

**Fluorescent Peptidyl Chemosensors for the Measurement of  
Divalent Metal Cation Concentrations**

Thesis by  
Grant Kingsley Walkup

In Partial Fulfillment of the Requirements  
for the Degree of  
Doctor of Philosophy

California Institute of Technology  
Pasadena, California

1998  
(Submitted May 5, 1998)

© 1998

Grant Kingsley Walkup

All Rights Reserved

For my wife,  
my parents,  
and  
my teachers.

## Acknowledgments

I would like to thank my advisor, Professor Barbara Imperiali, for her unending support throughout my graduate career. I can say without hesitation that she has truly been a mentor for me in every sense of the word. Her enthusiasm for science, and dedication to quality, exactness, and clarity shall always remain in my mind as an example to follow. Specifically, I want to thank her for tirelessly working to maintain an atmosphere in her labs that is simultaneously supportive of new ideas, while demanding of the best that one may do. It has been a pleasure and an honor to be her student.

Additionally, I owe a sizable debt to Robert Davis, who convinced me that I could get no better graduate education than that at Caltech—I think he was right. Undeniably, there is no institution better than its people and my stay at Caltech has been greatly enriched by the members of the Imperiali group. I was lucky to have been trained, advised, and befriended in my early days by Drs. Jeff Spencer, Bill Shrader, Stew Fisher, Keith Rickert, Ranabir Sinha Roy, Mary Struthers, Tamara Hendrickson, and Richard Cheng. I will also miss my talented and friendly co-workers Michael Shogren-Knaak, Vincent Tai, Kevin McDonnell, Dr. Jens Pohlmann, Jennifer Ottesen, Sarah O'Connor, Carlos Bosques, Angela Koehler, Maria Ufret, Dr. Paula Eason, Dr. Kazuaki Kudo, and Rob Dempski. I learned a lot from them, and without their presence, the lab would have been just another building.

The group of Dr. Alicia Torrado, Dr. Jean Ernest Sonha-Sonha, and Dr. Dierdre Pearce deserves special mention as collaborators on various different projects that I was associated with. It is in no small part due to their interest, advice, friendship, and hard work that I may view my graduate work as having been a success. I thank each of you for your enthusiasm, support, and excellence. Similarly, with the recent addition of Isaac Carrico to the chemosensor project, I expect that many more exciting results will be had.

This work could not have been completed without the continual support given me by my family. Mom and Dad, thank you for helping me to do what I believe in; it has

already started to pay off. Also, I must thank my wife for looking after me, making me happy when none other could, and working so hard to keep in balance the too-often-sacrificed necessities required for good mental health— eating, sleeping, and having fun. Traci, thank you, and now on to the “better,” we’ve done the “worse!”

Finally, the financial support of the NSF and the Caltech President’s Fund are gratefully acknowledged, as are the awards of a Glaxo Summer Fellowship and an NIH predoctoral training grant in biology and chemistry (GM07616).

## Abstract

Studies toward the production of fluorescent chemosensors for trace divalent metal ions have been conducted, with emphasis placed on the attainment of sufficient analyte selectivity and sensitivity for the measurement of environmental or biomedical samples. One technique that has historically been applied for the design of selective metal ion sensors is to prepare biosensors, devices that exploit proteins for their unmatched specificity in the recognition of small molecules. Alternately, the construction of abiotic chemosensors has been favored by other researchers, but the synthetic simplicity and enhanced durability exhibited by these agents comes at the expense of analyte-detection selectivity. By applying a strategy that is a hybrid of these approaches, selective and sensitive chemosensors for divalent zinc, copper, and nickel have been prepared. These devices combine the advantageous aspects of biosensors within a peptidyl architecture that by virtue of its synthetic origin contains an expanded repertoire of amino acids for metal ion binding and signaling.

Fluorescent chemosensors for Zn(II) have been prepared that are based upon the zinc finger domains and enable the quantitation of sub-micromolar concentrations of that ion in the presence of many other divalent ions. In addition, other fluorosensors have been prepared that employ nonnatural alpha-amino acid derivatives that contain the bidentate metal binding functionality of oxine (8-hydroxyquinoline). These also enable the selective detection of sub-micromolar concentrations of Zn(II), but require only seven amino acid residues as opposed to the 25 present in the zinc finger-based sensors.

By exploiting the metal binding properties of the amino terminal Cu(II)- and Ni(II)-binding (ATCUN) motif of the serum albumins, sensors have been prepared which enable the selective determination of sub-micromolar concentrations of the Cu(II) ion, even in the presence of elevated concentrations of Ni(II). Sensors for Ni(II) that employ a fluorescence resonance energy transfer (FRET) mechanism for analyte detection have also been prepared. In addition, studies have been performed to convert these solution-based chemosensing reagents into solid phase-attached devices, in order to perform real-time measurements with regenerable sensing materials.

## Table of Contents

<b>Abstract</b> .....	vi
<b>List of Figures</b> .....	xii
<b>List of Schemes</b> .....	xviii
<b>List of Tables</b> .....	xix
<b>List of Abbreviations</b> .....	xxi
<b>Chapter 1. Introduction</b> .....	1
Background and current limitations for metal cation sensing.....	2
The benefit of fluorescence.....	3
The need for selectivity.....	4
Synthetic chemosensors: advantages and limitations. ....	6
Metallopeptide design.....	9
Mechanisms of fluorescence signaling. ....	13
Microenvironment sensitive fluorescence: sensors for Zn(II). ....	13
Chelation-enhanced fluorescence: sensors for Zn(II). ....	13
Fluorescence quenching: sensors for Cu(II). ....	15
Fluorescence resonance energy transfer: sensors for Ni(II).....	15
References .....	17

**Chapter 2. Fluorescent Chemosensors for Divalent Zinc Based on the Zinc**

<b>Finger Domains</b> .....	27
Introduction .....	28
Results .....	31
Modular fluorophore incorporation. ....	31
First-generation design: FS01DMB. ....	35
Second generation design: FS02CMN, FS02DNS, and FS02NBD. ....	40
Third generation design: FS03DNS. ....	49
Fourth generation design, FS04DNS, FS04DNC. ....	57
Discussion .....	63
Selection of the peptidyl template. ....	63
Importance of metal-induced secondary structural changes. ....	64
Accommodation of the fluorophore within the hydrophobic cluster. ....	65
Ligand choice and zinc binding affinity. ....	66
Conclusion .....	71
Acknowledgment .....	71
Experimental .....	71
References .....	86

**Chapter 3. Fluorescent Peptidyl Chemosensors for Divalent Zinc**

<b>Incorporating Novel <math>\alpha</math>-Amino Acids that Contain 8-Hydroxyquinoline .....</b>	<b>94</b>
Introduction .....	95
Results and Discussion.....	101
Synthesis of Fmoc-2Oxn and Fmoc-5Oxn.....	101
Peptidyl incorporation of 2Oxn and 5Oxn and evalutaion of chemosensors. ....	107
Conclusion .....	114
Experimental .....	114
References .....	126
Spectra.....	129

<b>Chapter 4. Fluorescent Chemosensors Based on the Amino-Terminal Cu(II)- and Ni(II)-Binding Domain of the Serum Albumins .....</b>	<b>147</b>
Introduction .....	148
Results and Discussion.....	149
Selection of a peptidyl motif. ....	149
Preliminary investigation of fluorescence quenching with the ATCUN motif. ....	150
Investigation of the role of the fluorophore in signaling. ....	155
Investigations of the role of the position 3 residue in metal ion binding. ....	159
Solid phase immobilization studies.....	168
Conclusion .....	183
Acknowledgment .....	183
Experimental .....	184
References .....	191

<b>Chapter 5. Chemosensors for Ni(II) Based Upon the ATCUN Motif that Employ a FRET-Based Mechanism for Signal Transduction</b> .....	198
Introduction .....	199
Results and Discussion.....	203
Modeling studies. ....	203
Selection of fluorophore pairs. ....	205
Synthesis of chemosensors.....	210
Fluorescence characterization. ....	213
Calculation of $R_0$ s.....	215
Conclusion .....	217
Acknowledgment .....	218
Experimental .....	218
References .....	222

## List of Figures

### Chapter 1

- Figure 1-1.** The structures of some recently-reported fluorescent chemosensors for Cu(II) that use relatively simple metal-binding scaffolds. .... 7
- Figure 1-2.** The structures of some nonnatural  $\alpha$ -amino acids used for the construction of metallopeptides. .... 11
- Figure 1-3.** The structures of some nonstandard metal-binding amino acids developed in the Imperiali group. .... 12
- Figure 1-4.** The “microenvironment sensitive fluorescence” mechanism used in the chemosensors for Zn(II) presented in Chapter 2..... 14
- Figure 1-5.** The “chelation-enhanced fluorescence” mechanism used in the chemosensors for Zn(II) presented in Chapter 3..... 14
- Figure 1-6.** The fluorescence quenching mechanism used in the chemosensors for Cu(II) presented in Chapter 4. .... 15
- Figure 1-7.** The FRET-based mechanism of fluorescence modulation used in the chemosensors for Ni(II) presented in Chapter 5. .... 16

### Chapter 2

- Figure 2-1.** The structure of a typical zinc finger. .... 30
- Figure 2-2.** The structures of some fluorophores incorporated within zinc finger peptides and their spectral properties. .... 35
- Figure 2-3.** The solvent polarity-dependence fluorescence of a DMB model compound..... 36
- Figure 2-4.** Circular dichroism spectra of FS01DMB. .... 37
- Figure 2-5.** Absorption spectra of FS01DMB with Co(II) and Zn(II). .... 37
- Figure 2-6.** Apparent  $K_D$  determination for FS01DMB..... 38

<b>Figure 2-7.</b>	Peptide sequences modeled for residue replacement in the design of FS02. ....	41
<b>Figure 2-8.</b>	Metal coordination isomers of histidine.....	41
<b>Figure 2-9.</b>	Minimized structures of “CHHH” and “HCHH.”.....	42
<b>Figure 2-10.</b>	Fluorescence emission spectra FS02DNS with Zn(II).....	44
<b>Figure 2-11.</b>	Fluorescence quenching of dansyl asparagine and FS02DNS by Cu(II) and the rescue of emission with EDTA. ....	45
<b>Figure 2-12.</b>	Circular dichroism spectra FS02DNS with Zn(II). ....	46
<b>Figure 2-13.</b>	Absorbance spectra of FS02DNS and mag-fura-2 upon the addition of Zn(II). ....	48
<b>Figure 2-14.</b>	Fluorescence response of FS03DNS to the addition of various divalent metals. ....	51
<b>Figure 2-15.</b>	Fluorescence emission response of FS03DNS to increasing levels of Zn(II), in the presence of 50 mM Mg(II), and 100 $\mu$ M Co(II) ions. ....	52
<b>Figure 2-16.</b>	Ratiometric profiles of the fluorescence emission of FS03DNS for both the Zn(II)-bound species and the Co(II)-bound species. ....	53
<b>Figure 2-17.</b>	Ratiometric analysis of FS03DNS with various divalent metal ions. ....	54
<b>Figure 2-18.</b>	Circular dichroism spectra of FS03DNS. ....	54
<b>Figure 2-19.</b>	A typical competition experiment for Zn(II)-binding between FS03DNS and the metallochromic indicator PAR. ....	56
<b>Figure 2-20.</b>	A schematic representation of the Cys6 $\rightarrow$ Asp residue replacement made for the FS04 template. ....	58
<b>Figure 2-21.</b>	Comparison of the fluorescence enhancement of the DNS and DNC fluorophores in a variety of solvents. ....	60

<b>Figure 2-22.</b>	Circular dichroism spectra of FS04DNS with Zn(II).....	61
<b>Figure 2-23.</b>	Fluorescence emission spectra of FS04DNS with Zn(II), in the presence of various divalent metal ions. ....	61
<b>Figure 2-24.</b>	Absorption spectra from a typical competition assay for Zn(II) binding between FS04DNS and mag-fura-2. ....	62
<b>Figure 2-25.</b>	Fluorescence emission spectra of several peptide·Zn(II) complexes, corrected for the concentration of the fluorophore. ....	66
<b>Figure 2-26.</b>	The fluorescence emission spectrum of FS03DNS·Zn(II) in comparison with a DNS model compound in reference solvents.....	70
<b>Figure 2-27.</b>	A typical titration of mag-fura-2 with Zn(II). ....	78
<b>Figure 2-28.</b>	Concentration-corrected spectra of mag-fura-2 in the absence and presence of Zn(II). ....	79
<b>Figure 2-29.</b>	A representative plot used for determining the disassociation constant for the FS02DNS·Zn(II) complex. ....	81
<b>Figure 2-30.</b>	Analysis of the Zn(II) competition binding assay for FS04DNS. ....	81
<b>Figure 2-31.</b>	Analysis of the apparent $K_D$ for the FS04DNS·Zn(II) complex. ....	83
<b>Chapter 3</b>		
<b>Figure 3-1.</b>	A CPK model of the sensor FS03DNS, with the side chain of the Dap(dansyl) residue highlighted. ....	96
<b>Figure 3-2.</b>	8-Hydroxyquinoline forms fluorescent complexes with several metal ions. ....	97
<b>Figure 3-3.</b>	Fluorescence emission spectra of oxine, both before and after the addition of ZnCl <sub>2</sub> . ....	98
<b>Figure 3-4.</b>	Absorption spectra of oxine in the absence and presence of ZnCl <sub>2</sub> .....	99

<b>Figure 3-6.</b>	Structures and sequences of <b>P1</b> and <b>P2</b> . .....	107
<b>Figure 3-7.</b>	Absorption spectra from a typical titration of P1 with ZnCl <sub>2</sub> and the binding isotherm calculated using the data at 262 nm. ....	110
<b>Figure 3-8.</b>	Fluorescence emission spectra of <b>3</b> and <b>P1</b> showing the effect of added ZnCl <sub>2</sub> . .....	111
<b>Figure 3-9.</b>	Fluorescence emission spectra of a 1 μM solution of <b>P1</b> with increasing concentrations of ZnCl <sub>2</sub> . .....	111
<b>Figure 3-10.</b>	Measurements of the fluorescence emission response of P1 to various metal cations both in the presence and absence of ZnCl <sub>2</sub> . .....	113
 <b>Chapter 4</b>		
<b>Figure 4-1.</b>	A model of an ATCUN motif (Gly-Gly-His-CONH <sub>2</sub> ) displaying the metal ion bound with square planar geometry. ....	149
<b>Figure 4-2.</b>	Structures of the first generation of compounds based on the ATCUN motif. .....	151
<b>Figure 4-3.</b>	Fluorescence emission response of <b>1-3</b> , with an added equivalent of Ni(II) or Cu(II). .....	151
<b>Figure 4-4.</b>	Mechanisms for fluorescence quenching by the Cu(II) ion. ....	154
<b>Figure 4-5.</b>	Structures of and spectral data for the fluorophores investigated to increase the sensitivity of the sensors to Cu(II) or Ni(II) quenching. .....	156
<b>Figure 4-6.</b>	Fluorescence emission spectra of several fluorophores, compared with the absorption band of an ATCUN·Cu(II) complex. ....	156
<b>Figure 4-7.</b>	Structures of the second series of peptides used to investigate the role of the fluorophore in the preparation of fluorescent chemosensors. ....	157

<b>Figure 4-8.</b>	Fluorescence response of the ANT fluorophore compared with that of the DNS fluorophore upon the addition of an equivalent of Ni(II) or Cu(II).....	158
<b>Figure 4-9.</b>	Structures of the third series of peptidyl chemosensors prepared (9-18).....	160
<b>Figure 4-10.</b>	Fluorescence emission response of compounds <b>11</b> and <b>12</b> to an added equivalent of Ni(II) or Cu(II). ....	162
<b>Figure 4-11.</b>	Profiles of the rate of fluorescence emission quenching for compounds <b>1</b> , <b>13</b> , and <b>16</b> , upon the addition of an equivalent of Ni(II). ....	163
<b>Figure 4-12.</b>	The structure of <b>19</b> , a sensitive and selective chemosensor for divalent copper. ....	164
<b>Figure 4-13.</b>	Fluorescence emission spectra of <b>19</b> in response to increasing concentrations of Cu(II). ....	165
<b>Figure 4-14.</b>	Fluorescence emission spectra of <b>19</b> in response to various metal ions. ....	166
<b>Figure 4-15.</b>	A comparison of the structures of the Cu(II) complexes for glycyl-histidine and carnosine. ....	167
<b>Figure 4-16.</b>	Molecular model of a Gly- $\beta$ Ala-His tripeptide bound to Cu(II) that was constrained to maintain a square planar coordination geometry.....	168
<b>Figure 4-17.</b>	Structures of the monomers that comprise PEGA resin. ....	170
<b>Figure 4-18.</b>	The second (Xaa) and third (Yaa) residues of the ATCUN motif chosen for replacement.....	171
<b>Figure 4-19.</b>	Amino acid derivatives chosen for the replacement of the “Xaa” and “Yaa” residues of the ATCUN motif. ....	172

<b>Figure 4-20.</b>	Typical solid-phase quenching assay of Dap(DNS)- $\beta$ Ala-His-Ser-Ser-PEGA. ....	177
<b>Figure 4-22.</b>	Fluorescence emission spectra of Dap(DNS)-Sar-Thz-Ser-Ser-NH <sub>2</sub> in response to increasing concentrations of Cu(II). ....	179
<b>Figure 4-23.</b>	The Cu(II) binding isotherm calculated for Dap(DNS)-Sar-Thz-Ser-Ser-NH <sub>2</sub> obtained from the data presented in Figure 4-22. ....	179
<b>Figure 4-24.</b>	Fluorescence quenching of Dap(DNS)- $\beta$ Ala-His-Ser-Ser-PEGA after the addition of 1 mM Cu(II). ....	181
<b>Figure 4-25.</b>	Quantitative measurement of on-bead fluorescence quenching kinetics. ....	182
<b>Chapter 5.</b>		
<b>Figure 5-1.</b>	The mechanism of FRET-based chemosensing. ....	201
<b>Figure 5-2.</b>	The distance-dependence of FRET efficiency as a function of the characteristic $R_0$ for a donor and acceptor pair. ....	202
<b>Figure 5-3.</b>	Molecular model of an ATCUN motif in an extended, and metal-bound state. ....	203
<b>Figure 5-4.</b>	A typical donor-acceptor overlap, required for FRET. ....	206
<b>Figure 5-5.</b>	Structures and spectral properties of the donor fluorophores selected for incorporation within chemosensors. ....	207
<b>Figure 5-6.</b>	Structures of the fluorophore considered as energy acceptors and their spectral properties in relation to those of energy donors. ....	209
<b>Figure 5-7.</b>	Fluorescence emission spectra of peptide <b>F5</b> in response to the addition of NiCl <sub>2</sub> . ....	215

## List of Schemes

### Chapter 2

**Scheme 2-1.** The mechanism of microenvironment sensitive fluorescence. .... 30

**Scheme 2-2.** Method for modular fluorophore introduction. .... 33

### Chapter 3.

**Scheme 3-1.** Synthesis of Fmoc-2Oxn-OH..... 102

**Scheme 3-2.** Synthesis of Fmoc-5Oxn-OH..... 106

### Chapter 5

**Scheme 5-1.** Synthetic strategy for the preparation of fluorescent peptides..... 211

## List of Tables

### Chapter 1.

- Table 1-1.** Biological concentrations and limits of detection as determined by standard methods for the ions Cu(II) and Zn(II) ..... 2
- Table 1-2.** Some abiotic fluorescent chemosensors for Cu(II) and their conditions for operation. .... 8

### Chapter 2.

- Table 2-1.** Amino acid sequences of synthetic zinc finger peptides. .... 34
- Table 2-2.** Published solution structures of individual zinc finger domains. .... 50
- Table 2-3.** Apparent  $K_{DS}$  for the FS03DNS·Zn(II) complex calculated by competition with PAR..... 56
- Table 2-4.** Apparent  $K_{DS}$  for Peptide·Zn(II) Complexes..... 64
- Table 2-5.** Fluorescence emission properties of peptide·Zn(II) complexes. .... 68
- Table 2-6.** Fluorescence enhancements for ratiometric-based and intensity-based chemosensors for Ca(II)..... 69
- Table 2-7.** Calculated and observed electrospray mass values for the synthetic zinc finger peptides..... 74
- Table 2-8.** Parameters used for the modeling of the fluorescent sensing peptides. .... 84

### Chapter 3.

- Table 3-1.** Stability constants of oxine-metal complexes at 20 °C in 50% v/v aqueous dioxane. .... 101
- Table 3-2.** Apparent dissociation constants and stoichiometries measured for Zn(II)-complexes of various compounds. .... 108

**Chapter 4.**

<b>Table 4-1.</b>	Identities of the PEGA resin-bound peptides prepared.....	172
<b>Table 4-2.</b>	Time-dependent quenching of Dap(DNS)-Gly-His-Ser-Ser- PEGA in response to varying concentrations of Cu(II). .....	174
<b>Table 4-3.</b>	Time-dependent quenching of Dap(DNS)-Gly-His-Ser-Ser- PEGA in response to varying concentrations of Cu(II), with 20% v/v methanol. ....	174
<b>Table 4-4.</b>	Results from a typical Cu(II) quenching assay. ....	176
<b>Table 4-5.</b>	Results from a typical Ni(II) quenching assay. ....	176

**Chapter 5.**

<b>Table 5-1.</b>	Interatomic distances measured from the model ATCUN motif. ....	204
<b>Table 5-2.</b>	Sequences of the peptides prepared, and the number of pure isomers collected by HPLC.....	212
<b>Table 5-3.</b>	Spectral properties of the fluorescent peptides. ....	214
<b>Table 5-4.</b>	Quantum yields of the donor fluorophores measured in 0.15 M NaCl, 50 mM HEPES, pH 7.0. ....	216
<b>Table 5-5.</b>	Integrated overlap integrals ( $J$ ) and distances of 50% energy transfer ( $R_0$ ) calculated for several fluorophore pairs. ....	217

**List of Abbreviations**

AAS	Atomic absorption spectroscopy
Abs	Absorbance
Ac	Acetyl
alloc	Allyloxycarbonyl
ANT	9-Carboxamido-anthracene
ASV	Anode-stripping voltammetry
ATCUN	Amino-terminal Cu(II)- and Ni(II)-binding
AU	Absorption unit
$\beta$ Ala	$\beta$ -Alanine (3-amino-propanoic acid)
Bn	Benzyl
Boc	<i>tert</i> -Butyloxycarbonyl
BOP	Benzotriazole-1-yl-oxy-tris(dimethylamino)-phosphoniumhexafluoro-phosphate
BZX	2-Benzoxazole
calcd	Calculated
CCD	Charge-coupled device
CD	Circular dichroism
CHEF	Chelation-enhanced fluorescence
CMN	coumarin-3-carboxamido
COM	Coumarin 343
CZE	Capillary zone electrophoresis
Dab	( <i>S</i> )-2,4-Diaminobutyric acid
Dap	( <i>S</i> )-2,3-Diaminopropionic acid
DBU	1,7-Diazabicyclo[5,4,0]-undec-7-ene
DCM	Dichloromethane

de	Diastereomeric excess
DE	7-Diethylamino-coumarin-3-carboxylic acid
DIEA	Diisopropylethylamine
DIPCDI	Diisopropylcarbodiimide
DM	7-Dimethylamino-coumarin-4-acetic acid
DMAP	4- <i>N,N</i> -Dimethylaminopyridine
DMF	<i>N, N</i> -Dimethylformamide
DMSO	Dimethylsulfoxide
DNC	1- <i>N,N'</i> -Dimethylamino-naphthalene-5-carboxyl
DNS	5- <i>N,N</i> -Dimethylamino-naphthalene-1-sulfonyl
DSPC	Distearoyl phosphatidylcholine
DTNB	5,5'-Dithiobis(2-nitrobenzoic acid)
EDTA	Ethylenediaminetetraacetic acid
ee	Enantiomeric excess
EPPS	<i>N</i> -(2)-Hydroxyethylpiperazine- <i>N'</i> -(3)-propanesulfonic acid
ESI	Electrospray ionization
ETAAS	Electrothermal atomic absorbance spectroscopy
FAB	Fast atom bombardment mass spectrometry
FE	Fluorescence enhancement
Fen	( <i>S</i> )-2-Amino-3-(1,10-phenanthrol-2-yl)propionic acid
Fmoc	9-Fluorenylmethyloxycarbonyl
Fmoc-OSu	9-Fluorenylmethyloxycarbonylsuccinimidyl carbonate
FRET	Fluorescence resonance energy transfer
HATU	<i>O</i> -(7-Azabenzotriazol-1-yl)-1,1,3,3-tetramethyluronium hexafluorophosphate
Hcs	Homocysteine
HEPES	<i>N</i> -(2-Hydroxyethyl)piperazine- <i>N'</i> -(2-ethane-sulfonic acid)

HOAt	1-Hydroxy-7-azabenzotriazole
HOBt	1-Hydroxybenzotriazole
HOMO	Highest occupied molecular orbital
HPLC	High performance liquid chromatography
HRMS	High resolution mass spectrometry
Hse	Homoserine
ICPMS	Inductively coupled plasma mass spectroscopy
IDA	Iminodiacetic acid
K <sub>D</sub>	Dissociation constant
LDA	Lithium diisopropylamide
LUMO	Lowest unoccupied molecular orbital
max	Maximum
min	Minute
MS	Mass spectrometry
NBD	4-Nitrobenzo-2-oxa-1,3-diazole
nm	Nanometer
NMR	Nuclear magnetic resonance
obsd	Observed
OPfp	Pentafluorophenyl
Orn	Ornithine
PAL	5-(4'-Aminomethyl-3',5'-dimethoxyphenoxy)valeric acid
PAR	4-(2-Pyridylazo)resorcinol
PEG-PS	Polyethyleneglycol-grafted polystyrene
PEGA	Polyethyleneglycol-poly-( <i>N,N'</i> -dimethylacrylamide) copolymer
PET	Photoinduced electron transfer
ppb	Parts per billion
PRODAN	6-Propionyl-2-(dimethylamino)naphthalene

Pya	2-Pyridylalanine
PyBrOP	Bromo-tris-pyrrolidino-phosphonium hexafluorophosphate
RHD	Rhodamine B
RP	Reverse phase
Sar	Sarcosine ( <i>N</i> -methylglycine)
sec	Seconds
SPPS	Solid phase peptide synthesis
<sup>t</sup> Bu	<i>tert</i> -Butyl
TAPS	<i>N</i> -Tris(hydroxymethyl)methylaminopropanesulfonic acid
TEA	Triethylamine
TFA	Trifluoroacetic acid
TG	TentaGel, polystyrene–poly(ethyleneglycol)–tentacle copolymer
THF	Tetrahydrofuran
Thz	4-Thiazolylalanine
TLC	Thin layer chromatography
UV	Ultra violet
vis	Visible

**Chapter 1**  
**Introduction**

## Background and current limitations for metal cation sensing.

Divalent metal cations are ubiquitous biological cofactors, required for cellular processes as diverse as hydrolysis, electron transfer, and signal transduction;<sup>1,2</sup> consequently the maintenance of the proper levels of these species is essential for the health of both the environment as well as for individuals.<sup>3</sup> Cu(II) and Zn(II) are two such species, and aberrations in their physiological concentrations can have serious medical repercussions. Irregularity in Cu(II) transport, characteristic of Wilson's disease, leads to the accumulation of copper throughout the body, causing neurological damage and cirrhosis of the liver.<sup>4</sup> Minor deficiencies in zinc have similarly worrisome consequences, including stunted growth and severe skin disorders.<sup>5</sup> Despite the well-recognized importance of these and other divalent metal cations, current means for their detection and quantitation in biological or environmental samples are limited.

Current techniques available for accurately measuring Cu(II) and Zn(II) concentrations include atomic absorption spectroscopy (AAS), inductively-coupled plasma mass spectrometry (ICPMS), electroanalytical techniques such as anode stripping voltammetry (ASV), and chromatographic techniques using post-column colorimetric indicators.<sup>6-9</sup> The limits of detection of these analytes by such techniques, and average concentrations of Zn(II) and Cu(II) ions in some biological media are shown in Table 1-1.

**Table 1-1.** Biological concentrations and limits of detection as determined by standard methods for the ions Cu(II) and Zn(II)

Ion	Concentration ( $\mu\text{M}$ ) <sup>9-11</sup>		Limits of Detection ( $\mu\text{M}$ ) <sup>7,8</sup>		
	Plasma	Urine	AAS <sup>a</sup>	ICPMS <sup>b</sup>	ASV <sup>c</sup>
Cu(II)	12-26	0.2-1.0	0.3	0.2	0.3
Zn(II)	11-46	5-10	2	1	0.1

<sup>a</sup>Atomic absorption mass spectrometry, including electrothermal, and flame excitation.

<sup>b</sup>Inductively-coupled plasma mass spectrometry.

<sup>c</sup>Anode stripping voltammetry.

While the analytical techniques listed in Table 1-1 have impressive sensitivities, and biological samples *can* be analyzed by them, difficulties do arise due to the expense of analysis, sample preparation, or interference from the complicated broth of molecules and ions that typify biological specimens. For example, chloride, bromide, and phosphate ions (all present in high concentrations in biological and environmental samples) severely interfere with both AAS and ICPMS.<sup>6,7,10</sup> On the other hand, ASV analysis is often rendered impractical due to the presence of chelating agents and/or redox active molecules such as citrate.<sup>8</sup> The analysis of trace metal cations thus remains a significant challenge, and the desire for rapid, sensitive, and selective means for measuring these species continues to be a challenge.<sup>12</sup>

### **The benefit of fluorescence.**

The techniques mentioned above are limited in their usefulness for measuring trace Cu(II) or Zn(II) levels in biological or environmental samples, predominantly due to the complicated milieu of species present *de facto* in those specimens. However, the measurement of Cu(II) and Zn(II) ions in biological or environmental samples are amenable to analysis with appropriately constructed *fluorescent chemosensors*. The inherent sensitivity of fluorescence measurements easily accommodates the need to make determinations at the nM level (or lower).<sup>13-16</sup> Therefore, the task of producing an operational chemosensor requires the conjunction of a fluorophore that can interact with and signal in some way the occupancy of a metal ion-binding receptor, a topic that has been discussed at length.<sup>12,15-20</sup> Furthermore, the success of chemosensors for ions including sodium,<sup>21</sup> potassium,<sup>21</sup> magnesium,<sup>22</sup> calcium,<sup>23-25</sup> chloride,<sup>26</sup> as well as pH,<sup>27,28</sup> demonstrate convincingly that chemosensors can work exceptionally well in complex solutions once sufficiently selective binding domains have been developed.

Other criteria required for functional, real-time measurements within biological or environmental samples by fluorescent chemosensors have been delineated,<sup>14-16</sup> and are summarized below.

- The analyte should be able to bind to the receptor reversibly.
- Excitation of the fluorophore should be performed at as long a wavelength as possible to reduce background fluorescence from materials commonly found in biological, medicinal, or environmental samples.
- The signal being measured should not be effected substantially by adventitious fluorescence quenching agents, nor modulated by pH changes in the range expected for the environment in which it is to be applied.
- The chemosensor should be resistant to facile hydrolysis and oxidation reactions.

### **The need for selectivity.**

Yet among all these concerns, the central problem for the production of useful new fluorescent sensors for the detection of metal cations is the issue of selectivity.<sup>12,16</sup> The relative affinity of the chemosensor for the ion of interest must exceed the cumulative concentration excess imposed by all other competing species. In other words, one must consider the environment into which a sensor is to be placed in order to judge its effectiveness. On one hand, a chemosensor can have lower affinity for its intended analyte than for a competing species if the competitor is present at sufficiently low levels. For example, the well-known fluorescent indicator fura-2 binds Zn(II) with greater affinity than Ca(II), but remains a *cellular* probe for free calcium,<sup>29</sup> due to the composition of the environment to which it is applied. It is due in part to this reason that the remarkable cellular probes for Mg(II) and Ca(II) pioneered by Tsien have achieved such remarkable success; the divalent cations present in the highest (free) concentrations within cells are Mg(II) and Ca(II).<sup>15,29,30</sup> On the other hand, this selectivity requirement can present an awesome challenge for the measurement of trace metal cations. Consider, for example, a sensor for Zn(II) that is required for use in an environmental measurement, such as for the analysis of sea water. Under such conditions this device must compete with approximately 0.5 M sodium, 50 mM Mg(II), and 10 mM Ca(II) ions.<sup>6,8,31,32</sup> Thus

accurate measurements of Zn(II) concentrations near 100 nM requires sensors with greater than  $5 \times 10^5$  fold selectivity for Zn(II) against Mg(II).

Achieving selectivities of this magnitude is therefore required for the analysis of trace metal cation concentrations, and it is often very difficult to construct chemosensors with metal-binding motifs that fulfill these demands. In order to obtain selectivities of these magnitudes, researchers have frequently taken advantage of the (often unrivaled) ability of proteins for the recognition of small molecules— a trait that is exemplified by metal cation coordination. Indeed, the specific recognition of metal cations is central to regulation and catalysis in innumerable biological systems and consequently many proteins exhibit enviable metal-binding selectivity.<sup>1,33</sup> However, naturally occurring proteins typically lack the fluorescence characteristics of a useful sensor, and therefore strategies involving affinity labeling or other methods for the introduction of a fluorophore are required for signal transduction.<sup>34,35</sup> Thus, biological signal transducers, *i.e.*, “biosensors,” have been devised from existing proteins for the divalent cations of zinc,<sup>32,36,37</sup> mercury,<sup>38</sup> as well as copper and cobalt.<sup>39</sup>

While many of these biosensors can detect a specific divalent metal cation at nanomolar levels, problems associated with the use of these labile and complicated protein scaffolds for metal ion sensing still remain. For example, the sensors for Zn(II) mentioned above require the addition of an exogenous, diffusible fluorophore for the sensing process, a constraint that greatly complicates the measurement process.<sup>37</sup> Moreover, the Co(II) and Cu(II) sensing devices are too labile for application in sea water.<sup>39</sup> An additional limitation of these devices is the difficulty involved in making modifications to the signal transducer. Such modifications have been made but have required the precise atomic-level detail of high-quality X-ray structure analysis to achieve success.<sup>40</sup> In other words, the impressive selectivities and affinities afforded within the context of a biosensor can also provide an excessively restrictive burden of complexity for the design of new sensors.

**Synthetic chemosensors: advantages and limitations.**

In light of the opportunities for greater design flexibility, the production of purely synthetic sensing devices continues to be pursued. This alternate approach for the design of metal cation chemosensors therefore has foregone the complexity (and concomitant selectivity) of biologically-derived receptors, to build from first principles relatively small synthetic organic molecules comprising a metal binding site and a reporting fluorophore. A survey of the literature covering fluorescent chemosensors for Cu(II) provides insight into both the successes and limitations of this approach. Sensors for Cu(II) ion have been chosen for illustrative purposes in light of the fact that, *a priori*, the preparation of a binding domain selective for this ion should be comparatively easy. Because the Cu(II) ion is the most Lewis-acidic divalent transition metal cation in the third-row of the periodic table, it should (in the absence of specific ligand-field effects) bind to a given receptor with greater affinity than other divalent species.<sup>41,42</sup>

The structures of several of the most promising fluorescent chemosensors for Cu(II) are presented in Figure 1-1. Representative chemosensors have been selected from the work of several laboratories, including those of Fabbri<sup>43-45</sup> (**1-3**), Czarnik<sup>46,47</sup> (**4-5**), and Arnold<sup>48</sup> (**6**).

Inspection of these structures reveals that common to each is the use of the “receptor-spacer-fluorophore” paradigm for metal cation sensing.<sup>18-20</sup> Sensors **1-4** are “off” sensors which rely on photoinduced electron transfer (PET) from a bound metal ion to excited fluorophore to quench fluorescence. The workings of this frequently-used mechanism for transition metal cation sensing have been thoroughly reviewed.<sup>19,49-52</sup> Compounds **5** and **6** are both “on” sensors that operate using less commonly employed mechanisms for signal transduction. Chemosensor **5** is non-fluorescent in the form shown, but is a substrate for metal ion-catalyzed hydrolysis of the hydrazide to produce the intensely fluorescent compound rhodamine B. Chemosensor **6**, when present in

distearoyl phosphatidylcholine (DSPC) vesicles will, in the presence of various divalent cations, exhibit pyrene excimer fluorescence.

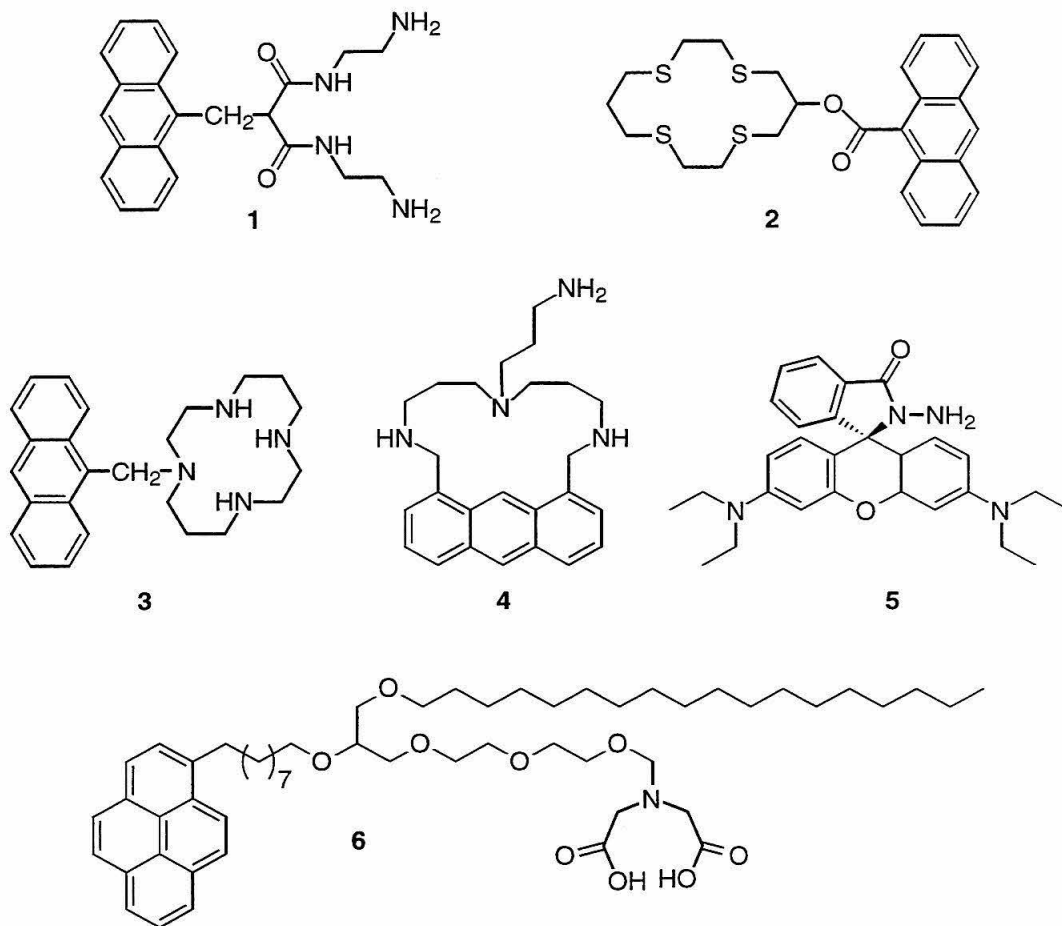


**Figure 1-1.** The structures of some recently-reported fluorescent chemosensors for Cu(II) that use relatively simple metal-binding scaffolds.

The most striking features shared by these chemosensors are the relatively simple metal-binding receptors used, at least in comparison to those found in biosensors. Indeed, the fact that these molecules may be readily synthesized without the construction of an elaborate and complex metal binding site is their main advantage. Yet despite the exceptional chemical properties of the Cu(II) ion (its unique position in the Irving-Willimas series that results in an intrinsic advantage in producing binding motifs that are selective for this species), these chemosensors do have shortcomings. These sensors

exhibit significant cross-reactivity with the Ni(II) ion, and/or incompatibility with solely aqueous solvent. A summary of the operating characteristics for fluorescent chemosensors **1-6** is presented in Table 1-2. For example, the experimental constraints imposed by sensors **1-3** (that are only functional in EtOH or 4:1 MeCN:H<sub>2</sub>O) are enormous, effectively eliminating the possibility of measuring ion concentrations within biological or environmental samples. Similarly, for **6**, the necessity of forming DSPC micelles is a significant drawback, effectively eliminating real time measurements. In this regard, chemosensors **4** and **5** are most suitable for application, but even these could be improved: the affinity of **4** for Cu(II) is too weak for effective measurements of trace (sub-micromolar) divalent copper concentrations, and the irreversible destruction of **5** also presents a significant logistical concern.

**Table 1-2.** Some abiotic fluorescent chemosensors for Cu(II) and their conditions for operation.

compound	competing ions <sup>a</sup>	solvent	comment	ref.
1	Ni(II)	4:1 MeCN:H <sub>2</sub> O	Ni(II) reactivity suppressed at pH (apparent) 7.1	43,44
2	Ni(II)	EtOH	Mn(II), Fe(II), Co(II) benign	45
3	Ni(II), Zn(II)	4:1 MeCN:H <sub>2</sub> O	Excessively slow metal binding at pH < 8	44
4	Hg(II)	H <sub>2</sub> O	Hg(II) K <sub>D</sub> < 1 μM Cu(II) K <sub>D</sub> = 56 μM	47
5	Hg(II)	4:1 H <sub>2</sub> O:MeCN	irreversible hydrolysis of hydrazide	46
6	—	H <sub>2</sub> O/DSPC	requires micelle formation, discontinuous	48

<sup>a</sup>Only those species are included that alter the measured signal for Cu(II) by ≥ 50% when present in equal quantities as the analyte.

<sup>b</sup>Distearoyl phosphatidylcholine.

The examples provided illustrate the dilemma to be faced during the design of new fluorosensors. Sensors with highly selective metal binding properties can be prepared through the production of biosensors, yet these suffer ultimately from the lability or complexity of the biologically-derived materials. Alternately, purely synthetic chemosensors that are rugged, easily prepared and can be systematically modified, have generally proven to exhibit insufficient selectivity for measuring a specific divalent metal cation. In order to resolve this dilemma, it makes sense to combine the advantageous aspects of both types of sensors for the development of new devices.

The chemosensors that will be presented in this dissertation have been developed using an approach that is a hybrid of the archetypal biosensor and abiotic sensor regimes. Synthetic chemosensors based upon the polypeptidyl architecture have been constructed that may therefore have access to the enviable metal binding selectivities exhibited by naturally occurring metalloptides and proteins. The inherently modular nature of the peptidyl scaffold offers unique design flexibility, allowing rapid and facile modifications to be made. And, by virtue of their synthetic origin, these sensors also enable the inclusion of an expanded menu of nonstandard amino acids.

This approach shares a great deal of similarity with one used in nature by microbes for the production of metal chelating motifs such as the siderophores.<sup>53-56</sup> These compounds, which combine unusual non-encoded metal-ligating amino acids within a peptidyl architecture, set an impressive precedent for the *specific* recognition of metal cations in the biosphere. So too, then, do the siderophores highlight the potential of peptidyl motifs for the design of new, selective metal cation chemosensors.

### **Metallopeptide design.**

In a general sense, this research falls within the field of metallopeptide design. Due to the tremendous importance of metal cations in biological systems, there has been wide-spread interest in the modification of existing metal-binding proteins, and in the *de novo* design of metalloptides and metalloproteins. A number of reviews covering these

topics have recently appeared.<sup>57-61</sup> In many cases, the focus of this research has been to better understand the reactivity or stability of a well-characterized protein, consequently analysis from the standpoint of metal binding *selectivity* has been of less concern. Recent examples of elegant metalloprotein engineering which fall into this category include the conversion of a zinc-copper superoxide dismutase to a blue copper protein,<sup>62-64</sup> and the investigations made into the workings of the catalytic zinc of carbonic-anhydrase.<sup>65,66</sup> Although little mention of metal binding selectivity is made in these reports, the bias is completely understandable and justifiable as the goal has been to understand the unique characteristics of the particular metal cation under investigation. Nonetheless, the qualities of reactivity and metal binding selectivity are tightly intertwined as both are controlled by subtle changes of both ligand type and geometry.<sup>1,2</sup>

Examples of engineering selective metal binding sites within proteins of *de novo* design are fewer in number, but excellent examples do exist. These include the construction of zinc-binding proteins by Regan and co-workers,<sup>67-69</sup> as well as proteins that bind either zinc<sup>70</sup> or mercury<sup>71</sup> described by DeGrado and associates. These proteins are either multimeric, or too large for practical application as chemosensors.

A powerful approach for minimizing the extent of peptidyl architecture required for constructing a high-affinity metal binding site involves the synthesis of nonstandard amino acids containing multidentate ligands. Several groups have prepared metallopeptides *via* this technique, with representative structures of such peptide-incorporated-amino acids shown in Figure 1-2. Residues incorporating the metal binding functionality of iminodiacetic acid (IDA) were first prepared by the Hopkins group,<sup>72,73</sup> with subsequent synthetic improvements made by Kazmierski.<sup>74,75</sup> Similarly Rana *et al.* have prepared peptides containing the ethylenediaminetetraacetic acid (EDTA) metal-binding core.<sup>76</sup> More recently Gilbertson has reported the preparation of peptides containing phosphine functionality.<sup>77,78</sup> Additionally, Sasaki<sup>79</sup> and Ghadiri<sup>80,81</sup> have

independently employed the bidentate 2,2'-bipyridine moiety (not incorporated within an  $\alpha$ -amino acid scaffold) as an *N*- or *C*-terminal modification of peptides.

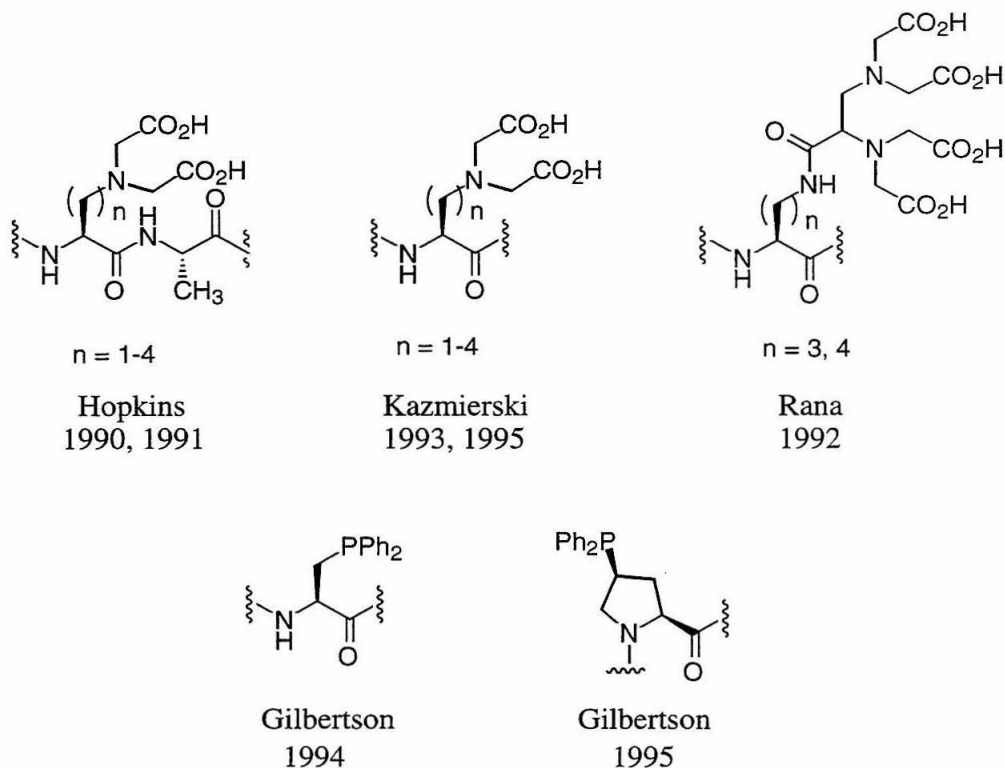


**Figure 1-2.** The structures of some nonnatural  $\alpha$ -amino acids used for the construction of metallopeptides.

Despite the opportunities provided by the inclusion of preorganized metal binding functionality or the availability of ligands not readily available to natural peptides, the goal of preparing a selective metal binding site has not been the focus of this research.<sup>82</sup> Instead the use of these nonstandard residues has been for the enhancement of peptide secondary or tertiary structure. The fact that high-affinity metal binding residues have been used predominantly to *reliably induce peptide folding* is tremendously important. As noted earlier, construction of a binding site that exhibits metal cation selectivity requires the judicious presentation of both ligand type and geometry. This feat, which is the hallmark of metalloproteins, requires the opposite relationship between peptide structure and metal binding than that observed in the studies mentioned above.

In contrast, a considerable amount of effort has been spent in the Imperiali group toward the evaluation of cation binding selectivity of metallopeptides of *de novo* design. Toward this end, numerous amino acids containing bidentate metal-ligating functionality have been synthesized and incorporated within peptides, some of which are shown in Figure 1-3. These include the  $\alpha$ -amino acid residues that incorporate 2,2'-bipyridine,<sup>83-85</sup> 1,10-phenanthroline and 2,9-dimethyl-1,10-phenanthroline (neocuproine),<sup>86</sup> as well as  $\omega$ -amino residue containing the 2,2'-bipyridine moiety as a backbone modification.<sup>87</sup> Insights into ways to tune metal ion binding affinity, provided by the inclusion of such residues within short peptides of *de novo* design provided much of the ground-rules (and inspiration) for the development of fluorescent chemosensors described in this thesis.

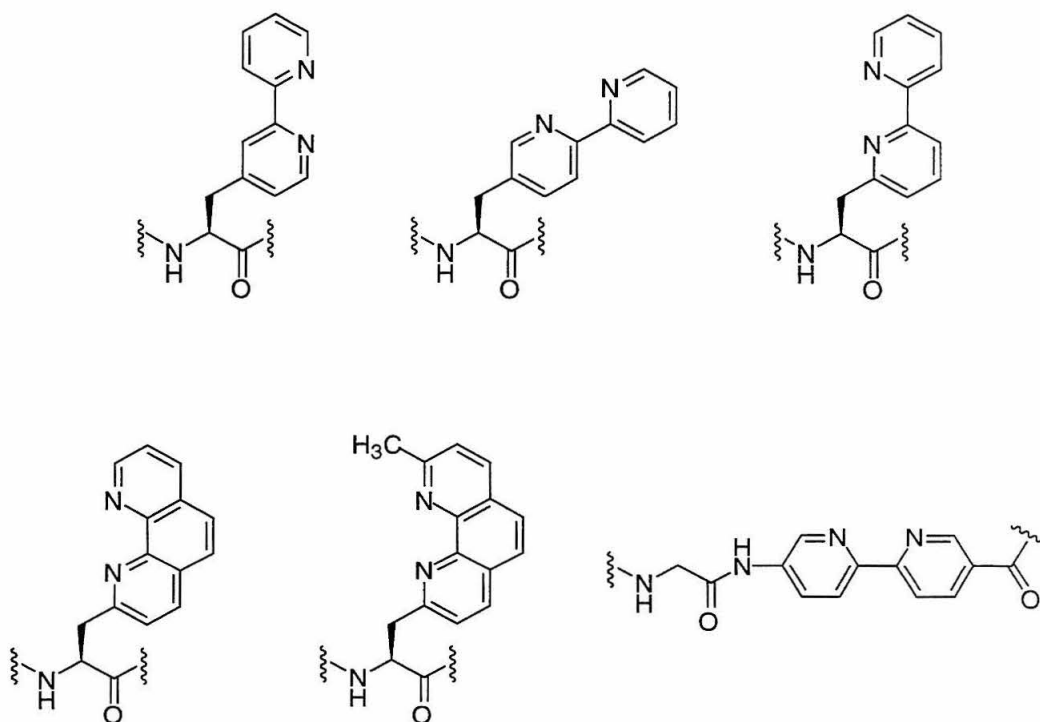


**Figure 1-3.** The structures of some nonstandard metal-binding amino acids developed in the Imperiali group.

## **Mechanisms of fluorescence signaling.**

Strategies from the related fields of biosensor-, metalloprotein-, metallopeptide-, and *de novo* protein design have been exploited to varying degrees in a “hybrid approach” for the development of the fluorosensors presented herein. Depending upon the characteristics of the particular ion of interest, different methods for the construction of the metal binding receptors and different means for modulating the fluorescence response of individual sensors have been employed. The remainder of this chapter summarizes the types of sensors that have been produced and describes in general terms the fluorescence mechanisms exploited in their design.

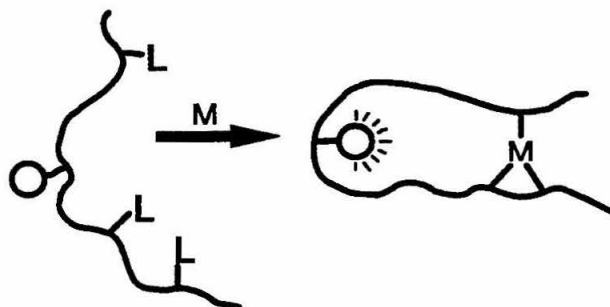
### *Microenvironment sensitive fluorescence: sensors for Zn(II).*

Highly sensitive and selective chemosensors for divalent zinc, based on the zinc finger domains, are presented in Chapter 2. These entities short (25-30 residue) protein domains that bind Zn(II) avidly, and with great selectivity.<sup>88-90</sup> Furthermore, zinc finger peptides have been shown to undergo reversible metal-induced folding, which assists in the packing of a central core of hydrophobic residues.<sup>91,92</sup> To include an optical element for reporting the metal binding event, fluorophores that exhibit solvent polarity-dependent fluorescence were incorporated in the place of residues known to participate in the composition of the hydrophobic core. This mechanism for signal transduction is shown schematically in Figure 1-4.

### *Chelation-enhanced fluorescence: sensors for Zn(II).*

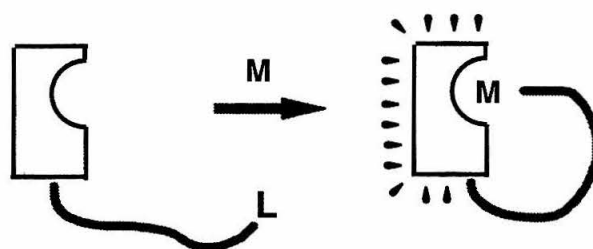
Other peptidyl fluorosensors for Zn(II), employing a different mechanism for signal transduction (Figure 1-5) are presented in Chapter 3. In contrast to the sensors patterned after the zinc-finger domains, these sensors were based upon the synthesis and peptide-incorporation of nonstandard  $\alpha$ -amino acids that contain the core metal-binding functionality of oxine (8-hydroxyquinoline). Oxine is a well known, bidentate, fluorochromic indicator for a number of species,<sup>93,94</sup> but that is insufficiently selective

for determining Zn(II) concentrations in complex mixtures of metal cations.<sup>32</sup> By incorporating this compact, self-contained fluorescence-modulated ligand within an amino acid derivative, and by the judicious provision of ancillary metal-binding ligands, selective chemosensors for Zn(II) containing only 7 residues have been prepared.



Metal coordination triggers a change in the fluorophore environment and an increase in the fluorescence signal.

**Figure 1-4.** The “microenvironment sensitive fluorescence” mechanism used in the chemosensors for Zn(II) presented in Chapter 2.

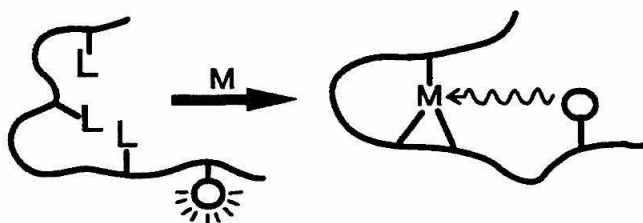


Metal coordination occurs with direct involvement of functionality from the fluorophore itself, resulting in enhanced emission.

**Figure 1-5.** The “chelation-enhanced fluorescence” mechanism used in the chemosensors for Zn(II) presented in Chapter 3.

*Fluorescence quenching: sensors for Cu(II).*

Chapter 4 presents fluorescent chemosensors for Cu(II) that employ yet another mechanism for fluorescence modulation. In order to attain highly avid and selective divalent copper binding, sensors were prepared using the three-residue consensus sequence of the amino terminal Cu(II)- and Ni(II)-binding (ATCUN) domains.<sup>95,96</sup> Due to the redox-active, paramagnetic, and therefore inherently quenching properties of the Cu(II) ion,<sup>97</sup> fluorophores were intentionally incorporated in proximity to the metal-binding site in order to report the occupancy of the sensor by that ion by a decrease in fluorescence (Figure 1-6). In addition, studies regarding the conversion of these soluble reagents to renewable solid-phase devices are discussed.



Metal coordination brings the fluorophore into proximity with the metal causing a decrease in fluorescence signal.

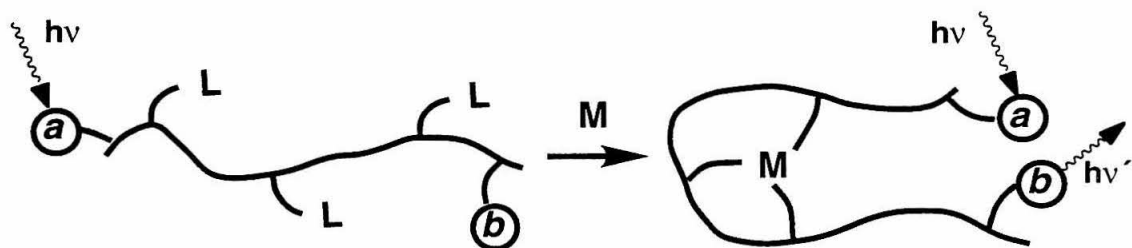
**Figure 1-6.** The fluorescence quenching mechanism used in the chemosensors for Cu(II) presented in Chapter 4.

*Fluorescence resonance energy transfer: sensors for Ni(II).*

Finally, the development of sensors for the Ni(II) ion are presented in Chapter 5. These devices have, like the sensors for Cu(II), relied on modifications to the ATCUN motif for cation binding. However, these chemosensors have been prepared by means of the attachment of two fluorophores, with optical output provided by the quantum-mechanical effect of fluorescence resonance energy transfer (FRET),<sup>98,99</sup> as illustrated in Figure 1-7. This technique has historically been used as a sensitive probe of intermolecular distances.<sup>100-104</sup> However, it is also well suited for sensor design, when

analyte-induced changes in interfluorophore distances can be engineered.<sup>105,106</sup>

Furthermore, FRET-based measurements have the advantages of accommodating long-wavelength fluorophores and enabling ratiometric measurements (which provides a control for variable instrument response).<sup>14,15</sup>



Metal binding causes a change in the distance between two fluorophores, *a* and *b*, resulting in enhanced energy transfer to, and thus greater emission from, the longer-wavelength fluorophore *b*.

**Figure 1-7.** The FRET-based mechanism of fluorescence modulation used in the chemosensors for Ni(II) presented in Chapter 5.

In summary, fluorescent chemosensors have been prepared that enable selective measurement of sub-micromolar levels of Zn(II), Cu(II), and Ni(II). Furthermore, the peptidyl architecture that underlies the construction of these devices is well-suited to performing analyses on biological or environmental samples; in contrast to many of the previously reported chemosensors which have been devised for the measurement of these species, all of the molecular devices reported in this dissertation are compatible with entirely aqueous solution, bind their analyte of interest reversibly, and tolerate high ionic strengths ( $\geq 0.15$  M NaCl). For each divalent metal cation addressed within this research, a sensor has been prepared that is *a priori* compatible with immobilization on a solid support, allowing for the eventual production of regenerable devices for real-time measurement of divalent metal cations. Furthermore, the strengths of the approaches taken for chemosensor design have not been exhausted; there is scope for continuous

refinement and improvement of these systems, as well as for addressing the measurement of other metal cations.

## References

1. "The Biological Chemistry of the Elements: The Inorganic Chemistry of Life," Fraústo da Silva, J. J. R.; Willams, R. J. P.; Clarendon Press: New York, 1993.
2. "Bioinorganic Chemistry," Bertini, I.; Gray, H. B.; Lippard, S. J.; Valentine, J. S.; University Science Books: Sausalito, 1994.
3. "Metal Ions in Biological Systems: Concepts on Metal Ion Toxicity," Sigel, H.; Marcel Dekker: New York, 1986.
4. "Biochemistry," Matthews, C. K.; van Holde, K. E.; Benjamin/Cummings: New York, 1990.
5. "Zinc Metabolism," Prasad, A. S.; Thomas: Springfield, Ill., 1966.
6. "Biological Trace Element Research— Multidisciplinary Perspectives," Subramanian, K. S.; Iyengar, G. V.; Okamoto, K.; ACS: Washington D. C., 1991.
7. "Principles of Instrumental Analysis," Skoog, D. A.; Leary, J. J.; Saunders College: Fort Worth, 1992.
8. "Trace Elements in Natural Waters," Salbu, B.; Steinnes, E.; CRC: Boca Raton, 1995.
9. "Determination of Transition Metals in Serum and Whole Blood by Ion Chromatography," Dionex Corp., Application note 108, **1996**.
10. "The Analysis of Biological and Clinical Materials," Delves, H. T. *Prog. Analyt. Atom. Spectrosc.* **1981**, 4, 1-48.
11. "Quantitation of Zinc in Nitric Acid-Digested Plasma by Atomic Absorption Spectrophotometry," Passey, R. B.; Maluf, K. C.; Fuller, R. *Anal. Biochem.* **1985**, 151, 462-465.
12. "Desperately Seeking Sensors," Czarnik, A. W. *Chem. Bio.* **1995**, 2, 423-428.
13. "Bioanalytical Applications of Fluorescence Spectroscopy," Bright, F. V. *Anal. Chem.* **1988**, 60, 1031A-1039A.

14. "Fluorescent Probes in Cellular and Molecular Biology," Slavik, J.; CRC Press: Boca Raton, 1994.
15. "Fluorescent and Photochemical Probes of Dynamic Biochemical Signals inside Living Cells," In *Fluorescent Chemosensors for Ion and Molecule Recognition*; Tsien, R. Y.; Czarnik, A. W.; ACS, Washington D.C., 1993; pp 130-146.
16. "Supramolecular Chemistry, Fluorescence, and Sensing," In *Fluorescent Chemosensors for Ion and Molecule Recognition*; Czarnik, A. W.; Czarnik, A. W.; ACS, Washington D.C., 1993; pp 1-9.
17. "Chemical Communication in Water Using Fluorescent Chemosensors," Czarnik, A. W. *Acc. Chem. Res.* **1994**, *27*, 302-308.
18. "Molecular Fluorescent Signalling with 'Fluor-Spacer-Receptor' Systems: Approaches to Sensing and Switching Devices via Supramolecular Photophysics," Bissell, R. A.; de Silva, A. P.; Gunaratne, H. Q. N.; Lynch, P. L. M.; Maguire, G. E. M., et al. *Chem. Soc. Rev.* **1992**, 187-195.
19. "Signaling Recognition Events with Fluorescent Sensors and Switches," de Silva, A. P.; Gunaratne, H. Q. N.; Gunnlaugsson, T.; Huxley, A. J. M.; McCoy, C. P., et al. *Chem. Rev.* **1997**, *97*, 1515-1566.
20. "Sensors and Switches from Supramolecular Chemistry," Fabbrizzi, L.; Poggi, A. *Chem. Soc. Rev.* **1995**, 197-202.
21. "Fluorescent Indicators for Cytosolic Sodium," Minta, A.; Tsien, R. Y. *J. Biol. Chem.* **1989**, *264*, 19449-19457.
22. "A Fluorescent Indicator for Measuring Cytosolic Free Magnesium," Raju, B.; Murphy, E.; Levy, L. A.; Hall, R. D.; London, R. E. *Am. J. Physiol.* **1989**, *256*, C540-C548.
23. "New Calcium Indicators and Buffers with High Selectivity against Magnesium and Protons: Design, Synthesis, and Properties of Prototype Structures," Tsien, R. Y. *Biochemistry* **1980**, *19*, 2396-2404.

24. "A New Generation of Ca<sup>2+</sup> Indicators with Greatly Improved Fluorescence Properties," Grynkiewicz, G.; Poenie, M.; Tsien, R. Y. *J. Biol. Chem.* **1985**, *260*, 3440-3450.
25. "Fluorescent Indicators for Cytosolic Calcium Based on Rhodamine and Fluorescein Chromophores," Minta, A.; Kao, J. P. Y.; Tsien, R. Y. *J. Biol. Chem.* **1989**, *264*, 8171-8178.
26. "Membrane Chloride Transport Measured Using a Chloride-Sensitive Fluorescent Probe," Illsley, N. P.; Verkman, A. S. *Biochemistry* **1987**, *26*, 1215-1219.
27. "Application of a New pH-Sensitive Fluorophore (Carboxy-SNARF-1) for Intracellular pH Measurement in Small, Isolated Cells," Buckler, K. J.; Vaughan-Jones, R. D. *Pflüg. Arch. Eur. J. Phys.* **1990**, *417*, 234-239.
28. "Intracellular pH Measurement Using Single Excitation-Dual Emission Fluorescence Ratios," Bassnett, S.; Reinisch, L.; Beebe, D. C. *Am. J. Physiol.* **1990**, *258*, C171-C178.
29. "Intracellular Ionized Calcium," June, C. H.; Rabinovitch, P. S. *Meth. Cell Biol.* **1994**, *41*, 149-174.
30. "Handbook of Fluorescent Probes and Research Chemicals," Haugland, R. P.; Molecular Probes: 1996.
31. "Trace Elements in Sea Water," Bruland, K. W.; Rilet, J. P.; Chester, R.; Academic Press, London, 1975; pp 157-220.
32. "Enzyme-Based Fiber Optic Zinc Biosensor," Thompson, R. B. *Anal. Chem.* **1993**, *65*, 730-734.
33. "Structural Aspects of Metal Liganding to Functional Groups in Proteins," Glusker, J. P. *Adv. Prot. Chem.* **1991**, *42*, 1-76.
34. "Fluorescent Protein Biosensors: Measurement of Molecular Dynamics in Living Cells," Giuliano, K. A.; Post, P. L.; Hahn, K. M.; Taylor, D. L. *Ann. Rev. Biophys. Biomol. Struct.* **1995**, *24*, 405-434.

35. "Biosensors," Turner, A. P. F. *Curr. Opin. Struct. Biol.* **1994**, *5*, 49-53.
36. "Lifetime-Based Fluorescence Energy Transfer Biosensing of Zinc," Thompson, R. B.; Patchan, M. W. *Anal. Biochem.* **1995**, *227*, 123-128.
37. "Structure-Based Design of a Sulfonamide Probe for Fluorescence Anisotropy Detection of Zinc with a Carbonic Anhydrase-Based Biosensor," Elbaum, D.; Nair, S. K.; Patchan, M. W.; Thompson, R. B.; Christianson, D. W. *J. Am. Chem. Soc.* **1996**, *118*, 8381-8387.
38. "A Luminescence-Based Mercury Biosensor," Virta, M.; Lampinen, J.; Karp, M. *Anal. Chem.* **1995**, *67*, 667-669.
39. "Fiber Optic Biosensor for Co(II) and Cu(II) Based on Fluorescence Energy Transfer with an Enzyme Transducer," Thompson, R. B.; Ge, Z.; Patchan, M.; Huang, C.-C.; Fierke, C. A. *Biosensors & Bioelectronics* **1996**, *11*, 557-564.
40. "Structure-Assisted Redesign of a Protein-Zinc-Binding Site with Femtomolar Affinity," Ippolito, J. A.; Baird, T. T. J.; McGee, S. A.; Christianson, D. W.; Fierke, C. A. *Proc. Natl. Acad. Sci. U.S.A.* **1995**, *92*, 5017-5021.
41. "The Stability of Transition-Metal Complexes," Irving, H.; Williams, R. J. P. *J. Chem. Soc.* **1953**, 3192-3210.
42. "Advanced Inorganic Chemistry," Cotton, F. A.; Wilkinson, G.; Wiley: New York, 1988.
43. "An Anthracene-Based Fluorescent Sensor for Transition Metal Ions," Fabbrizzi, L.; Licchelli, M.; Pallavicini, P.; Perotti, A.; Sacchi, D. *Angew. Chem. Int. Ed. Engl.* **1994**, *33*, 1975-1977.
44. "Fluorescent Sensors for Transition Metals Based on Electron-Transfer and Energy-Transfer Mechanisms," Fabbrizzi, L.; Licchelli, M.; Pallavicini, P.; Perotti, A.; Taglietti, A., et al. *Chemistry a European Journal* **1996**, *2*, 75-82.
45. "A Fluorescent Chemosensor for the Copper(II) Ion," De Santis, G.; Fabbrizzi, L.; Licchelli, M.; Mangano, C.; Sacchi, D., et al. *Inorg. Chem. Acta* **1997**, *257*, 69-76.

46. "A Long-Wavelength Fluorescent Chemodosimeter Selective for Cu(II) Ion in Water," Dujols, V.; Ford, F.; Czarnik, A. W. *J. Am. Chem. Soc.* **1997**, *119*, 7386-7387.
47. "A Fluorescent Chemosensor Signalling Only Hg(II) and Cu(II) in Water," Yoon, J.; Ohler, N. E.; Vance, D. H.; Aumiller, W. D.; Czarnik, A. W. *Tetrahedron Lett.* **1997**, *38*, 3845-3848.
48. "Metal-Induced Dispersion of Lipid Aggregates: A Simple, Selective, and Sensitive Fluorescent Metal Ion Sensor," Sasaki, D. Y.; Shnek, D. R.; Pack, D. W.; Arnold, F. H. *Angew. Chem. Int. Ed. Engl.* **1995**, *34*, 905-907.
49. "Fluorescent PET (Photoinduced Electron Transfer) Sensors," Bissell, R. A.; de Silva, A. P.; Gunaratne, H. Q. N.; Lynch, P. L. M.; Maguire, G. E. M., et al. *T. Curr. Chem.* **1993**, *168*, 223-264.
50. "Luminescence and Charge Transfer. Part 2. Aminomethyl Anthracene Derivatives as Fluorescent PET (Photoinduced Electron Transfer) Sensors for Protons," Bissell, R. A.; Calle, E.; de Silva, A. P.; de Silva, S. A.; Gunaratne, H. Q. N., et al. *J. Chem. Soc., Perkin Trans. II* **1992**, 1559-1564.
51. "Luminescence and Charge Transfer. Part 3. The Use of Chromophores with ICT (Internal Charge Transfer) Excited States in the Construction of Fluorescent PET (Photoinduced Electron Transfer) pH Sensors and Related Absorption pH Sensors with Aminoalkyl Side Chains," de Silva, A. P.; Gunarantne, H. Q. N.; Lynch, P. L. M.; Patty, A. J.; Spence, G. L. *J. Chem. Soc., Perkin Trans. II* **1993**, 1611-1616.
52. "Luminescence and Charge Transfer. Part 4. 'On-off' Fluorescent PET (Photoinduced Electron Transfer) Sensors with Pyridine Receptors: 1,3-Diaryl-5-pyridyl-4,5-dihydropyrazoles," de Silva, A. P.; Gunaratne, H. Q. N.; Lynch, P. L. M. *J. Chem. Soc., Perkin Trans. II* **1995**, 685-690.
53. "Microbial Iron Transport," Guerinot, M. L. *Annu. Rev. Microbiol.* **1994**, *48*, 743-772.

54. "Coordination Chemistry of Siderophores - Thermodynamics and Kinetics of Iron Chelation and Release," Albrechtgary, A. M.; Crumbliss, A. L. **1998**, *35*, 239-327.
55. "Complexation of Iron by Siderophores - A Review of Their Solution and Structural Chemistry and Biological Function," Raymond, K. N.; Muller, G.; Matzanke, B. F. *T. Curr. Chem.* **1984**, *123*, 49-102.
56. "Marine Metabolites and Metal Ion Chelation: The Facts and the Fantasies," Michael, J. P.; Pattenden, G. *Angew. Chem. Int. Ed. Engl.* **1993**, *32*, 1-23.
57. "Metalloprotein Design," Hellinga, H. W. *Curr. Opin. Biotechnology* **1996**, *7*, 437-441.
58. "Interfacial Metal-Binding Site Design," Matthews, D. J. *Curr. Opin. Biotechnology* **1995**, *6*, 419-424.
59. "The Design of Metal-Binding Sites in Proteins," Regan, L. *Ann. Rev. Biophys. Biomol. Struct.* **1993**, *22*, 257-281.
60. "Metalloprotein Design," Berg, J. M. *Curr. Opin. Struct. Biol.* **1993**, *3*, 585-588.
61. "Engineering Metal-Binding Sites in Proteins," Lu, Y.; Valentine, J. S. *Curr. Opin. Struct. Biol.* **1997**, *7*, 495-500.
62. "Redesign of a Type-2 into a Type-1 Copper Protein - Construction and Characterization of Yeast Copper-Zinc Superoxide-Dismutase Mutants," Lu, Y.; Gralla, E. B.; Roe, J. A.; Valentine, J. S. *J. Am. Chem. Soc.* **1992**, *114*, 3560-3562.
63. "Construction of a Blue Copper Site at the Native Zinc Site of Yeast Copper-Zinc Superoxide-Dismutase," Lu, Y.; Lacroix, L. B.; Lowery, M. D.; Solomon, E. I.; Bender, C. J., et al. *J. Am. Chem. Soc.* **1993**, *115*, 5907-5918.
64. "New Type-2 Copper-Cysteinate Proteins - Copper Site Histidine-to-Cysteine Mutants of Yeast Copper-Zinc Superoxide-Dismutase," Lu, Y.; Roe, J. A.; Bender, C. J.; Peisach, J.; Banci, L., et al. *Inorg. Chem.* **1996**, *35*, 1692-1700.
65. "Histidine-Carboxamide Ligand Substitutions in the Zinc-Binding Site of Carbonic Anhydrase-II Alter Metal Coordination Geometry but Retain Catalytic Activity,"

- Lesburg, C. A.; Huang, C. C.; Christianson, D. W. *Biochemistry* **1997**, *36*, 15780-15791.
66. "Carbonic-Anhydrase - Evolution of the Zinc-Binding Site by Nature and by Design," Christianson, D. W.; Fierke, C. A. *Acc. Chem. Res.* **1996**, *29*, 331-339.
67. "Characterization of Metal Binding by a Designed Protein: Single Ligand Substitutions at a Tetrahedral Cys<sub>2</sub>His<sub>2</sub> Site," Klemba, M.; Regan, L. *Biochemistry* **1995**, *34*, 10094-10100.
68. "Novel Metal-Binding Proteins by Design," Klemba, M.; Dardner, K. H.; Marino, S.; Clarke, N. D.; Regan, L. *Nature Struct. Biol.* **1995**, *2*, 368-373.
69. "A Tetrahedral Zinc(II)-Binding Site Introduced into a Designed Protein," Regan, L.; Clarke, N. D. *Biochemistry* **1990**, *29*, 10878-10883.
70. "De Novo Design of a Zn<sup>2+</sup>-Binding Protein," Handel, T.; DeGrado, W. F. *J. Am. Chem. Soc.* **1990**, *112*, 6710-6711.
71. "De Novo Design of Mercury-Binding Two- and Three-Helical Bundles," Diekmann, G. R.; McRorie, D. K.; Tierney, D. L.; Utschig, L. M.; Singer, C. P., et al. *J. Am. Chem. Soc.* **1997**, *119*, 6195-6196.
72. "Metal Ion Enhanced Helicity in Synthetic Peptides Containing Unnatural, Metal-Ligating Residues," Ruan, F.; Chen, Y.; Hopkins, P. B. *J. Am. Chem. Soc.* **1990**, *112*, 9403-9404.
73. "Synthesis of Peptides Containing Unnatural, Metal-Ligating Residues: Aminodiacetic Acid as a Peptide Side Chain," Ruan, F.; Chen, Y.; Itoh, K.; Sasaki, T.; Hopkins, P. B. *J. Org. Chem.* **1991**, *56*, 4347-4354.
74. "Efficient Synthesis of Metal Binding Peptides Incorporating Aminodiacetic Acid Based Ligands," Kazmierski, W. M. *Int. J. Pep. Protein Res.* **1995**, *45*, 241-247.
75. "Metal Chelating Amino Acids in the Design of Peptides and Proteins. Synthesis of N<sup>α</sup>-Fmoc/Bu<sup>t</sup> Protected Amino Acids Incorporating Aminodiacetic Acid Moiety," Kazmierski, W. M. *Tetrahedron Lett.* **1993**, *34*, 4493-4496.

76. "Synthesis of a Metal-Ligating Amino Acid Suitable for Solid Phase Assembly of Peptides," Rana, T. M.; Ban, M.; Hearst, J. E. *Tetrahedron Lett.* **1992**, 33, 4521-4524.
77. "Versatile Building Block for the Synthesis of Phosphine-Containing Peptides: The Sulfide of Diphenylphosphinoserine," Gilbertson, S. R.; Chen, G.; McLoughlin, M. J. *Am. Chem. Soc.* **1994**, 116, 4481-4482.
78. "Synthesis of Thiophosphoryl Derivatives of Proline: Building Blocks for Phosphanyl-Substituted Peptides with  $\beta$ -Turns," Gilbertson, S. R.; Pawlick, R. V. *Angew. Chem. Int. Ed. Engl.* **1996**, 35, 902-904.
79. "Iron(II) Organizes a Synthetic Peptide into Three-Helix Bundles," Lieberman, M.; Sasaki, T. *J. Am. Chem. Soc.* **1991**, 113, 1470-1471.
80. "Peptide Architecture: Design of Stable  $\alpha$ -Helical Metallopeptides via a Novel Exchange-Inert Ru<sup>III</sup> Complex," Ghadiri, M. R.; Fernholz, A. K. *J. Am. Chem. Soc.* **1990**, 112, 9633-9635.
81. "A Convergent Approach to Protein Design. Metal Ion-Assisted Spontaneous Self-Assembly of a Polypeptide into a Triple-Helix Bundle Protein," Ghadiri, M. R.; Soares, C.; Choi, C. *J. Am. Chem. Soc.* **1992**, 114, 825-831.
82. Indeed, the residues shown in Figure 1-2 which allow the introduction of the complete IDA or EDTA moieties within peptides should be expected to display the same metal-binding preferences as the parent ligands. In this regard there has been no attempt at obtaining selective metal binding with these residues.
83. "(S)- $\alpha$ -Amino(2,2'-bipyridine)-6-Propanoic Acid: A Versatile Amino Acid for *de novo* Metalloprotein Design," Imperiali, B.; Fisher, S. L. *J. Am. Chem. Soc.* **1991**, 113, 8527.
84. "Stereoselective Synthesis and Peptide Incorporation of (S)- $\alpha$ -Amino-(2,2'-bipyridine)-6-Propanoic Acid," Imperiali, B.; Fisher, S. L. *J. Org. Chem.* **1992**, 57, 757.

85. "Chemoenzymatic Synthesis of 2-Amino-3-(2,2'-bipyridinyl)propanoic Acids," Imperiali, B.; Prins, T. J.; Fisher, S. L. *J. Org. Chem.* **1993**, *58*, 1613-1616.
86. "Metallopeptide Design: Tuning the Metal Cation Affinities with Unnatural Amino Acids and Peptide Secondary Structure," Cheng, R. P.; Fisher, S. L.; Imperiali, B. *J. Am. Chem. Soc.* **1996**, *118*, 11349-11356.
87. "New Synthetic Amino Acids for the Design and Synthesis of Peptide-Based Metal Ion Sensors," Torrado, A.; Imperiali, B. *J. Org. Chem.* **1996**, *61*, 8940-8948.
88. "Complexes of Zinc Finger Peptides with Ni<sup>2+</sup> and Fe<sup>2+</sup>," Krizek, B. A.; Berg, J. M. *Inorg. Chem.* **1992**, *31*, 2984-2986.
89. "Ligand Variation and Metal Ion Binding Specificity in Zinc Finger Peptides," Krizek, B. A.; Merkle, D. L.; Berg, J. M. *Inorg. Chem.* **1993**, *32*, 937-940.
90. "On the Metal Ion Specificity of 'Zinc Finger' Proteins," Berg, J. M.; Merkle, D. L. *J. Am. Chem. Soc.* **1989**, *111*, 3759-3761.
91. "Time-Resolved Energy Transfer Measurements of Donor-Acceptor Distance Distributions and Intramolecular Flexibility of a CCHH Zinc Finger Peptide," Eis, P. S.; Lakowicz, J. R. *Biochemistry* **1993**, *32*, 7981-7993.
92. "Metal-Dependent Folding of a Single Zinc Finger from Transcription Factor IIIA," Frankel, A. D.; Berg, J. M.; Pabo, C. O. *Proc. Natl. Acad. Sci. U.S.A.* **1987**, *84*, 4841-4845.
93. "Chapter 18: Spectrofluorimetry," In *Vogel's Textbook of Quantitative Chemical Analysis*; Vogel, A. I.; Wiley, New York, 1989; pp 731-740.
94. "Fluorescence Derivatization," Seitz, W. R. *CRC Crit. Rev. Anal. Chem.* **1980**, *8*, 367-405.
95. "Amino Terminal Cu(II)- and Ni(II)-Binding (ATCUN) Motif of Proteins and Peptides: Metal Binding, DNA Cleavage, and Other Properties," Harford, C.; Sarkar, B. *Acc. Chem. Res.* **1997**, *30*, 123-130.

96. "Intrinsic Stoichiometric Equilibrium Constants for the Binding of Zinc(II) and Copper(II) to the High Affinity Site of Serum Albumin," Masuoka, J.; Hegenauer, J.; Van Duke, B. R.; Saltman, P. *J. Biol. Chem.* **1993**, *268*, 21533-21537.
97. "Principles of Fluorescence Spectroscopy," Lakowicz, J. R.; Plenum Press: New York, 1983.
98. "Fluorescence Resonance Energy Transfer," Selvin, P. R. *Meth. Enzym.* **1995**, *246*, 300-334.
99. "Resonance Energy Transfer," Van Der Meer, B. W.; Coker, G. I.; Chen, S.-Y. S.; VCH: New York, 1994.
100. "Energy Transfer: A Spectroscopic Ruler," Stryer, L.; Haugland, R. P. *Proc. Natl. Acad. Sci. U.S.A.* **1967**, *38*, 719-725.
101. "Fluorescence Energy Transfer as a Spectroscopic Ruler," Stryer, L. *Ann. Rev. Biochem.* **1978**, *47*, 819-846.
102. "Metal Ions as Donors and Acceptors of Fluorescence," In *Methods for Determining Metal Ion Environments in Proteins*; Holmquist, B.; Darnall, W. D. Wilkins, R. G.; Elsevier, New York, 1980; pp 75-93.
103. "The Use of Singlet-Singlet Energy Transfer to Study Macromolecular Assemblies," Fairclough, R. H.; Cantor, C. R. *Meth. Enzym.* **1976**, *278*, 347-379.
104. "Intramolecular Transfer of Excitation from Tryptophan to 1-Dimethylaminonaphthalene-5-sulfonamide in a Series of Model Compounds," Conrad, R. H.; Brand, L. *Biochemistry* **1968**, *7*, 777-787.
105. "Ion Recognition Detected by Changes in Photoinduced Charge or Energy Transfer," In *Fluorescent Chemosensors for Ion and Molecule Recognition*; Valeur, B.; Bourson, J.; Pouget, J.; Czarnik, A. W.; ACS, Washington D.C., 1993; pp 25-44.
106. "Fluorescence Ratio Imaging of Cyclic AMP in Single Cells," Adams, S. R.; Harootunian, A. T.; Buechler, Y. J.; Taylor, S. S.; Tsien, R. Y. *Nature* **1991**, 694-697.

## Chapter 2. Fluorescent Chemosensors for Divalent Zinc Based on the Zinc Finger Domains

Reprinted in part with permission from "Design and Evaluation of a Peptidyl Fluorescent Chemosensor for Divalent Zinc," Walkup, G. K.; Imperiali, B. *J. Am. Chem. Soc.* **1996**, *118*, 3053-3054. Copyright 1996 American Chemical Society.

Reprinted in part with permission from "Fluorescent Chemosensors for Divalent Zinc Based on Zinc Finger Domains—Enhanced Oxidative Stability, Metal Binding Affinity, and Structural and Functional Characterization," Walkup, G. K.; Imperiali, B. *J. Am. Chem. Soc.* **1997**, *119*, 3443-3450. Copyright 1997 American Chemical Society.

## Introduction

Fluorescent indicators have revolutionized the process of quantifying metal cations in aqueous media, and in particular within biological samples. The success of fluorescent indicators for the intracellular measurement of sodium and potassium,<sup>1</sup> calcium,<sup>2,3</sup> magnesium,<sup>4</sup> and pH<sup>5,6</sup> is well known. Due to the success of these agents, the design and production of fluorescent chemosensors for other species continues to be an active area of interest.

The central problem in the production of new fluorescent sensors for the detection of metal cations lies in selectivity.<sup>7</sup> In fact, there are successful intracellular fluorescent probes only for the divalent cations Mg(II) and Ca(II), which are present at the highest concentration within the cell. For example, the concentration of ionized Zn(II) within a cell or in sea water is commonly 10<sup>6</sup>-fold lower than that of Mg(II) or Ca(II).<sup>8,9</sup> Thus, the fluorescent indicator fura-2 may bind Zn(II) with greater affinity than Ca(II), but it remains a *cellular* probe for free calcium. In order to prevent spurious cross-talk, the relative affinity of the sensor for the ion of interest must exceed the cumulative concentration excess imposed by all other competing species. Typically, this difficulty has been addressed by the exploitation of proteins for their unmatched selectivity in binding small molecules.<sup>10</sup> Thus biological signal transducers, i.e., “biosensors,” have been devised from existing proteins for the divalent cations of zinc,<sup>11,12</sup> mercury,<sup>13</sup> as well as copper and cobalt,<sup>14</sup> and even organic molecules such as cAMP.<sup>15</sup>

The need for new chemosensors for these and other analytes continues to exist.<sup>16</sup> Although the analyte binding selectivity which may be obtained with a biosensor is remarkable, the complexity of a large biomolecule can impose greater design constraints relative to an abiotic sensing molecule. For example, proteins typically lack the fluorescence characteristics of a useful sensor, and thus a strategy involving affinity labeling or an auxiliary diffusible fluorophore is required for signal transduction. In this light, the production of a purely synthetic chemosensor is desirable as there is greater

flexibility for systematic variation of the analyte-binding and fluorescent moieties of the sensor.

In order to marry the advantageous aspects of biosensors with those of more simple abiotic chemosensors, the remarkable metal-binding properties of the zinc finger domains<sup>17-19</sup> have been exploited. (The production of peptidyl motifs with tunable metal binding properties,<sup>20</sup> as well as those with novel fluorescent signaling capabilities,<sup>21</sup> highlight the applicability of this “hybrid approach” for the production of peptidyl chemosensors.)

Zinc finger peptides bind the Zn(II) ion avidly, with dissociation constants as low as 5.7 pM reported for a particular peptide-Zn(II) complex,<sup>22</sup> and with great selectivity as well.<sup>22,23</sup> A single zinc finger domain is 25-30 residues in length and may be described by the consensus sequence (F/Y)-X-C-X<sub>2-4</sub>-C-X<sub>3</sub>-F-X<sub>5</sub>-L-X<sub>2</sub>-H-X<sub>3-5</sub>-H-X<sub>2-6</sub>.<sup>19,24</sup> Importantly, peptides of these lengths are easily accessible *via* solid phase peptide synthesis techniques, enabling the rapid production of analogous molecules to be used for Zn(II) sensing. Furthermore, zinc fingers have been shown to undergo reversible metal-induced folding,<sup>18,25</sup> in which the Zn(II) ion nucleates a cluster of hydrophobic residues (underlined above). A schematic diagram depicting the structure of a representative zinc finger in the metal-bound state is illustrated in Figure 2-1, highlighting both the metal-ligating and hydrophobic core residues.

Naturally occurring zinc fingers lack a sufficiently sensitive optical handle that may be used to probe the occupancy of the metal-binding site. Because Zn(II) binding drives the folding of these domains, the presence of this ion is causative of changes in the microenvironment experienced by the residues that coalesce to form the hydrophobic cluster. The fluorescence emission of such a fluorophore-bearing residue can therefore serve as an optical reporter of the zinc binding event, as depicted in Scheme 2-1.

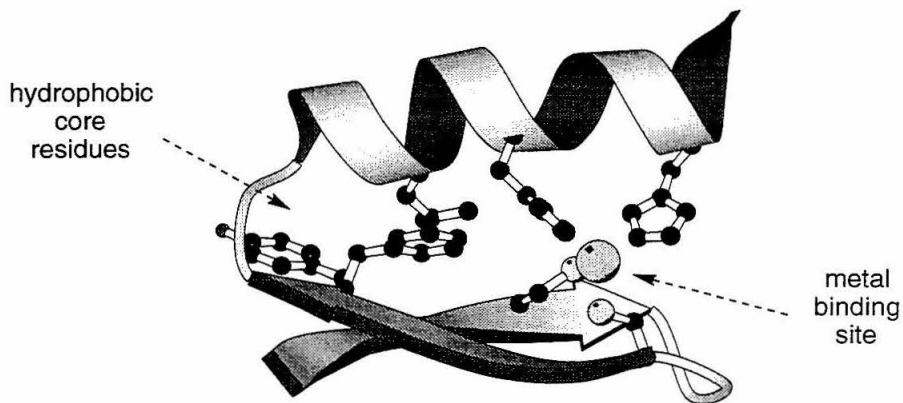
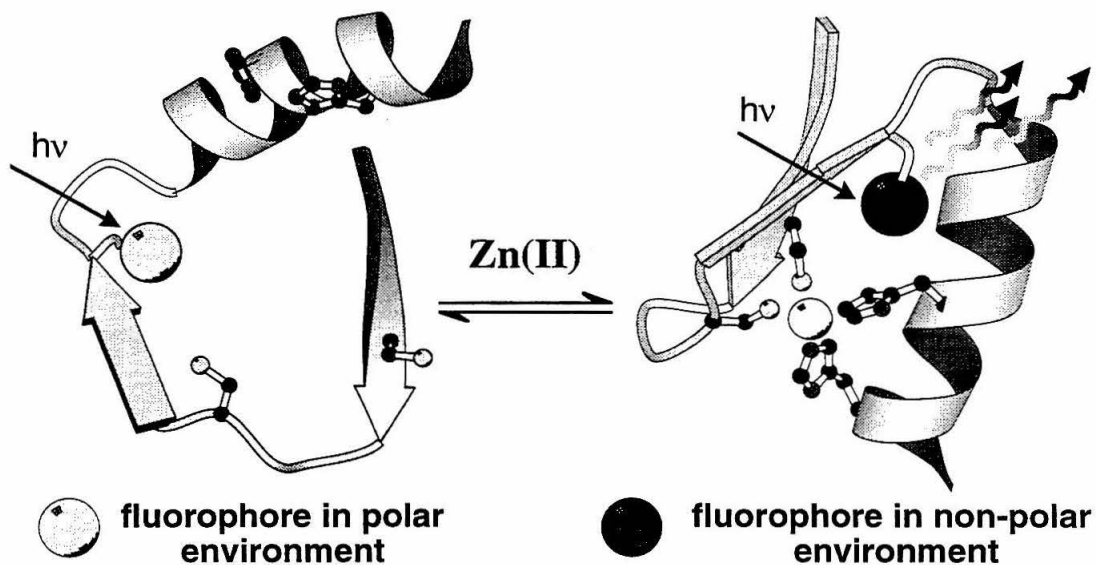


**Figure 2-1.** The structure of a typical zinc finger, highlighting the metal-ligating and hydrophobic core residues. (The coordinates of Xfin<sup>26</sup> were used to prepare this diagram, using the program Molscript.)<sup>27</sup>

**Scheme 2-1.** The mechanism of microenvironment sensitive fluorescence.



The design, synthesis, and characterization of a family of zinc finger peptides which incorporate residues containing fluorophores are described in the remainder of this chapter. Through an iterative process of design, many topics have been addressed in the studies of these fluorescent chemosensors. These include peptide folding; characterization, design and synthesis of the fluorophore moiety; reconstitution of the metal-binding ligation sphere to exhibit greater oxidative stability while preserving Zn(II) binding selectivity, as well as characterization of the zinc binding affinity of many of the peptides.

These studies have resulted in the production of highly sensitive and selective chemosensors for divalent zinc, capable of detecting nanomolar concentrations of Zn(II) in the presence of vast excesses of competing species. In addition, a chemosensor with enhanced oxidative stability relative to the native zinc finger domains has also been prepared and characterized.

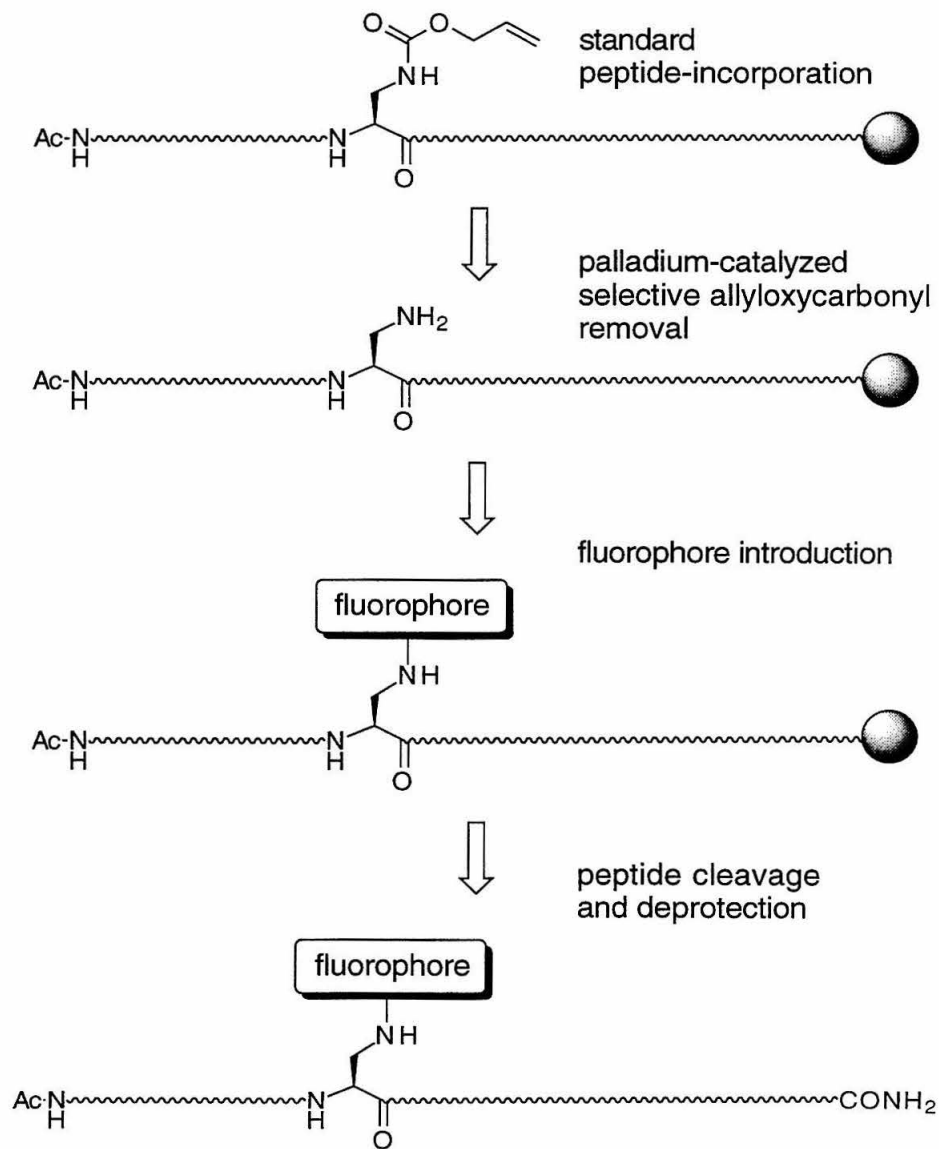
## **Results**

### **Modular fluorophore incorporation.**

A key feature in the synthesis of these peptides is the residue (*S*)-2,3-diamino-*N*<sup>α</sup>-9-fluorenylmethyloxycarbonyl-*N*<sup>β</sup>-allyloxycarbonyl propanoic acid (Fmoc-L-Dap(alloc)-OH).<sup>28</sup> This residue may be incorporated at any position within the polypeptide chain. At the completion of synthesis but prior to cleavage from the resin, the side chain of this residue may be selectively deprotected under mild conditions using a palladium catalyst.<sup>29</sup> The liberated amine is then available for coupling with a variety of fluorophores, as shown in Scheme 2-2. The modularity of peptide synthesis is preserved through this strategy for fluorophore introduction.

The sequences of the peptides discussed in this chapter are shown in Table 2-1. The amino acid sequence of each “fluorescent sensor” peptide has been denoted with the first four letters of its name (i.e., FS01, FS02, etc.), with the last three letters representing the fluorophore incorporated (see below). The standard 1-letter convention for naming

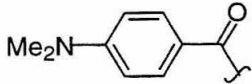
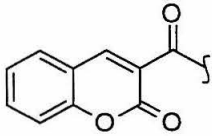
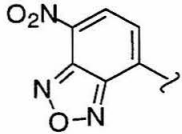
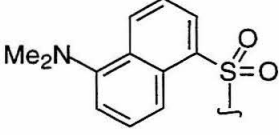
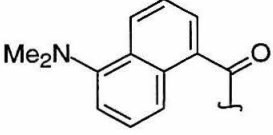
amino acids has been adopted with the addition of the nonstandard amino acid (*S*)-2,3-diaminopropanoic acid (L-Dap) which is represented by the letter B. The three letters in parentheses following this residue denote which chromophore is covalently attached to the side chain amine of this residue. The abbreviations used, and the structures they represent are: DMB = 4-*N,N'*-dimethylaminobenzoic acid, DNS = 5-*N,N'*-dimethylamino-naphthalene-1-sulfonamide (dansyl), CMN = coumarin-3-carboxamide, DNC = 1-*N,N'*-dimethylamino-naphthalene-5-carboxamide. A summary of some of the fluorescence properties of these molecules<sup>30</sup> are shown in Figure 2-2.

**Scheme 2-2.** Method for modular fluorophore introduction.

**Table 2-1.** Amino acid sequences of the synthetic zinc finger peptides.

peptide	sequence <sup>a</sup>
FS01DMB	Ac-B(DMB)ACDICGKNFSQSDELTTTHIRTHT-NH <sub>2</sub>
FS02CMN	Ac-B(CMN)ACDIHGKNFSQSDELTTTHIRTHT-NH <sub>2</sub>
FS02DNS	Ac-B(DNS)ACDIHGKNFSQSDELTTTHIRTHT-NH <sub>2</sub>
FS02NBD	Ac-B(NBD)ACDIHGKNFSQSDELTTTHIRTHT-NH <sub>2</sub>
FS03DNS	Ac-YQCQYCEKRB(DNS)ADSSNLKTHIKTKHS-NH <sub>2</sub>
FS04DNC	Ac-YQCQYDEKRB(DNC)ADSSNLKTHIKTKHS-NH <sub>2</sub>
FS04DNS	Ac-YQCQYDEKRB(DNS)ADSSNLKTHIKTKHS-NH <sub>2</sub>

<sup>a</sup>The standard 1-letter convention for naming amino acids has been followed. The residue "B" refers to (*S*)-(2,3)-diaminopropanoic acid, or *L*-β-amino alanine (Baa). The three letters in parentheses following this residue denote the covalently attached chromophore; DMB = 4-*N,N'*-dimethylaminobenzoic acid, DNS = 5-*N,N'*-dimethylamino-naphthalene-1-sulfonamide (dansyl), CMN = coumarin-3-carboxamide, DNC = 1-*N,N'*-dimethylamino-naphthalene-5-carboxamide.

		$\lambda_{\text{ex}}$ nm	$\lambda_{\text{em}}$ nm	Q
	<b>DMB</b>	<b>310</b>	<b>475 - 525</b>	<b>0 - 0.1</b>
	<b>CMN</b>	<b>315</b>	<b>400 - 450</b>	<b>0.05 - 0.3</b>
	<b>NBD</b>	<b>480</b>	<b>510 - 545</b>	<b>0.05-0.3</b>
	<b>DNS</b>	<b>340</b>	<b>500 - 550</b>	<b>0.05 - 0.5</b>
	<b>DNC</b>	<b>340</b>	<b>500 - 550</b>	<b>0.05 - &gt; 0.5</b>

**Figure 2-2.** The structures of some fluorophores incorporated within zinc finger peptides and their spectral properties. Q is the solvent-dependent quantum yield (values taken from the literature<sup>30</sup>).

### First-generation design: FS01DMB.

The initial design of a fluorescent zinc finger peptide was based upon the sequence and structural information available from a crystal structure of Zif268.<sup>31</sup> The microenvironment sensitive fluorophore 4-dimethylaminobenzamide (DMB) was chosen for its unique spectroscopic properties. Unlike most solvent sensitive fluorophores, which respond to increasingly nonpolar environments with greater fluorescence observed at shorter wavelengths, this molecule responds to decreasing microenvironment polarity with the production a significantly red-shifted emission.<sup>32-36</sup> Furthermore, a cyclodextrin-based chemosensor that exploits this property of DMB chromophore for polarity-dependent signaling in aqueous solution has been previously reported.<sup>37</sup> An

example of the fluorescence changes exhibited by the DMB chromophore as it is probed in water or acetonitrile are shown in Figure 2-3.

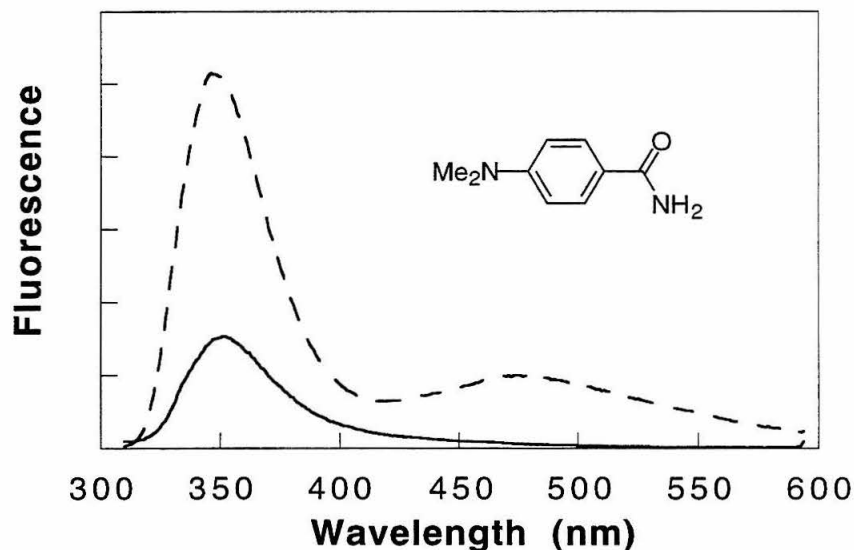


**Figure 2-3.** The solvent polarity-dependence fluorescence of a DMB model compound. Emission spectra were taken of 10  $\mu\text{M}$  solutions of the fluorophore in water (solid line, pH 7.0, 50 mM HEPES) and in acetonitrile (dashed line).

Unfortunately, fluorescence emission spectra of the peptide FS01DMB did not display any change upon the addition of divalent zinc. In order to probe whether metal-dependent structural changes could be observed, circular dichroism (CD) studies were undertaken. The CD spectra of FS01DMB at pH 7.0, alone, and in the presence of an excess of Zn(II) are shown in Figure 2-4. The structural changes which accompany zinc addition are similar to those seen for other zinc finger peptides.<sup>18,38,39</sup> Additionally, the Zn(II)-induced change in the CD spectra is pH dependent, with no structural change apparent at  $\text{pH} \leq 4$  (data not shown). Again, this is similar to the behavior of zinc finger peptides that have been characterized previously.<sup>40</sup>

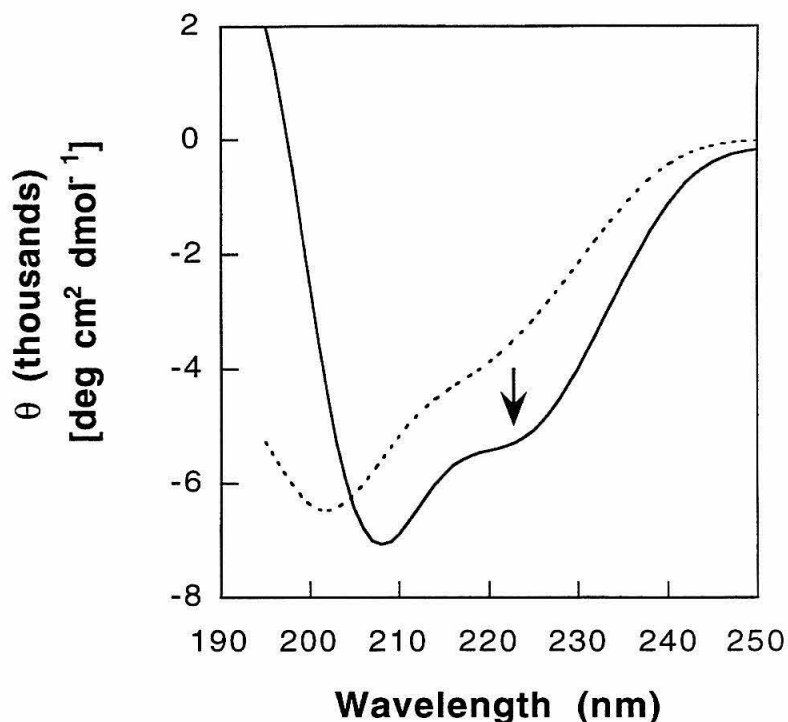


**Figure 2-4.** Circular dichroism spectra of a 12.9  $\mu$ M solution of FS01DMB in 0.5 mM HEPES, pH 7.0 in both the absence (dashed line) and presence (solid line) of 14  $\mu$ M divalent zinc.

The metal binding affinity of this peptide was probed by UV-vis spectroscopy to verify that the peptidyl template would bind Zn(II) with the avidity characteristic of the zinc finger domains and test whether the incorporation of the fluorescent probe significantly interferes with zinc binding. Because Zn(II) is a spectroscopically silent ion with an electronic configuration of  $d^{10}$ , the determination of the Zn(II) binding affinity of zinc fingers has commonly been determined through competition experiments with Co(II).<sup>17,41</sup> Within the tetrahedral  $S_2N_2$  coordination geometry of a zinc finger, a  $d-d$  transition of bound Co(II) is observed.<sup>42</sup> This technique was used to probe the Zn(II) binding properties of FS01DMB. The metal cation titration of FS01DMB was monitored by UV-vis spectroscopy as illustrated in Figure 2-5. The dissociation constant for both the Co(II) and Zn(II)-bound species were obtained from calculations using the absorption data obtained at 645 nm.

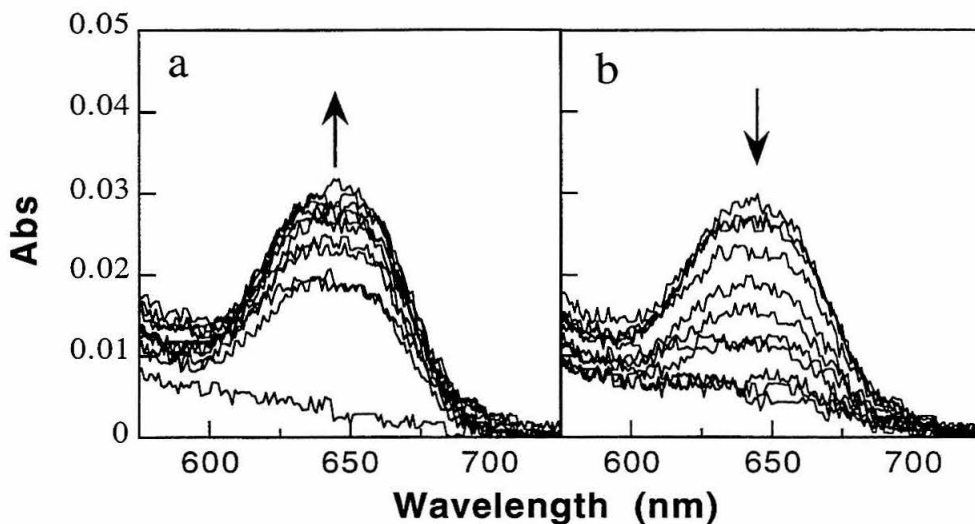


**Figure 2-5.** (a) Absorption spectra of 3.3  $\mu\text{M}$  FS01DMB (path length = 10 cm) upon addition of  $\text{CoCl}_2$  up to 100  $\mu\text{M}$  in 10 mM HEPES, pH 7.0. (b) Absorption spectra of the same upon the subsequent addition of  $\text{ZnCl}_2$  up to 8.5  $\mu\text{M}$ .

Mathematical treatment of the data was based on a simple two-state equilibrium described by the Scott equation.<sup>43</sup> Dissociation constants were obtained from an iterative calculation procedure in which successive approximations of  $[M^{2+}]_{free} / b\Delta A$  (ordinate) are plotted against  $[M^{2+}]_{free}$  (abscissa), where  $[M^{2+}]_{free}$  is the free divalent metal in solution,  $b$  is the path length of the cell, and  $\Delta A$  is the absorbance change observed. For initial calculations, only the higher metal concentrations were plotted in the assumption that  $[M^{2+}]_{total} \approx [M^{2+}]_{free}$ . By doing so,  $[M^{2+}]_{free}$  were estimated more accurately, and the procedure repeated until convergence occurred. From the final plot, the apparent dissociation constant is obtained from the y-intercept/slope. In the case of the Zn(II) titration, a relative dissociation constant was determined, which was multiplied by the Co(II) complex  $K_D$  to give the apparent peptide-Zn(II) complex  $K_D$ . Representative plots showing the final iteration of calculations for both Co(II) addition and Zn(II) competition are shown in Figure 2-6. The dissociation constants obtained were 2.8  $\mu\text{M}$  for the Co(II) complex and 7 pM for the Zn(II) complex.

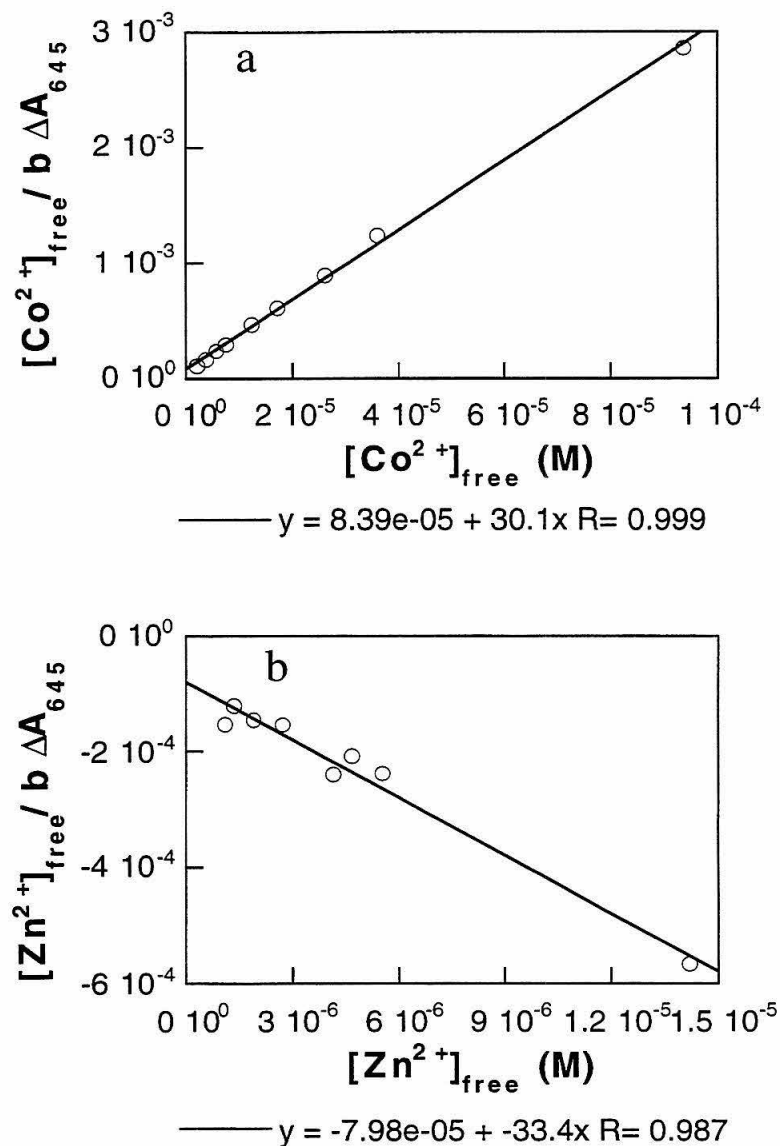


**Figure 2-6.** Analysis of the data obtained from Figure 2-5 where 3.3  $\mu\text{M}$  FS01DMB is titrated with  $\text{CoCl}_2$  up to 100  $\mu\text{M}$  followed by titration with  $\text{ZnCl}_2$  up to 8.5  $\mu\text{M}$ . The ratio of y-intercept/slope gives the apparent dissociation constant of (a) 2.8  $\mu\text{M}$  for the Co(II) complex, and (b) 7 pM for the Zn(II) complex.

**Second generation design: FS02CMN, FS02DNS, and FS02NBD.**

The environmental polarity dependence of long-wavelength emission for the DMB chromophore (and in particular the large change in quantum yield reported for model compounds of this type) stimulated the initial interest in this group as a fluorescent reporter. However, with the undesirable emission properties of FS01DMB, other fluorophores were investigated for the next generation peptide. Fluorophores were chosen to be small in size in order to be well accommodated within the hydrophobic cluster, yet with known polarity dependent emission properties. As a result, the fluorophores coumarin-3-carboxamide (CMN), 5-*N,N'*-dimethylamino-naphthalene-1-sulfonamide (dansyl, DNS), and 4-nitro-2-oxa-1,3-diazole (NBD) were chosen for incorporation within the FS02 template.

The other change made in the design of FS02 was to replace one of the two cysteines of the motif. Solutions of FS01 were particularly prone to intramolecular disulfide formation, even when great care was taken in handling them. Replacement of either Cys<sup>3</sup> or Cys<sup>6</sup> with a histidine residue to create a CysHis<sub>3</sub> motif would change the coordination sphere to one which could still bind metal cations, but remove the possibility of intramolecular disulfide formation.

Molecular modeling was performed to evaluate which of the two cysteine residues was structurally best suited to be replaced with a histidine residue, and that could preserve the tetrahedral coordination sphere of the parent structure. Consequently, both the "HCHH" and "CHHH" peptide structures (see Figure 2-7) were analyzed using, as starting coordinates, the coordinates from the Zif268 structure that was the basis for peptide FS01.

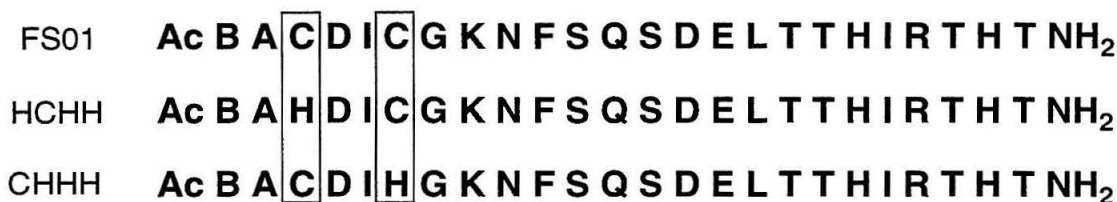


**Figure 2-7.** Peptide sequences modeled for residue replacement. The metal ligating residues considered for replacement are highlighted.

Modeling was performed using INSIGHT (v 2.3.0) and DISCOVER (v 2.9.5) using the CVFF force field (Biosym, San Diego). The starting structures used were the minimized FS01 peptide coordinates (based upon Zif268) with the appropriate cysteine residue replaced with histidine. As the composition of the coordination sphere was judged to be most important in these studies, all modeling was performed with NBD derivatized L-Dap incorporated as the fluorophore. Although metal ligation most commonly occurs through the  $\epsilon$  nitrogen atom in protein structures,<sup>44</sup> this is not exclusively the case and was not assumed for the purposes of modeling. Thus, two different minimizations were performed for each sequence, with the appropriate distance restraints applied to force either an  $N^\delta$  or  $N^\epsilon$  metal-histidine interaction (Figure 2-8). The C-terminal histidines were restrained with the native  $N^\epsilon$  coordination geometry intact.

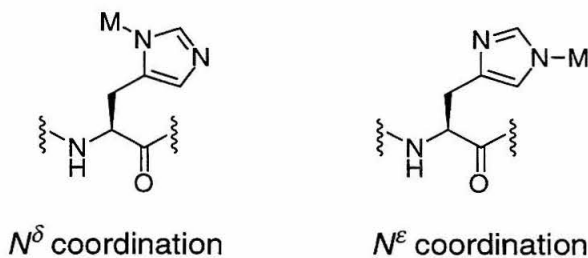


**Figure 2-8.** Metal coordination isomers of histidine.

It immediately became apparent that the  $N^\delta$  coordination isomers for both the CHHH and HCHH peptides was less well tolerated, causing catastrophic disruption of the zinc finger fold, and were not considered further. The final, minimized structures of the

$N^E$  isomers for both of the two peptides modeled are shown in Figure 2-9. Analysis shows that the CHHH peptide can more easily adopt a tetrahedral coordination geometry, and as a result of these studies, the CHHH motif was selected for development as the peptidyl template for FS02.

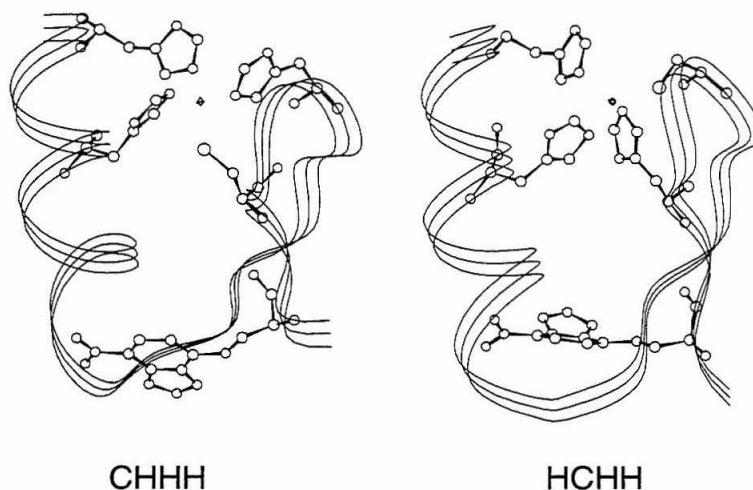


**Figure 2-9.** Minimized structures of CHHH and HCHH peptides, highlighting the metal-binding residues.

The peptide FS02 was prepared using standard Fmoc-based synthesis techniques, *via* the scheme for modular fluorophore introduction described above. While FS02DNS, and FS02CMN were successfully purified, the final peptide FS02NBD did not survive the cleavage reaction from the resin. Consequently, the effect of Zn(II) on the fluorescence emission of FS02DNS and FS02CMN was investigated. Whereas the dansylated peptide FS02DNS showed metal-induced fluorescence changes, FS02CMN did not. In light of these results, only FS02DNS was investigated further.

The fluorescence emission response of FS02DNS to Zn(II), Cu(II), and Co(II) ions was investigated. The effect of these ions upon FS02DNS was to slightly increase, weakly quench, and strongly quench fluorescence emission respectively. Representative

fluorescence emission spectra for each of these ions are shown in Figure 2-10. The change in signal observed with Zn(II) and Co(II) was readily reversible by the addition of EDTA. However, Cu(II) induced quenching of emission was not fully rescued by the addition of EDTA when present in *ca.* two-fold excess to added divalent copper.

To probe the nature of Cu(II) quenching FS02DNS fluorescence, further experiments were performed. Dansyl asparagine (DNS-Asn), and FS02DNS at similar concentrations were titrated with solutions of CuCl<sub>2</sub> and EDTA, and fluorescence emission spectra were acquired. The emission at 550 nm for each of these titrations are shown in Figure 2-11. Both fluorophores are quenched similarly by the addition of CuCl<sub>2</sub>. However, FS02DNS is quenched more efficiently, particularly for the first equivalent of Cu(II) added. All of the fluorescence of DNS-Asn was regained with the addition of stoichiometric EDTA, whereas only 70% of FS02-DNS emission was recovered with excess EDTA. These observations suggest that the Cu(II)·EDTA complex does not inherently quench the emission of the DNS fluorophore and that FS02DNS therefore binds Cu(II) strongly, being able to effectively compete with EDTA. Such tight binding of the Cu(II) ion is remarkable (at pH 7.0  $\log K_A \text{ EDTA} \cdot \text{Cu(II)} = 15.5$ ).<sup>45</sup>

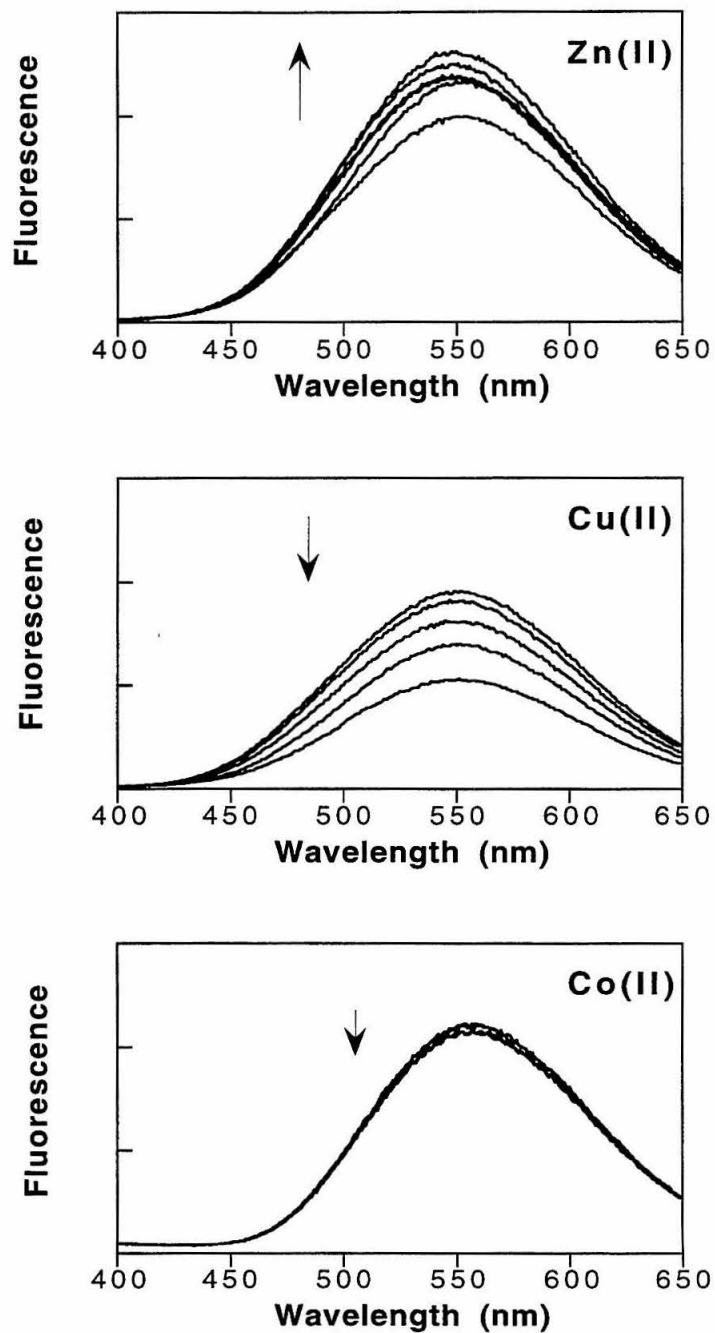


**Figure 2-10.** Fluorescence emission spectra FS02DNS (20  $\mu\text{M}$ ) in 50 mM HEPES, pH 7.0 with increasing amounts of added metal salt (in equivalents):  $\text{ZnCl}_2$  0, 0.2, 0.4, 0.6, 0.8, 1.0;  $\text{CuCl}_2$  0, 0.2, 0.4, 0.6, 0.8, 1.0;  $\text{CoCl}_2$  0, 1, 5, 10, 20. Excitation was performed at 333 nm.

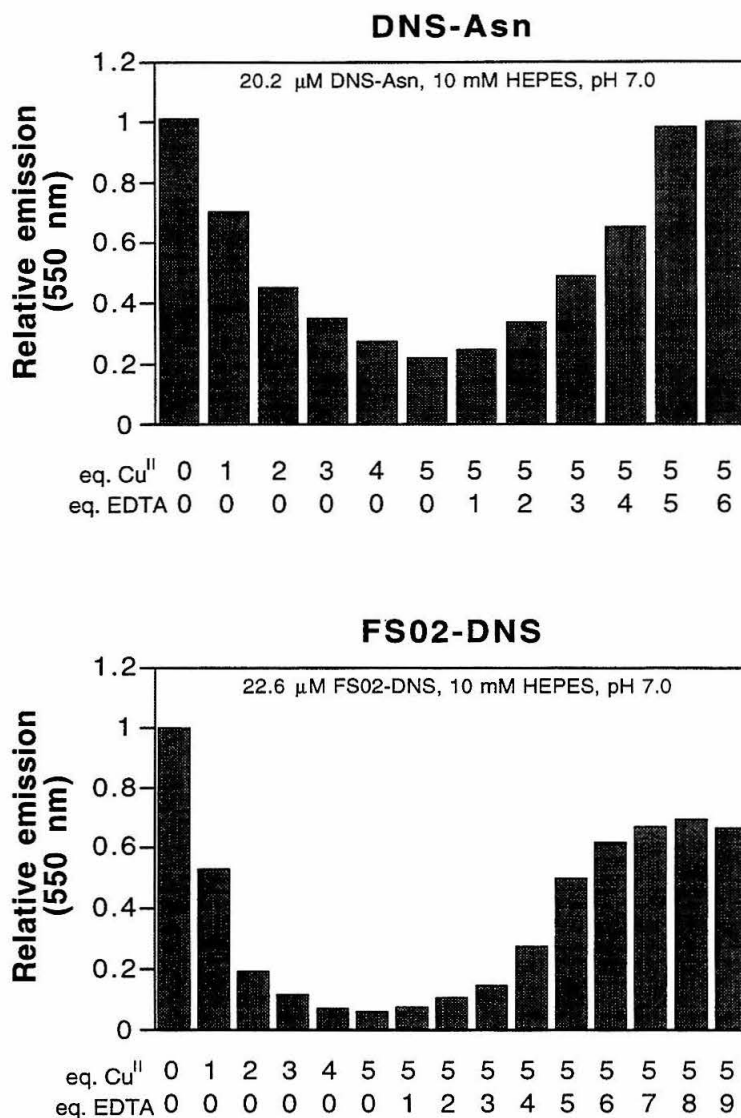


**Figure 2-11.** Fluorescence quenching of dansyl asparagine and FS02DNS by Cu(II) and the rescue of emission with EDTA.

To confirm that FS02DNS was binding these metals in the same manner as the native zinc fingers, and that 1:1 metal : peptide complexes were formed, UV-vis and circular dichroism experiments were performed. Absorption spectra of FS02DNS with Co(II) did not show significant absorbance in the region between 550 nm and 700 nm which is diagnostic for Co(II) in a tetrahedral coordination environment. (Co(II)

complexes with tetrahedral coordination geometry and at least one sulfur ligand show a *d-d* transition centered near 600 nm.)<sup>41</sup> However, titration with Cu(II) did produce a band at 550 nm ( $\epsilon \approx 133 \text{ M}^{-1} \text{ cm}^{-1}$ ) implying that copper is *probably* not bound with octahedral geometry but rather with 4- or 5-coordinate geometry (data not shown).<sup>46</sup>

Analysis of FS02DNS by circular dichroism revealed that the peptide is relatively structured in the absence of divalent metals, compared to other zinc finger peptides (Figure 2-12), and the addition of Zn(II) did not produce a spectrum similar to those reported for individual native zinc fingers domains.<sup>18,38,47</sup> In addition, neither Co(II) nor Cu(II) induced signs of secondary structure in this peptide (data not shown).

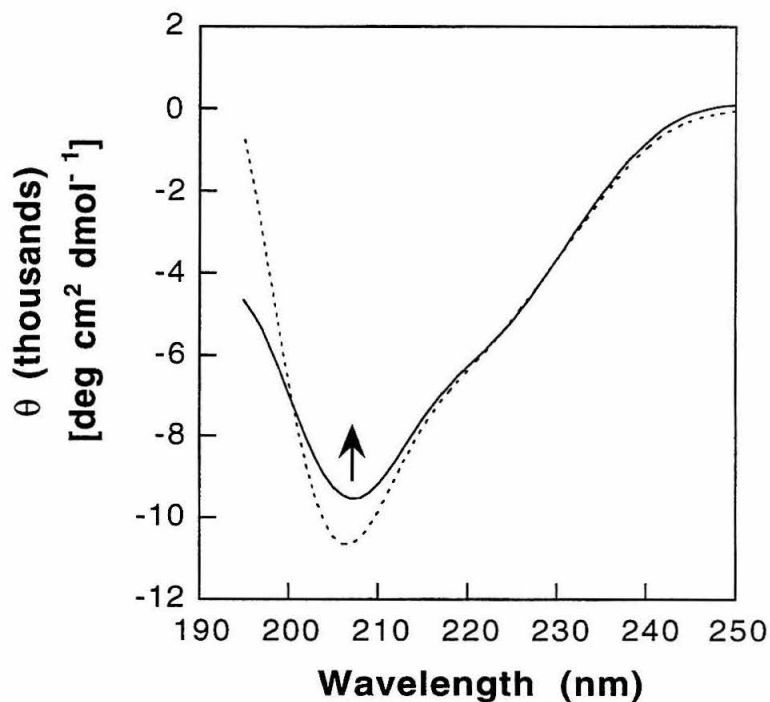


**Figure 2-12.** Circular dichroism spectra of 9.2  $\mu\text{M}$  FS02DNS upon the addition of  $\text{ZnCl}_2$ , in 0.5 mM HEPES, pH 7.0. Dashed line, no  $\text{ZnCl}_2$ ; solid line with 10.1  $\mu\text{M}$   $\text{ZnCl}_2$ .

Because FS02DNS titrations with Co(II) did not provide a spectroscopic handle which could be used to elucidate the affinity of this peptide for Zn(II), this information was determined by competition experiments with furaptra (mag-fura-2).<sup>4</sup> Mag-fura-2 forms a 1:1 complex with Zn(II), with a dissociation constant of 20 nM determined *via* fluorescence measurements.<sup>48</sup> However, large shifts in the UV-vis absorption spectrum are observed upon the addition of Zn(II) as well. Consequently, the competition was monitored by absorption spectroscopy, to avoid interference from the fluorescence of the peptide itself.

In the absence of divalent zinc, the absorbance maximum of mag-fura-2 occurs at 366 nm, with an extinction coefficient of  $29900 \text{ M}^{-1} \text{ cm}^{-1}$ . Bound to Zn(II), the absorbance maximum red-shifts to 325 nm, and the extinction coefficient at 366 nm lowers to  $1880 \text{ M}^{-1} \text{ cm}^{-1}$ . (Extinction coefficients for mag-fura-2 both in the presence and absence of Zn(II) had to be determined; for details see the experimental section at the end of this chapter.) A typical titration in which aliquots of  $\text{ZnCl}_2$  are added to a solution of FS02DNS and mag-fura-2, and the corresponding binding isotherm for the formation peptide·Zn(II) complex are shown in Figure 2-13. The dissociation constant calculated for the FS02DNS·Zn(II) complex was  $3.0 (\pm 0.5) \text{ nM}$ . (Further details concerning the calculation of the apparent dissociation constant of the FS02DNS·Zn(II) complex are presented in the experimental section.)

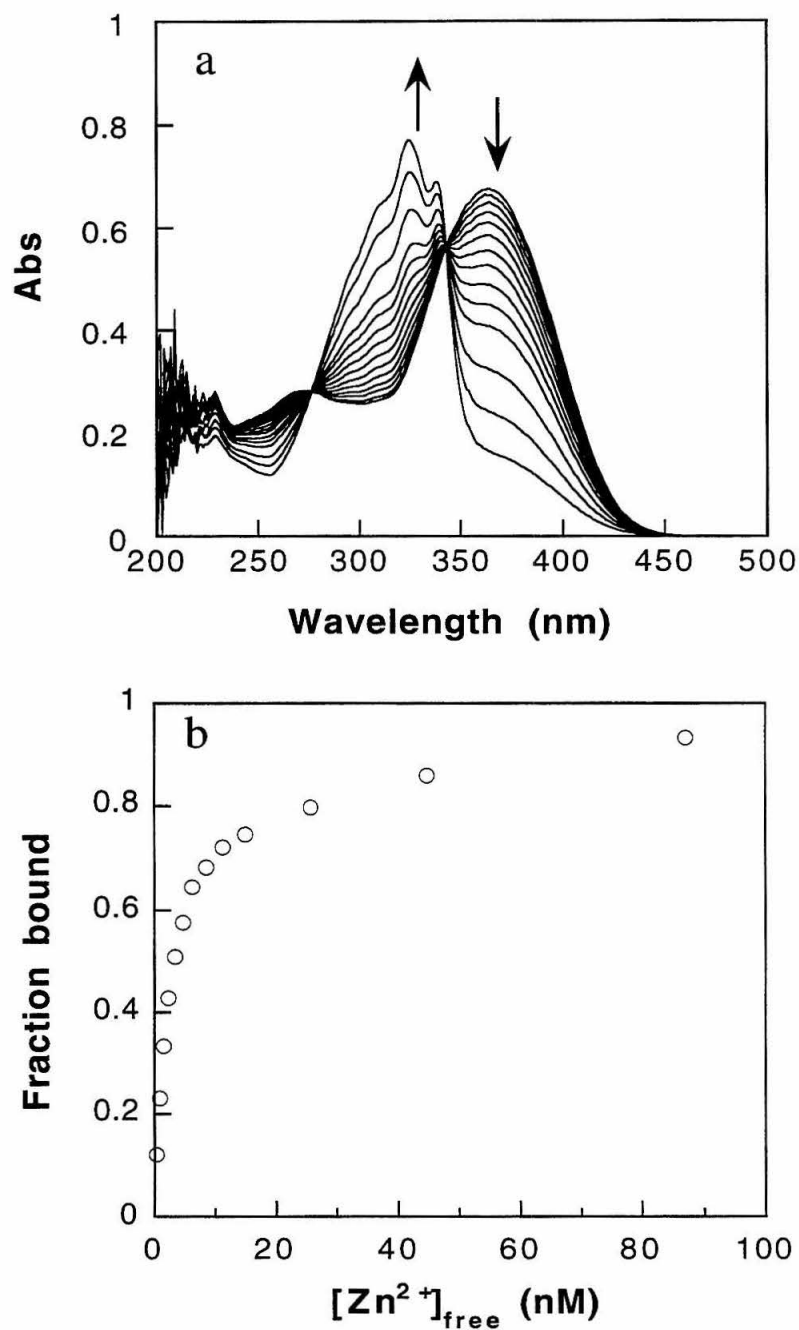


**Figure 2-13.** (a) Absorption spectra of 13.0  $\mu\text{M}$  FS02DNS and 22.6  $\mu\text{M}$  magfura-2 upon addition of  $\text{ZnCl}_2$  up to 32  $\mu\text{M}$  in 150 mM NaCl, 50 mM HEPES, pH 7.0. (b) The binding isotherm calculated from the data in tile a.

**Third generation design: FS03DNS.**

The results from the first two generations of fluorescent sensing peptides indicated that judicious placement of the fluorophore is required for the generation of a significant change in fluorescence upon metal binding. In the design of the next generation peptides (FS03), attempts to solve the difficulty of dithiol oxidation were temporarily foregone, and Cys<sub>2</sub>His<sub>2</sub> zinc fingers were once again investigated due to their proven ability to selectively bind divalent zinc. The positioning of the residue (from the hydrophobic cluster) to be replaced was reevaluated, as the position 1 replacements which were made in FS01 and FS02 failed to show significant protection from solvent in the metal-bound state. For the mechanism of microenvironment sensitive fluorescence to work, the peptidyl template must be able to tolerate the inclusion of the chromophore, a residue that is considerably larger than naturally-occurring amino acids, within the hydrophobic cluster.

To assist in this task, the *solution* structures of individual zinc finger domains (Table 2-2) were consulted<sup>26,49-51</sup> to determine which template could best accommodate a bulky fluorophore at the position of the zinc finger consensus sequence which contains the aromatic residue of the hydrophobic cluster. As a result of these studies, the peptide “ZFY-swap”<sup>47,52</sup> was selected as the best candidate for development. Moreover, Phe<sup>10</sup> of that sequence chosen for replacement with the dansylated Dap amino acid derivative. (The FS01 and FS02 templates incorporated the fluorophore at position 1.) This decision was considerably aided by the excellent structural studies involving mutations made within the hydrophobic cluster of this peptide.<sup>49,53,54</sup> As an added benefit, ZFY-swap is known to undergo large changes in total secondary structure, particularly  $\alpha$ -helical structure, upon metal addition.<sup>47</sup>

**Table 2-2.** Published solution structures of individual zinc finger domains.

PDB #	identity	reference
1ZNF	Xfin-31	26
3ZNF	Human enhancer binding protein (average of 41 SA runs)	51
4ZNF	Human enhancer binding protein (best 41 SA runs)	51
5ZNF	ZFY-6T	52
7ZNF	ZFY-swap	52
1ARD	Yeast alcohol dehydrogenase transcription factor (res. 102-130)	50
1ARE	As above, with H118A mutation	50
1ARF	As above, with H118Y mutation	50

The fluorescence response of FS03DNS to the divalent metal cations Zn(II), Co(II), and Ni(II) was assessed to determine the zinc-sensing ability of this peptide. While Zn(II) produces a significant increase in fluorescence, the latter two ions slightly diminish the amount of DNS emission. The effect of these species on the fluorescence of FS03DNS is shown in Figure 2-14.

The fluorescence emission properties of FS03DNS are sensitive to the presence of nanomolar concentrations of Zn(II) (Figure 2-15). Upon excitation at 333 nm, the response (at 475 nm) is linear between 0.1 and 1  $\mu\text{M}$  Zn(II). Since a potential application of this zinc sensor is for the analysis of sea water, these studies were carried out in the presence of other metal cations including 0.5 M Na<sup>+</sup>, 50 mM Mg(II) and 100  $\mu\text{M}$  Co(II). It is notable that the chemosensor is compatible with these competing species.<sup>8</sup>

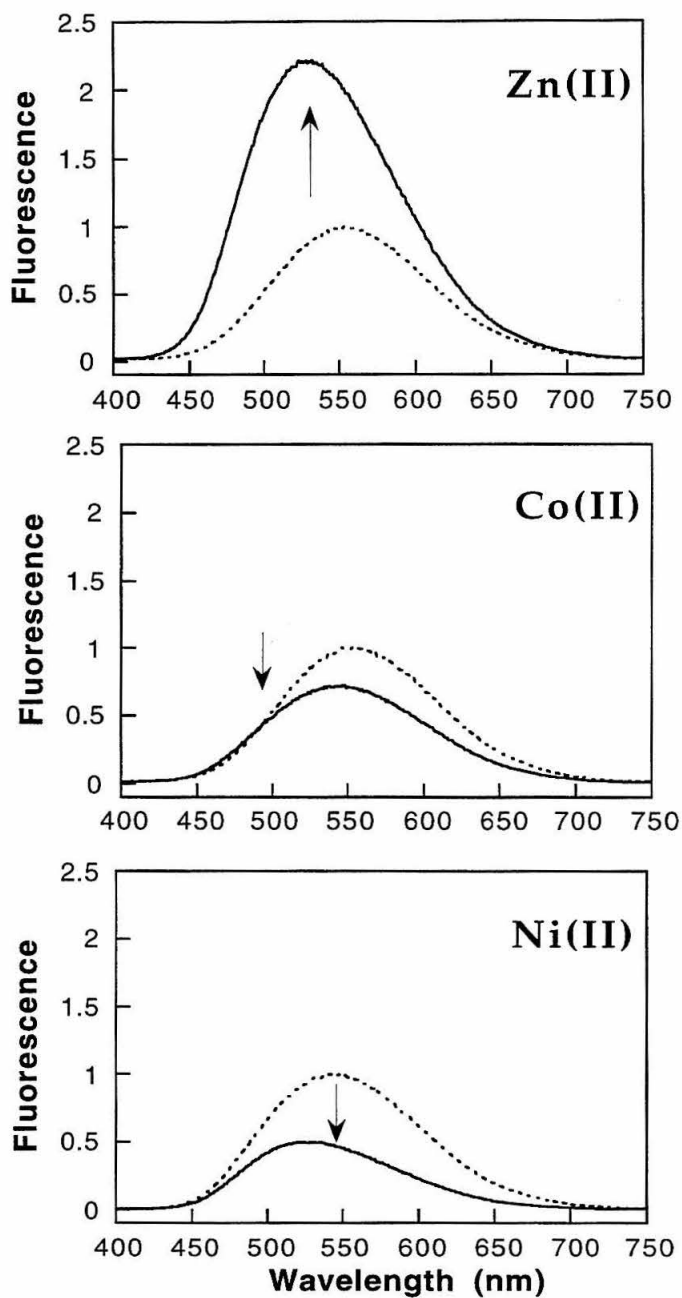


**Figure 2-14.** Fluorescence response of FS03DNS to the addition of various divalent metals. Data were acquired in 50 mM HEPES, pH 7.0 with 17  $\mu$ M fluorescent sensor before (dashed lines) and after (solid lines) the addition of 10 eq.  $\text{ZnCl}_2$ , 10 eq.  $\text{CoCl}_2$ , and 50 eq.  $\text{NiCl}_2$  respectively. Excitation at 333 nm.

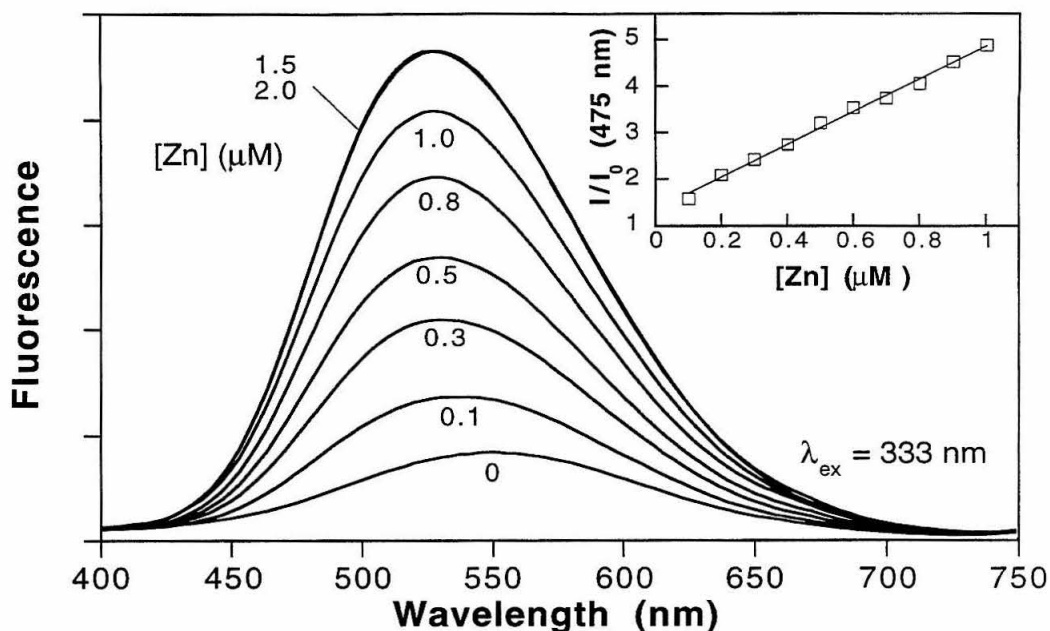


**Figure 2-15.** Fluorescence emission response of FS03DNS to increasing levels of Zn(II) ( $\mu\text{M}$ ) in the presence of Mg(II) (50 mM), and Co(II) (100  $\mu\text{M}$ ) ions; excitation at 333 nm. Spectra were acquired with 1.4  $\mu\text{M}$  FS03DNS, 50 mM HEPES, pH 7.0,  $\mu = 0.5$  (NaCl), 3.5  $\mu\text{M}$  EDTA. Addition of EDTA was required to complex adventitious metal ions and establish the initial baseline prior to metal addition. The relative increase in fluorescence at 475 nm is linear between 0.1 and 1.0  $\mu\text{M}$  Zn(II).

Ratiometric analysis of the emission spectra is possible, due to a blue-shift in the fluorescence upon metal binding. Because the maximum of the zinc-bound species (525 nm) is not widely separated from the emission maximum of the cobalt-bound species (550) or from the emission maximum of the peptide in the absence of divalent metals (560 nm), the fluorescence emission measured at 525 nm and 650 nm were selected. Although the relative emission profiles for the Zn(II) and Co(II)-bound species show that these wavelengths do not coincide with the maximal ratio (Figure 2-16), the wavelength with maximal total signal (525 nm) is employed. And, because no negative ratio is observed at any wavelength, the choice of the reference wavelength is rendered somewhat arbitrary. Hence 650 nm was selected for the normalization wavelength as it

was the longest wavelength which did not suffer from disruptive scattering effects near 665 nm (double the excitation wavelength).

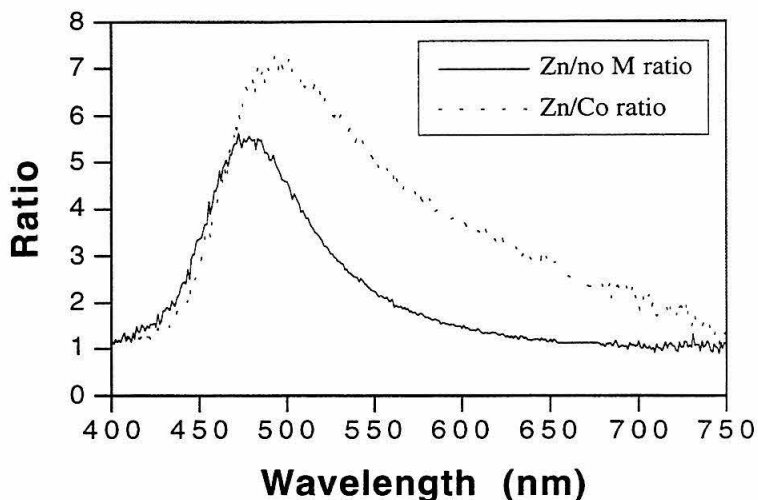


**Figure 2-16.** Ratiometric profiles of the fluorescence emission of FS03DNS for both the Zn(II)-bound species (dotted line) and the Co(II)-bound species (solid line).

An example of the response obtained through the use of ratiometric analysis, which highlights the minimal effect of competing ions toward the measurement of Zn(II) with FS03DNS, is presented in Figure 2-17. Furthermore, the reversibility of the chemosensor is also demonstrated by the addition of excess EDTA to the analysis mixture.

The structural response of FS03DNS to different divalent metal cations is markedly different (Figure 2-18). In the absence of divalent metal cations, the CD spectrum of FS03DNS appears to be predominantly random coil, similar to other zinc finger domains, and the FS03DNS·Zn(II) species has a CD spectrum that is characteristic of natural Zn(II)-bound zinc finger domains. By comparison, the FS03DNS·Co(II) species has a CD spectrum which is much less negative at 222 nm than the FS03DNS·Zn(II) complex, suggesting that less helical content is present in the Co(II) complex.

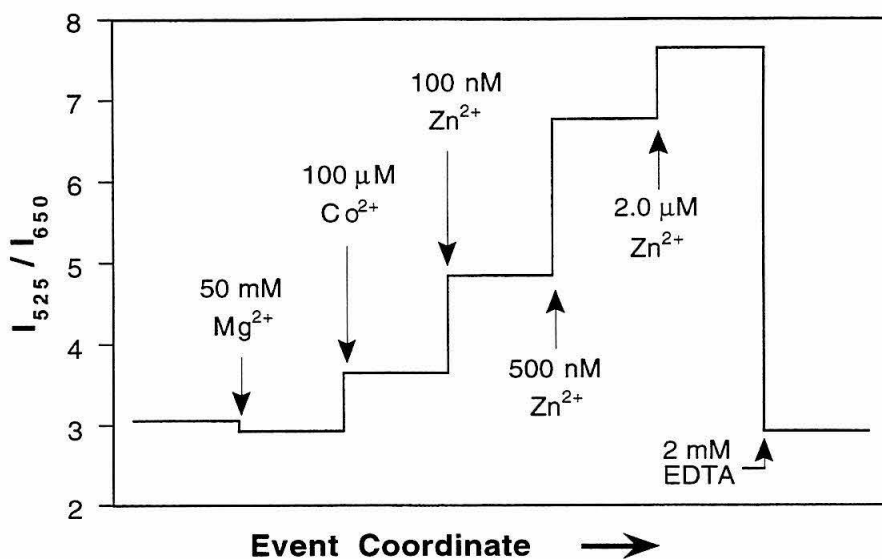


**Figure 2-17.** Ratiometric analysis of the fluorescence emission changes upon the addition of various divalent metals. Initial conditions are 1.4  $\mu\text{M}$  FS03DNS, 50 mM HEPES, pH 7.0, 3.5  $\mu\text{M}$  EDTA,  $\mu = 0.5$  (NaCl). Arrows represent the addition of concentrated metal stocks to give the indicated composition.

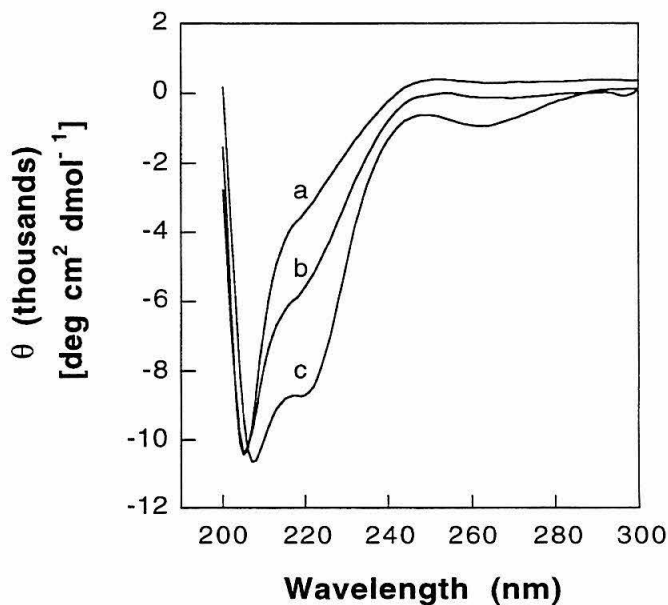


**Figure 2-18.** Circular dichroism spectra of FS03DNS in 0.5 mM HEPES, pH 7.0; (a) FS03DNS only, 9.6  $\mu\text{M}$  peptide; (b) FS03DNS-Co(II), 12.3  $\mu\text{M}$  peptide, 120  $\mu\text{M}$  CoCl<sub>2</sub>; (c) FS03DNS-Zn(II), 12.2  $\mu\text{M}$  FS03DNS, 14.5  $\mu\text{M}$  ZnCl<sub>2</sub>.

In order to better characterize the metal ion binding selectivity of FS03DNS, efforts were directed towards the elucidation of the apparent dissociation constant of the FS03DNS·Zn(II) complex. However, much like the peptide FS02DNS, the Co(II) complex of FS03DNS did not display a diagnostic *d-d* absorption band between 600 and 700 nm. However, the zinc binding affinity of FS03DNS is too great to be assayed accurately by competition with mag-fura-2. An alternate indicator, 4-(2-pyridylazo)resorcinol (PAR) was selected. PAR forms both 1:1 and 2:1 complexes with Zn(II), with stepwise apparent affinity constants of  $4.0 \times 10^6 \text{ M}^{-1}$  and  $5.5 \times 10^5 \text{ M}^{-1}$  respectively (at pH 7.0,  $\mu = 0.1$ ).<sup>55</sup> Addition of Zn(II) to a solution of PAR produces an intense absorbance at 500 nm ( $\Delta\epsilon = 6.6 \times 10^4 \text{ M}^{-1} \text{ cm}^{-1}$ ) which has been used for the determination of low picomolar protein-zinc dissociation constants.<sup>56</sup>

The results from a typical competition experiment are shown in Figure 2-19. Incremental additions of FS03DNS to a solution containing PAR and Zn(II) results in a decrease in the fraction of PAR involved in the PAR<sub>2</sub>Zn complex, resulting in a diminution of the PAR<sub>2</sub>Zn signal observed at 500 nm.

Due to the mathematical complications resulting from the fact that PAR forms both 1:1 and 2:1 complexes with Zn(II), competition experiments were performed using an excess of PAR, sufficient to assure  $\geq 99\%$  of the Zn(II) bound to PAR was in the 2:1 ligand:metal form. Additionally, competition experiments were performed with nominal PAR concentrations of 200  $\mu\text{M}$ , 240  $\mu\text{M}$ , and 300  $\mu\text{M}$  to assure that the zinc binding competition was, in fact, adequately represented by a simple equilibrium that did not require the consideration of 1:1 Zn(II):PAR complexes. (Further details regarding the calculation of apparent dissociation constants are presented in the experimental section of this chapter.) A summary of the values obtained for the apparent dissociation constant ( $K'_D$ ) for the FS03DNS·Zn(II) complex calculated by this method are summarized in Table 2-3. The average value determined was 140 ( $\pm 30$ ) pM.

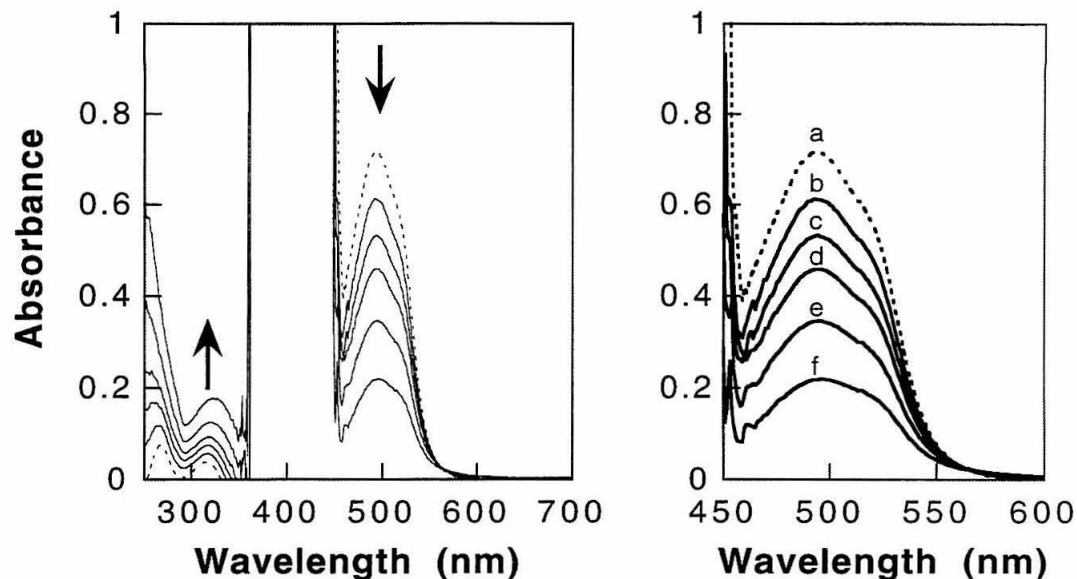


**Figure 2-19.** A typical competition experiment, showing the addition of FS03DNS to a solution of PAR and Zn(II). The spectra were blanked against a solution consisting of 50 mM HEPES, pH 7.0 with  $[\text{PAR}]_{\text{total}} = 240 \mu\text{M}$  at the initial volume of  $1000 \mu\text{L}$ . The individual spectra displayed were acquired after the addition of: a)  $10.6 \mu\text{M ZnCl}_2$ ; b)  $3.49 \mu\text{M FS03DNS}$ ; c)  $6.96 \mu\text{M FS03DNS}$ ; d)  $10.4 \mu\text{M FS03DNS}$ ; e)  $17.3 \mu\text{M FS03DNS}$ ; f)  $27.5 \mu\text{M FS03DNS}$ . The final volume of the solution was  $1018 \mu\text{L}$ .

**Table 2-3.** Values of the apparent dissociation constant for the FS03DNS·Zn(II) complex calculated by competition with PAR.

$K'_D$ (pM)	std. dev. ( $2\sigma$ )	$[\text{PAR}]_{\text{total}}$ ( $\mu\text{M}$ )
143	$40^a$	200
120	$30^a$	240
153	$60^a$	300
$140^b$	$34^c$	

<sup>a</sup>Error within one experiment.

<sup>b</sup>Average concentration.

<sup>c</sup>Error across experiments ( $n=3$ ).

**Fourth generation design, FS04DNS, FS04DNC.**

With the next generation design of sensors, the problem of intramolecular disulfide formation was again addressed through the replacement of one of the metal-coordinating ligands with a redox stable amino acid. The sites considered for ligand replacement were (as before) the cysteine residues Cys<sup>3</sup> and Cys<sup>6</sup>. Histidine, 3-thienyl alanine, aspartic acid, and glutamic acid were modeled for replacement using a combination of Insight and Discover (Molecular Simulations, Inc.) as well as Sculpt (Interactive Simulations) modeling software. The parent sequence of FS03DNS was used in the modeling studies, namely a truncated 25 amino acid version ZFY-SWAP.<sup>47</sup> In order to analyze the geometrical consequences of ligand replacement in the metal binding site without the interference of other factors, no attempt was made to model the inclusion of the fluorophore-bearing residue. Thus modeling was performed with residue 10 left as phenylalanine, and the ligand replacements were analyzed for their ability to maintain the parent structure.

Based upon these studies, Cys<sup>6</sup> was selected for replacement with aspartic acid. An acidic residue was deemed better at replacing cysteine as the negative charge of the ligand is preserved, enabling an overall neutral peptide-metal ligation sphere analogous to that achieved at neutral pH for the native Cys<sub>2</sub>His<sub>2</sub> coordination sphere. Furthermore, the acidic amino acids are known to have relaxed geometrical constraints for metal binding compared to histidine,<sup>44,57,58</sup> a prediction that was borne out by the modeling studies. Finally, aspartic acid matched the steric requirements of the metal-binding site better than glutamic acid or the heterocyclic groups considered, and removal of Cys<sup>6</sup> left a site with much less sterically challenging geometry for ligand replacement than did Cys<sup>3</sup>. A schematic representation of a typical Cys<sup>6</sup>→Asp minimized structure is shown in Figure 2-20.

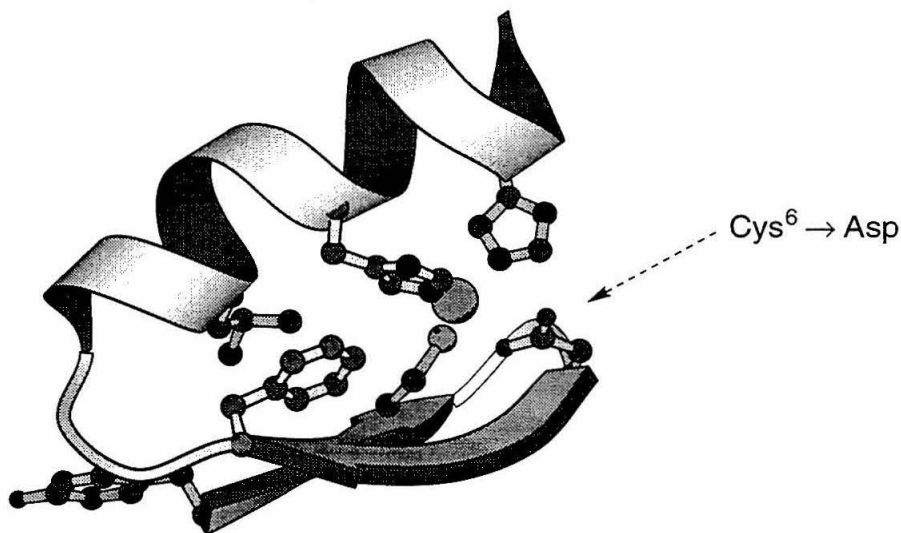


**Figure 2-20.** A schematic representation of the Cys<sup>6</sup> → Asp residue replacement made for the FS04 template, modeled from the coordinates of ZFY-Swap.

In addition to redesigning the composition of the metal ligating residues for FS04, the identity of the reporting fluorophore was again investigated in order to maximize metal-induced changes in fluorescence. As in previous modeling and chemical studies involving fluorophore replacement, emphasis was placed on the inclusion of a small, neutral fluorophore to allow for incorporation within the hydrophobic cluster of the zinc finger domain. Whereas only commercially available fluorophores were considered in prior studies, the success of FS03DNS as a chemosensor for Zn(II) provided impetus to expand the scope of fluorophore choice to include those requiring greater synthetic effort to prepare.

The PRODAN (6-propionyl-2-(dimethylamino)naphthalene) fluorophore is known to show exceptionally large microenvironment-sensitive changes in both emission wavelength and quantum yield,<sup>59,60</sup> and is relatively small, having only two annulated rings. Presumably, the solvent sensitivity of this fluorophore is due to the large separation of the dimethylamino and ketone groups, which results in the formation of a large excited-state dipole moment. Thus the 2,6-substituted naphthalene should be the

most solvent-sensitive isomer of this family. Although the amine to carbonyl distance may be used as an empirical guide to solvent sensitivity,<sup>33,36,59</sup> comparison of the properties of 1,4- 1,5- and 2,5-substituted dimethylamino / carbonyl naphthalene compounds reveals that the 1,5 isomer shows vastly greater fluorescence changes with solvent polarity.<sup>61</sup> Given that the sulfonamide-linked fluorophore of FS03DNS was the 1,5-substituted isomer, and that a carbonyl-linked 1,5-substituted dimethylamino-naphthalene fluorophore shows even greater solvent-sensitivity, this isomer was chosen for investigation as another reporter group. Accordingly this compound was synthesized, and incorporated in the FS04 template. (The details of the synthesis of this compound are at the end of the chapter.)

Model studies were performed to compare the solvent-dependent fluorescence enhancement (FE) for the DNS and DNC fluorophores in a variety of solvents. The fluorescence enhancement of the DNC group is much greater than that of DNS in nonpolar solvent. Figure 2-21 shows the fluorescence enhancement (integrated emission intensity) of both the dansyl group and the DNC group, with each fluorophore normalized to water. Although the greater FE for the DNC group is much larger than that for the dansyl group in nonpolar solvent (dioxane), the FE is about equal or less in polar, protic solvents.

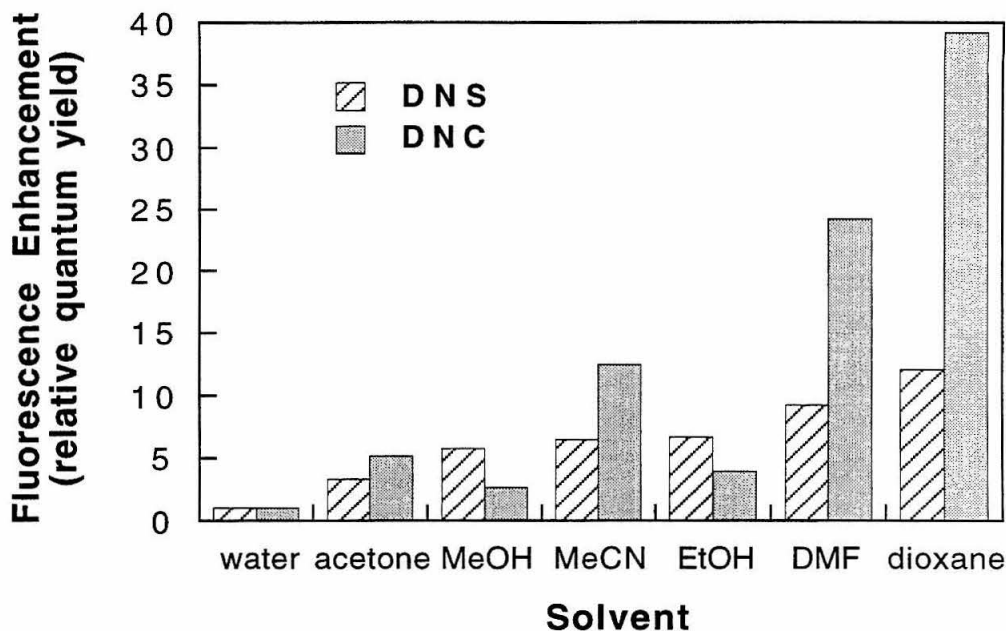


**Figure 2-21.** Comparison of the fluorescence enhancement of the DNS and DNC fluorophores, in a variety of solvents. Data represent integrated emission, and are independently normalized such that the value in water is unity.

Although model studies support the notion that the enhanced solvent sensitivity of the DNC group is significant when compared to the DNS fluorophore, the fluorescence response of the peptide FS04DNC to divalent zinc was disappointingly minimal (data not shown). As a consequence, only the structural, fluorescence, and Zn(II) binding properties of peptide FS04DNS were studied further.

The modification of the ligand sphere of the zinc finger made in the construction of FS04DNS has little effect upon the extent of metal-induced structural change (Figure 2–22). The fluorescence properties of FS04DNS retain the Zn(II) sensitivity observed for FS03DNS. More importantly, FS04DNS is compatible with redox active metal cations such as Cu(II). The fluorescence emission response of FS04DNS to increasing concentrations of divalent zinc in the presence of competing species is shown in Figure 2-23.

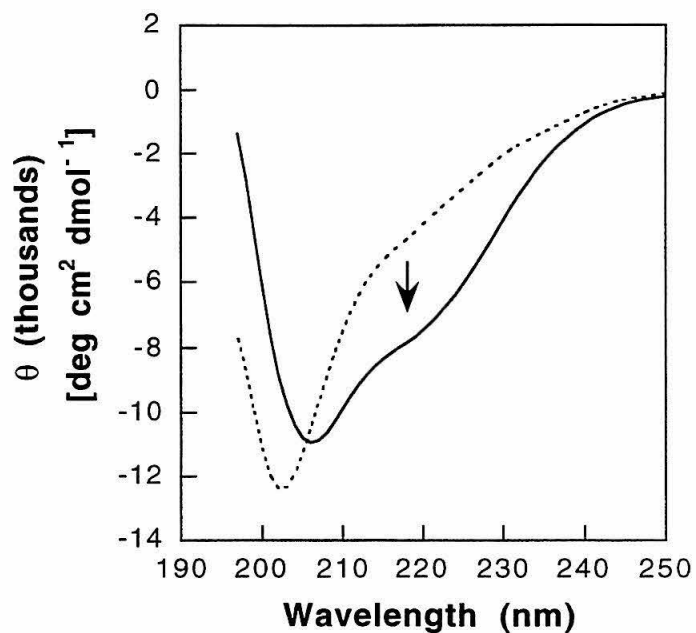


**Figure 2-22.** Circular dichroism spectra of 8.6  $\mu\text{M}$  FS04DNS upon the addition of  $\text{ZnCl}_2$ , in 0.5 mM HEPES, pH 7.0. Dashed line, no  $\text{ZnCl}_2$ ; solid line with 10  $\mu\text{M}$   $\text{ZnCl}_2$ .

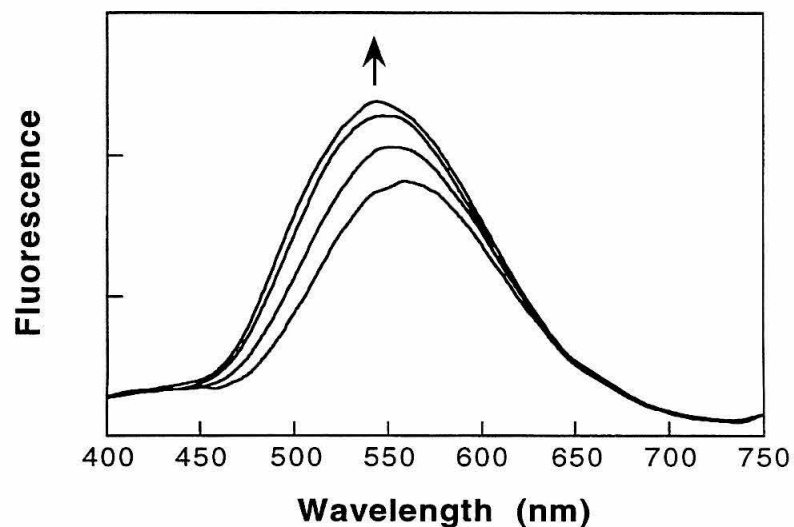


**Figure 2-23.** Fluorescence emission spectra of 1.3  $\mu\text{M}$  FS04DNS upon the addition of  $\text{ZnCl}_2$  up to 7  $\mu\text{M}$  in 50 mM HEPES, pH 7.0, 0.5 M NaCl, 50 mM  $\text{MgCl}_2$ , 10 mM  $\text{CaCl}_2$ , and 0.1  $\mu\text{M}$  each  $\text{FeCl}_2$ ,  $\text{CoCl}_2$ ,  $\text{NiCl}_2$ ,  $\text{CuCl}_2$ ,  $\text{CdCl}_2$ .

The Zn(II) binding affinity of the peptide FS04DNS was evaluated by a competition assay with mag-fura-2. Spectra from a typical titration are shown in Figure 2-24. Analysis revealed that treatment of the binding competition assuming 1:1 peptide:metal complex formation (as described for FS02DNS) did not suitably model the data. Initial formation of 2:1 peptide:Zn(II) complexes have been observed for other zinc finger peptides,<sup>62,63</sup> including a zinc finger-derived fluorosensor.<sup>64</sup> In those systems, Cys<sub>4</sub>·Zn(II) complexes are formed at low Zn(II) concentrations due to the preference of the zinc ion for a soft ligand.<sup>22,65</sup> It is presumed that the proposed CysHis<sub>2</sub>Asp coordination sphere of FS04DNS operates within the same manifold, preferring at low Zn(II) concentrations to bind thiolate ligands to divalent zinc in the place of *N* or *O* ligands.

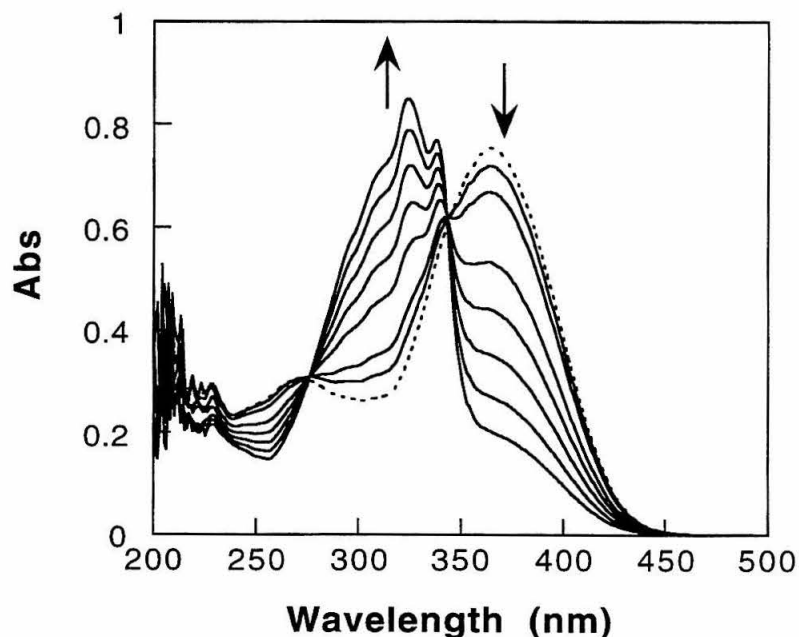


**Figure 2-24.** Absorption spectra from a typical competition assay between FS04DNS and mag-fura-2 (34  $\mu\text{M}$ ) blanked against 15  $\mu\text{M}$  FS04DNS, 50 mM HEPES, pH 7.0,  $\mu = 0.15$  (NaCl) with increasing concentrations of ZnCl<sub>2</sub>. Dotted line, no ZnCl<sub>2</sub>; solid lines, 2.00  $\mu\text{M}$  ZnCl<sub>2</sub>, 3.98  $\mu\text{M}$  ZnCl<sub>2</sub>, 9.24  $\mu\text{M}$  ZnCl<sub>2</sub>, 13.2  $\mu\text{M}$  ZnCl<sub>2</sub>, 17.1  $\mu\text{M}$  ZnCl<sub>2</sub>, 21.1  $\mu\text{M}$  ZnCl<sub>2</sub>, 25  $\mu\text{M}$  ZnCl<sub>2</sub>.

To further probe the Zn(II)-binding behavior of FS04DNS, the apparent dissociation constant for the FS04DNS·Zn(II) complex was calculated from each spectrum in the mag-fura-2 competition experiment by applying a mathematical treatment analogous to that described for the PAR-competition assays used with the peptide FS03DNS. At low concentrations of free Zn(II) (< 20 nM), the apparent dissociation constant of the FS04DNS·Zn(II) complex is indeterminate by this method. However, at free Zn(II) concentrations greater than 20 nM, the 1:1 complex is the dominant peptide:metal species and the apparent dissociation constant of the FS04DNS·Zn(II) complex is obtained as 65 ( $\pm$  5) nM.

## **Discussion**

The development of an oxidatively robust fluorescent peptidyl chemosensor for divalent zinc has been presented. Several synthetic zinc-finger peptides have been characterized by a variety of techniques including CD, UV-vis, and fluorescence spectroscopy. For many of these, the apparent dissociation constant of the peptide-zinc complex has been determined, and all bind divalent zinc with high affinity. A summary of the zinc binding affinities that have been determined are presented in Table 2-4. A summary of the fluorescence emission properties of the dansylated peptides is presented in Table 2-5. Furthermore, the peptides FS03DNS and FS04DNS are useful as sensors for divalent zinc having appreciable fluorescence response, with FS04DNS being an oxidatively robust fluorosensor.

### **Selection of the peptidyl template.**

A metal cation chemosensor requires two parts of equal importance; a metal binding moiety and a fluorescent signaling moiety. The central challenge for the production of new chemosensors for divalent metal cations remains one of selectivity. The remarkably avid and selective binding of Zn(II) exhibited by the zinc finger peptides was therefore exploited for the metal binding (sensing) event. The native zinc finger

peptides, however, lack a spectroscopic handle of sufficient sensitivity to signal this metal-dependent change. In these peptides a structural change from predominantly random coil to folded domains occurs upon binding Zn(II). This conformational change serves to alter the microenvironment of specific residues from being solvent exposed to participating in a hydrophobic cluster. Thus, to transduce this metal-binding event in a chemosensor, a fluorophore-bearing residue was incorporated in the place of the residues involved in the hydrophobic cluster of a zinc finger peptide.

**Table 2-4.** Apparent Dissociation Constants for Peptide·Zn(II) Complexes.

peptide	coordination sphere	$K'_D$
FS01DMB	Cys <sub>2</sub> His <sub>2</sub>	7 pM <sup>a</sup>
FS02DNS	CysHis <sub>3</sub>	3 nM <sup>b</sup>
FS03DNS	Cys <sub>2</sub> His <sub>2</sub>	140 pM <sup>c</sup>
FS04DNS	CysAspHis <sub>2</sub>	65 nM <sup>b,d</sup>

<sup>a</sup>Determined by competitive titration with Co(II) and Zn(II). <sup>b</sup>Determined by competition with the indicator mag-fura-2 for Zn(II). <sup>c</sup>Determined by competition with the indicator 4-(2-pyridylazo)resorcinol for Zn(II). <sup>d</sup>Initially forms a presumed 2:1 peptide:metal complex at low concentrations ( $\leq 20$  nM) of free Zn(II), the value represents the apparent value at  $\geq 20$  nM free Zn(II).

### Importance of metal-induced secondary structural changes.

The efficacy of this mechanism of microenvironment-sensitive fluorescence for signal transduction depends on the magnitude of the change experienced by the fluorophore. It is therefore expected that a large change in secondary structure upon binding Zn(II) would be accompanied by a concomitant change in fluorescence. Interpretation of the CD data is subject to the caveat that the fluorophores used in this study could contribute to the spectra in a manner unlike native proteins. Specifically, the

negative ellipticity observed for FS03DNS·Zn(II) between 250 and 280 nm (Figure 2-18) is a feature not commonly observed for zinc-finger complexes, and may result from the dansyl chromophore. However, the CD spectra of all the peptide-Zn(II) complexes obtained bear resemblance to those of naturally occurring zinc finger domains, regardless of the incorporated fluorophore. These results suggest that the CD spectra are not dominated by specific fluorophore-related effects. In any case, it is likely that a metal-dependent change in the CD spectrum for a given peptide is indicative of a concomitant change in the microenvironment of the fluorophore, whether it results solely from changes in secondary structural content or includes a contribution from the fluorophore itself.

This expectation is borne out by the CD studies performed on these peptides. Both FS01DMB and FS02DNS, which are derived from Zif268, show small changes in structure upon Zn(II) addition (Figures 2-4 and 2-12 respectively). By comparison, the Zn(II)-induced structural changes of FS03DNS and FS04DNS, which are derived from ZFY-swap, are much larger (Figures 2-18 and 2-22 respectively). Since FS02DNS, FS03DNS and FS04DNS share the same fluorophore, the effect of structural change upon fluorescence may be compared directly with the caveat that the fluorophore is attached at a different position within the primary sequence of the former peptide. In these cases, larger metal-induced changes in secondary structure measured by CD correlate with larger changes in fluorescence emission. These results highlight the importance of the inherent structural content of the peptidyl template in the absence of metal cations for fluorescence signaling.

#### **Accommodation of the fluorophore within the hydrophobic cluster.**

Of paramount importance for the production of a sizeable fluorescence response is the ability of the folded peptidyl template to accommodate the presence of a bulky fluorophore. For the dansyl chromophore, increasing emission intensity with increasing blue-shift indicates that the fluorophore is in a less polar microenvironment. Thus the

protection of the fluorophore from bulk solvent provided by the peptidyl template may be estimated qualitatively from the emission spectra. Concentration-corrected fluorescence emission spectra of the model compound dansyl asparagine and the zinc complexes of FS02DNS, FS03DNS, and FS04DNS are presented for comparison in Figure 2-25. The fluorescence from the zinc complexes of FS03DNS and FS04DNS are the most blue-shifted and intense, indicating more complete accommodation of the dansyl group as a member of the hydrophobic cluster. However, the emission of the FS04DNS·Zn(II) complex is diminished considerably relative to that of FS03DNS·Zn(II), which differs in only one residue. Clearly a subtle interplay exists between the geometry of the metal ligating residues and the topology of the folded peptide.

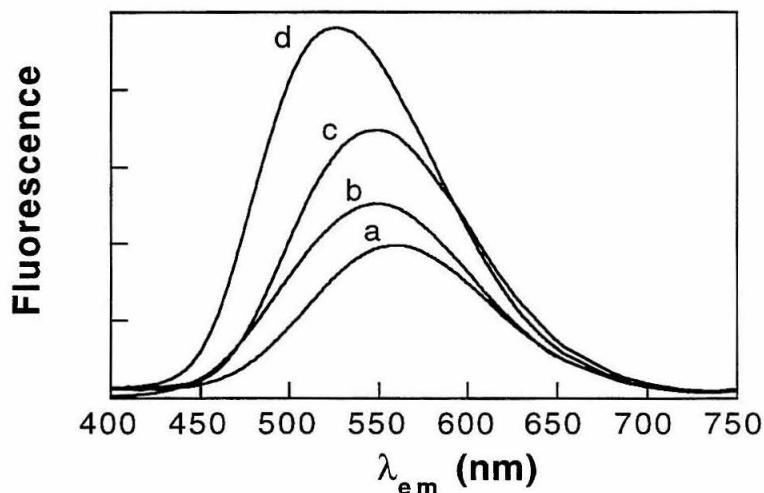


**Figure 2-25.** Fluorescence emission spectra of several peptide·Zn(II) complexes, corrected for the concentration of the fluorophore, as compared to the model compound dansyl asparagine. a) dansyl asparagine b) FS02DNS·Zn(II) c) FS04DNS·Zn(II) d) FS03DNS·Zn(II).

#### **Ligand choice and zinc binding affinity.**

To construct an oxidatively robust sensor from the zinc finger template requires the substitution of one of the metal binding cysteines. However, substitution of the cysteine residues, which comprise the native metal coordination sphere, for other

naturally occurring metal-binding residues reduces the Zn(II) binding affinity exhibited by the template (Table 2-4). This is presumably due to the preference of ions with electronic configurations of  $d^{10}$  for soft ligands.<sup>66</sup> Thus the peptides FS01DMB and FS03DNS with  $S_2N_2$  metal binding sites have the highest affinity for Zn(II), followed by FS02DNS with a  $SN_3$  site, and ultimately by FS04DNS which has an  $SN_2O$  ligation sphere.

Initial access to an oxidatively robust fluorescent chemosensor for divalent zinc was obtained in the peptide FS02DNS by making the substitution Cys<sup>6</sup>→His in the parent sequence of FS01DMB. While this peptide was tolerant of redox active metal ions, the fluorescence response to Zn(II) was too small to be useful as a sensitive probe of divalent zinc concentrations. In addition, fluorescence emission experiments carried out with competing Cu(II) and Zn(II) indicated that FS02DNS bound divalent copper with at least two orders of magnitude preference over zinc (data not shown). Based upon this knowledge, alternate ligating residues were considered for incorporation in the place of cysteine for the design of FS04DNS. Aspartic acid was selected as a replacement for Cys<sup>6</sup> to most closely mimic the steric and charge neutralization properties of the thiolate ligand. In addition, the carboxylate ligand exhibits flexible coordination geometry,<sup>67</sup> which was expected to relax the stringent steric requirements for metal ligation.

Modification of the ligation sphere of FS03DNS resulted in the production of a fluorescent peptidyl chemosensor for divalent zinc with enhanced oxidative stability. The fluorescence response of FS04DNS is responsive to sub-micromolar to micromolar concentrations Zn(II), in the presence of redox active metal cations including Cu(II) and Fe(II), as well as vast excesses of the competing divalent cations Mg(II) and Ca(II) (Table 2-5). It is particularly relevant that this chemosensor is compatible with a  $\geq 50,000$  fold excess of Mg(II) and  $\geq 10,000$  fold excess of Ca(II), given that these species are normally present in great excess in biological samples.

**Table 2-5.** Fluorescence emission properties of peptide·Zn(II) complexes.

peptide	$[\lambda_{\max}^{\circ}]^b$	$[\lambda_{\max}^{\text{Zn}}]^c$	$[F_{\lambda_{\max}^{\text{Zn}}}^{\text{Zn}}]^d$	$[\text{FE}_{\lambda_{\max}}]^e$
FS02DNS	552	548	1.3	1.3
FS03DNS	560	525	2.4	3.0
FS04DNS	560	543	1.7	1.8
DNS-Asn <sup>a</sup>	560	560	–	–

Data were acquired with excitation at 333 nm in 50 mM HEPES, pH 7.0, 0.5 M NaCl. Data for FS03DNS was acquired with the addition of 50 mM MgCl<sub>2</sub>, 10 mM CaCl<sub>2</sub>, 100 μM CoCl<sub>2</sub>. Data for FS04DNS was acquired with the addition of 50 mM MgCl<sub>2</sub>, 10 mM CaCl<sub>2</sub>, and 0.1 μM each FeCl<sub>2</sub>, CoCl<sub>2</sub>, NiCl<sub>2</sub>, CuCl<sub>2</sub>, CdCl<sub>2</sub>.

<sup>a</sup>Dansyl asparagine.

<sup>b</sup>Wavelength of maximum emission for the peptide in the absence of divalent zinc.

<sup>c</sup>Wavelength of maximum emission for the peptide·Zn(II) complex.

<sup>d</sup>Fluorescence intensity of the peptide·Zn(II) complex at  $\lambda_{\max}^{\text{Zn}}$  normalized such that the fluorescence intensity at  $\lambda_{\max}^{\circ} = 1$ .

<sup>e</sup>The fluorescence enhancement at the wavelength  $\lambda_{\max}^{\text{Zn}}$ ; defined as  $\text{FE}_{\lambda_{\max}}^{\text{Zn}} \equiv F_{\lambda_{\max}}^{\text{Zn}} / I$  where I is the fluorescence intensity at  $\lambda_{\max}^{\text{Zn}}$  in the absence of divalent zinc.

The relative change in quantum yield or fluorescence enhancement (FE) of FS03DNS is the largest for the peptides studied, with a value of 2.4 between the metal free and zinc bound state. Significant effort has been directed towards increasing the magnitude of this change, as it is very small when compared to other intensity-based fluorescent chemosensors. However, this FE is on par with those for commonly employed ratiometric sensors (Table 2-6). This is one of the major advantages of a ratiometric sensor: small fluorescence changes allow precise measurements of amount of analyte bound. This result suggests that an alternate tactic to consider for the continued improvement of fluorescent sensors of this class is to increase the spectral separation of the fluorescence from the metal-bound and free species, rather than the fluorescence enhancement.

**Table 2-6.** Fluorescence enhancements for ratiometric-based and intensity-based chemosensors for Ca(II).<sup>3,68</sup>

fluorophore	FE
ratiometric sensors	
Fura-2	2.1
Indo-1	1.5
intensity sensors	
Calcium Green-1	~14
Calcium Green-2	~100
Fluo-3	~50

The extent of the fluorescence increase, and the magnitude of the blue-shift caused by Zn(II) addition to these fluorescent sensors can be compared with the equivalent change in fluorescence for a model dansyl compound between different solvents. Concentration-corrected fluorescence emission spectra of dansyl asparagine

were collected under a variety of conditions, including polar and non-polar, protic and non-protic solvents. A comparison of these with a spectrum of FS03DNS·Zn(II), the zinc-bound form of the sensor that shows the greatest Zn(II)-induced change in fluorescence, is shown in Figure 2-26. Undoubtedly, the magnitude of the fluorescence changes demonstrated by the fluorophore within the peptidyl context may include contributions from effects in addition to those experienced in the structurally more simple model compound. (For example, the folded form of the sensor could potentially protect the fluorophore from an excited-state proton transfer quenching interaction, whereas the model compound could not.) However, this “ballpark” comparison may become helpful for the continued design of other sensors as it provides an estimate of how large a change in microenvironment is experienced by the fluorophore.

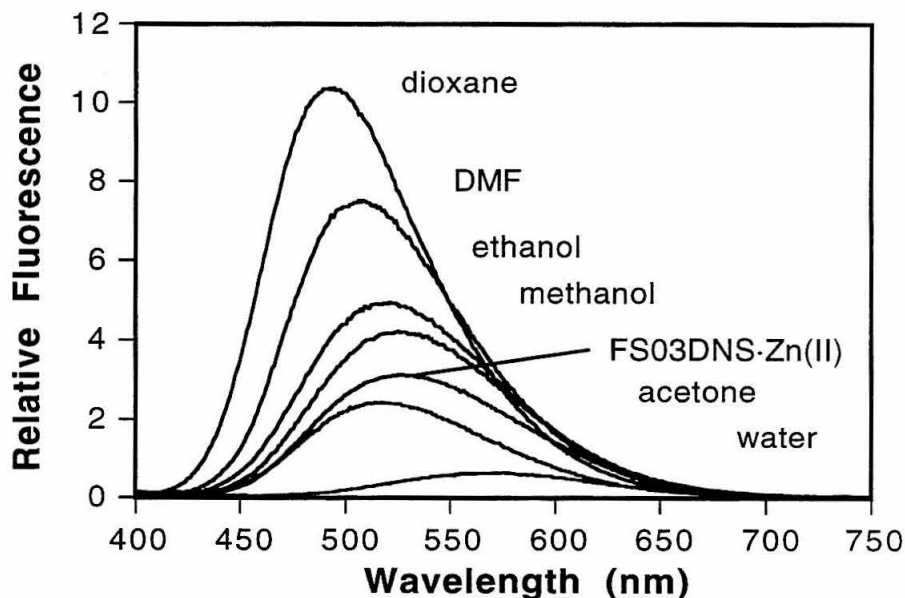


**Figure 2-26.** The microenvironment sensitive fluorescence of the DNS fluorophore in the FS03DNS·Zn(II) suggests the fluorophore experiences an environment similar in polarity to acetone or methanol. The model compound dansyl asparagine was used for measurements in the reference solvents.

## Conclusion

The zinc finger motif provides an architecture which is viable for the production of fluorescent sensors. The ease with which the peptide scaffold may be modulated provides opportunity for the continued elaboration of this design. The affinity of the zinc finger motif for divalent zinc may be varied by the choice of chelating residues as well as the overall amino acid sequence. Through the modification of ligand type, a fluorescent chemosensor for divalent zinc with enhanced oxidative stability has been produced (FS04DNS). Future modifications to this design may include the peptide incorporation of nonnatural, bidentate chelating residues to augment the metal binding selectivity of the motif as well as the incorporation of ligands with metal-modulated fluorescence properties.

## Acknowledgment

Both Richard Cheng and Ranabir Sinha Roy provided helpful advice regarding the measurement of apparent peptide-metal complex dissociation constants. The bulk of this work has appeared in the following publications:

- (1) "Design and Evaluation of a Peptidyl Fluorescent Chemosensor for Divalent Zinc," Walkup, G. K.; Imperiali, B. *J. Am. Chem. Soc.* **1996**, *118*, 3053-3054.
- (2) "Fluorescent Chemosensors for Divalent Zinc Based on Zinc Finger Domains—Enhanced Oxidative Stability, Metal Binding Affinity, and Structural and Functional Characterization," Walkup, G. K.; Imperiali, B. *J. Am. Chem. Soc.* **1997**, *119*, 3443-3450.

In addition, we note the subsequent report of another sensor developed along similar lines,<sup>64</sup> but which uses two fluorophores and a resonant energy transfer mechanism for signal transduction.

## Experimental

*Peptide synthesis.* Peptides were synthesized on a Milligen 9050 peptide synthesizer at a 0.125 mmole scale. Fmoc-PAL-PEG-PS (PerSeptive) resin (0.21

mmol/g) was used to afford carboxy-terminal primary amides. Couplings were performed at a concentration of 0.3 M acylating reagent and 1-hydroxybenzotriazole (HOBt), in a volume sufficient to achieve a three-fold excess of amino acid to resin-bound amine. Pentafluorophenyl ester / HOBt chemistry was employed for all residues except Fmoc-L-Dap(alloc)-OH which was coupled by *in situ* active ester generation using HOBt / *N,N'*-diisopropylcarbodiimide activation. A double-coupling procedure was employed, with coupling reactions of 45 minutes, followed by a 10 minute wash with 0.3 M acetic anhydride/HOBt solution in 9:1 DMF / dichloromethane to cap any unreacted amines. Removal of the Fmoc group was performed with piperidine (20% v/v in DMF) with a standard wash duration of 7 minutes. After addition of the final residue, the amino-terminus was acetyl-capped (DMF / acetic anhydride / triethylamine, 4 mL:63  $\mu$ L:94  $\mu$ L) for 0.5 h then washed with DMF ( $5 \times 10$  mL) and MeOH ( $5 \times 10$  mL). Residual solvent was removed under reduced pressure.

*Allyloxycarbonyl removal.* The method of Kates et al.<sup>29</sup> was employed with some minor modifications. A typical procedure for removal of the allyloxycarbonyl (alloc) group was as follows. Under a blanket of nitrogen, a 20-mL plastic, stoppered vial was charged with resin from the completed peptide synthesis (300 mg, 0.21 meq/g, 63  $\mu$ mol), and 5 mL of a solvent cocktail (CHCl<sub>3</sub> / morpholine / AcOH, 90:5:5). The resin was allowed to swell 10 min, to which tetrakis(triphenylphosphine)palladium (200 mg, 173  $\mu$ mol) was added under a blanket of nitrogen. The vial was capped, shielded from light, and placed on a wrist-action shaker at low speed for 2 h. The resin was filtered, washed with CHCl<sub>3</sub> ( $5 \times 10$  mL), and a palladium chelating cocktail (DMF / diethyldithiocarbamic acid·3H<sub>2</sub>O / triethylamine, 25 mL:225 mg:250  $\mu$ L). Traces of this solution were removed with a basic wash (0.5% v/v triethylamine in DMF), and a final wash with methanol. The resin was transferred to a clean plastic vial, and the residual solvent removed under reduced pressure.

*Fluorophore coupling.* Lyophilized resin was taken directly from the alloc-removal procedure, and allowed to swell in DMF (5 mL). For addition of the dansyl group, 10 equivalents (based on resin-bound amine) of dansyl chloride was added, followed by 10 equivalents of triethylamine. Coupling of fluorophores containing a carboxylic acid (CMN, DMB, DNC) was performed with standard (benzotriazol-1-yloxy-tris-(dimethylamino)phosphonium hexafluorophosphate (BOP) coupling. In all cases, after the addition of the acylating reagent, the vial was capped under a blanket of nitrogen, and placed on a wrist-action shaker at low speed for 2 h. The resin was filtered, washed with a basic wash ( $5 \times 10$  mL, see above), washed with DMF ( $5 \times 10$  mL), then finally washed with MeOH ( $5 \times 10$  mL). The resin was transferred to a clean 20 mL polyethylene vial, and residual solvent was removed under reduced pressure prior to peptide cleavage.

*Peptide cleavage and purification.* Peptides were cleaved after fluorophore coupling using 10 mL of Reagent K<sup>69</sup> (trifluoroacetic acid / H<sub>2</sub>O / ethanedithiol / thioanisole / phenol, 82.5:5:5:5:2.5) with a 2 h incubation period. The resin was filtered, the filtrate concentrated to *ca.* 2 mL volume, and precipitated with ether / hexane 2:1 at -20 °C for 30 min. The supernatant was decanted, and the solid triturated with ether / hexane 2:1 ( $5 \times 50$  mL). The resultant solid was resuspended in water (20 mL), lyophilized, and then purified to homogeneity by reverse phase (C<sub>18</sub>) high-performance liquid chromatography (HPLC). The identity of each peptide was confirmed by electrospray mass spectroscopy (Table 2-7).

*Peptide stock solutions.* After HPLC purification, the fractions containing pure peptide were lyophilized, and resuspended in hydrogen-sparged water to retard oxidation. When not in use, stocks were stored at -80 °C. The concentration of the stock solutions was determined by reaction with Ellman's reagent, 5,5'-dithiobis(2-nitrobenzoic acid) (DTNB).<sup>70</sup> These assays were performed in triplicate, with excellent agreement (< 5% variance) between runs. From the concentration of the stock solution, the extinction

coefficient of the peptide was determined at a wavelength appropriate for the fluorophore present. All peptide concentrations determined subsequently were based on this value. As the reduced and oxidized (disulfide) forms of the peptides are separable by HPLC, aliquots of the stock solution were periodically checked to assure that no detectable oxidation had occurred.

**Table 2-7.** Calculated and observed electrospray mass values for the synthetic zinc finger peptides.

peptide	formula [M+ H] <sup>+</sup>	MW calcd	MW obsd
FS01DMB	C <sub>120</sub> H <sub>188</sub> O <sub>40</sub> N <sub>37</sub> S	2853.2	2852.6
FS02DNS	C <sub>126</sub> H <sub>192</sub> O <sub>42</sub> N <sub>39</sub> S <sub>2</sub>	2973.3	2973.5
FS02CMN	C <sub>124</sub> H <sub>185</sub> O <sub>42</sub> N <sub>41</sub> S	2912.2	2912.6
FS03DNS	C <sub>138</sub> H <sub>214</sub> O <sub>42</sub> N <sub>42</sub> S <sub>3</sub>	3230.7	3231.0
FS04DNC	C <sub>140</sub> H <sub>214</sub> O <sub>43</sub> N <sub>42</sub> S	3203.6	3203.8
FS04DNS	C <sub>139</sub> H <sub>215</sub> O <sub>44</sub> N <sub>42</sub> S <sub>2</sub>	3240.5	3241.3

*Metal stock solutions.* Stock solutions of divalent metal cations were prepared from analytical grade salts, and dissolved in high purity water obtained from a Milli-Q (Millipore) filtration apparatus. The concentration of each stock solution was determined by titration against a standardized solution of EDTA (Aldrich) in the presence of an appropriate metallochromic indicator.<sup>71</sup>

*Buffer preparation.* All buffers were prepared in acid-washed polyethylene containers using high-purity water obtained from a Milli-Q filtration apparatus. Sodium chloride and 4-(2-hydroxyethyl)-1-piperazineethanesulfonic acid (HEPES) were obtained from Sigma and used without further purification. After preparation of the buffer, the solution was passed through a 30 cm × 1.5 cm column of freshly regenerated Chelex resin

(sodium form, Bio-Rad Laboratories).<sup>72</sup> This buffer was tested for metal ion impurities by the addition of 100  $\mu\text{M}$  4-(2-pyridylazo)resorcinol (PAR) followed by the addition of 1 mM EDTA, pH 7.0. The absorbance change at 500 nm in a 1.0 cm cell upon the addition of EDTA was  $\leq 0.003$ , indicating that  $\leq 50$  nM divalent metal was present (assuming all metal ion impurities were Zn(II),  $\Delta\epsilon_{500} = 6.6 \times 10^4$ ). This buffer analysis was performed periodically to test against buffer contamination.

*Circular dichroism.* Spectra were recorded on a Jasco J600 circular dichroism spectrometer. The peptide concentration in each assay was determined spectrophotometrically on a Shimadzu UV-160 UV-vis spectrophotometer fitted with a circular cell holder. Except for pH dependence studies, which were performed in unbuffered water, spectra were acquired in 0.5 mM HEPES, pH 7.0. In general, a nominal concentration of 10  $\mu\text{M}$  peptide was used in a 1.0 cm cell. Spectra were baseline corrected and noise reduced using the Jasco software.

*Emission fluorescence assay.* Assays were performed with a SLM-Aminco SPF-500c spectrofluorometer at room temperature in 50 mM HEPES buffer, pH 7.0, 0.5 M NaCl in a stoppered 750  $\mu\text{L}$  (1cm  $\times$  3mm) quartz fluorometer cell. The concentration of peptide in a given assay was determined by absorption spectroscopy immediately prior to the fluorescence experiment. Emission spectra were accumulated at 1 nm intervals with the following parameters: excitation band pass = 4 nm, emission band pass = 2 nm, lamp potential = 975 V, gain = 10, filter (time constant) = 3.

### **Competitive zinc binding with 4-(2-pyridylazo)resorcinol (PAR).**

A method for the determination of sub-picomolar protein-zinc dissociation constants has been described previously,<sup>55</sup> and a modified version of this procedure was employed. Because PAR forms both 1:1 and 2:1 complexes with Zn(II), an excess of PAR sufficient to bind  $\geq 99\%$  of the zinc in the 2:1 PAR:Zn(II) form must be used. Thus the binding the equilibrium may be expressed as in equation 1. Under these conditions,

the apparent affinity constant of the peptide may be obtained by solving equation 2 for  $K'_{\text{Pep}}$ .



$$\frac{[\text{Zn}\cdot\text{Pep}][\text{PAR}]^2}{[\text{Pep}][\text{PAR}_2\text{Zn}]} = \frac{K'_{\text{Pep}}}{\beta'_{\text{PAR}}} \quad (2)$$

The dissociation constant of the Zn·Pep complex was calculated by substituting into equation 2. Equations 3-6 were used to calculate the individual components of equation 2. Competition experiments were performed with nominal PAR concentrations of 200  $\mu\text{M}$ , 240  $\mu\text{M}$ , and 300  $\mu\text{M}$  to assure that the zinc binding competition is adequately represented by equation 1.

$$[\text{PAR}_2\text{Zn}] = \frac{A_{500}}{\Delta\epsilon_{500}} \quad \text{where } \Delta\epsilon_{500} = 6.6 \times 10^4 \quad (3)$$

$$[\text{PAR}] = [\text{PAR}]_{\text{total}} - 2[\text{PAR}_2\text{Zn}] \quad (4)$$

$$[\text{Zn}\cdot\text{Pep}] = [\text{PAR}_2\text{Zn}]_{\text{initial}} - [\text{PAR}_2\text{Zn}] \quad (5)$$

$$[\text{Pep}] = [\text{Pep}]_{\text{total}} - [\text{Zn}\cdot\text{Pep}] \quad (6)$$

*Competition assay with PAR.* Assays were performed on a Beckman DU-700 UV-vis spectrophotometer at room temperature using a standard 1.0 cm path length cell. Repeat runs were performed at a variety of PAR concentrations to assure that a simple zinc binding competition was in effect. A typical assay is described. Aliquots of HEPES buffer (979  $\mu\text{L}$ ) and the PAR stock solution (21  $\mu\text{L}$ ) were mixed in a cuvette and the spectrophotometer was blanked against this solution. A 1.9  $\mu\text{L}$  aliquot of 5.30 mM Zn(II) was added, and the UV-vis spectrum was acquired between 200 and 700 nm. The increased absorbance at 500 nm results from the formation of the  $\text{PAR}_2\text{Zn}$  complex which has a  $\Delta\epsilon = 6.6 \pm 0.2 \times 10^4 \text{ M}^{-1} \text{ cm}^{-1}$ , corrected for pH.<sup>55</sup> Aliquots of a 1.75 mM stock solution of FS03DNS were added in 2.0  $\mu\text{L}$  increments, and the absorption spectrum recorded.

*PAR stock solution.* The monosodium salt hydrate of 4-(2-pyridylazo)resorcinol was obtained from Aldrich, and dried under reduced pressure over P<sub>2</sub>O<sub>5</sub> for two days at 50 °C. A 9.62 mM solution of PAR was then prepared by dissolving 22.8 mg of the freshly dried material in 10.0 mL of water. After dissolution, this stock solution was stored in the dark at 4 °C.

### **Characterization of Mag-fura-2 extinction coefficient**

Mag-fura-2 is typically used to detect the concentration of divalent metal cations *via* ratiometric fluorescent techniques. In those experiments, the indicator is present in a concentration low enough that its metal binding affinity does not significantly alter the concentration of free metal ions: the concentration of the indicator does not need to be known precisely. Perhaps for this reason, no literature data was available on the extinction coefficient of this compound, even in the papers describing its synthesis,<sup>4</sup> or the determination of its Zn(II) complex K<sub>D</sub>.<sup>48</sup> A determination of the absorbance properties of mag-fura-2 was performed by titration of a concentrated (~20 μM) solution of the indicator with a standardized solution of ZnCl<sub>2</sub>. The results of a typical titration are shown in Figure 2-27.

The titration was performed with the concentration of the indicator roughly 1000-fold that of the K<sub>D</sub> of its Zn(II) complex, so that the addition of zinc would be “quantitative” for early additions. The metal free species has an absorbance maximum at 366 nm, whereas the Zn(II)-bound species maximum is at 325 nm. Isosbestic points were observed at 276 nm and at 343 nm. For each addition of ZnCl<sub>2</sub>, the fraction of free indicator was calculated using the absorbance data at 336 nm, using equation 7. By using data from early points of the titration to extrapolate to zero free indicator, the total quantity of mag-fura-2 in the solution was determined.

$$\text{fraction free} = \frac{1}{A_i} \left[ A - \frac{(A_i - A)}{(A_i - A_f)} A_f \right] \quad (7)$$

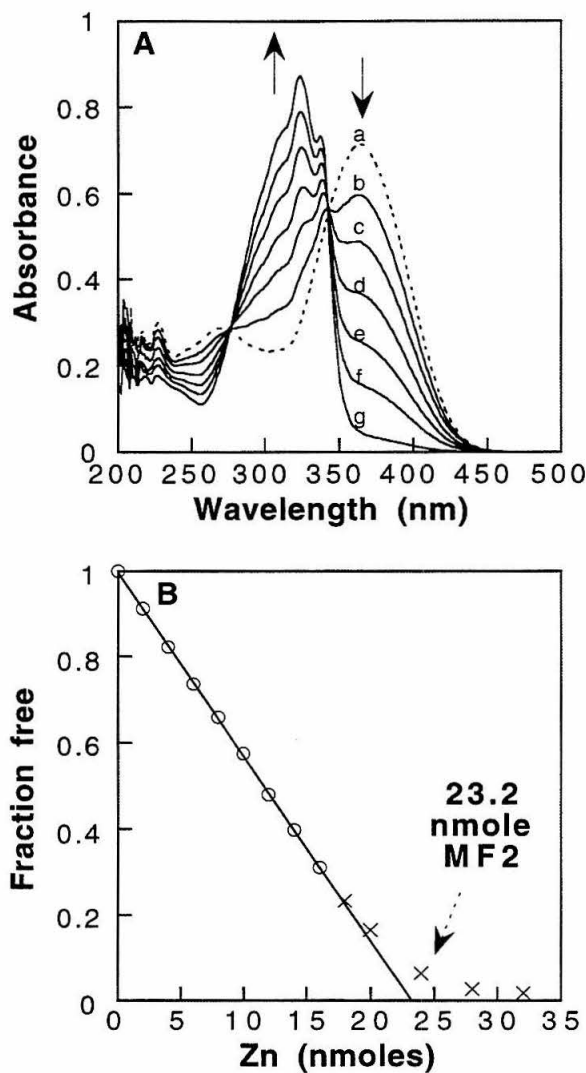


**Figure 2-27.** A typical titration of mag-fura-2 with ZnCl<sub>2</sub>. The assay was performed in 50 mM HEPES, pH 7.0,  $\mu = 0.15$  (NaCl). Plot A: Selected spectra showing increasing concentration of Zn(II); a) mag-fura-2 only ( $\approx 20 \mu\text{M}$ ), b)  $4 \mu\text{M}$  ZnCl<sub>2</sub>, c)  $8 \mu\text{M}$  ZnCl<sub>2</sub>, d)  $12 \mu\text{M}$  ZnCl<sub>2</sub>, e)  $16 \mu\text{M}$  ZnCl<sub>2</sub>, f)  $20 \mu\text{M}$  ZnCl<sub>2</sub>, g)  $230 \mu\text{M}$  ZnCl<sub>2</sub>. Plot B: Determination of the quantity of mag-fura-2 titrated, using the 366 nm wavelength data in plot A.

The absorbance characteristics of mag-fura-2 in both the free and Zn(II) bound state are shown in Figure 2-28. The values obtained for the absorbance maxima are, as expected, within 15% of those reported for the similar fluorescent indicator, fura-2.<sup>3</sup>

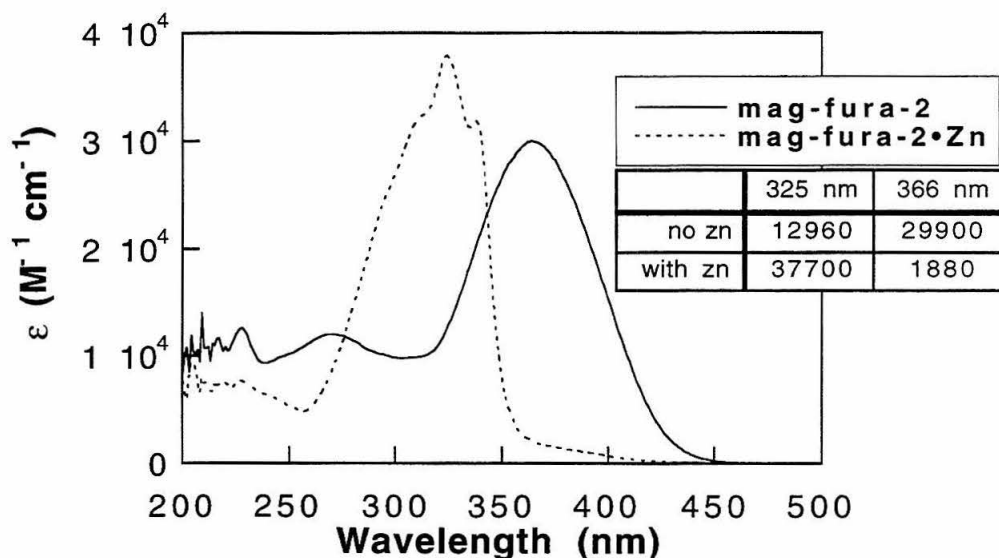


**Figure 2-28.** Concentration-corrected spectra of mag-fura-2 in the absence and presence of Zn(II).

### Competitive zinc binding with mag-fura-2.

The apparent disassociation constant of the mag-fura-2·Zn(II) complex is 20 nM at pH 7.0 and ionic strength 0.15.<sup>48</sup> Consequently, assays performed with mag-fura-2 were conducted in 50 mM HEPES buffer, pH 7.0,  $\mu=0.15$  (NaCl), which was treated to remove adventitious divalent metal ions, and tested for impurities as described above. An aliquot of peptide stock solution (sufficient to deliver 15-30 nmole of peptide) was added to a 1.0 cm cuvette followed by buffer to bring the volume up to 960  $\mu\text{L}$ . The spectrophotometer was blanked against this solution, then 9.0  $\mu\text{L}$  of the stock mag-fura-2 solution was added. The concentration of the mag-fura-2 actually delivered was calculated from the absorbance at 366 nm ( $\epsilon_{366} = 29900 \text{ M}^{-1} \text{ cm}^{-1}$ ). Small aliquots of a

standardized 1.00 mM solution of ZnCl<sub>2</sub> (2.0-4.0 μL) were added, with spectra taken between additions.

Dissociation constants were extracted using literature methods.<sup>43</sup> The variables Q and P are solved for using equations 8 and 9 respectively.

$$Q = \frac{\varepsilon - \varepsilon_{\text{IL}}}{\varepsilon_1 - \varepsilon} \quad (8)$$

$$P = L_t - \frac{1}{Q} K_I - \frac{I_t}{Q+1} \quad (9)$$

Q is equal to the ratio of free indicator to metal-bound indicator,  $\varepsilon$ ,  $\varepsilon_1$ , and  $\varepsilon_{\text{IL}}$  are the observed, free indicator, and metal-bound indicator extinction coefficients respectively. P is the concentration of peptide-metal complex,  $L_t$  is the total ligand (metal) concentration,  $K_I$  is the association constant for the indicator-metal complex, and  $I_t$  is the total indicator concentration.

It can be shown that these variables are related as in equation 10. Thus the binding affinity of the peptide is determined by plotting  $S_t/P$  as a function of Q, where  $S_t$  is the total substrate (peptide) concentration, and  $K_{\text{Pep}}$  is the association constant of interest.

$$\frac{S_t}{P} = \frac{K_I}{K_{\text{Pep}}} Q + 1 \quad (10)$$

A representative plot for FS02DNS is shown in Figure 2-29. In this plot, the slope is equal to  $K_D K_I$  where  $K_D$  is the apparent disassociation constant of interest, and  $K_I$  is the association constant of the mag-fura-2-Zn complex ( $50 \times 10^6 \text{ M}^{-1}$ ). The  $K_D$  determined for the FS02DNS-Zn complex is  $2.9 \pm 0.5 \text{ nM}$  (mean  $\pm \sigma$ ,  $n = 3$ ).

Analysis of the data obtained in the competition of FS04DNS and mag-fura-2 for Zn(II) binding, however, revealed that complex formation with 1:1 peptide:metal stoichiometry did not occur at low concentrations of free Zn(II). Of particular importance for the binding constant determination method described above, the plot should pass through the point (0, 1) if the assumption of 1:1 binding stoichiometry is valid. A plot of the data treated in this manner for FS04DNS is presented in Figure 2-30.

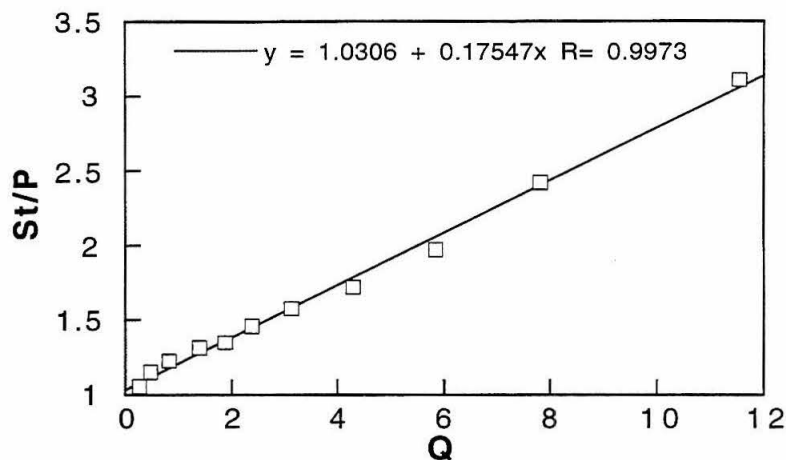


**Figure 2-29.** A representative plot used for determining the disassociation constant for the FS02DNS·Zn complex; these data were calculated using the data obtained as in Figure 2-13. The slope is equal to  $K_D K_I$  where  $K_D$  is the disassociation constant of interest, and  $K_I$  is the association constant of the magfura-2·Zn complex ( $50 \times 10^6 \text{ M}^{-1}$ ).

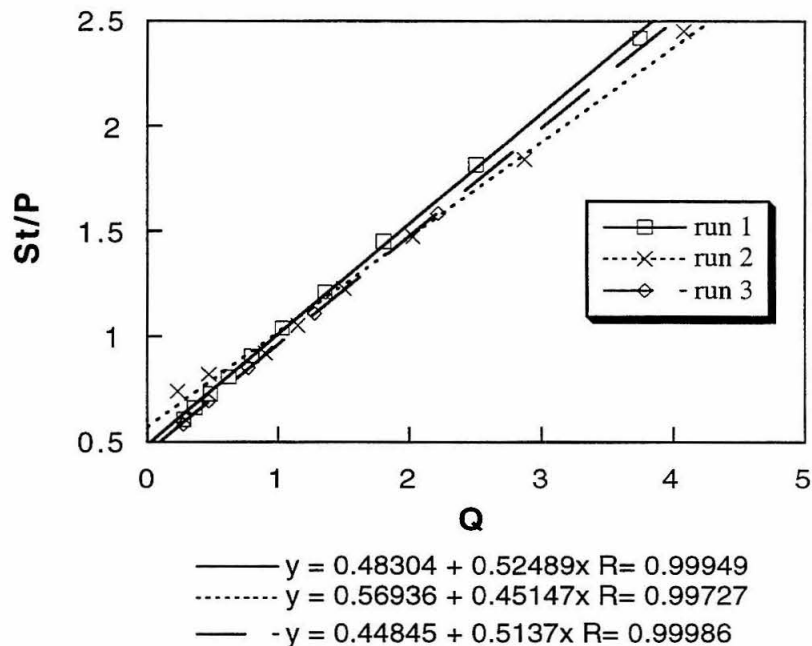


**Figure 2-30.** Analysis of the Zn(II) competition binding assay for FS04DNS revealed that 1:1 peptide:metal complex stoichiometry was not formed. Data were obtained as described in Figure 2-24.

To further probe the zinc binding behavior of FS04DNS, an alternate method was applied,<sup>55,56</sup> wherein the apparent dissociation constant for a presumed peptide:metal complex is calculated for each spectrum in Figure 2-24. The metal binding competition is modeled by plotting  $Zn_{free}$  (abscissa) against  $[ZnI][Pep]/[ZnPep][I]$  (ordinate) where  $ZnI$  is the amount of indicator-bound zinc,  $Pep$  is free FS04DNS,  $ZnPep$  is metal-bound FS04DNS, and  $I$  is indicator which remains unbound. When the plot as described above has a slope of zero, a 1:1 peptide:metal binding stoichiometry is indicated, and the equilibrium manifold as expressed in equation 11 is being sampled.



The ratio  $[ZnI][Pep]/[ZnPep][I]$  is equal to  $K'_D / K_I$ , or the ratio of the apparent dissociation constant of the  $ZnPep$  complex and the indicator-zinc complex (which is known to be 20 nM).<sup>48</sup> Individual values of  $ZnI$ ,  $Pep$ ,  $ZnPep$ , and  $I$  are calculated using equations 12-15.

$$I = A_{366} / 29900 \text{ M}^{-1} \quad (12)$$

$$[ZnI] = [I_{total}] - [I] \quad (13)$$

$$[ZnPep] = [Zn_{total}] - [ZnI] \quad (14)$$

$$[Pep] = [Pep_{total}] - [ZnPep] \quad (15)$$

The data from the mag-fura-2 competition assay treated as described above is presented in Figure 2-31. At values of  $Zn_{free} < 20$  nM, an apparent dissociation constant for the  $ZnPep$  complex is not well described. However, at concentrations of  $Zn_{free}$  above this threshold, the plot has a slope of zero, and a 1:1 peptide:metal complex apparent dissociation constant of 65 ( $\pm 5$ ) nM is described.

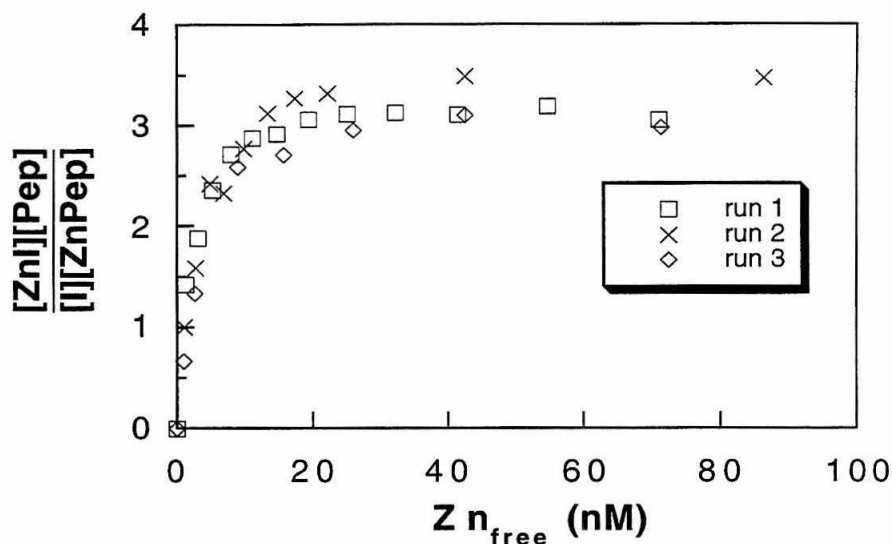


**Figure 2-31.** Analysis of the apparent dissociation constant for the FS04DNS·Zn(II) complex showing 1:1 peptide:metal stoichiometry is observed at free Zn(II) concentrations > 20 nM.

### Molecular modeling

Modeling was performed using InsightII and Discover software (Biosym, San Diego) with the CVFF force field. Coordinates for initial structures were obtained from either Zif268 (PDB accession #1ZAA),<sup>31</sup> or from ZFY-Swap (PDB accession #7ZNF),<sup>52</sup> depending upon the peptide being modeled. After the appropriate metal ligating residues were replaced, minimizations were performed. A typical minimization protocol consisted of 100 steps of steepest descent minimization followed by 1000 steps of conjugate gradient minimization using the restraint parameters shown in Table 2-8. Because the CVFF force field is not parameterized for Zn(II), this atom was replaced with a center-of-mass pseudoatom, using the four ligating atoms as vertices. The restraint distances (flat bottom well) and force constants used were the same as those used in the geometry/molecular dynamics protocol reported for the zinc finger structure of Xfin.<sup>26</sup>

**Table 2-8.** Parameters used for the modeling of the fluorescent sensing peptides.

parameter	value
upper bound	2.2 Å
lower bound	1.5 Å
upper K	400 kcal mole <sup>-1</sup> Å <sup>-2</sup>
lower K	100 kcal mole <sup>-1</sup> Å <sup>-2</sup>
max force	1000 kcal mole <sup>-1</sup> Å <sup>-1</sup>

### Synthesis of the DNC fluorophore

5-*N,N'*-Dimethylamino-1-naphthoic acid was synthesized from 1-naphthoic acid in two steps. First, 5-nitro-1-naphthoic acid was prepared by nitration *via* the method of Ekstrand,<sup>73</sup> as repeated in more recent literature by Bell and Morgan,<sup>74</sup> and Nakayama et al.<sup>75</sup> Following separation of the 5-nitro- and 8-nitro isomers by recrystallization, reductive methylation of the 5-nitro compound was accomplished using the method of Bergel and Stock.<sup>76</sup>

**5-Nitro-1-naphthoic acid.** Synthesis of this compound is well documented in the literature; synthetic details are reported here in case this synthesis is to be repeated in the Imperiali lab. Naphthoic acid (96% 1-isomer, remainder 2-isomer) was obtained from Aldrich, and recrystallized from hot toluene twice to afford pale caramel-colored flakes. A 250 mL round bottom flask, equipped with a stir bar and reflux condenser was charged with 1-naphthoic acid (10 g, 58 mmole), and high-purity concentrated nitric acid (40 mL,  $\rho = 1.42$ , 15.8 N, 630 mmole) was added cautiously. The flask was heated on an oil bath to 85 °C, and the reaction stirred for 1.5 hours. At that time, the contents of the flask had changed appearance to a lemon-yellow slurry. Water (20 mL) was added to disperse the slurry, and stirring was continued an additional 3 h. The flask was removed from the oil-

bath and the contents poured onto ~50 mL of ice. The precipitate was filtered, washed with water, and the yellow solid transferred to a 500 mL glass beaker. The solid was dissolved in 150 mL of 10% w/v Na<sub>2</sub>CO<sub>3</sub> and filtered. This solution was allowed to cool, then acidified with 6N HCl dropwise. (Caution. Solution foams and forms a solid simultaneously.) The solid was dried to afford 11 g of mixed nitro-isomers. Recrystallization from 300 mL of hot ethanol (95%) gave 4.12 g (33%) of the desired compound.

**1-*N,N'*-Dimethylamino-5-naphthoic acid.** A 100 mL, 2-neck round bottom flask was fitted with one septum, and charged with a stir bar, 5-nitro-1-naphthoic acid (1.00 g, 4.61 mmole), ethanol (23 mL), NaOAc.3H<sub>2</sub>O (1.25 g, 9.2 mmole), 37% w/v formaldehyde in water (2.5 mL, 1 g formaldehyde, 33 mmole), and 10% Pd/C (0.8 g). A H<sub>2</sub>-filled balloon was attached to the flask via a stopcock, the flask was evacuated, and then placed under a hydrogen atmosphere. Analysis by TLC showed no starting material remained after 36 h. The slurry was filtered through celite, and the eluent concentrated to dryness. Water (75 mL) was added, and the solution extracted with CH<sub>2</sub>Cl<sub>2</sub> (5 × 25 mL). The organic layers were combined, dried (Na<sub>2</sub>SO<sub>4</sub>), and concentrated to *ca.* 5 mL volume. Purification was performed by flash chromatography using Florisil as the stationary phase, eluting with CH<sub>2</sub>Cl<sub>2</sub> (200 mL) followed by 95:5 CH<sub>2</sub>Cl<sub>2</sub> : MeOH (200 mL), 90:10 CH<sub>2</sub>Cl<sub>2</sub> : MeOH (200 mL) and finally the remainder of the product removed from the column with methanol. Pure product (307 mg, 31%) was obtained from the first 600 mL of eluent. The methanol fractions contained the desired compound and silica. These fractions were pooled, dissolved in CHCl<sub>3</sub> (40 mL), and washed with water (3 x 30 mL) to afford a further 0.17 g (17%) for a combined 48% yield.

In later experiments it was determined that the crude product could be dissolved in CH<sub>2</sub>Cl<sub>2</sub>, washed with water, and then recrystallized by vapor diffusion from CH<sub>2</sub>Cl<sub>2</sub> with a surrounding atmosphere of hexanes to give pure product in similar yield.

## References

1. "Fluorescent Indicators for Cytosolic Sodium," Minta, A.; Tsien, R. Y. *J. Biol. Chem.* **1989**, *264*, 19449-19457.
2. "New Calcium Indicators and Buffers with High Selectivity against Magnesium and Protons: Design, Synthesis, and Properties of Prototype Structures," Tsien, R. Y. *Biochemistry* **1980**, *19*, 2396-2404.
3. "A New Generation of  $\text{Ca}^{2+}$  Indicators with Greatly Improved Fluorescence Properties," Grynkiewicz, G.; Poenie, M.; Tsien, R. Y. *J. Biol. Chem.* **1985**, *260*, 3440-3450.
4. "A Fluorescent Indicator for Measuring Cytosolic Free Magnesium," Raju, B.; Murphy, E.; Levy, L. A.; Hall, R. D.; London, R. E. *Am. J. Physiol.* **1989**, *256*, C540-C548.
5. "Intracellular pH Measurement Using Single Excitation-Equal Emission Fluorescence Ratios," Bassnett, S.; Reinisch, L.; Beebe, D. C. *Am. J. Physiol.* **1990**, *258*, C171-C178.
6. "Cytoplasmic pH and free  $\text{Mg}^{2+}$  in lymphocytes," Rink, T. J.; Tsien, R. Y.; Pozzan, T. *J. Cell Biol.* **1982**, *95*, 189-196.
7. "Supramolecular Chemistry, Fluorescence, and Sensing," In *Fluorescent Chemosensors for Ion and Molecule Recognition*; Czarnik, A. W.; Czarnik, A. W.; ACS, Washington D.C., 1993; pp 1-9.
8. "Trace Elements in Sea Water," Bruland, K. W.; Rilet, J. P.; Chester, R.; Academic Press, London, 1975; pp 157-220.
9. "The Biological Chemistry of the Elements: The Inorganic Chemistry of Life," Fraústo da Silva, J. J. R.; Willams, R. J. P.; Clarendon Press: New York, 1993.
10. "Fluorescent Protein Biosensors: Measurement of Molecular Dynamics in Living Cells," Giuliano, K. A.; Post, P. L.; Hahn, K. M.; Taylor, D. L. *Ann. Rev. Biophys. Biomol. Struct.* **1995**, *24*, 405-434.

11. "Enzyme-Based Fiber Optic Zinc Biosensor," Thompson, R. B. *Anal. Chem.* **1993**, *65*, 730-734.
12. "Lifetime-Based Fluorescence Energy Transfer Biosensing of Zinc," Thompson, R. B.; Patchan, M. W. *Anal. Biochem.* **1995**, *227*, 123-128.
13. "A Luminescence-Based Mercury Biosensor," Virta, M.; Lampinen, J.; Karp, M. *Anal. Chem.* **1995**, *67*, 667-669.
14. "Fiber Optic Biosensor for Co(II) and Cu(II) Based on Fluorescence Energy Transfer with an Enzyme Transducer," Thompson, R. B.; Ge, Z.; Patchan, M.; Huang, C.-C.; Fierke, C. A. *Biosensors & Bioelectronics* **1996**, *11*, 557-564.
15. "Fluorescence Ratio Imaging of Cyclic AMP in Single Cells," Adams, S. R.; Harootunian, A. T.; Buechler, Y. J.; Taylor, S. S.; Tsien, R. Y. *Nature* **1991**, 694-697.
16. "Desperately Seeking Sensors," Czarnik, A. W. *Chem. Bio.* **1995**, *2*, 423-428.
17. "On the Metal Ion Specificity of "Zinc Finger" Proteins," Berg, J. M.; Merkle, D. L. *J. Am. Chem. Soc.* **1989**, *111*, 3759-3761.
18. "Metal-dependent Folding of a Single Zinc Finger from Transcription Factor IIIA," Frankel, A. D.; Berg, J. M.; Pabo, C. O. *Proc. Natl. Acad. Sci. U.S.A.* **1987**, *84*, 4841-4845.
19. "Protein Motifs 5: Zinc Fingers," Klug, A.; Schwabe, J. W. R. *FASEB J.* **1995**, *9*, 597-604.
20. "Metallopeptide Design: Tuning the Metal Cation Affinities With Unnatural Amino Acids and Peptide Secondary Structure," Cheng, R. P.; Fisher, S. L.; Imperiali, B. *J. Am. Chem. Soc.* **1996**, *118*, 11349-11356.
21. "New Synthetic Amino Acids for the Design and Synthesis of Peptide-Based Metal Ion Sensors," Torrado, A.; Imperiali, B. *J. Org. Chem.* **1996**, *61*, 8940-8948.
22. "Ligand Variation and Metal Ion Binding Specificity in Zinc Finger Peptides," Krizek, B. A.; Merkle, D. L.; Berg, J. M. *Inorg. Chem.* **1993**, *32*, 937-940.

23. "Complexes of Zinc Finger Peptides with Ni<sup>2+</sup> and Fe<sup>2+</sup>," Krizek, B. A.; Berg, J. M. *Inorg. Chem.* **1992**, *31*, 2984-2986.
24. "Zinc Finger Domains: From Predictions to Design," Berg, J. M. *Acc. Chem. Res.* **1995**, *28*, 14-19.
25. "Time-Resolved Energy Transfer Measurements of Donor-Acceptor Distance Distributions and Intramolecular Flexibility of a CCHH Zinc Finger Peptide," Eis, P. S.; Lakowicz, J. R. *Biochemistry* **1993**, *32*, 7981-7993.
26. "Three-Dimensional Solution Structure of a Single Zinc Finger DNA-Binding Domain," Lee, M. S.; Gippert, G. P.; Soman, K. V.; Case, D. A.; Wright, P. E. *Science* **1989**, *245*, 635-637.
27. "MOLSCRIPT: A Program to Produce Both Detailed and Schematic Plots of Protein Structure," Kraulis, P. J. *J. Appl. Crystallogr.* **1991**, *24*, 946-950.
28. Sinha Roy, R., Ph.D. Thesis, California Institute of Technology, **1996**.
29. "Automated Allyl Cleavage for Continuous-Flow Synthesis of Cyclic and Branched Peptides," Kates, S. A.; Daniels, S. B.; Albericio, F. *Anal. Biochem.* **1993**, *212*, 303-310.
30. "Covalent Fluorescent Probes," In *Excited States of Biopolymers*; Haugland, R. P.; Sheiner, R. F.; Plenum, New York, 1983; pp 29-58.
31. "Zinc Finger-DNA Recognition: Crystal Structure of a Zif268-DNA Complex at 2.1 Å," Pavletich, N. P.; Pabo, C. O. *Science* **1991**, *252*, 809-817.
32. "Solvation of TICT States in Solvent Mixtures," Ghoneim, N.; Suppan, P. *Pure & Appl. Chem.* **1993**, *65*, 1739-1743.
33. "Twisted Intramolecular Charge Transfer States (TICT). A New Class of Excited States With a Full Charge Separation," Grabowski, Z. R.; Rotkiewicz, K.; Siemiarczuk, A.; Cowley, D. J.; Baumann, W. *Nouv. J. Chim.* **1979**, *3*, 443-454.
34. "Charge Separation in Excited States of Decoupled Systems- TICT Compounds and Implications Regarding the Development of New Laser Dyes and the Primary

- Processes of Vision and Photosynthesis,” Rettig, W. *Angew. Chem. Int. Ed. Engl.* **1986**, *25*, 971-988.
35. “Chemical Reactivity of the TICT states. Unusual Quenching by Fluoride Ion and by Hard and Soft Bases,” Kolos, R.; Grabowski, Z. R. *Journal of Molecular Structure* **1982**, *84*, 251-258.
36. “Twisted Intramolecular Charge Transfer (TICT) Excited States: Energy and Molecular Structure,” Grabowski, Z. R.; Dobkowski, J. *Pure & Appl. Chem.* **1983**, *55*, 245-252.
37. “Fluorescent Sensors of Molecular Recognition. Modified Cyclodextrins Capable of Exhibiting Guest-Responsive Twisted Intramolecular Charge Transfer Fluorescence,” Hamasaki, K.; Ikeda, H.; Nakamura, A.; Ueno, A.; Toda, F., et al. *J. Am. Chem. Soc.* **1993**, *115*, 5035-5040.
38. “Zinc-Dependent Structure of a Single-Finger Domain of Yeast ADR1,” Párraga, G.; Horvath, S. J.; Eisen, A.; Taylor, W. E.; Hood, L. E., et al. *Science* **1988**, *241*, 1489-1492.
39. “Alternating Zinc-Finger Motifs in the Human Male-Associated Protein ZFY,” Weiss, M. A.; Mason, K. A.; Dahl, C. E.; Keutmann, H. T. *Biochemistry* **1990**, *29*, 5660-5664.
40. “A Consensus Zinc Finger Peptide: Design, High-Affinity Metal Binding, a pH-Dependent Structure, and a His to Cys Sequence Variant,” Krizek, B. A.; Amann, B. T.; Kilfoil, V. J.; Merkle, D. L.; Berg, J. M. *J. Am. Chem. Soc.* **1991**, *113*, 4518-4523.
41. “Cobalt as Probe and Label of Proteins,” Maret, W.; Vallee, B. L. *Meth. Enzym.* **1993**, *226*, 52-71.
42. “High Spin Cobalt(II) as a Probe for the Investigation of Metalloproteins,” Bertini, I.; Luchinat, C. *Adv. Inorg. Biochem.* **1984**, *6*, 71-111.

43. "Binding Constants: The Measurement of Molecular Complex Stability," Connors, K. A.; Wiley-Interscience: New York, 1987.
44. "Geometry of Interaction of Metal Ions with Histidine Residues in Protein Structures," Chakrabarti, P. *Protein Eng.* **1990**, *4*, 57-63.
45. "Stability Constants of Metal Complexes," In *Data for Biochemical Research*; Dawson, R. M. C.; Elliott, D. C.; Elliott, W. H.; Jones, K. M.; Clarendon, Oxford, 1986; pp 399-415.
46. "Bonding and Spectra of Complexes," In *Inorganic Chemistry*; Shriver, D. E.; Atkins, P. W.; Langford, C. H.; W. H. Freeman, New York, 1990; pp 434-464.
47. "Alternating Zinc-Finger Motifs in the Human Male-Associated Protein ZFY: Defining Architectural Rules by Mutagenesis and Design of an "Aromatic Swap" Second-Site Revertant," Weiss, M. A.; Keutmann, H. T. *Biochemistry* **1990**, *29*, 9808-9813.
48. "Measurement of Free Zn<sup>2+</sup> Ion Concentration With the Fluorescent Probe Magfura-2 (Furaptra)," Simons, T. J. B. *J. Biochem. Biophys. Methods* **1993**, *27*, 25-37.
49. "Architectural Rules of the Zinc-Finger Motif: Comparative Two-Dimensional NMR Studies of Native and 'Aromatic-Swap' Domains Define a 'Weakly Polar Switch,'" Kochoyan, M.; Keutmann, H. T.; Weiss, M. A. *Proc. Natl. Acad. Sci. U.S.A.* **1991**, *88*, 8455-8459.
50. "Structures of DNA-Binding Mutant Zinc Finger Domains: Implications for DNA Binding," Hoffman, R. C.; Horvath, S. J.; Klevit, R. E. *Protein Sci.* **1993**, *2*, 951-965.
51. "High Resolution Three-Dimensional Structure of a Stable Zinc Finger from Human Enhancer Binding Protein," Omichinski, J. G.; Clore, G. M.; Appella, E.; Sakaguchi, K.; Gronenborn, A. M. *Biochemistry* **1990**, *29*, 9324-9334.
52. "Alternating Zinc Fingers in the Human Male-Associated Protein ZFY: 2D NMR Structure of an Even Finger and Implications for "Jumping-Linker" DNA

- Recognition,” Kochoyan, M.; Keutmann, H. T.; Weiss, M. A. *Biochemistry* **1991**, *30*, 3371-3386.
53. “Two-Dimensional NMR Studies of the Zinc Finger Motif: Solution Structures and Dynamics of Mutant ZFY Domains Containing Aromatic Substitutions in the Hydrophobic Core,” Qian, X.; Weiss, M. A. *Biochemistry* **1992**, *31*, 7463-7476.
54. “Aromatic-Aromatic Interactions in the Zinc Finger Motif,” Jasnoff, A.; Kochoyan, M.; Frenkel, E.; Lee, J. P.; Weiss, M. A. *J. Mol. Biol.* **1992**, *225*, 1035-1047.
55. “The Use of 4-(2-Pyridylazo)resorcinol in Studies of Zinc Release from *Escherichia coli* Aspartate Carbamoylase,” Hunt, J. B.; Neece, S. H.; Ginsburg, A. *Anal. Biochem.* **1985**, *146*, 150-157.
56. “Characterization of Indo-1 and Quin-2 as Spectroscopic Probes for  $Zn^{2+}$ -Protein Interactions,” Jefferson, J. R.; Hunt, J. B.; Ginsburg, A. *Anal. Biochem.* **1990**, *187*, 328-336.
57. “Interaction of Metal Ions with Carboxylic and Carboxamide Groups in Protein Structures,” Chakrabarti, P. *Protein Eng.* **1990**, *4*, 49-56.
58. “Systematics in the Interaction of Metal Ions with the Main-Chain Carbonyl Group in Protein Structures,” Chakrabarti, P. *Biochemistry* **1990**, *29*, 651-658.
59. “Effects of Solvents on Fluorescence Emission,” In *Principles of Fluorescence Spectroscopy*; Lakowicz, J. R.; Plenum Press, New York, 1983; pp 189-218.
60. “Synthesis and Spectral Properties of a Hydrophobic Fluorescent Probe: 6-Propionyl-2-(dimethylamino)naphthalene,” Weber, G.; Farris, F. J. *Biochemistry* **1979**, *18*, 3075-3078.
61. “Interaction of Fluorescent Adenine Nucleotide Derivatives with the ADP/ATP Carrier in Mitochondria. A. Comparison of Various 3'-O-Ester Adenine Nucleotide Derivatives,” Mayer, I.; Dahms, A. S.; Riezler, W.; Klingenberg, M. *Biochemistry* **1984**, *23*, 2436-2442.

62. "Metal-Binding and Folding Properties of a Minimalist Cys<sub>2</sub>His<sub>2</sub> Zinc Finger Peptide," Michael, S. F.; Kilfoil, V. J.; Schmidt, M. H.; Amann, B. T.; Berg, J. M. *Proc. Natl. Acad. Sci. U.S.A.* **1992**, *89*, 4796-4800.
63. "Metal Binding Properties of Single Amino Acid Deletion Mutants of Zinc Finger Peptides: Studies Using Cobalt (II) as a Spectroscopic Probe," Shi, Y. G.; Beger, R. D.; Berg, J. M. *Biophys. J.* **1993**, *64*, 749-753.
64. "A Fluorescent Zinc Probe Based on Metal-Induced Peptide Folding," Godwin, H. A.; Berg, J. M. *J. Am. Chem. Soc.* **1996**, *118*, 6514-6515.
65. "Acids and Bases," Pearson, R. G. *Science* **1966**, *151*, 172-177.
66. "Advanced Inorganic Chemistry," Cotton, F. A.; Wilkinson, G.; John Wiley & Sons, Inc.: New York, 1988.
67. "Structural Aspects of Metal Liganding to Functional Groups in Proteins," Glusker, J. P. *Adv. Prot. Chem.* **1991**, *42*, 1-76.
68. "Handbook of Fluorescent Probes and Research Chemicals," Haughland, R. P.; Molecular Probes: 1996.
69. "A Cleavage Method Which Minimizes Side Reactions Following Fmoc Solid Phase Peptide Synthesis," King, D. S.; Fields, C. G.; Fields, G. B. *Int. J. Pep. Protein Res.* **1990**, *36*, 255-266.
70. "Reassessment of Ellman's Reagent," Riddles, P. W.; Blakeley, R. L.; Zerner, B. *Meth. Enzym.* **1983**, *91*, 49-60.
71. "Vogel's Textbook of Quantitative Inorganic Analysis," Bassett, J.; Denney, R. C.; Jeffery, G. H. Mendham, J.; William Clowes: London, 1978.
72. "Elimination of Adventitious Metals," Holmquist, B. *Meth. Enzym.* **1988**, *158*, 6-12.
73. Ekstrand, A. G. *J. Prakt. Chem* **1888**, *38*, 139.
74. "The Optical Resolution of 1,1'-Dinaphthyl-5,5'-dicarboxylic Acid," Bell, F.; Morgan, W. H. D. *J. Chem. Soc.* **1954**, 1716-1718.

75. "Synthesis and Structure-Activity Study of Protease Inhibitors. II. Amino- and Guanidino-Substituted Naphthoates and Tetrahydronaphthoates," Nakayama, T.; Okutome, T.; Matsui, R.; Kurumi, M.; Sakurai, Y., et al. *Chem. Pharm. Bull. Jpn.* **1984**, *32*, 3968-3980.
76. Bergel; Stock *J. Chem. Soc.* **1959**, 90.

**Chapter 3. Fluorescent Peptidyl Chemosensors for Divalent Zinc  
Incorporating Novel  $\alpha$ -Amino Acids that Contain 8-Hydroxyquinoline**

Reprinted in part with permission from *J. Org. Chem.*, submitted for publication.  
Unpublished work copyright 1998 American Chemical Society.

## Introduction

The fluorescent chemosensors based upon the zinc finger domains, presented in Chapter 2, enable sensitive and selective measurements of Zn(II) in aqueous media. Of the peptides presented, FS03DNS enables the detection of 100 nM increments of free Zn(II) in the presence of excess competing species, yet suffers from oxidative degradation by the formation of an intramolecular disulfide. The peptide FS04DNS was designed to address this limitation, resulting in the production of a chemosensor with enhanced oxidative stability.

These results were immensely encouraging, and provided the initial “proof of concept” for the design of peptidyl fluorescent chemosensors. However, from the standpoint of chemosensor design, there are several features of these devices that were identified as targets for improvement. First, the zinc-induced fluorescence increase and zinc-binding selectivity of the oxidatively robust peptide were reduced relative to the parent motif. Because the sensors FS03DNS and FS04DNS differed only in the identity of a single metal-binding residue, this result suggests that the mechanism of signal transduction, i.e., *microenvironment sensitive fluorescence*, is dependent upon small changes in the peptide primary sequence. This is an undesirable result as the fluorophore and metal-ligating residues of those constructs were desired to act independently; the choice of residues used to construct of the selective metal-binding site should not be limited by unpredictable effects on the fluorescence response of the sensor. In addition, relatively small increases in fluorescence enhancement (FE) were observed, even for the most responsive chemosensor, FS03DNS, suggesting that the magnitude of the microenvironment change experienced by the reporting group could be a limiting factor in the continued development of these devices. Indeed, solvent-sensitive fluorophores such as the dansyl group are considerably larger than the naturally encoded amino acids, and can dominate even “large” peptidyl motifs. This “steric dilemma” is graphically demonstrated in Figure 3-1, wherein the side chain of the Dap(dansyl) residue is

highlighted in a CPK model of FS03DNS. The construction of even larger sensing molecules is of course possible, but is effectively invalidated if sensors compatible with solid-phase attachment are considered. Such a modification would allow the production of regenerable sensing materials, but obtaining materials of sufficient purity is rendered excessively difficult for motifs  $\geq 10$  residues in length.

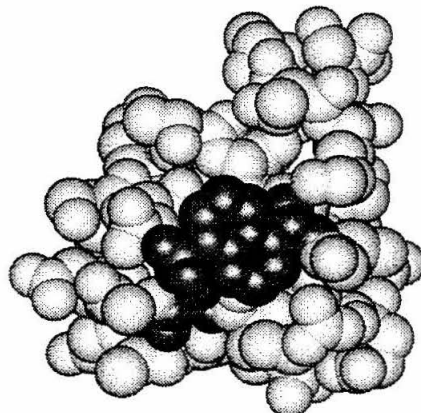


**Figure 3-1.** A CPK model of the sensor FS03DNS, with the side chain of the Dap(dansyl) residue highlighted. The fluorophore is too large to be accommodated within, yet may associate beside the hydrophobic cluster.

To address these difficulties, new strategies for producing selective sensors for Zn(II) were considered, with attention directed towards minimizing the amount of peptidyl architecture required for sensing. The well-known ligand 8-hydroxyquinoline (oxine) has historically found use as an analytical reagent for the fluorometric quantitation of Zn(II),<sup>1</sup> as well as other metal ions (Figure 3-2).<sup>2</sup> However, this ligand has insufficient Zn(II)-binding selectivity to be applied toward Zn(II) measurements in complex solutions.<sup>3</sup>

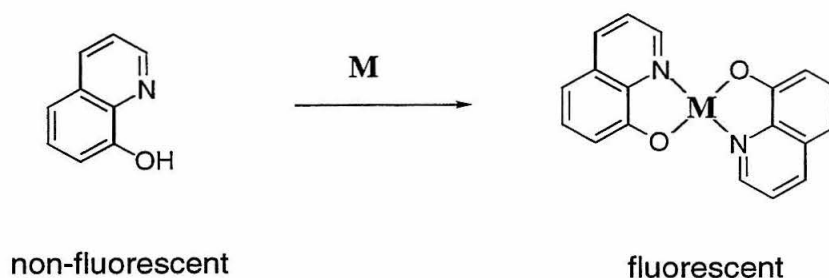


**Figure 3-2.** 8-Hydroxyquinoline forms fluorescent complexes with several metal ions.

Regardless of the insufficient selectivity of 8-hydroxyquinoline for direct use as a  $\text{Zn(II)}$  sensor, oxine and its derivatives display impressive chelation-enhanced fluorescence (CHEF) in the presence of the appropriate metal ions; the fluorescence spectra for a typical titration of oxine with  $\text{ZnCl}_2$  in aqueous solution is shown in Figure 3-4. CHEF is a commonly occurring phenomenon, observed for a variety of organic fluorophores. This mechanism has been exploited extensively in the design of sensors (for  $\text{Na}^+$ ,  $\text{K}^+$ , and pH), and has been extensively reviewed.<sup>4-9</sup> While no *general* explanation of this photophysical mechanism has been developed,<sup>5</sup> the cause of the CHEF observed for oxine is well understood.

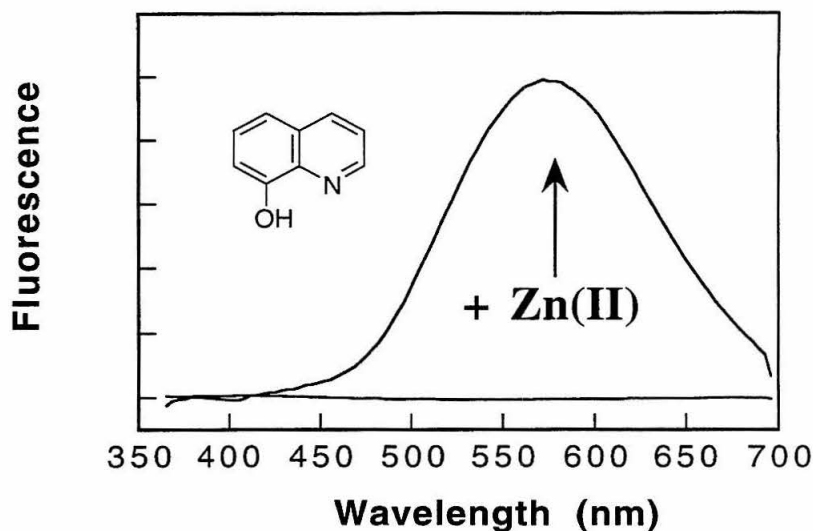


**Figure 3-3.** Fluorescence emission spectra of oxine ( $40 \mu\text{M}$ ) in 50 mM HEPES, pH 7.0, both before and after the addition of  $\text{ZnCl}_2$  ( $75 \mu\text{M}$ ). Excitation performed at 355 nm.

The increase in fluorescence observed upon the binding of an appropriate metal ion to oxine results from a change in the electronic properties of the ligand, producing a longer-wavelength absorbance for the ligand-metal complex than is present for the ligand itself (Figure 3-4). An advantage of using this fluorescence mechanism for signal transduction is that excitation of the ligand-metal complex can be performed at a wavelength that the ligand itself does not absorb (e.g., 355 nm). Due to this fact, the relative increase in quantum yield upon  $\text{Zn(II)}$  binding is theoretically infinite and in practice very large FEs can be observed.

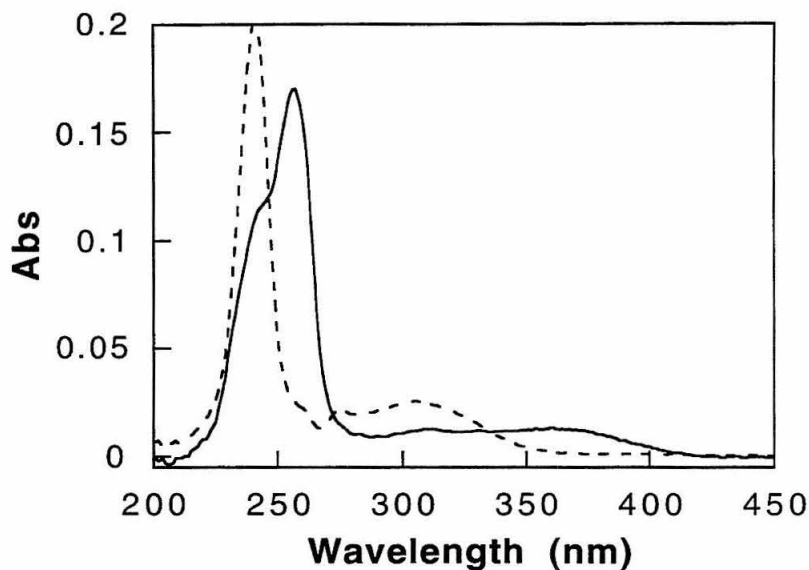


**Figure 3-4.** Absorption spectra of 8.0  $\mu\text{M}$  oxine in the absence (dashed line) and presence (solid line) of 1 equivalent  $\text{ZnCl}_2$ . Spectra were taken in a 1.0 cm cuvette at pH 7.0 in 50 mM HEPES.

With the impressive precedent of attaining highly selective  $\text{Zn(II)}$ -binding peptidyl motifs described in Chapter 2, efforts were directed towards harnessing the fluorescence properties of this ligand within the framework of nonstandard  $\alpha$ -amino acid derivatives suitable for solid phase peptide synthesis (Figure 3-5); two regioisomers with differing points of side chain attachment were prepared to allow for the construction of peptidyl motifs with different chelation geometries. The availability of such oxine-containing residues would enable the production of peptidyl chemosensors that employ a “direct” mechanism of fluorescence modulation, reducing the requirements for structural complexity and bulk demanded of the peptidyl host.

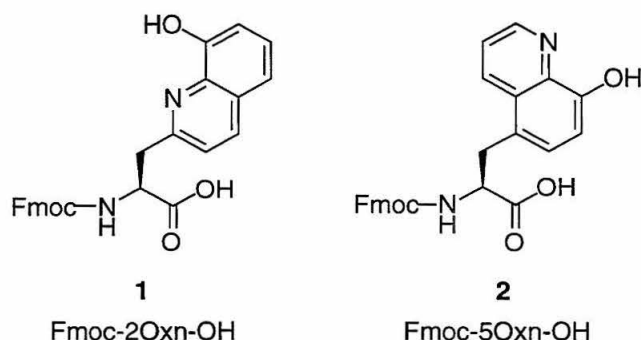


**Figure 3-5.** The chemical structures of Fmoc-2Oxn-OH and Fmoc-5Oxn-OH.

For the production of Zn(II) chemosensors containing the oxine chromophore, it is important to bear in mind that ions other than those that produce CHEF can also bind, and produce an absorption band similar to that observed for Zn(II). The presence of this band is a necessary but not a sufficient condition for fluorescence. The outcome of this result is that *fluorescence* selectivity and *metal-binding* selectivity operate independently for this ligand.

Indeed, the bidentate metal-binding provided by this ligand provides a competent nucleus for the facile construction of a metal binding site that may be modulated through the appropriate delivery of accessory functionality. Oxine is known to form both 1:1 and 2:1 ligand:metal complexes with a variety of metal cations, many of these with high affinity (see Table 3-1). Because the proposed peptidyl chemosensors that will employ the oxine-containing amino acid have been designed to contain a 1:1 peptide:metal complex, it is most meaningful to compare the  $\log K_1$  values shown in Table 3-1. In the absence of other factors, oxine is selective for binding Ni(II) and Cu(II) by >1 and >3 orders of magnitude respectively. These data highlight the importance that the peptidyl host must have for the ultimate generation of metal binding selectivity.

**Table 3-1.** Stability constants of oxine-metal complexes at 20 °C in 50% v/v aqueous dioxane.<sup>10</sup>

	Mg(II)	Zn(II)	Ni(II)	Cu(II)
log K <sub>1</sub>	5.04	9.34	10.43	13.03
log K <sub>2</sub>	4.29	8.22	9.97	12.35

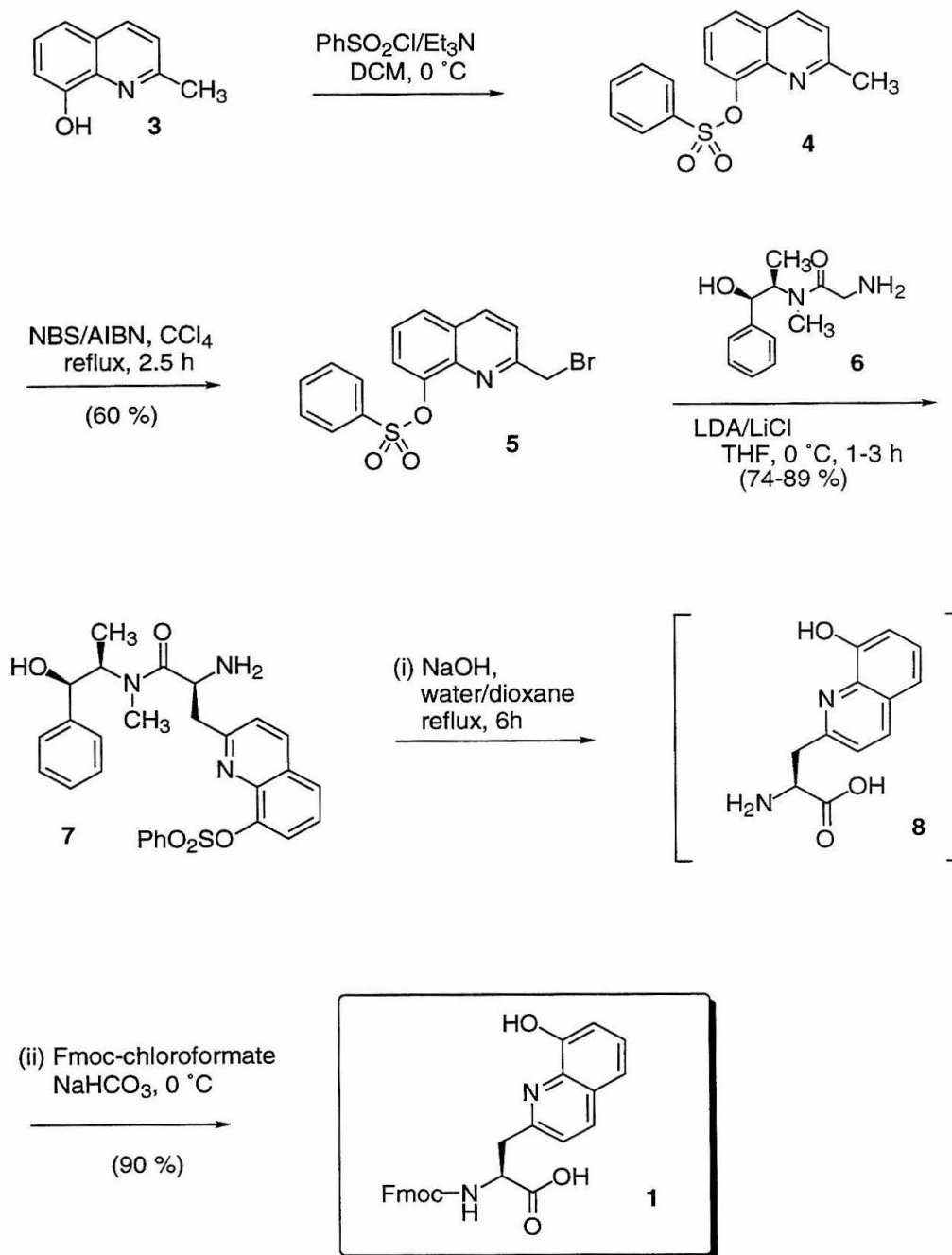
The remainder of this chapter presents the syntheses of (*S*)-2-amino-*N*<sup>α</sup>-9-fluorenylmethoxycarbonyl-3-(oxine-2-yl)-propanoic acid (Fmoc-2Oxn-OH, **1**), and (*S*)-2-amino-*N*<sup>α</sup>-9-fluorenylmethoxycarbonyl-3-(oxine-5-yl)-propanoic acid (Fmoc-5Oxn-OH, **2**), and the peptide-incorporation of these residues in heptapeptides capable of reporting sub-micromolar levels of Zn(II).

## Results and Discussion

### Synthesis of Fmoc-2Oxn and Fmoc-5Oxn.

The synthesis of **1**, employing the Myers pseudoephedrine glycinamide alkylation<sup>11,12</sup> in the key stereogenic step, is outlined in Scheme 1. Starting from commercially available 8-hydroxy-2-methylquinoline (**3**), bromide **4** was prepared in two steps *via* protection of the phenol as the benzenesulfonate ester, followed by free radical bromination. The (*R, R*)-(-) enantiomer of pseudoephedrine glycinamide (**6**) was chosen for alkylations in order to yield as the major diastereomer, the α-amino acid derivative **7** possessing the L-configuration.

## Scheme 3-1. Synthesis of Fmoc-2Oxn-OH.



The optimal temperature for the Myers' alkylation procedure have been shown to vary depending on the reactivity of the electrophile,<sup>12</sup> and generally a compromise between chemical yield and diastereoselectivity must be made. Alkylations attempted with both **5** and **13** at -78 °C and -45 °C suffered from precipitation of the bromide. Consequently, alkylations were performed by adding one equivalent of **5** or **13** in chilled (0 °C) THF to 1.0- 2.0 equivalents of the enolate of pseudoephedrine glycinamide, also at 0 °C. After addition of the electrophile, the reaction vessel was transferred to a 0 °C ice bath and allowed to stir until consumption of the bromide was complete (~2-4 hours). Based on these studies, the use of a two-fold excess of the chiral auxiliary **6** per equivalent of electrophile is recommended in order to drive reactions to completion within 1-3 hours when conducted at 0 °C. While no attempt was made to determine the diastereoselectivity of the alkylation reaction, isolated yields of **7** as high as 89% were achieved, in > 95% de as determined by <sup>1</sup>H NMR.

The sensitivity of the alkylation reaction to exogenous moisture has been carefully documented previously.<sup>12</sup> However, the maintenance of scrupulously dry apparatus and reagents is of such critical importance that it deserves additional mention. Particular care should be taken to assure that the chiral auxiliary is absolutely dry: anhydrous pseudoephedrine glycinamide is extremely hygroscopic and should be handled with careful attention to avoid water contamination. The crystalline monohydrate of pseudoephedrine glycinamide and the anhydrous powder have melting points of 84-86 °C and 78-80 °C respectively.<sup>13</sup> Additionally, it has been noted that anhydrous **6** dissolves rapidly in dry THF, whereas the monohydrate dissolves sluggishly. Lyophilization of **6** from benzene has proven to be a reliable method for the dehydration of a partially hydrated sample. (Precipitation from dry toluene often produces an oil rather than a powder.)

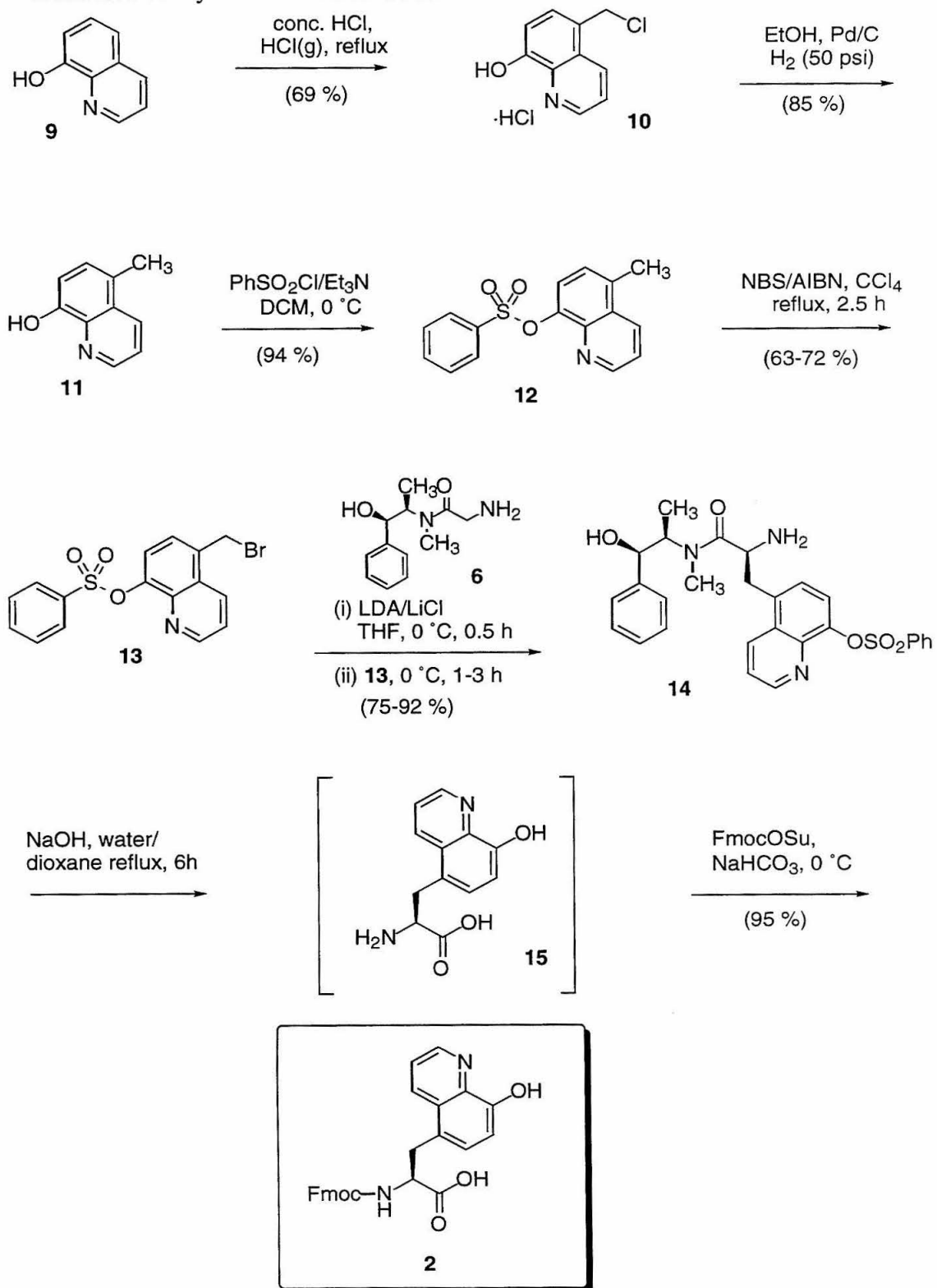
Hydrolysis of purified **7** was performed under basic conditions (0.5 M NaOH, 4 eq.) in refluxing 1:1 water:dioxane for 4-6 hours. At the end of this time, the dioxane

was removed under reduced pressure, followed by extraction of the liberated pseudoephedrine into dichloromethane (DCM). The *N*-methyl amide of alkylated pseudoephedrine glycinamide derivatives is hydrolyzed under relatively mild conditions (1,5 *N*→*O* acyl migration is proposed to facilitate the process). As a result, the removal of the chiral auxiliary is usually complete after 1-2 h. However, complete removal of the benzenesulfonate aryl ester requires protracted reaction times. Even under these conditions any racemization of the resultant  $\alpha$ -amino acid (**8**) was negligible; chiral HPLC analysis of the hydrolysis products shows that the deprotected amino acid is formed in  $\geq 95$  % ee. Rather than purify the intermediate amino acid **8**, the basic aqueous solution resulting from the hydrolysis reaction was instead buffered with NaHCO<sub>3</sub>, and the  $\alpha$ -amine protected as the 9-fluorenylmehyloxycarbonyl (Fmoc) derivative to provide **1** in 90% yield and > 95% ee. (The optical integrity of compounds **1** and **2** were verified by chiral HPLC analysis after removal of the *N* $\alpha$ -Fmoc protecting group; for details see the experimental section.)

The synthesis of **2**, outlined in Scheme 3-2, was performed using a strategy analogous to that used for the preparation of **1**. Commercial availability of methyl-substituted 8-hydroxyquinoline derivatives is limited to the 2-substituted compound. Accordingly, methods for constructing other methyl-substituted 8-hydroxyquinolines were assessed. Several of these compounds are accessible *via* the Skraup reaction, yet in low yields.<sup>14</sup> Alternately, construction of the 5-chloromethylated derivative of 8-hydroxyquinoline (**10**) may be achieved in moderate yields *via* electrophilic aromatic substitution of oxine.<sup>15</sup> Despite the prior mention of the unusually reactive chloride **10** under neutral or basic conditions, as well as low solubility in non-reacting solvents, initial attempts were made to protect the phenol of the intermediate 6-chloromethyl hydrochloride salt **10** directly. These efforts were not successful, and were abandoned in favor of the high chemical yield of conversion to 8-hydroxy-5-methylquinoline (**11**). Protection of this intermediate as the benzenesulfonate ester (**12**), and subsequent

conversion to the bromide (**13**), was performed under analogous conditions used to prepare the 2-bromomethyl product **5**.

As for the preparation of **7**, stereoselective alkylation of **13** (to yield product **14**) was performed with two equivalents of **6** to drive the reaction to completion within 3 h at 0 °C. Finally, hydrolysis to provide  $\alpha$ -amino acid **15**, and subsequent Fmoc protection of this (non-isolated) intermediate was performed to provide **2** in excellent yield with high optical purity (> 99% ee).

**Scheme 3-2.** Synthesis of Fmoc-5Oxn-OH.

### Peptidyl incorporation of 2Oxn and 5Oxn and evaluation of chemosensors.

In order to demonstrate the utility of these newly developed residues, **1** and **2** were used for the preparation of heptapeptides *via* standard Fmoc-based solid phase peptide synthesis techniques.<sup>16</sup> Peptides **P1** and **P2** thus contain the oxine functionality formally attached to the side chain of an *N*-terminal alanine residue through the 2-position (2Oxn) and 5-position (5Oxn) of the heterocycle respectively. Furthermore, the sequences of these peptides were designed to contain the internal sequence -Val-Pro-DSer-Phe- which has been demonstrated in prior studies to promote reverse-turn formation in solution.<sup>17</sup> Flanking residues are therefore placed in proximity (underlined in Figure 3-6); this arrangement has been observed to result in enhanced metal-binding properties when appropriate metal-ligation residues are incorporated at these positions.<sup>18,19</sup> In order to simultaneously enhance the metal binding *selectivity* of **P1** and **P2** for Zn(II), cysteine was incorporated as the additional intended ligand, which by virtue of its soft character may be expected to favor binding Zn(II),<sup>20</sup> particularly in comparison to the hard ions Mg(II) and Ca(II) which also form fluorescent complexes with oxine.

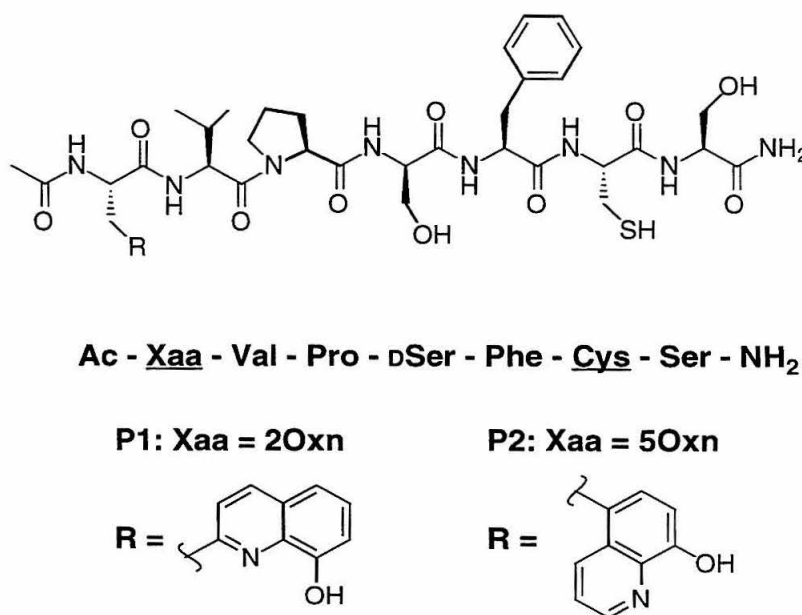


**Figure 3-6.** Structures and sequences of **P1** and **P2**.

In order to evaluate the potential of **P1** and **P2** as chemosensors for Zn(II), efforts were directed toward the measurement of the apparent dissociation constants ( $K_{\text{Ds}}$ ) of their respective Zn(II) complexes. As revealed by prior studies of peptides that contain residues with metal-ligating functionality flanking a reverse turn element,<sup>18,19,21,22</sup> **P1** and **P2** were expected to bind Zn(II) with greater affinity than the model compounds **3** and **11**, and thus these were assayed as well. Unfortunately, it quickly became apparent that **P2** suffered from rapid oxidation to form a disulfide-linked dimer under normal handling conditions (pH 7.0, rt, exposed to air), particularly in the presence of Zn(II). This behavior was confirmed by spectrophotometric analysis using Ellman's reagent, 5,5'-dithiobis(2-nitrobenzoic acid (DTNB)). As a consequence, studies of the metal-binding and fluorescence properties of **P2** were curtailed, in favor of analyzing the stable oxidation product, **P2\***. In stark contrast to **P2**, the compound **P1** suffered from little (if any) oxidative degradation over the course of a typical titration experiment (~1 h).

Metal binding titrations monitoring both UV-vis and fluorescence emission were performed at room temperature in pH 7.0 buffer (50 mM HEPES), in the presence of 150 mM NaCl to determine the apparent dissociation constants ( $K_{\text{Ds}}$ ) for the Zn(II) complexes of **3**, **11**, **P1**, and **P2\*** (Table 3-2).

**Table 3-2.** Apparent dissociation constants and stoichiometries measured for Zn(II)-complexes.

compound	$K_{\text{D}}^a$	$K_{\text{D}}^b$	stoichiometry <sup>a</sup>
<b>3</b>	17 $\mu\text{M}$	17 $\mu\text{M}$	1:1
<b>11</b>	3 $\mu\text{M}$	3 $\mu\text{M}$	1:1
<b>P1</b>	100 nM	< 200 nM	1:1
<b>P2*</b>	130 nM	< 200 nM	1:1

<sup>a</sup>Determined by UV-vis.

<sup>b</sup>Determined by fluorescence.

Mathematical extraction of apparent dissociation constants was performed by using a modified Scott analysis,<sup>23</sup> similar to that described in Chapter 2. Determination of binding affinity by this method gives reliable information regarding the complex stoichiometry only for UV-vis experiments, in which the change in extinction coefficient ( $\Delta\epsilon$ ) of the ligand is calculated; the analog of this property for measurements involving fluorescence emission is the change in quantum yield ( $\Delta\Phi$ ) which is significantly more difficult to measure accurately. It is due to uncertainty in this parameter that the threshold for measuring the  $K_D$  by this technique is less sensitive than that obtained by UV-vis. In any event, the values calculated by the two different methods are in excellent agreement, and despite this apparent paradox, fluorescence analysis of these compounds is more sensitive and can be performed on vastly smaller quantities of material than possible by UV-vis. The results from a typical (UV-vis) titration experiment of **P1**, and a corresponding binding isotherm, are presented in Figure 3-7.

Both **P1** and **P2\*** bind Zn(II) avidly with 1:1 stoichiometry, with  $K_D$ s of 100 and 130 nM respectively. Furthermore, these values indicate 170-fold and 23-fold enhancements in Zn(II) binding affinity relative to that of the respective 8-hydroxyquinoline model compounds with the appropriately positioned methyl substitution. These results suggest that the cysteine residue of **P1** assists in metal binding, and in the case of **P2\*** may explain the unusually facile oxidation of **P2** as resulting from a preorganization of two molecules for dimer formation.

Because the fluorescence and Zn(II)-binding properties of **P1** were in accord with the intended design, and could therefore be more readily interpreted within the scope of rational design, the continued analysis of the fluorescence and metal binding selectivity of this class of sensors focused on this compound. The significance of the enhancement in binding affinity of **P1** for Zn(II) is highlighted by a comparison of the fluorescence response of 10  $\mu$ M solutions of **3** and **P1** to Zn(II), when excited at 355 nm; **P1** is a decidedly more sensitive sensor for divalent zinc than is **3** (Figure 3-8). Furthermore, at

lower concentrations of the chemosensor, sub-micromolar concentrations of Zn(II) are clearly distinguishable, with the limit of detection less than 250 nM (Figure 3-9).

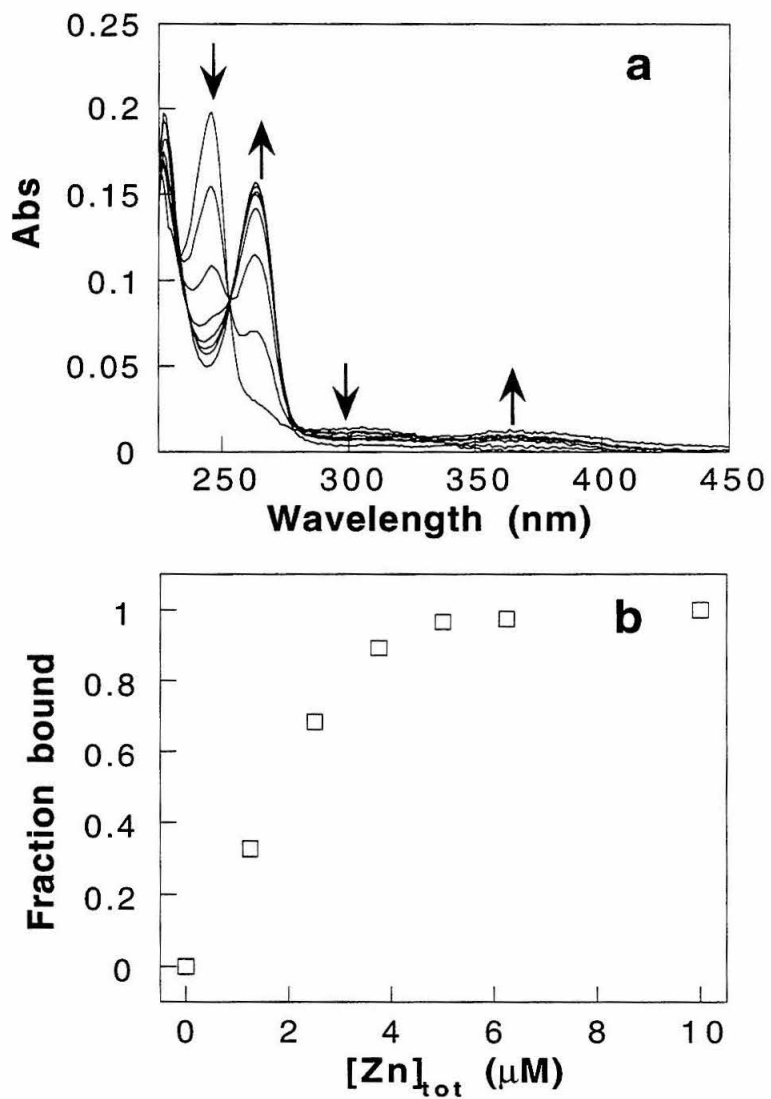


**Figure 3-7.** (a) Absorption spectra from a typical titration of **P1** (4.0 μM) with ZnCl<sub>2</sub> in increments up to 10 μM. (b) The binding isotherm calculated using the data at 262 nm taken from panel a. Data were acquired in a 1.0 cm cell in 50 mM HEPES, 150 mM NaCl, pH 7.0.

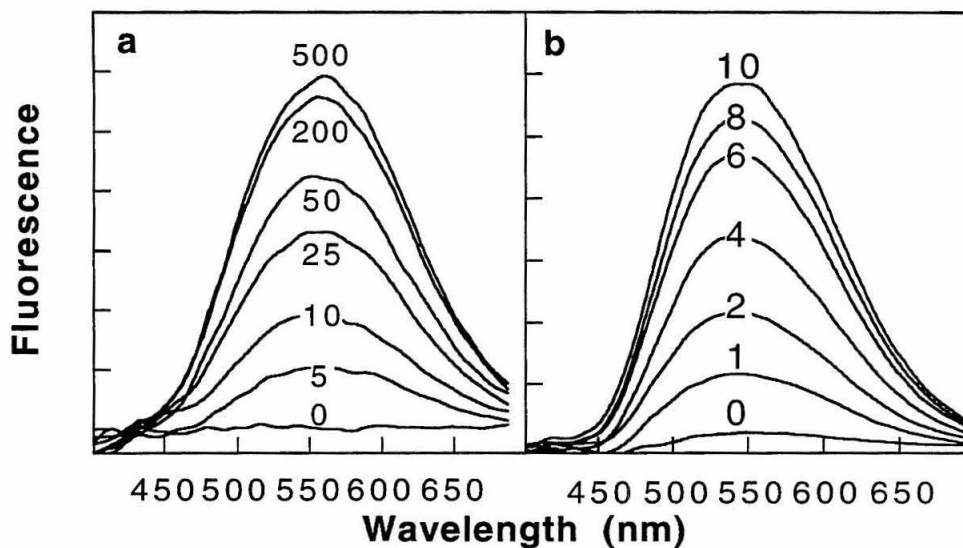


**Figure 3-8.** Fluorescence emission spectra of 10  $\mu\text{M}$  solutions of **3** (panel a) and **P1** (panel b) taken after the addition of the indicated concentration of  $\text{ZnCl}_2$  (in  $\mu\text{M}$ ). Spectra were taken at room temperature in 50 mM HEPES, pH 7.0, 150 mM NaCl, and have been baseline subtracted against a sample containing buffer only.

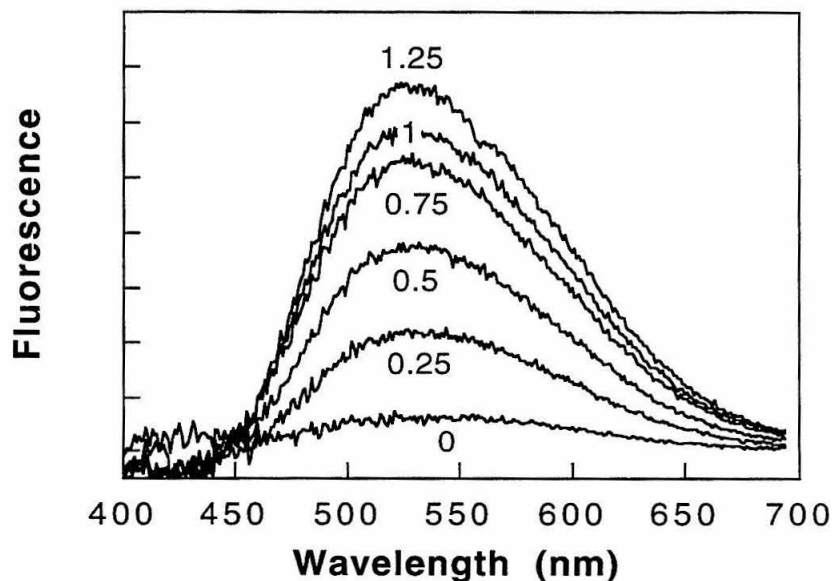


**Figure 3-9.** Fluorescence emission spectra of a 1  $\mu\text{M}$  solution of **P1** taken after the addition of the indicated concentration of  $\text{ZnCl}_2$  (in  $\mu\text{M}$ ). Spectra were acquired using the same buffer and conditions described for Figure 3-8.

As mentioned in the introduction to this chapter, the fluorescence characteristics of the oxine moiety shows fluorescence selectivity independently of its metal-binding selectivity. The evaluation of a chemosensor that uses this ligand for optical reporting should address these properties separately. In light of this fact, a series of experiments were performed to determine both the fluorescence- and binding-selectivity of **P1** with a variety of metal ions.

Specifically, the fluorescence selectivity was assessed by measuring the response of a 10  $\mu\text{M}$  solution of **P1** to an equivalent of a given metal (Figure 3-10a). It can easily be seen that at these concentrations of ions, the response of **P1** to Zn(II) is much greater than for other ions, and most notably so for Mg(II) and Ca(II) which have traditionally presented the greatest challenge for the design of chemosensors for Zn(II). At these concentrations, the Cd(II) ion also produces some CHEF; however, the presence of this ion is rare at such elevated levels. A slight increase in fluorescence is also noted after the addition of Cu(II); this species does not form fluorescent complexes with oxine, and it is therefore likely that the  $d_{10}$  species Cu(I) is generated in situ by virtue of the thiolate ligand.

The issue of metal binding selectivity was addressed in a similar manner, but through competition experiments in which the *diminution* in fluorescence is measured when a solution containing 10  $\mu\text{M}$  each of **P1** and  $\text{ZnCl}_2$  is titrated with an equivalent of a competing cation (Figure 3-10b). From the results of this experiment it can be seen that only Fe(II), Cu(II), and to a lesser extent, Cd(II) effectively compete with **P1** for binding Zn(II).

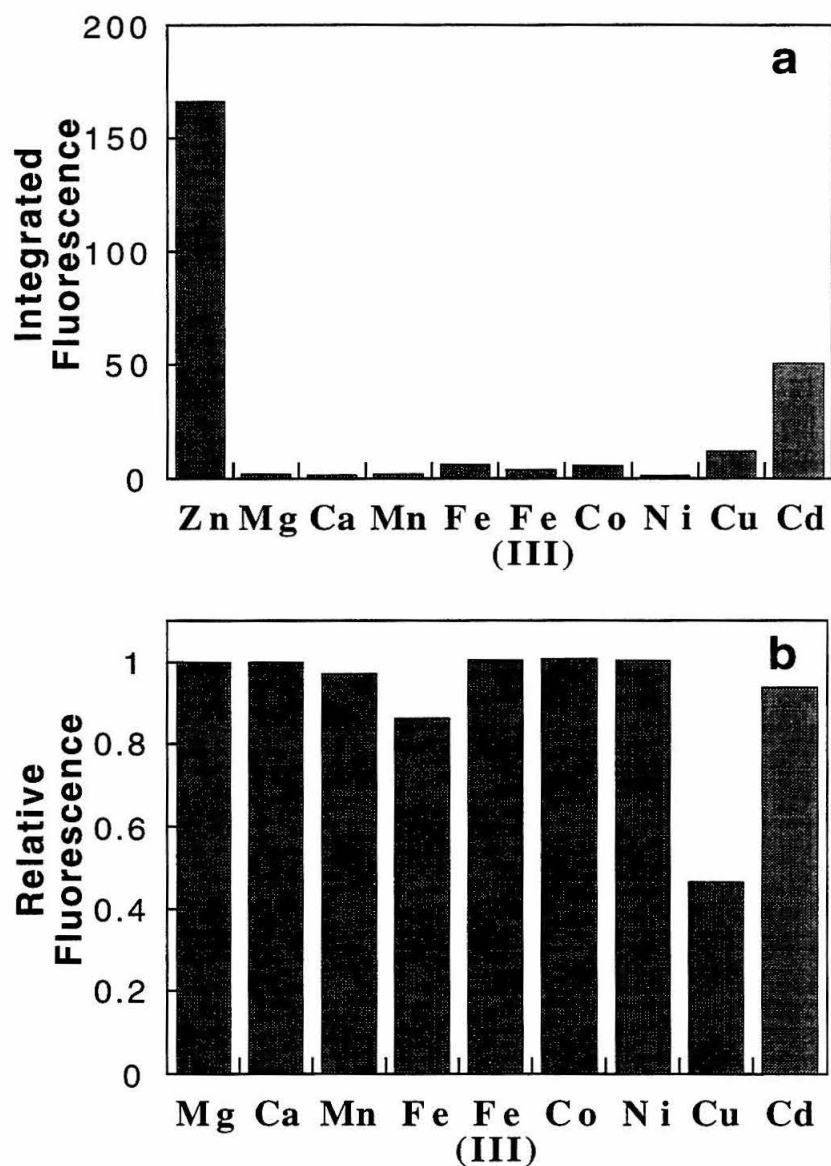


**Figure 3-10.** Measurements of the fluorescence emission of **P1** demonstrate the fluorescence selectivity (panel a) and metal-binding selectivity (panel b) of this chemosensor. (a) Integrated fluorescence emission of a 10  $\mu\text{M}$  solution of **P1** upon the addition of the indicated metal cation. (b) Integrated fluorescence emission of a 10  $\mu\text{M}$  solution of **P1** with an equivalent each of  $\text{ZnCl}_2$  and the indicated metal cation. Measurements were performed in 50 mM HEPES, pH 7.0, 150 mM NaCl. Excitation at 355 nm.

## Conclusion

The stereoselective synthesis and peptide incorporation of two novel  $\alpha$ -amino acids that contain the bidentate metal-binding functionality of oxine (8-hydroxyquinoline) has been presented. One of the resulting peptidyl fluorescent chemosensors for Zn(II), **P1**, enables the measurement of sub-micromolar concentrations of divalent zinc, even in the presence of elevated concentrations of competing metal ions. These results demonstrate that the sensitive and selective reporting of Zn(II) is feasible within short, 7-residue peptides. The new oxine-containing residues **1** and **2** will therefore undoubtedly be useful tools in the continuing development of other peptidyl fluorescent chemosensors for Zn(II).

## Experimental

### General experimental procedures.

Unless otherwise noted, all reagents and solvents obtained from commercial suppliers were of the highest possible purity and used without further purification. Tetrahydrofuran and diethylether were distilled from sodium benzophenone ketyl. Diisopropylamine, dichloromethane (DCM), 2-butanol and toluene were distilled from calcium hydride. Lithium chloride was dried under vacuum at 150 °C for  $\geq 12$  h, and flame dried immediately prior to use. *n*-Butyllithium was titrated with an analytically prepared solution of 2-butanol in toluene using 2,2'-bipyridyl in diethylether as indicator.<sup>12,24</sup> Anhydrous reactions were performed in oven-dried glassware under a positive pressure of nitrogen. Thin layer chromatography was performed using plates obtained from EM (SiO<sub>2</sub> 60, F-254). Flash column chromatography was carried out according to the procedure of Still,<sup>25</sup> using 230-400 mesh silica gel. <sup>1</sup>H and <sup>13</sup>C NMR spectra were recorded at 300 MHz and 75 MHz respectively in CDCl<sub>3</sub>, unless otherwise noted. All melting points reported are uncorrected.

**Chiral HPLC Analysis.**

HPLC analysis to evaluate the optical purity of **1** and **2** was performed on a CrownPak CR (+) analytical column (Daicel), eluting with 0.1 N aqueous HClO<sub>4</sub>, flow rate 0.5 ml/min, UV detection (320 nm). Analyses were performed on aliquots of the intermediate  $\alpha$ -amino acids taken from the hydrolyses of **6** and **9**, as well as of samples resulting from deprotection of the *N* $\alpha$ -Fmoc-amino acids **1** and **2** by treatment with 20% piperidine in DMF. In order to confirm the chromatographic profile of enantiomers, samples of the *N* $\alpha$ -Fmoc-deprotected amino acids were racemized by treatment with 25% by weight NaOH. Retention times: 2Oxn, 14.0 min (D), 15.0 min (L); 5Oxn, 10.1 min (D), 12.7 min (L).

**Peptide synthesis.**

Peptides were assembled on macro crown supports (Chiron, 6  $\mu$ mole/crown) using standard Fmoc chemistry batch synthesis techniques. Iterative removal of *N* $\alpha$ -Fmoc protecting groups was performed with piperidine (20% v/v in DMF) for 10 min followed by washing with DMF (2  $\times$  5 min), MeOH (1  $\times$  2 min, 2  $\times$  5 min), allowing the support to dry (5 min), and then re-swelling the support in DMF (5 min). Coupling reactions were carried out using diisopropylcarbodiimide/1-hydroxybenzotriazole (DIPCDI/HOBt) activation chemistry using 0.1 M active ester in sufficient volume of DMF to provide a 6-fold excess of coupling reagent to support-bound amine for a minimum of 4 h. At the completion of the synthesis, the final Fmoc protecting group was removed, and the *N*-terminal  $\alpha$ -amine acetylated with 1 mL of 0.1 M acetic anhydride, 0.1 M diisopropylethylamine (DIEA) for 2 h. Following acetylation, an additional piperidine deblock cycle was performed to deprotect any aryl acetate ester that formed during the acetylation procedure. Final peptide deprotection was achieved with 5% v/v triisopropylsilane in TFA. The crude peptide was precipitated into 1:1 diethylether/hexanes, triturated using the same solvent (3  $\times$  5 mL), and purified to homogeneity by reverse phase (C<sub>18</sub>) HPLC.

**Ac-2Oxn-Val-Pro-dSer-Phe-Cys-Ser-NH<sub>2</sub> (P1).** HPLC (C<sub>18</sub>; solvent A = water, 0.1% v/v TFA; solvent B MeCN, 0.1% v/v TFA)*t<sub>R</sub>* (linear gradient 0-70% B over 25 minutes) = 18.5 min; UV (0.1 N NaOH),  $\lambda_{\max}$  (nm) = 335; MS (electrospray) calcd for C<sub>42</sub>H<sub>56</sub>N<sub>9</sub>O<sub>11</sub>S [M+H]<sup>+</sup> 894.3, found 894.3.

**Ac-5Oxn-Val-Pro-dSer-Phe-Cys-Ser-NH<sub>2</sub> (P2).** HPLC (C<sub>18</sub>, solvent A = water, 0.1% v/v TFA; solvent B MeCN, 0.1% v/v TFA)*t<sub>R</sub>* (linear gradient 0-70% B over 25 minutes) = 17.9 min; UV (0.1 N NaOH),  $\lambda_{\max}$  (nm) = 366; MS (electrospray) calcd for C<sub>42</sub>H<sub>56</sub>N<sub>9</sub>O<sub>11</sub>S [M+H]<sup>+</sup> 894.3, found 894.3.

### Metal binding studies

Absorption spectra were obtained on a Beckman DU-7000 spectrophotometer using 1.0 cm path length quartz cuvettes. The concentrations of the peptide stock solutions were determined spectrophotometrically using the characteristic absorption band of the deprotonated (hydroxyquinolate) 8-hydroxyquinoline core, determined in 0.1 N NaOH, 1 mM EDTA, using analytically prepared solutions of the model compounds **3** and **11**. (**3**  $\lambda_{\max}$  = 355 nm,  $\epsilon_{\max}$  = 3500 M<sup>-1</sup> cm<sup>1</sup>; **11**  $\lambda_{\max}$  = 366 nm,  $\epsilon_{\max}$  = 3350 M<sup>-1</sup> cm<sup>-1</sup>.) The Zn(II) binding studies were carried out according to the procedures presented in Chapter 2. In brief, aqueous solutions of known peptide concentrations (1-10  $\mu$ M) were titrated with standardized metal solutions at room temperature in 50 mM HEPES buffer, 150 mM NaCl at pH 7.0. The apparent dissociation constants ( $K_D$ ) were calculated using an iterative process based on the Scott equation:<sup>23</sup>

$$\frac{b \cdot [M]}{\Delta A} = \frac{[M]}{[\text{Pep}]_t \cdot \Delta \epsilon} + \frac{K_D}{[\text{Pep}]_t \cdot \Delta \epsilon}$$

where  $b$  = cell path length,  $[M]$  = free metal cation concentration,  $\Delta A$  = change in absorbance due to complex formation,  $[\text{Pep}]_t$  = total peptide in solution,  $\Delta \epsilon$  = change in molar absorptivity due to complex formation.

**Synthesis.**

**8-Benzenesulfonyloxy-2-methylquinoline (4).** 8-Hydroxy-2-methylquinoline (**3**) (5.0g, 31.4 mmole, 1 eq) was dissolved in DCM (30 mL) and chilled to 0 °C with constant stirring. Triethylamine (5.29 mL, 37.7 mmole, 1.2 eq) was added followed by the dropwise addition of benzenesulfonyl chloride (4.41 mL, 34.5 mmole, 1.1 eq) dropwise over 15 min. After 0.5 h, the clear solution had become a white slurry, and the ice bath was removed. The reaction was allowed to warm to room temperature and was stirred for an additional 1.5 hours. Water (10 mL) was added and the biphasic reaction mixture stirred vigorously an additional 0.5 h to quench any remaining benzenesulfonyl chloride. The slurry was transferred to a separatory funnel, and the volume of DCM increased to 100 mL. The organic layer was washed with 100 mL of saturated aqueous K<sub>2</sub>CO<sub>3</sub>. The layers were separated, and the aqueous layer extracted with DCM (2 × 50 mL). The organic layers were combined, dried (K<sub>2</sub>CO<sub>3</sub>), and concentrated to afford the desired product as a white solid (9.33 g, 99%): mp 109-110 °C; R<sub>f</sub> = 0.18 (75:25 hexanes:EtOAc), R<sub>f</sub> = 0.33 (100:1 DCM:EtOAc); <sup>1</sup>H NMR δ 7.96 (m, 3H), 7.68 (dd, *J* = 1.2, 8.1 Hz, 1H), 7.64 (dd, *J* = 1.2, 7.8 Hz, 1H), 7.56 (tt, *J* = 2.1, 7.5 Hz, 1H), 7.35-7.45 (m, 3H), 7.19 (d, *J* = 8.4 Hz, 1H), 2.50 (s, 3H); <sup>13</sup>C NMR δ 25.1, 122.6, 123.0, 125.0, 126.7, 127.8, 128.4, 128.8, 133.6, 135.6, 136.7, 140.8, 145.0, 159.5; IR (thin film, cm<sup>-1</sup>) 3064, 1605, 1371, 1188; HRMS (FAB) calcd for C<sub>16</sub>H<sub>14</sub>NO<sub>3</sub>S [M+H]<sup>+</sup> 300.0694, found 300.0691.

**8-Benzenesulfonyloxy-2-bromomethylquinoline (5).** 8-Benzenesulfonyloxy-2-methylquinoline (5.0g, 16.6 mmole, 1.0 eq) was placed in a round bottom flask with deoxygenated CCl<sub>4</sub> (40 mL), fitted with a reflux condenser and heated to reflux to dissolve. *N*-bromosuccinimide (4.14 g, 23.2 mmole, 1.4 eq) was added, followed by 2,2'-azobis(2-methylpropionitrile) (AIBN, 295 mg, 1.55 mmole, 0.1 eq) and reflux continued. Additional aliquots of AIBN (295 mg) were added at 0.5 h intervals until a total of 5 additions had been made. At 0.5 h after the final addition, the reaction flask

was allowed to cool to room temperature, and the solvent was removed under reduced pressure. The resulting residue was suspended in EtOAc (400 mL), transferred to a separatory funnel, and washed with 1:1 saturated aqueous  $\text{Na}_2\text{CO}_3:\text{Na}_2\text{SSO}_3$  (300 mL). The layers were separated, and the aqueous layer extracted with EtOAc (75 mL). The organic layers were combined, dried ( $\text{K}_2\text{CO}_3$ ), and concentrated. The resulting residue was dissolved in a minimal quantity of chloroform, and purified by silica flash chromatography (eluent 75:25 hexanes:EtOAc,  $R_f = 0.22$ ). Both starting material (1.7 g) and the product were collected by concentration of the appropriate fractions. NMR analysis of the product revealed the presence of a contaminant (singlet at 1.73 ppm,  $\text{CDCl}_3$ ) which was assigned to the radical termination product 2,3-dicyano-2,3-dimethylbutane. Recrystallization from hot EtOAc/hexanes provided the pure bromide **5** (3.25 g, 71% based on recovery of starting material) as a crystalline white solid: mp 138-139 °C;  $R_f = 0.40$  (65:35 hexanes/EtOAc)  $R_f = 0.60$  (100:1 DCM:EtOAc).  $^1\text{H}$  NMR  $\delta$  8.12 (d,  $J = 8.4$  Hz, 1H), 7.98 (dd,  $J = 8.4, 1.2$  Hz, 2H), 7.74 (d,  $J = 8.1$  Hz, 2H), 7.61 (m, 1H), 7.45-7.6 (m, 4H), 4.44 (s, 2H);  $^{13}\text{C}$  NMR  $\delta$  33.9, 122.0, 123.8, 126.6, 126.7, 128.5, 128.7, 128.8, 134.0, 137.0, 137.1, 140.2, 145.3, 157.3; IR (thin film,  $\text{cm}^{-1}$ ) 3605, 1600, 1503, 1468, 1449, 1431, 1368, 1188, 1068, 1046; HRMS (FAB) calcd for  $\text{C}_{16}\text{H}_{13}\text{NO}_3\text{SBr}$   $[\text{M}+\text{H}]^+$  377.9800, found 377.9797.

The synthesis of the following two compounds have already been reported,<sup>15</sup> but with little experimental data. More complete descriptions of the synthesis are provided below.

**5-Chloromethyl-8-hydroxyquinoline (10).** 8-Hydroxyquinoline (**9**) (14.5 g, 100 mmole, 1.0 eq), 12 N HCl (16 mL, 192 mmole, 1.92 eq), and formaldehyde (37 wt. % in water, 5.5 g, 180 mmole, 1.8 eq) were combined in a round bottom flask, and stirred magnetically, forming a lemon-yellow precipitate. HCl (g) was bubbled through the slurry with constant stirring for 90 minutes, during which time the precipitate dissolved and another yellow precipitate formed. The solids were collected on a sintered glass

funnel, washed with ice-cold water (50 mL) and dried by aspiration on the funnel for 1 h. The solid was triturated from diethylether (4 × 100 mL), and transferred to a 250 mL round bottom flask. Toluene (50 mL) was added and the solvent removed under reduced pressure to remove residual HCl. The solid was then dried under high vacuum for 12 h to yield a lemon yellow power, 15.8 g, 69%. <sup>1</sup>H NMR (DMSO-*d*<sub>6</sub>) δ 12.5 (broad s, 1H), 9.26 (dd, 1H, *J* = 8.7 Hz, 1.2 Hz), 9.13 (dd, 1H, *J* = 5.1 Hz, 1.2 Hz), 8.14 (dd, 1H, *J* = 5.4 Hz, 8.7 Hz), 7.87 (d, 1H, *J* = 8.1 Hz), 7.54 (d, 1H, *J* = 8.1 Hz), 5.32 (s, 2H).

**8-Hydroxy-5-methylquinoline (11).** Hydrochloride salt **10** (10.6 g, 46.1 mmole, 1.0 eq) was added to a slurry of degassed methanol (200 mL) and Pd/C (10 wt. %, 1.0 g, 0.94 mmole, 0.02 eq) in a 500 mL hydrogenation chamber, and immediately aspirated of air. The reaction vessel was mounted within a hydrogenation apparatus and H<sub>2</sub> (50 psi) was delivered to the vessel with constant rocking. After 4 hours, hydrogen consumption had ceased, and the green slurry was filtered through celite to remove the palladium catalyst. The filtrate was collected, and concentrated to afford a yellow residue which was transferred to a separatory funnel with water (75 mL) and chloroform (75 mL). Ammonium hydroxide (2N) was added slowly to the separatory funnel with continual shaking, which produced a white precipitate in the aqueous layer that slowly dissolved into the organic layer. When the pH of the aqueous layer reached 8, the layers were separated and the aqueous layer extracted with CHCl<sub>3</sub> (75 mL). The organic layers were combined, and concentrated to afford a greenish-brown solid. Toluene (3 × 50 mL) was added to the solid and removed under reduced pressure to remove residual water. The resulting solid was dried under high vacuum for 12 h, then sublimed under high vacuum at 80 °C to afford 6.23 g (85%) of **11** as crystalline white prisims. TLC R<sub>f</sub> = 0.45 (95:5 CHCl<sub>3</sub>:MeOH), R<sub>f</sub> = 0.27 (65:35 hexanes:EtOAc); <sup>1</sup>H NMR δ 8.80 (dd, *J* = 1.5, 4.2 Hz), 8.30 (dd, *J* = 1.5, 8.7 Hz, 1H), 8.2 (s, 1H, broad), 7.48 (dd, *J* = 4.2, 8.7 Hz, 1H), 7.28 (dd, *J* = 0.6, 7.8 Hz, 1H), 7.09 (d, *J* = 7.8 Hz, 1H), 2.60 (s, 1H); <sup>13</sup>C NMR δ 17.7, 109.4,

117.8, 121.2, 124.3, 127.5, 132.9, 138.4, 147.3, 150.4. HRMS (FAB) calcd for  $C_{10}H_{10}NO$   $[M+H]^+$  160.0762, found 160.0764.

**8-Benzenesulfonyloxy-5-methylquinoline (12).** 8-Hydroxy-5-methylquinoline (**11**) (6.23 g, 39.1 mmole, 1.0 eq) was dissolved in DCM (90 ml) and chilled to 0 °C with constant stirring. Triethylamine (6.58 mL, 46.9 mmole, 1.2 eq) was added followed by the dropwise addition of benzenesulfonyl chloride (5.48 mL, 43.0 mmole, 1.1 eq) over 15 min. After 0.5 h, the clear solution had become a white slurry, and stirring was continued overnight (10 h). Water (20 mL) was added and the biphasic mixture was stirred vigorously for 1 h to assure consumption of the remaining benzenesulfonyl chloride. The organics were removed under reduced pressure, and the aqueous phase transferred to a separatory funnel. Saturated aqueous  $Na_2CO_3$  (100 mL) was added and extracted with EtOAc (2 × 75 mL). The organic layers were combined, dried ( $K_2CO_3$ ), and concentrated to afford a white solid. The solid was dissolved in a minimal quantity of  $CHCl_3$ , and loaded onto a silica flash column (eluent 65:35 hexanes:EtOAc,  $R_f = 0.21$ ) to afford the desired product (10.95 g, 94%): mp 106-108 °C;  $R_f = 0.4$  (1:1 hexanes:EtOAc).  $^1H$  NMR  $\delta$  8.77 (dd,  $J = 1.5, 4.2$  Hz, 1H), 8.26 (dd,  $J = 1.5, 8.7$  Hz, 1H), 7.98 (dd,  $J = 0.6, 7.2$  Hz, 2H), 7.59 (tt,  $J = 1.2, 7.5$  Hz, 1H), 7.4-7.5 (m, 3H), 7.4 (dd,  $J = 4.2, 8.7$  Hz, 1H), 7.32 (dd,  $J = 0.9, 7.8$  Hz, 1H), 2.65 (s, 3H);  $^{13}C$  NMR  $\delta$  18.3, 121.3, 122.1, 122.5, 126.1, 128.7, 132.3, 133.7, 134.1, 136.3, 138.6, 141.5, 143.9, 150.1; IR (thin film,  $cm^{-1}$ ) 3062, 1598, 1500, 1472, 1448, 1369, 1188, 1048, 846, 807; HRMS (FAB) calcd for  $C_{16}H_{14}NO_3S$   $[M+H]^+$  300.0694, found 300.0697.

**8-Benzenesulfonyloxy-5-bromomethylquinoline (13).** 8-(benzenesulfonyloxy)-5-methylquinoline (**12**) (1.28 g, 4.28 mmole, 1.0 eq) was placed in a round bottom flask with deoxygenated  $CCl_4$  (30 mL), fitted with a reflux condenser and heated to reflux to dissolve. *N*-bromosuccinimide (1.07 g, 6.0 mmole, 1.4 eq) was added, followed by AIBN (70 mg, 0.43 mmole, 0.1 eq) and reflux continued. Additional aliquots of AIBN (70 mg) were added at 0.5 h intervals until a total of 5 additions had been made. At 0.5 h

after the final addition, the reaction flask was allowed to cool to room temperature, and the solvent was removed under reduced pressure. The resulting residue was suspended in EtOAc (50 mL), transferred to a separatory funnel, and washed with 1:1 saturated  $\text{Na}_2\text{CO}_3:\text{Na}_2\text{SSO}_3$  (50 mL). The layers were separated, and the aqueous layer extracted with EtOAc (50 mL). The organic layers were combined, dried ( $\text{K}_2\text{CO}_3$ ), and concentrated. The resulting residue was dissolved in a minimal quantity of  $\text{CHCl}_3$ , and purified by silica flash chromatography (eluent 75:25 hexanes:EtOAc,  $R_f = 0.13$ ) to yield **13** (1.02 g, 63%) as a white solid: mp 142-142 °C;  $R_f = 0.22$  (65:35 hexanes:EtOAc),  $R_f = 0.60$  (95:5 DCM/Et<sub>2</sub>O). <sup>1</sup>H NMR  $\delta$  8.83 (dd,  $J = 1.8, 4.2$  Hz, 1H), 8.44 (dd,  $J = 1.5, 8.7$  Hz, 1H), 8.00 (dd, 1,2, 8.4 Hz, 2H), 7.63 (m, 1H), 7.56 (d, 4.2 Hz, 2H), 7.4-7.5 (m, 3H), 4.87 (s, 2H); <sup>13</sup>C NMR ( $\text{CDCl}_3$ )  $\delta$  29.2, 121.9, 122.0, 127.4, 127.6, 128.7, 128.9, 132.1, 133.0, 134.0, 136.0, 142.0, 146.1, 150.8; IR (thin film,  $\text{cm}^{-1}$ ) 3063, 1598, 1501, 1472, 1449, 1373, 1188, 1050, 807; HRMS (FAB) calcd for  $\text{C}_{16}\text{H}_{13}\text{NO}_3\text{SBr}$   $[\text{M}+\text{H}]^+$  377.9800, found 377.9800.

**[(*R,R*)-2*S*]-*N*-(2-Hydroxy-1-methyl-2-phenylethyl)-*N*-methyl-2-amino-3-[2-(8-benzenesulfonyloxy)quinolinyl]propionamide (7).** A solution of *n*-butyllithium in hexanes (2.30 M, 1.70 mL, 3.90 mmole, 3.9 eq.) was added to a solution of diisopropylamine (560  $\mu\text{l}$ , 4.0 mmole, 4.0 eq) in deoxygenated THF (2 mL) at 0 °C. After 15 minutes, the resulting solution of lithium diisopropylamide (+ 2 mL wash) was transferred *via* cannula over 5 min to a stirred slurry of anhydrous (*R,R*)-(-) pseudoephedrine glycinamide (454 mg, 2.0 mmole, 2.0 eq) and flame-dried lithium chloride (509 mg, 12.0 mmole, 12.0 eq) in deoxygenated THF (5 mL) at 0 °C. After 30 min at 0 °C, a solution of **5** (378 mg, 1.0 mmole, 1.0 eq) in THF (5 mL + 2 mL wash) at 0 °C was added slowly to the yellow enolate solution. The reaction mixture was stirred for 3 h at 0 °C. Water (30 mL) was added, and the resulting biphasic mixture was warmed to room temperature and the THF removed under reduced pressure. The pH of the solution was made strongly basic by the addition of aqueous NaOH (2 mL, 2 N), and the resulting

aqueous phase was extracted with chloroform (3 × 20 mL). The combined organic layers were dried (K<sub>2</sub>CO<sub>3</sub>), filtered, and concentrated under reduced pressure. The residue was purified by chromatography on silica gel eluting with DCM/MeOH/Et<sub>3</sub>N (92:4:4). The C-alkylated diastereomers were separable under these conditions and only those fractions containing the pure major diastereomer were collected. After concentration of the appropriate fractions, the product residue was concentrated from toluene (2 × 25 mL), and then chloroform (2 × 25 mL) to remove residual triethylamine. This afforded **7** as a pale yellow granular solid (0.47 g, 89%): mp 67-69 °C; R<sub>f</sub> = 0.44 (90:5:5 CHCl<sub>3</sub>/MeOH/TEA), R<sub>f</sub> = 0.28 (95:5:1 CHCl<sub>3</sub>/MeOH/NH<sub>4</sub>OH) ; <sup>1</sup>H NMR (approximately 2:1 rotamer ratio, \* denotes minor rotamer) δ 8.65\* (d, J = 8.4 Hz, 0.33 H), 8.04 (d, J = 8.4 Hz, 0.67 H), 7.9-8 (m, 2 H), 7.2-7.8 (m, 12 H), 4.74\* (d, J = 8.1 Hz, 0.33 H), 4.61 (d, J = 8.1 Hz, 0.67 H), 4.4-4.6 (m, 2H), 3.46\* (dd, J = 3.6, 14.7 Hz, 0.33 H), 3.28\* (dd J = 8.1, 14.7 Hz, 0.33H), 3.09 (dd, J = 5.1, 14.7 Hz, 0.67 H), 3.04 (s, 2H), 2.96\* (s, 1H), 2.93 (dd, J = 8.4, 14.7 Hz, 0.67 H), 1.5-2.5 (broad s, 3H), 1.04\* (d, J = 6.6 Hz, 1H), 0.99 (d, J = 6.9 Hz, 2 H); <sup>13</sup>C NMR δ 14.1, 15.5, 27.2, 31.3, 43.9, 51.2, 57.0, 57.7, 75.1, 75.4, 121.5, 122.0, 123.3, 123.5, 125.0, 125.1, 126.5, 126.6, 126.8, 127.1, 127.4, 127.8, 128.1, 128.2, 128.3, 128.4, 128.8, 128.9, 133.8, 135.8, 136.4, 140.9, 141.6, 142.0, 145.0, 159.9, 160.4, 174.8, 175.9; IR (thin film, cm<sup>-1</sup>) 3360 (broad), 3062, 2982, 1625, 1449, 1372, 1189, 1068, 1047, 788, 758; HRMS (FAB) calcd for C<sub>28</sub>H<sub>30</sub>N<sub>3</sub>O<sub>5</sub>S [M+H]<sup>+</sup> 520.1906, found 520.1909; [α]<sub>D</sub><sup>20</sup> = +61° (c = 1.0, CHCl<sub>3</sub>).

**[(R,R)-2S]-N-(2-Hydroxy-1-methyl-2-phenylethyl)-N-methyl-2-amino-3-[5-(8-benzenesulfonyloxy)quinolinyl]propionamide (14).** A solution of *n*-butyllithium in hexanes (2.40 M, 1.63 mL, 3.90 mmole, 3.9 eq.) was added to a solution of diisopropylamine (560 μl, 4.0 mmole, 4.0 eq) in deoxygenated THF (2 mL) at 0 °C. After 15 minutes, the resulting solution of lithium diisopropylamide (+ 2 mL wash) was transferred via cannula over 5 min to a stirred slurry of anhydrous (*R, R*)-(-) pseudoephedrine glycineamide (454 mg, 2.0 mmole, 2.0 eq) and flame-dried lithium

chloride (509 mg, 12 mmole, 12 eq) in deoxygenated THF (5 mL) at 0 °C. After stirring 30 minutes at 0 °C, a solution of **13** (378 mg, 1.0 mmole, 1.0 eq) in THF (3 mL + 2 mL wash) at 0 °C was added slowly to the yellow enolate solution. The mixture was stirred for 2 h. at 0 °C. Water (30 mL) was added, and the resulting biphasic mixture was warmed to room temperature and the THF removed under reduced pressure. The pH of the solution was made strongly basic by the addition of NaOH (2 mL, 2N), and the resulting aqueous phase was extracted with chloroform (3 × 25 mL). The combined organic layers were dried over anhydrous potassium carbonate, filtered, and concentrated under reduced pressure. The residue was purified by chromatography on silica gel by gradient elution with DCM/MeOH/Et<sub>3</sub>N (96.5:1.5:2 → 92:4:4). The C-alkylated diastereomers were separable under these conditions and only those fractions containing the pure major diastereomer were collected. After concentration of the appropriate fractions, the product residue was concentrated from toluene (2 × 25 mL), and then chloroform (2 × 25 mL), to remove residual triethylamine. The product **14** was isolated as a pale yellow granular solid (482 mg, 92%): R<sub>f</sub> = 0.55 (85:15:1 CHCl<sub>3</sub>:MeOH:NH<sub>4</sub>OH), R<sub>f</sub> = 0.23 (90:5:5 CHCl<sub>3</sub>:MeOH:Et<sub>3</sub>N). <sup>1</sup>H NMR (1:2:3 rotameric forms, \* denotes minor rotamer) δ 8.78\* (d, J = 2.5 Hz, 0.3 H), 8.74 (d, J = 2.5 Hz, 0.7 H), 8.57\* (d, J = 7.5 Hz, 0.3 H), 8.39 (d, J = 7.5 Hz, 0.7 H), 7.95-8.0 (m, 1.3 H), 7.2-7.6 (m, 11.4 H), 7.04\* (d, J = 3.5 Hz, 0.3 H), 4.60 (m, 0.7 Hz), 4.43\* (d, 8 Hz, 0.3 H), 4.35 (d, 8 Hz, 0.7 H), 4.2\* (m, 0.3 H), 4.14 (m, 0.7 H), 4.01\* (m, 0.3 H), 3.66\* (dd, J = 5 Hz, 14 Hz, 0.3 H), 3.0-3.5 (m, 3.7 H), 2.91\* (s, 0.9 H), 2.23 (s, 2.1 H), 0.92\* (d, J = 6 Hz, 0.9 H), 0.46 (d, J = 6 Hz, 2.1 H); <sup>13</sup>C NMR (contributions from both rotamers listed) δ, 13.9, 14.0, 15.6, 27.2, 29.5, 37.6, 37.8, 51.8, 52.1, 55.2, 55.5, 58.0, 70.7, 71.2, 74.6, 75.2, 76.7, 121.95, 122.0, 126.7, 126.8, 127.3, 128.0, 128.3, 128.4, 128.5, 128.6, 128.7, 128.8, 132.2, 132.6, 133.2, 133.9, 134.0, 136.1, 136.2, 141.3, 141.4, 141.5, 141.8, 144.4, 144.6, 150.2, 150.5, 174.9, 186.7; IR (thin film, cm<sup>-1</sup>) 3350 (broad), 3062, 2980,

1626, 1501, 1472, 1449, 1371, 1188, 1048, 850, 808, 744; HRMS (FAB) calcd for  $C_{28}H_{30}N_3O_5S$   $[M+H]^+$  520.1906, found 520.1906;  $[\alpha]^{20}_D = +12^\circ$  ( $c = 1.0$ ,  $CHCl_3$ ).

**(S)-2-amino-*N* $^{\alpha}$ -9-fluorenylmethoxycarbonyl-3-(oxine-2-yl)-propanoic acid**

(1) Alkylated pseudoephedrine derivative **7** (100 mg, 0.192 mmole, 1.0 eq) was dissolved in deoxygenated dioxane (1.5 mL) and deoxygenated aqueous NaOH (0.5 M, 1.54 mL, 0.768 mmole, 4 eq.) was added and the reaction mixture heated to reflux. After 4 h, TLC analysis of the amber solution (*n*-BuOH/AcOH/H<sub>2</sub>O/EtOAc 1:1:1:1) showed that only the deprotected amino acid ( $R_f = 0.23$ ) remained as a UV- ninhydrin- and FeCl<sub>3</sub>-active species. The solution was cooled, and the dioxane removed under reduced pressure. The aqueous solution was washed with DCM (3 × 5 mL) to remove pseudoephedrine. A small aliquot of the aqueous phase (20 μL) was removed for chiral HPLC analysis, the remainder was chilled to 0 °C, and NaHCO<sub>3</sub> (64 mg, 0.768 mmole, 4.0 eq) was added. A solution of 9-fluorenylmethoxycarbonylchloroformate (60 mg, 0.23 mmole, 1.2 eq) in dioxane (1.5 mL) was added, and the reaction mixture stirred for 8 h. The dioxane was removed under reduced pressure, and HCl (1 N) was added dropwise until the solution was *ca.* pH 4. Water was added to increase the volume to *ca.* 10 mL, and the solution was extracted with DCM (3 × 10 mL). The organic layers were concentrated and the resulting yellow residue was concentrated from toluene (2 × 25 mL) to remove traces of water. The residue was dissolved in CHCl<sub>3</sub> (2 mL) and precipitated by addition to a rapidly stirred solution of 1:1 hexanes/ether (25 mL). The yellow precipitate was filtered and dried under vacuum 6 h to afford 81 mg (90%) of pale yellow solid.  $R_f = 0.70$  (85:15:3 CHCl<sub>3</sub>:MeOH:AcOH); <sup>1</sup>H NMR (MeOH-*d*<sub>4</sub>)  $\delta$  3.64 (t,  $J = 9.9$  Hz, 1 H), 3.7-4.5 (m, 3H), 4.81 (m, 1H), 7.0-8.0 (m, 12 H), 8.9 (d,  $J = 8.7$  Hz, 1H); <sup>13</sup>C NMR  $\delta$  38.1, 46.3, 47.0, 52.8, 67.1, 115.0, 117.3, 119.9, 122.7, 124.7, 127.0, 127.2, 127.6, 127.8, 129.4, 141.1, 141.7, 143.6, 143.8, 154.7, 156.2; IR (thin film, cm<sup>-1</sup>) 3000 (broad), 2919, 1717, 1640, 1602, 1544, 1445, 1312, 1224, 1017, 760, 743; HRMS (FAB)

calcd for C<sub>27</sub>H<sub>23</sub>N<sub>2</sub>O<sub>5</sub> [M+H]<sup>+</sup> 455.1607, found 455.1605; [ $\alpha$ ]<sub>D</sub><sup>20</sup> = -340° (*c* = 0.5, 9:1 MeOH/1.0 N aqueous HCl).

**(S)-2-amino-N<sup>α</sup>-9-fluorenylmethoxycarbonyl-3-(oxine-5-yl)-propionic acid**

(2). Alkylated pseudoephedrine derivative **14** (100 mg, 0.192 mmole, 1.0 eq) was dissolved in deoxygenated dioxane (1.5 mL) and deoxygenated aqueous NaOH (0.5 M, 1.54 mL, 0.768 mmole, 4 eq.) was added and the reaction mixture heated to reflux. After 6 h, the solution was deep yellow, and analysis by TLC (1:1:1:1 *n*-butanol:AcOH:water:EtOAc) showed that only the deprotected amino acid (*R<sub>f</sub>* = 0.23) remained as a UV- ninhydrin- and FeCl<sub>3</sub>-active species. The solution was cooled, and the dioxane removed under reduced pressure. The aqueous solution was washed with DCM (3 × 5 mL) to remove pseudoephedrine. A small aliquot of the aqueous phase (20 μL) was removed for chiral HPLC analysis, and the remainder was chilled to 0 °C, and NaHCO<sub>3</sub> (64 mg, 0.768 mmole, 4.0 eq) was added. A solution of *N*(9-fluorenylmethoxycarbonyloxy)succinimide (78 mg, 0.23 mmole, 1.2 eq) in dioxane (1.5 mL) was added, and the reaction mixture stirred for 8 h. The dioxane was removed under reduced pressure, and HCl (1 N) was added dropwise until the solution was *ca.* pH 4. Water (5 mL) was added, and the solution cooled to 4 °C, and held at that temperature for an hour during which time a yellow precipitate formed. The solution was filtered, and washed with cold water. The solid was transferred to a round bottom flask, and concentrated from toluene several times to remove traces of water. The resulting pale yellow solid was dried under vacuum 6 h to afford 90 mg (95%) of **2**: *R<sub>f</sub>* = 0.37 (85:15:3 CHCl<sub>3</sub>:MeOH:AcOH); mp 114-116 °C; <sup>1</sup>H NMR (MeOH-*d*<sub>4</sub>) δ 3.27 (dd, *J* = 4.5 Hz, 14.1 Hz, 1 H), 3.65 (dd, *J* = 4.5 Hz, 14.1 Hz, 1 H), 3.86 (d, *J* = 6.9 Hz, 2H), 4.01 (t, *J* = 4.5 Hz, 1H), 4.45 (m, 1H), 7.02 (d, *J* = 7.8 Hz, 1H), 7.1-7.8 (m, 10H), 8.61 (d, *J* = 7.8 Hz, 1H), 8.78 (d, *J* = 4.2 Hz, 1H); <sup>13</sup>C NMR (DMSO-*d*<sub>6</sub>) δ 32.3, 46.5, 55.0, 65.6, 114.3, 120.1, 122.0, 125.1, 125.2, 127.0, 127.1, 137.6, 127.8, 130.9, 140.6, 140.8, 143.6, 143.7, 144.6, 155.9, 172.9; IR (thin film, cm<sup>-1</sup>) 3000 (broad), 3067, 2924, 1713, 1598, 1581,

1505, 1476, 1449, 1232, 1078, 1050, 759, 740; HRMS (FAB) calcd for C<sub>27</sub>H<sub>23</sub>N<sub>2</sub>O<sub>5</sub> [M+H]<sup>+</sup> 455.1607, found 455.1599; [ $\alpha$ ]<sub>D</sub><sup>20</sup> = -5° (c = 0.5, 9:1 MeOH/1.0 N HCl<sub>aq</sub>).

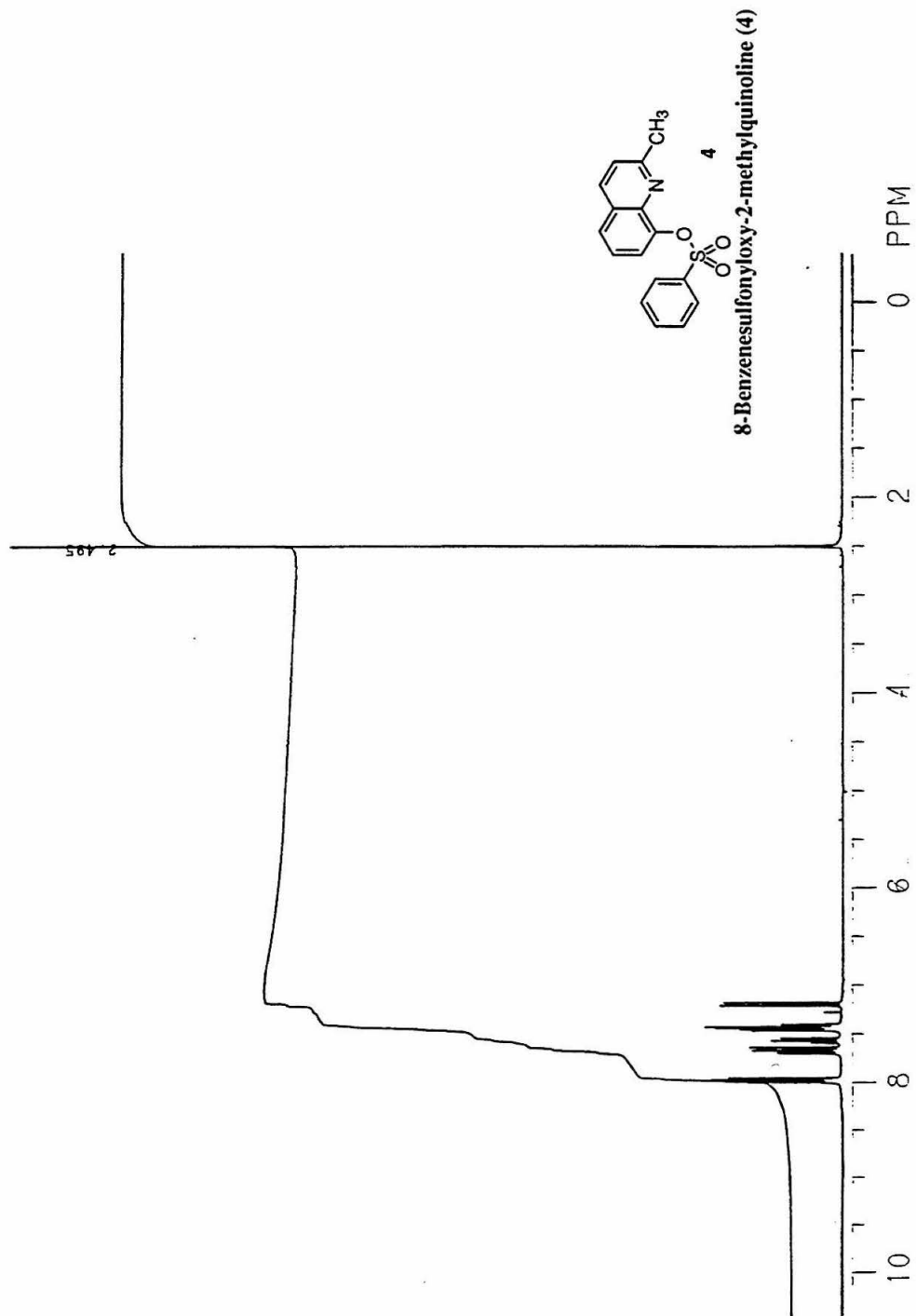
## References

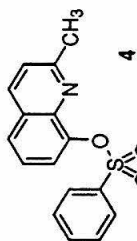
1. "Chapter 18: Spectrofluorimetry," In *Vogel's Textbook of Quantitative Chemical Analysis*; Vogel, A. I.; Wiley, New York, 1989; pp 731-740.
2. "Fluorescence Derivatization," Seitz, W. R. *CRC Crit. Rev. Anal. Chem.* **1980**, 8, 367-405.
3. "A Fluorescent Sensor for Aluminum(III), Magnesium(II), Zinc(II) and Cadmium(II) Based on Electrostatically Immobilized Quinolin-8-ol Sulfonate," Zhujun, Z.; Seitz, W. R. *Anal. Chim. Acta* **1985**, 171, 251-258.
4. "Unimolecular Photochemistry of Anthracenes," Becker, H. D. *Chem. Rev.* **1993**, 93, 145-172.
5. "Supramolecular Chemistry, Fluorescence, and Sensing," In *Fluorescent Chemosensors for Ion and Molecule Recognition*; Czarnik, A. W.; ACS, Washington D.C., 1993; pp 1-9.
6. "Fluorescent Signal Transduction in Molecular Sensors," In *Fluorescent Chemosensors for Ion and Molecule Recognition*; Czarnik, A. W.; ACS, Washington D.C., 1993; pp 104-129.
7. "Chemical Communication in Water Using Fluorescent Chemosensors," Czarnik, A. W. *Acc. Chem. Res.* **1994**, 27, 302-308.
8. "Signaling Recognition Events with Fluorescent Sensors and Switches," de Silva, A. P.; Gunaratne, H. Q. N.; Gunnlaugsson, T.; Huxley, A. J. M.; McCoy, C. P., et al. *Chem. Rev.* **1997**, 97, 1515-1566.
9. "Handbook of Fluorescent Probes and Research Chemicals," Haugland, R. P.; Molecular Probes: 1996.

10. "The Stabilities of Some Metal Complexes of 8-Hydroxyquinoline and Related Substances," Irving, H.; Rossotti, H. S. *J. Chem. Soc.* **1954**, 2910-2918.
11. "A Practical Method for the Synthesis of D- or L- $\alpha$ -Amino Acids by the Alkylation of (+)- or (-)-Pseudoephedrine Glycinamide," Myers, A. G.; Gleason, J. L.; Yoon, T. *J. Am. Chem. Soc.* **1995**, *117*, 8488-8489.
12. "Highly Practical Methodology for the Synthesis of D- and L- $\alpha$ -Amino Acids, *N*-Protected  $\alpha$ -Amino Acids, and *N*-Methyl- $\alpha$ -amino Acids," Myers, A. G.; Gleason, J. L.; Yoon, T.; Kung, D. W. *J. Am. Chem. Soc.* **1997**, *119*, 656-673.
13. "A One-Step Synthesis of Pseudoephedrine Glycinamide, a Versatile Precursor for the Synthesis of  $\alpha$ -Amino Acids," Myers, A. G.; Yoon, T.; Gleason, J. L. *Tetrahedron Lett.* **1995**, *36*, 4555-4558.
14. "Synthesis of the Quinoline Ring System," In *Quinolines. The Chemistry of Heterocyclic Compounds*; Jones, G.; Jones, G.; Wiley Interscience, New York, 1977; pp 93-318.
15. "Amino- and Chloromethylation of 8-Quinolinol. Mechanism of Preponderant *ortho* Substitution in Phenols under Mannich Conditions," Burckhalter, J. H.; Leib, R. I. *J. Org. Chem.* **1961**, *26*, 4078-4083.
16. "Solid-Phase Peptide Synthesis Utilizing 9-Fluorenylmethoxycarbonyl Amino-Acids," Fields, G. B.; Noble, R. L. *Int. J. Pep. Protein Res.* **1990**, *35*, 161.
17. "A Conformational Study of Peptides with the General Structure Ac-L-Xaa-Pro-D-Xaa-L-Xaa-NH<sub>2</sub>: Spectroscopic Evidence for a Peptide with Significant  $\beta$ -Turn Character in Water and in Dimethyl Sulfoxide," Imperiali, B.; Fisher, S. L.; Moats, R. A.; Prins, T. J. *J. Am. Chem. Soc.* **1992**, *114*, 3182-3188.
18. "The Reverse Turn as a Template for Metal Coordination," Imperiali, B.; Kapoor, T. M. *Tetrahedron* **1993**, *49*, 3501-3510.

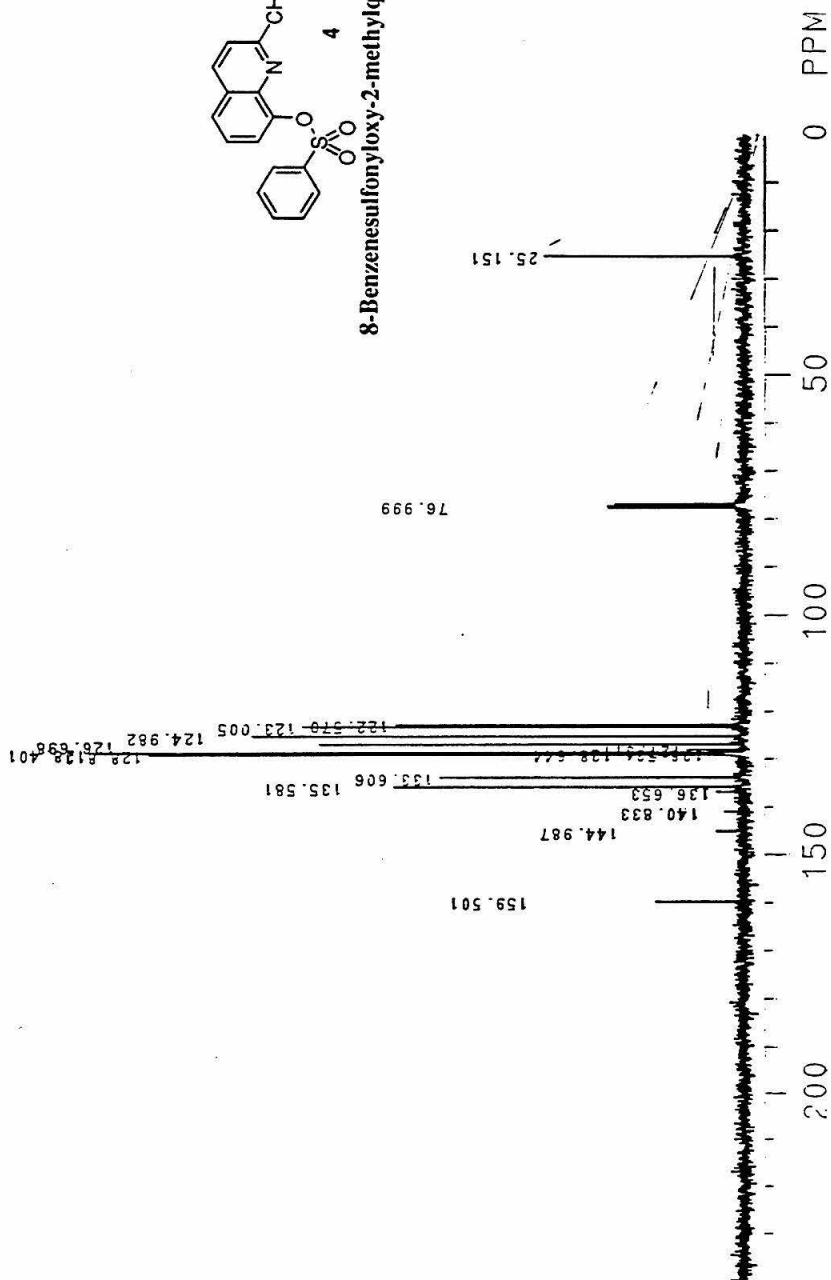
19. "Metallopeptide Design: Tuning the Metal Cation Affinities with Unnatural Amino Acids and Peptide Secondary Structure," Cheng, R. P.; Fisher, S. L.; Imperiali, B. *J. Am. Chem. Soc.* **1996**, *118*, 11349-11356.
20. "The Biological Chemistry of the Elements: The Inorganic Chemistry of Life," Fraústo da Silva, J. J. R.; Willams, R. J. P.; Clarendon Press: New York, 1993.
21. "(S)- $\alpha$ -Amino(2,2'-bipyridine)-6-Propanoic Acid: A Versatile Amino Acid for *de novo* Metalloprotein Design," Imperiali, B.; Fisher, S. L. *J. Am. Chem. Soc.* **1991**, *113*, 8527.
22. "Stereoselective Synthesis and Peptide Incorporation of (S)- $\alpha$ -Amino-(2,2'-bipyridine)-6-Propanoic Acid," Imperiali, B.; Fisher, S. L. *J. Org. Chem.* **1992**, *57*, 757.
23. "Binding Constants: The Measurement of Molecular Complex Stability," Connors, K. A.; Wiley-Interscience: New York, 1987.
24. "Colored Indicators for Simple Direct Titration of Magnesium and Lithium Reagents," Watson, S. C.; Eastham, J. F. *J. Organometal. Chem.* **1967**, *9*, 165-168.
25. "Rapid Chromatographic Technique for Preparative Separations with Moderate Resolution," Still, W. C.; Kahn, M.; Mitra, A. *J. Org. Chem.* **1978**, *43*, 2923.

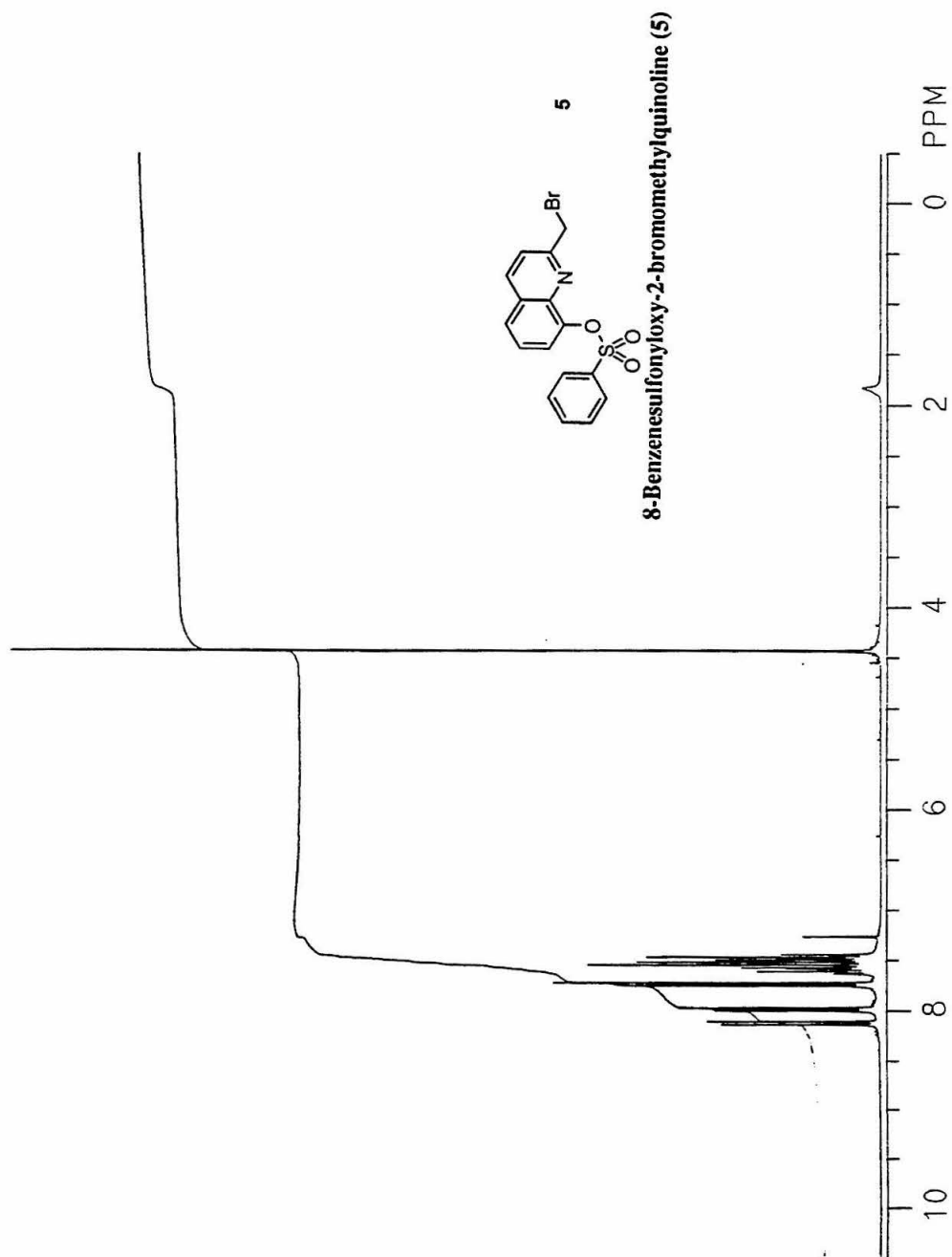
**Spectra to accompany Chapter 3.**

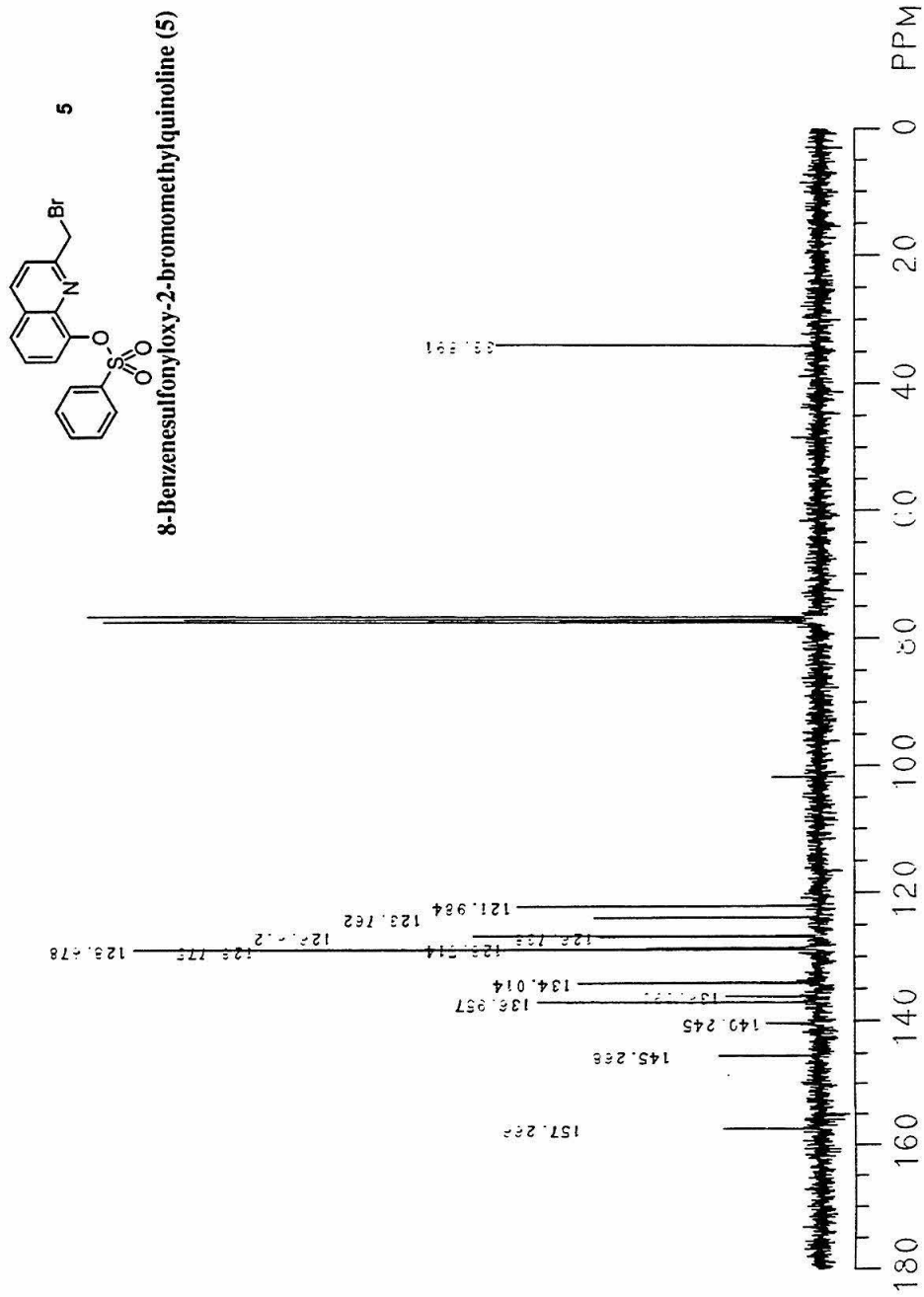


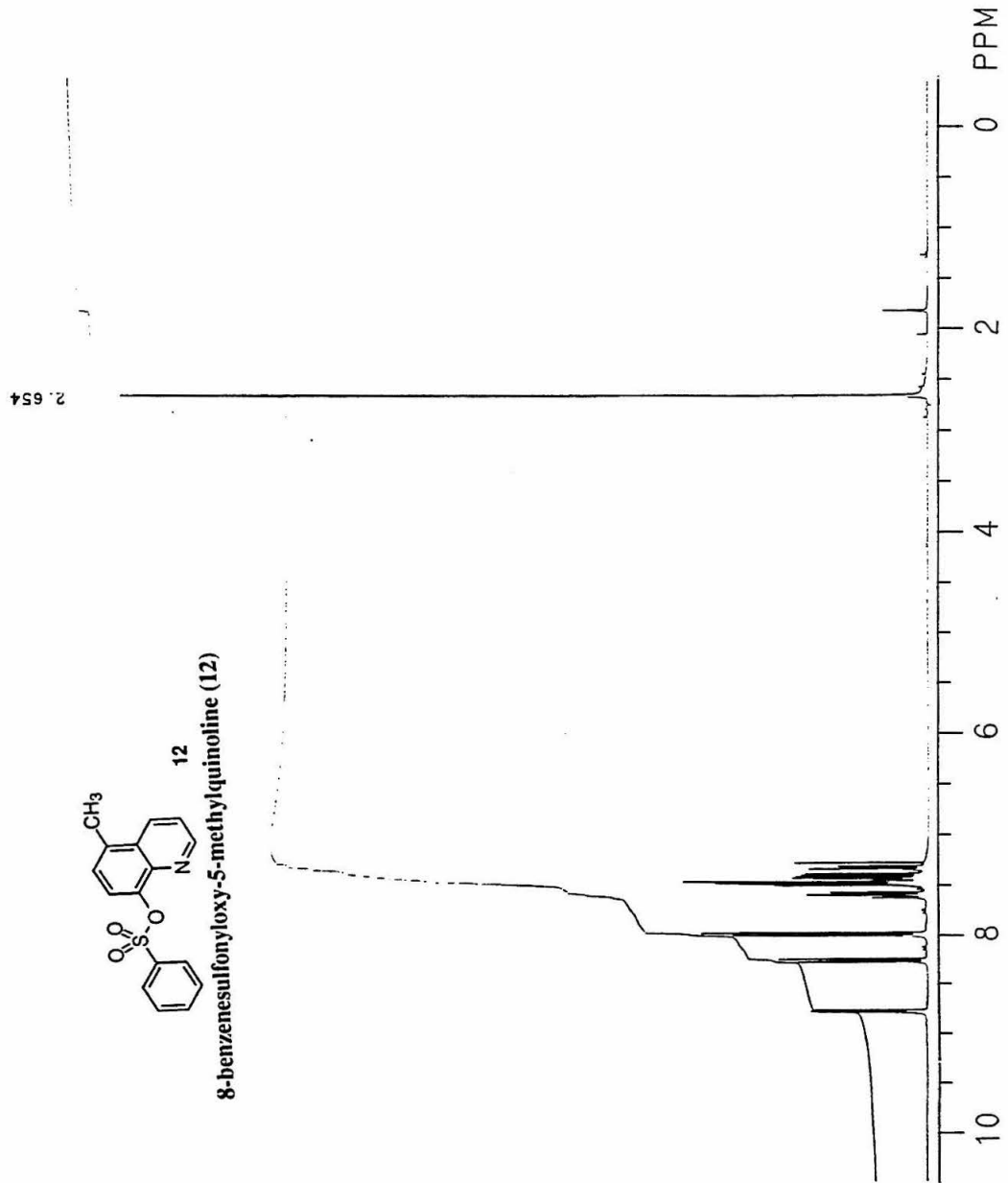


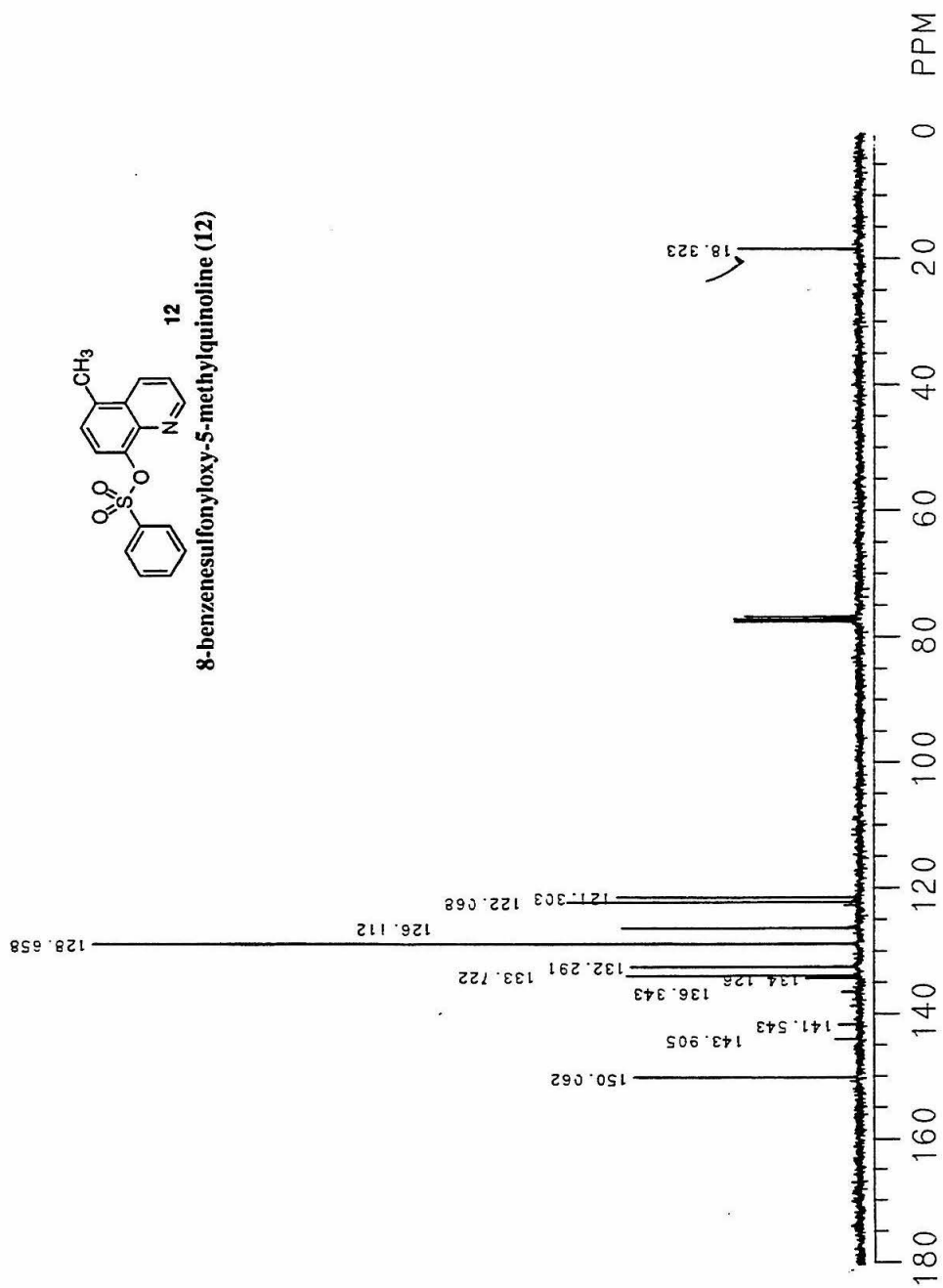
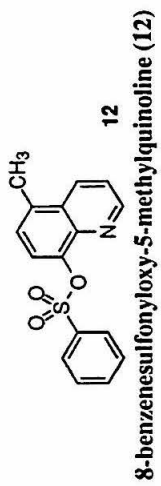
8-Benzenesulfonyloxy-2-methylquinoline (4)

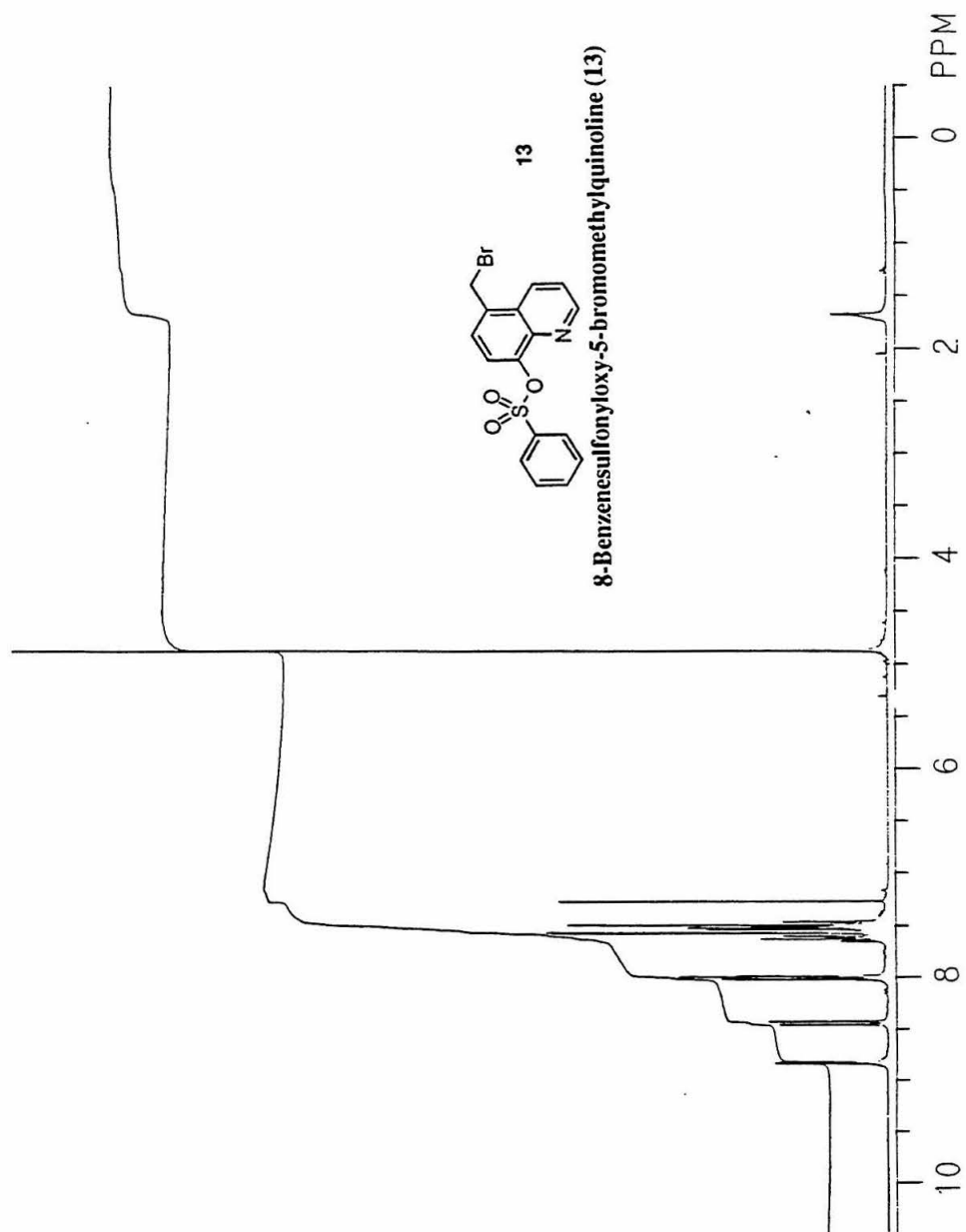


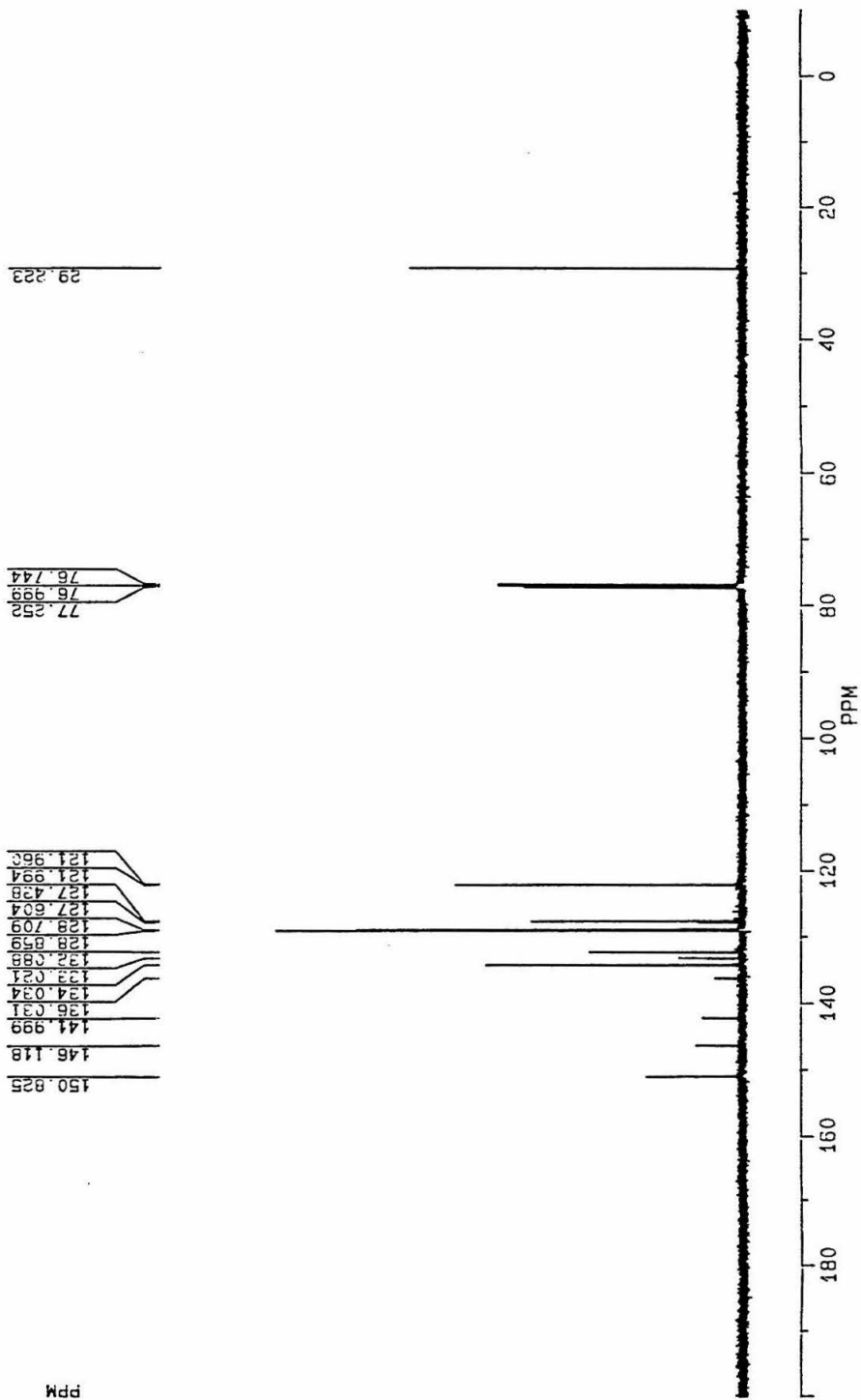
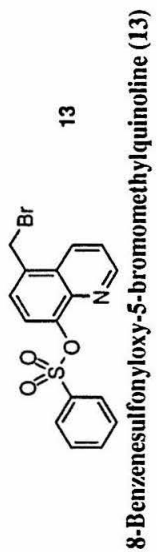


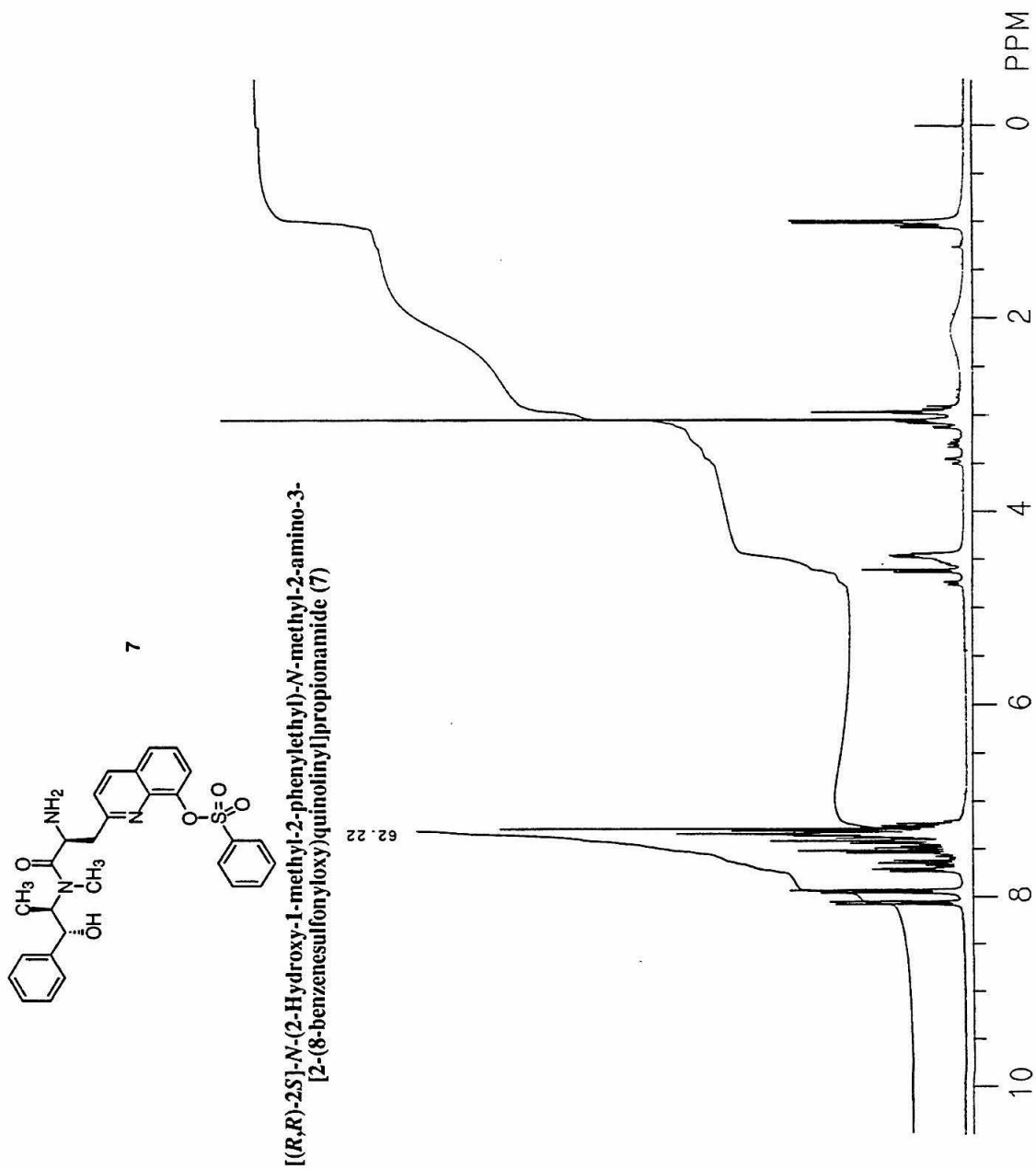


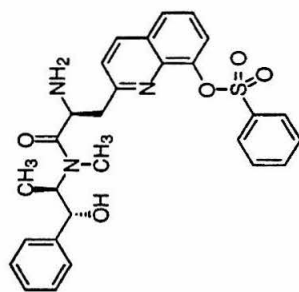




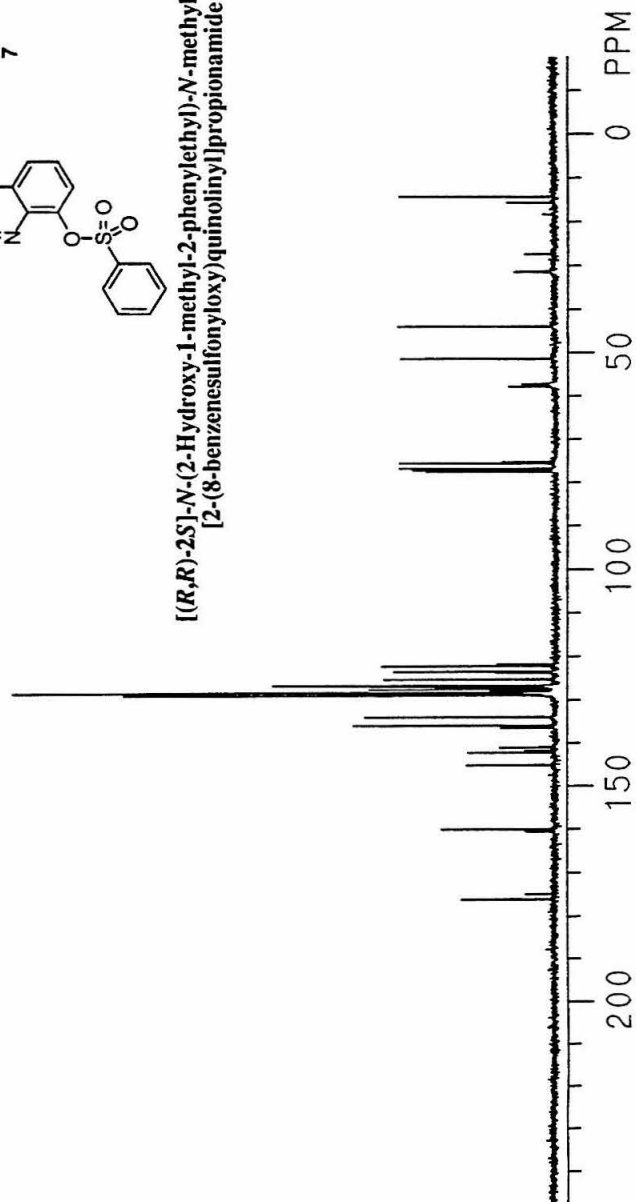


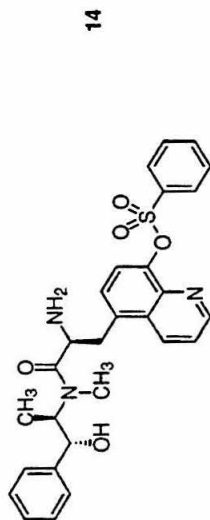




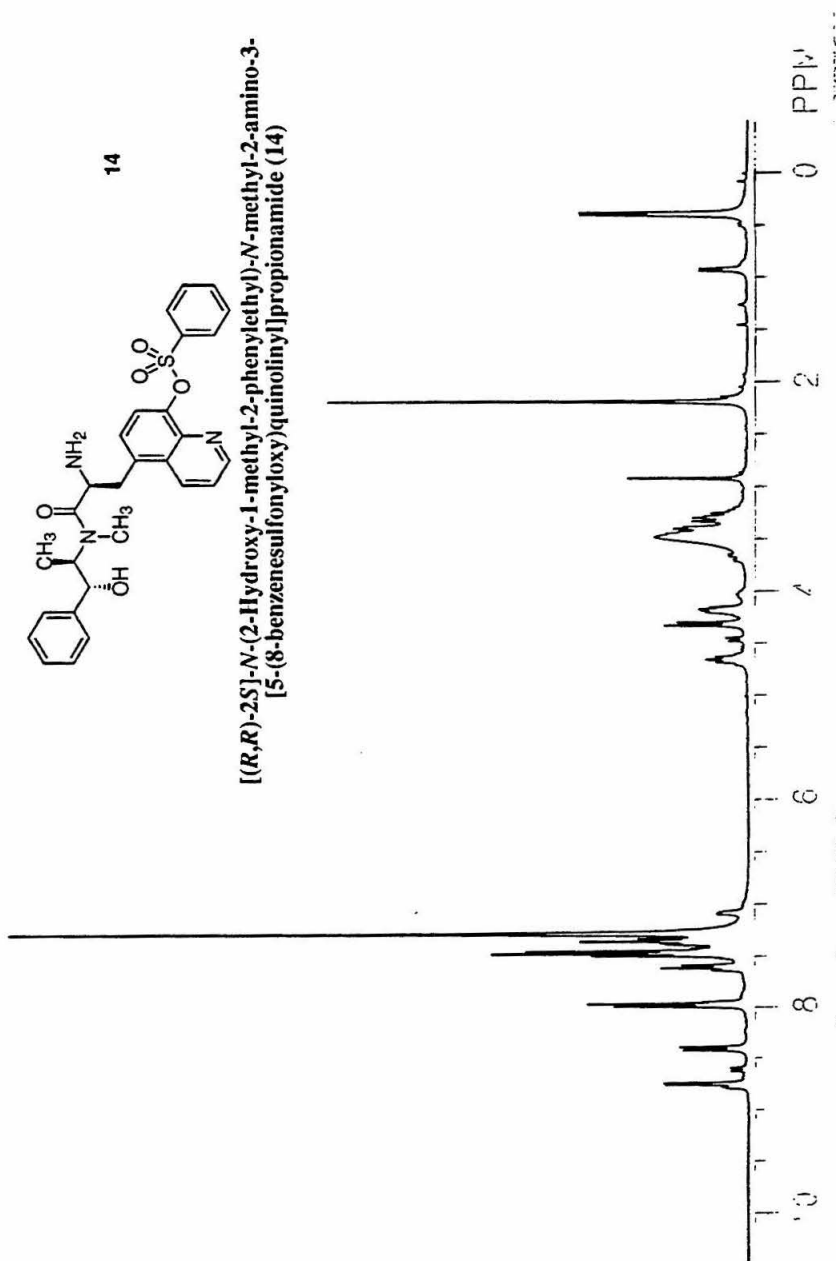


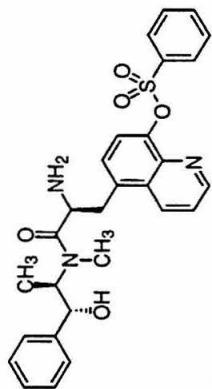
**[(*R,R*)-2*S*]-*N*-(2-Hydroxy-1-methyl-2-phenylethyl)-*N*-methyl-2-amino-3-[2-(8-benzenesulfonyloxy)quinoliny]propionamide (7)**





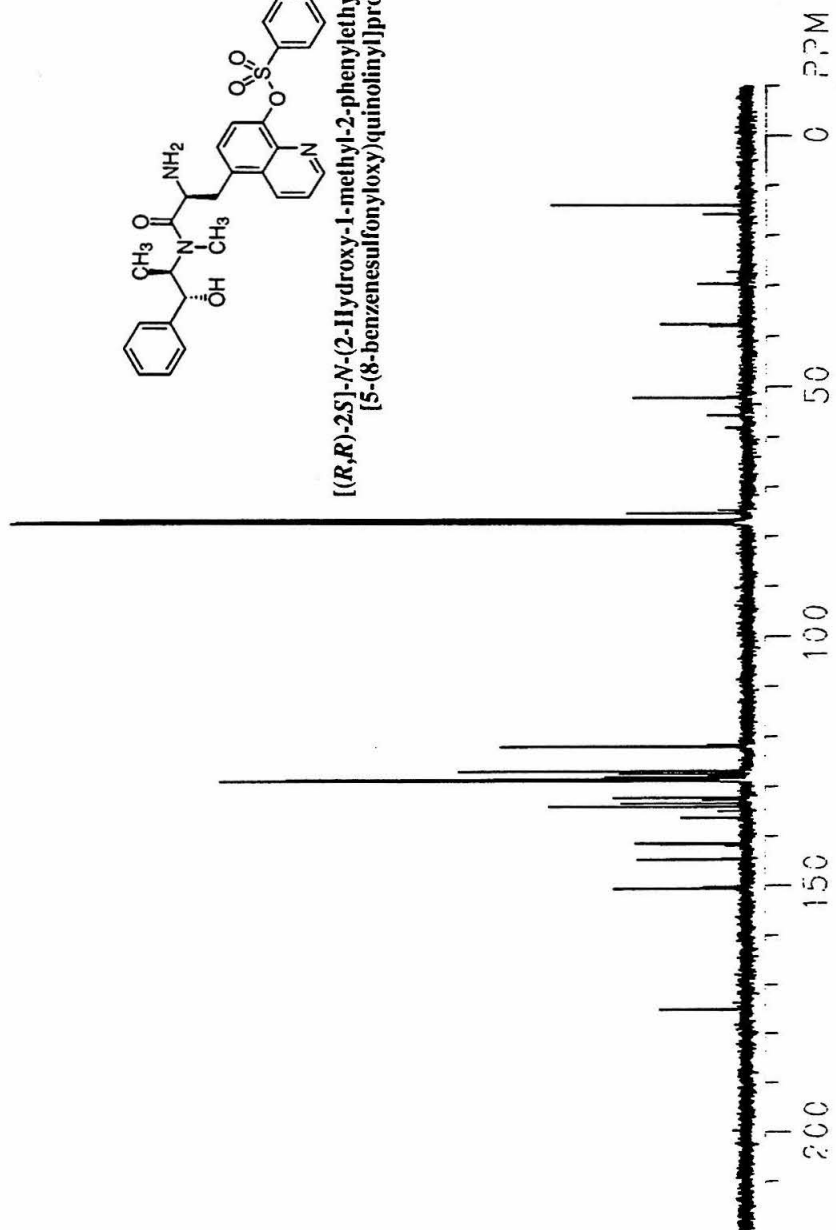
**[(*R,R*)-2*S*]-*N*-(2-Hydroxy-1-methyl-2-phenylethyl)-*N*-methyl-2-amino-3-[5-(8-benzenesulfonyloxy)quinolinyl]propionamide (14)**

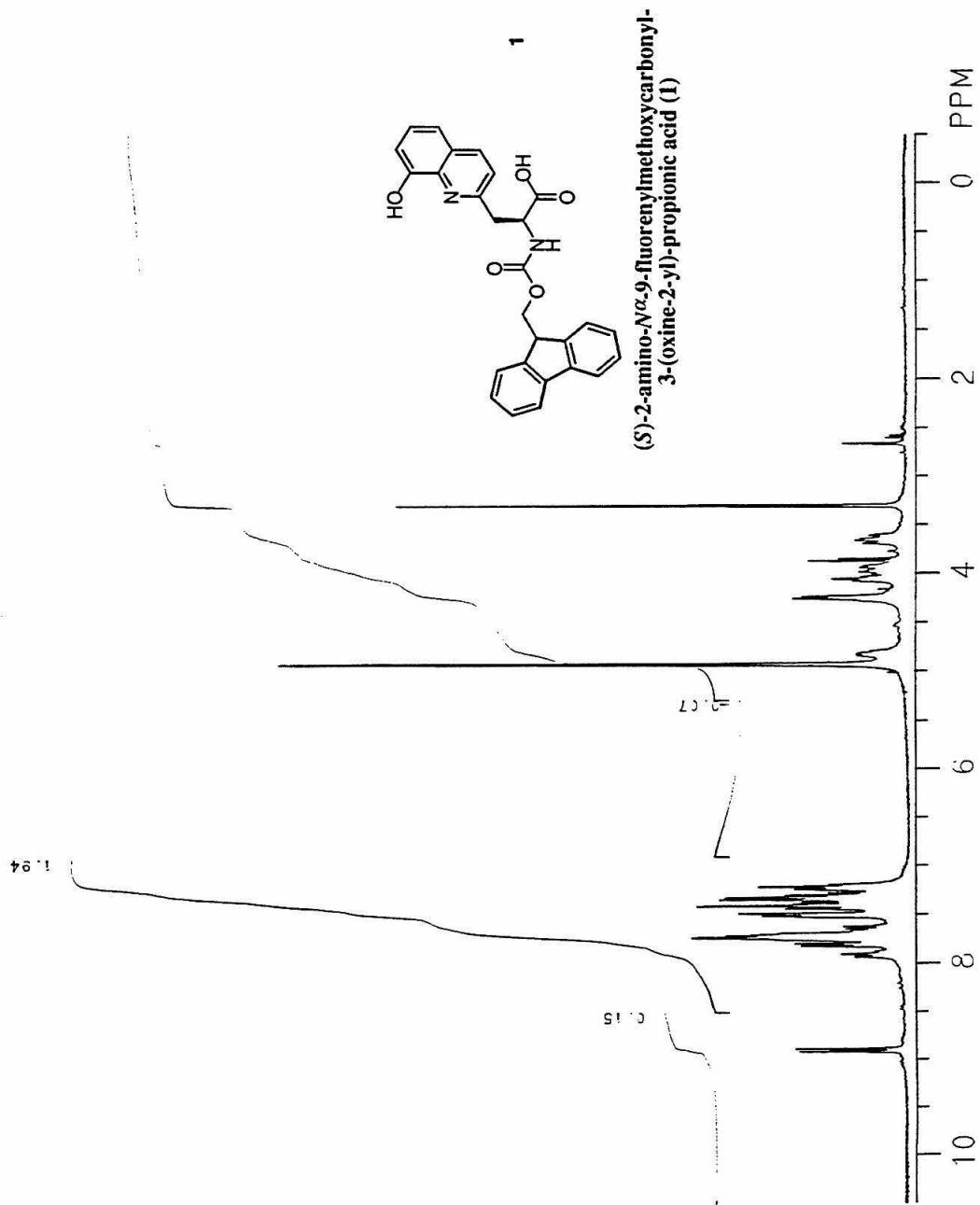


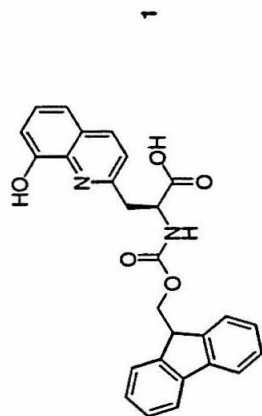


14

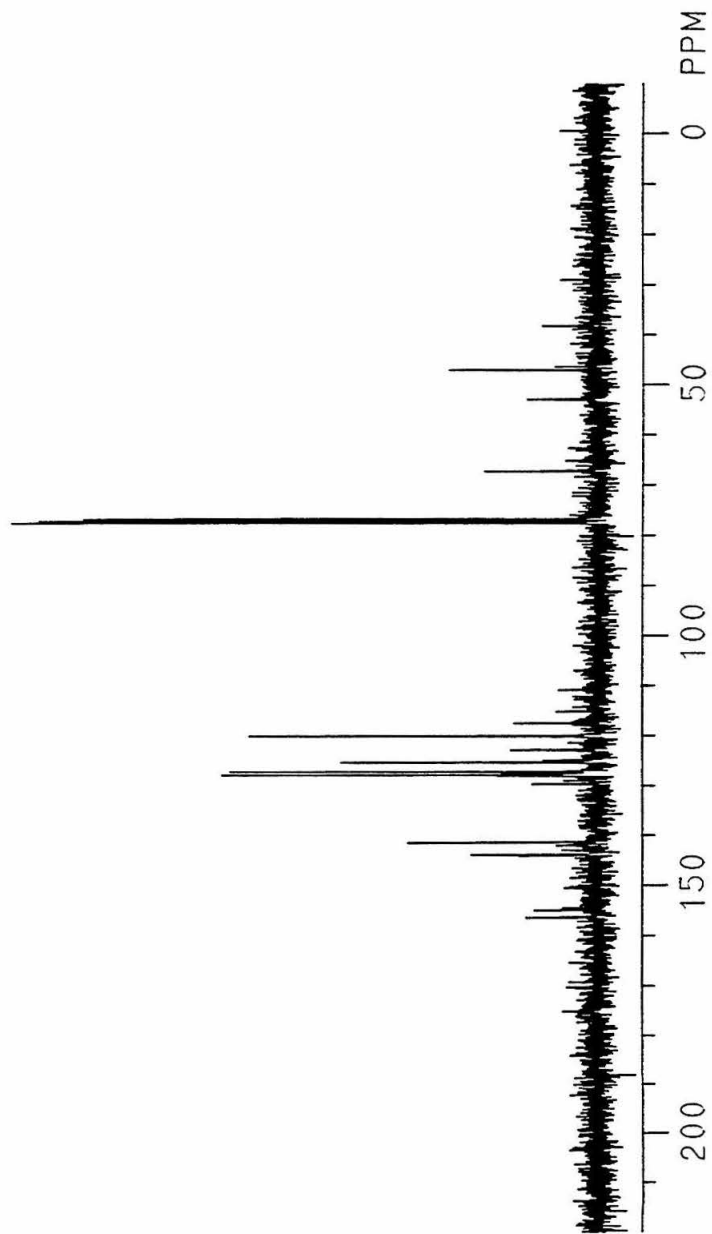
[(*R,R*)-2*S*]-*N*-(2-*H*ydroxy-1-methyl-2-phenylethyl)-*N*-methyl-2-amino-3-[5-(8-benzenesulfonyloxyquinolinyl)propionamide (14)

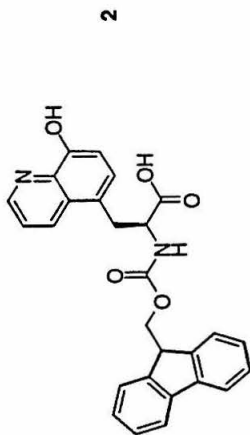




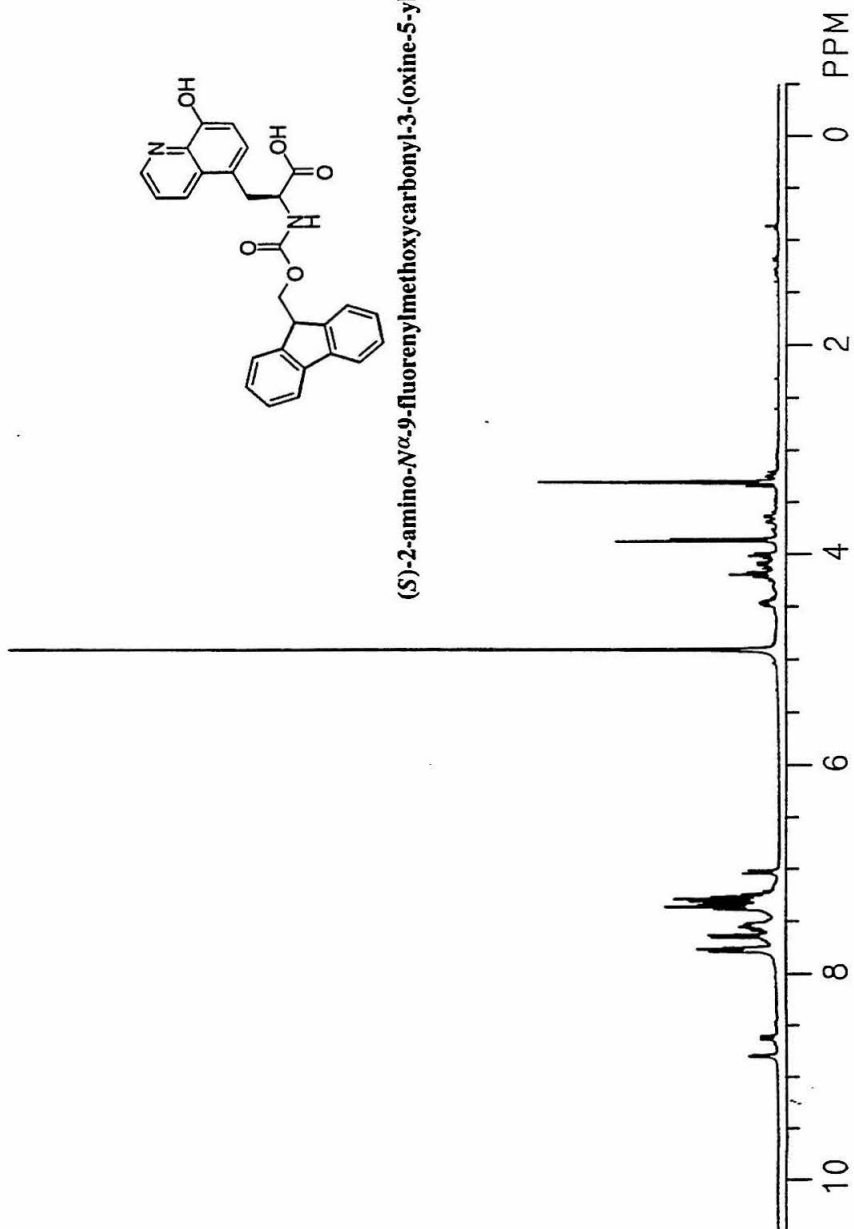


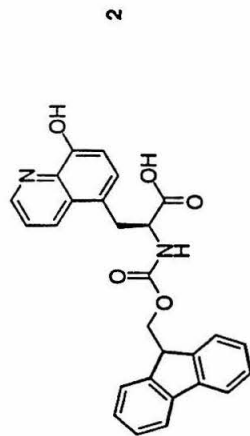
(*S*)-2-amino-*N* $\alpha$ -9-fluorenylmethoxycarbonyl-3-(oxine-2-yl)-propionic acid (1)



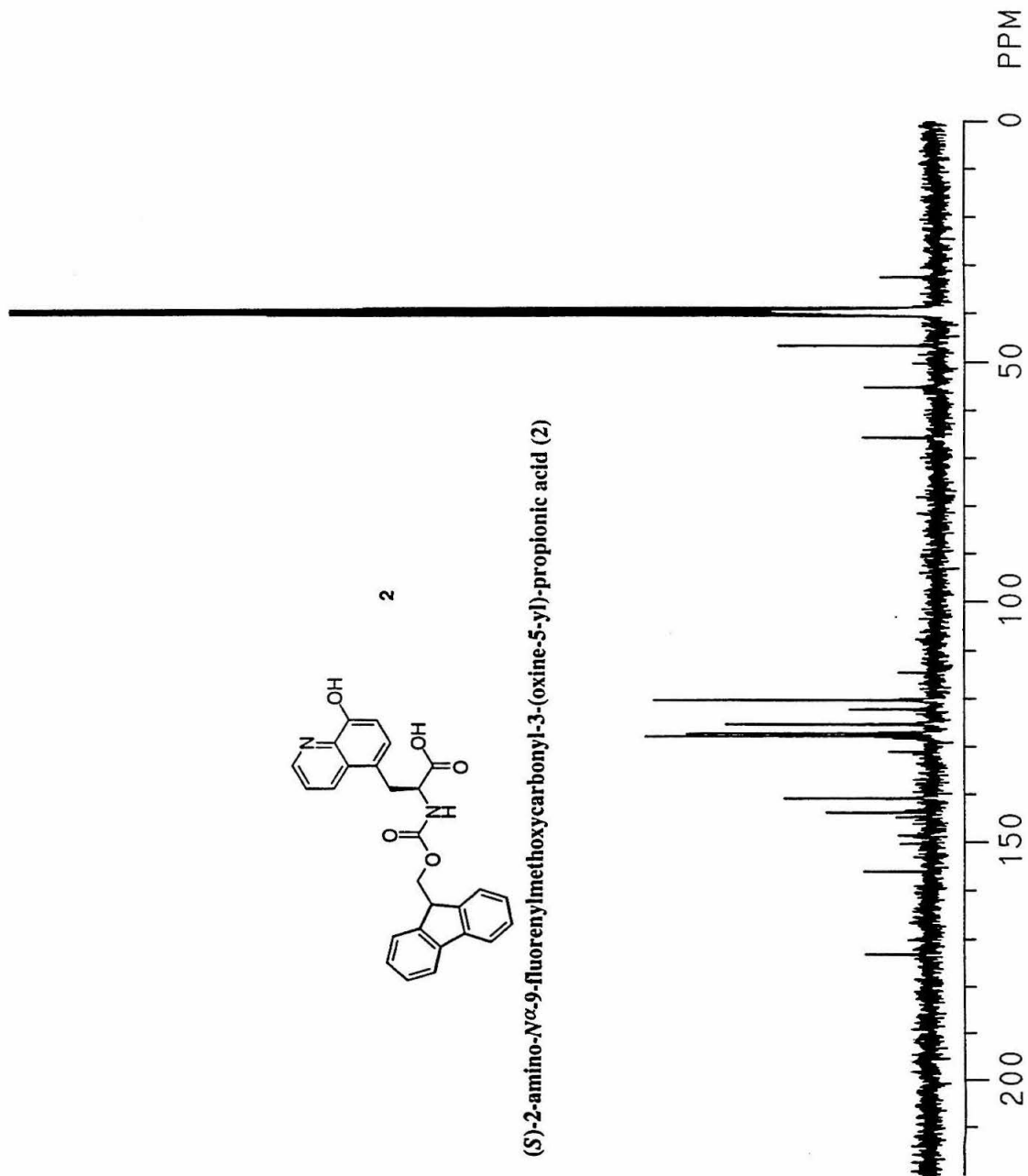


*(S)*-2-amino-*N* $\alpha$ ,9-fluorenylmethoxycarbonyl-3-(oxine-5-yl)-propionic acid (**2**)

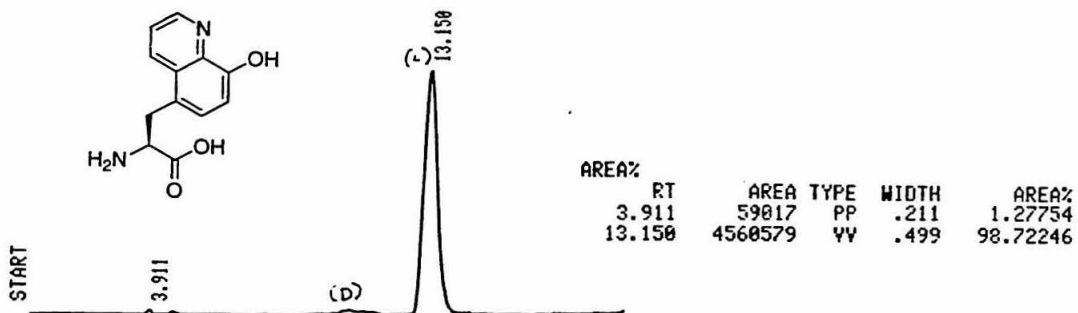
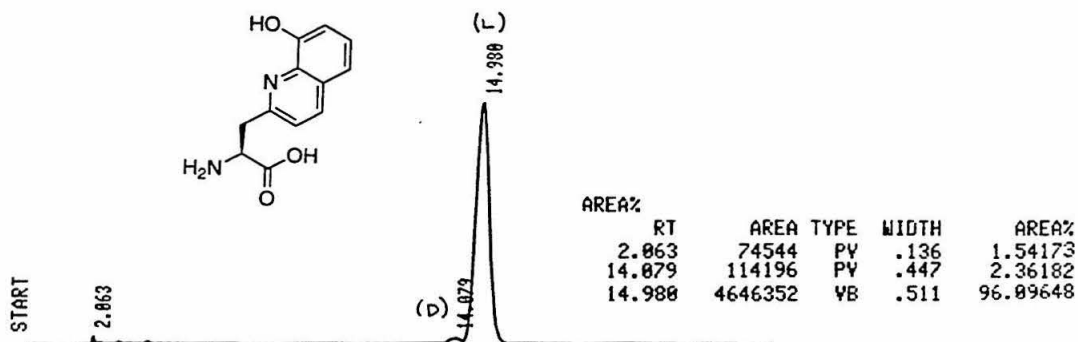




(S)-2-amino-N $\alpha$ -9-fluorenylmethoxycarbonyl-3-(oxine-5-yl)-propionic acid (2)



## CrownPak CR (+) Chiral HPLC Analysis

**Conditions:**0.5 mL min<sup>-1</sup>, 0.1 N HClO<sub>4</sub> mobile phase

UV detection at 320 nm.

Chart speed 0.5 cm min<sup>-1</sup>

scale: 1 division = 1 cm

**Chapter 4. Fluorescent Chemosensors Based on the Amino-Terminal  
Cu(II)- and Ni(II)-Binding Domain of the Serum Albumins**

Reprinted in part with permission from "Exploiting Polypeptide Motifs for the Design of Selective Cu(II) Ion Chemosensors," Torrado, A.; Walkup, G. K.; Imperiali, B. *J. Am. Chem. Soc.* **1997**, *120*, 609-610. Copyright 1997 American Chemical Society.

## Introduction

The production of fluorescent devices for the sensing and reporting of chemical events is currently of significant importance for both chemistry and biology.<sup>1</sup> As presented in Chapter 1, the traditional analytical methods for measuring the concentrations of Cu(II) in biological or environmental samples are limited. In response to this, many researchers have directed efforts toward the production of fluorescent chemosensors for metal ions, with particular attention being given to divalent copper. Methods for the determination of Cu(II) in aqueous or aqueous/organic solution have been described which fall into the categories of biosensors,<sup>2</sup> chemosensors,<sup>3-8</sup> and chemodosimeters.<sup>9</sup> (See Chapter 1.) However, the goal of producing a sensor with that exhibits reversible, selective and sensitive signaling of Cu(II) in aqueous solution that would enable real time measurements for this ion has remained elusive.

The success of the fluorosensors for Zn(II) presented in Chapter 2 and Chapter 3 serves to highlight the versatility of the peptidyl architecture for the production of new chemosensors. By exploiting the synthetic simplicity and structural diversity of this class of molecules, the production of robust, small-molecule chemosensors that exhibit reversible signaling and operate in aqueous solution at neutral pH (without the requirement for organic cosolvents) has been clearly demonstrated. In order to address the specific problem of Cu(II) sensing, the focus of this research was once again directed toward the construction of a selective metal-binding site. As in previous studies, the intended use for such a sensor is ultimately for the measurement of environmental or biological samples, and sufficient detection selectivity is of prime concern to assure that a measurement in the appropriate concentration range can be made, even in the presence of elevated levels of competing divalent cations.

## Results and Discussion

### Selection of a peptidyl motif.

In order to afford high affinity Cu(II) binding, the amino terminal Cu(II)- and Ni(II)-binding (ATCUN) motif found of the serum albumins was selected.<sup>10,11</sup> The serum albumins bind both Cu(II) and Ni(II) avidly, with intrinsic affinity constants on the order of  $10^{11} \text{ M}^{-1}$  for the protein-Cu(II) complex.<sup>12</sup> (Dissociation constants for ATCUN-Cu(II) complexes are frequently misstated as being  $\sim 10^{-17} \text{ M}$ , an occurrence that probably results from as interpreting the *overall* stability constant, which includes  $\text{H}^+$  terms, as the *intrinsic*, pH 7, formation constant.)<sup>12,13</sup> Regardless, the simple tripeptide sequence Gly-Gly-His,<sup>14-18</sup> and other related sequences,<sup>19-21</sup> effectively mimic these binding characteristics, competing with the intact protein for Cu(II) binding.<sup>15</sup> Crystallographic and potentiometric studies have shown that the histidine-derived imidazole  $\delta$ -nitrogen, the *N*-terminal  $\alpha$ -amine, and two intervening (deprotonated) amide nitrogens, are recruited as ligands at neutral pH to form a tetradentate 1:1 peptide:metal complex with slightly distorted square-planar geometry (Figure 4-1).<sup>22</sup>

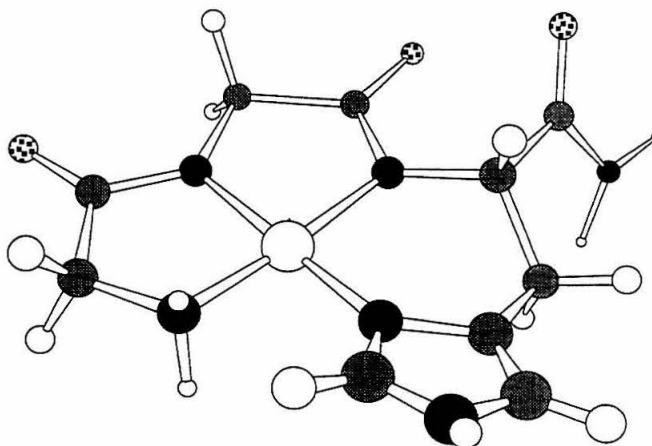
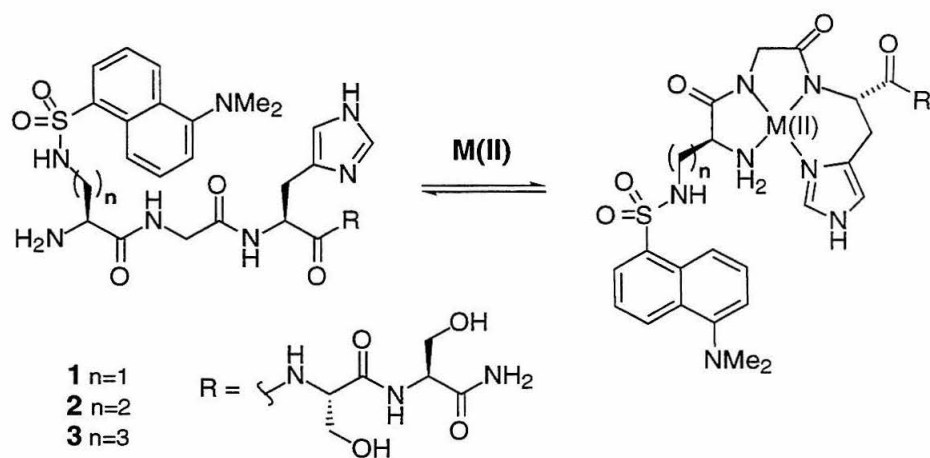


Figure 4-1. A model of an ATCUN motif (Gly-Gly-His-CONH<sub>2</sub>) displaying the metal ion bound with square planar geometry.

As this peptidyl motif selectively targets Ni(II) and Cu(II) ions, intramolecular quenching of an appropriately incorporated fluorophore represents a convenient means for signaling cation binding. Because the *N*-terminal amine is stringently required for high affinity binding, the ATCUN motif for metal binding is limited to the *N*-terminus of naturally encoded peptides. However, substitution of the amino-terminal glycine for a residue with an amine-containing side chain has been shown to allow elaboration of the motif while preserving the metal binding characteristics.<sup>23,24</sup> By applying this strategy, the preparation of peptides that exhibit avid metal cation binding with a coupled fluorescent probe for optical signal transduction is enabled. Furthermore, by the incorporation of a differentially protected *N*<sup>ω</sup>-Fmoc-diamino acid as the *N*-terminal residue, the introduction of a wide variety of amine-reactive fluorophore labeling reagents may be effected in a standard peptide-lengthening protocol thereby assuring synthetic simplicity.

#### **Preliminary investigation of fluorescence quenching with the ATCUN motif.**

In order to gain information as to the properties one might expect from such ATCUN-based fluorescent chemosensors, a family of peptides were prepared, containing a pendant 5-*N*, *N*'-dimethylamino-naphthalene-1-sulfonyl (DNS) fluorophore at varying distances from the metal-binding site. The *N*-terminal amino acid was substituted with residues which contain a side chain amine with varying lengths of intervening methylene units linking it to the  $\alpha$ -carbon. The representative amino acids incorporated at this position are (*S*)-2,3-diaminopropanoic acid (Dap), L-( $\alpha,\gamma$ )-diaminobutyric acid (Dab), and L-ornithine (Orn) (Figure 4-2). In addition, two *C*-terminal serine residues were appended to assure aqueous solubility.



**Figure 4-2.** The first generation of compounds based on the ATCUN motif. Both Ni(II) and Cu(II) bind with high affinity, thereby quenching fluorescence.

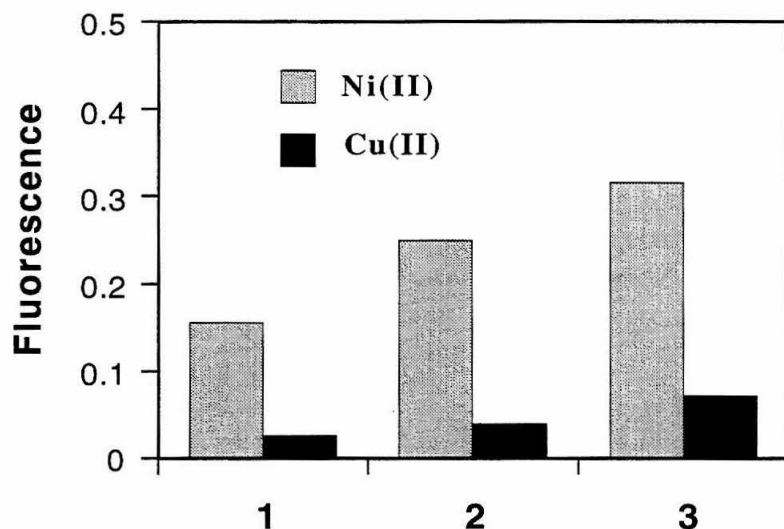


**Figure 4-3.** Fluorescence emission at 570 nm of **1-3**, with an added equivalent of Ni(II) or Cu(II). The compound with the shortest linker (**1**) is most effectively quenched, and Cu(II) is a more effective quencher than Ni(II). Results have been normalized such that in the absence of metal cations the fluorescence is equal to unity. Measurements were performed with 10  $\mu$ M chemosensor, excitation at 333 nm in 0.15 M NaCl, 50 mM HEPES, pH 7.0.

Preliminary studies centered on the response of peptides **1-3** to Ni(II) and Cu(II). Fluorescence emission spectra were collected in 50 mM HEPES, 0.15 M NaCl (pH 7.0) with 10  $\mu$ M peptide, and the effect of an added equivalent of Ni(II) or Cu(II) determined (Figure 4-3). In all cases, the titration of divalent metal ion stocks into solutions of chemosensor were indicative of tight binding; a linear increase in fluorescence quenching was observed until the chemosensor was saturated at one equivalent of added metal, and further addition of divalent metal produced no further quenching (data not shown).

These studies revealed that a shorter linkage from the peptidyl backbone to the fluorophore resulted in more efficient fluorescence quenching, and that the addition of Cu(II) produced a greater change in the DNS fluorescence than did Ni(II). For example, one equivalent of Cu(II) leaves < 5% of the initial emission intensity (measured at 570 nm), while for Ni(II), 30-40% of the original emission intensity remained. For all peptides, the addition of excess EDTA to the assay mixture reversed the metal ion-induced fluorescence quenching. Furthermore, 100  $\mu$ M concentrations of Mn(II) and Co(II), and millimolar levels of Mg(II), Ca(II), Zn(II), or Cd(II) have no effect on the fluorescence of these chemosensors. The ferrous ion has a slight quenching effect; at 10  $\mu$ M chemosensor, an equivalent of Fe(II) causes ~5% quenching.

The Ni(II)- or Cu(II)-induced quenching of a variety of fluorophores has been a common theme in the design of chemosensors for these species. In general, transition metal cations can quench fluorescence by two distinct mechanisms, photoinduced electron transfer (PET) and energy transfer.<sup>25,26</sup> For the Ni(II) and Cu(II) ions, accession of either of these mechanisms is a possibility. This is particularly so in light of the fact that the ATCUN motif presents a very strong-field coordination environment by virtue of the amine and two deprotonated amide ligands,<sup>22</sup> which provide stabilization of these towards being oxidized (if only transiently) to the trivalent species.<sup>27</sup>

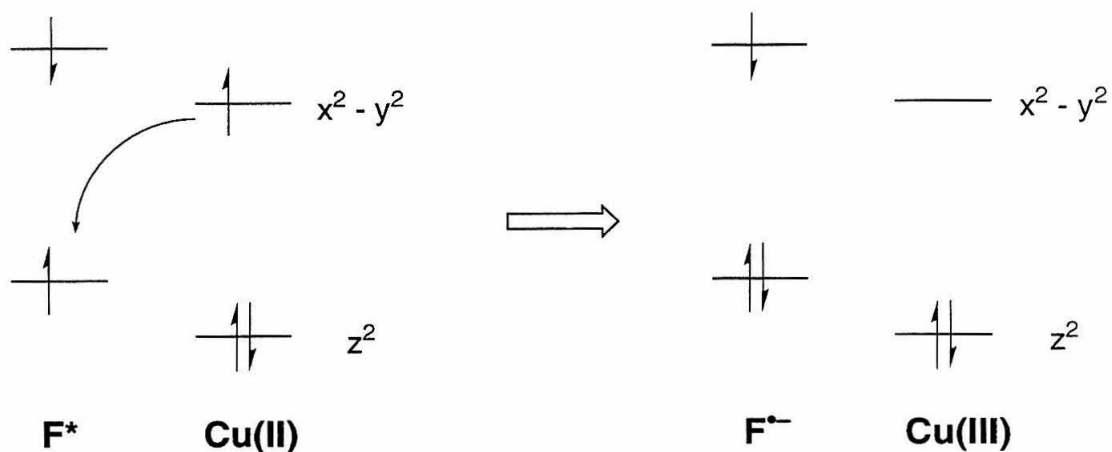
The workings of both mechanisms may be explained through a frontier molecular orbital analysis;<sup>6</sup> a qualitative representation of the relevant molecular orbitals involved

in a Cu(II)-fluorophore quenching interaction are presented in Figure 4-4. Specifically, the frontier orbitals for Cu(II) ion in a strong field square planar coordination geometry are the  $x^2-y^2$  and  $z^2$  orbitals.<sup>28</sup> In the case of electron transfer quenching, the energetics of the (singly occupied)  $x^2-y^2$  orbital, relative to those of the excited state of the fluorophore, are such that the Cu(II) ion can donate an electron to ground-state HOMO of the fluorophore (Figure 4-4a). After this occurrence, the resulting radical anion (fluorophore) cannot relax to the ground state with radiative emission: it is quenched. Eventually, recombination to regenerate the starting species can occur. Alternately, in an energy transfer mechanism (Figure 4-4b) the relaxation of the fluorophore from the excited state is coupled with a promotion of a Cu(II) electron to the  $x^2-y^2$  orbital, which can readily relax without emission.<sup>25</sup>

Experiments may be done to elucidate which of these mechanisms is in operation for a given chemosensor; at cryogenic temperatures in glassy solids, electron transfer rates are drastically slowed or stopped, while FRET processes are not. Accordingly, there have been extensive studies done to determine whether particular sensors owe their signaling behavior to a PET or FRET mechanism.<sup>6,29-36</sup> However, a strong argument can be made that knowledge of the *exact* mechanism of fluorescence modulation for a chemosensor is not necessary as long as the fluorescence response of the chemosensor is reliable, sensitive and selective.

Importantly, the results obtained from the analysis of **1-3** indicate that a reversible, intramolecular quenching mechanism is in operation, and that the chemosensors are robust under the conditions used. Furthermore, the inherent metal-binding selectivity of the modified ATCUN motif is sufficient to perform sensitive monitoring for a subset of the divalent metal cations, namely Cu(II) and Ni(II).

### a. Electron Transfer



### b. Energy Transfer

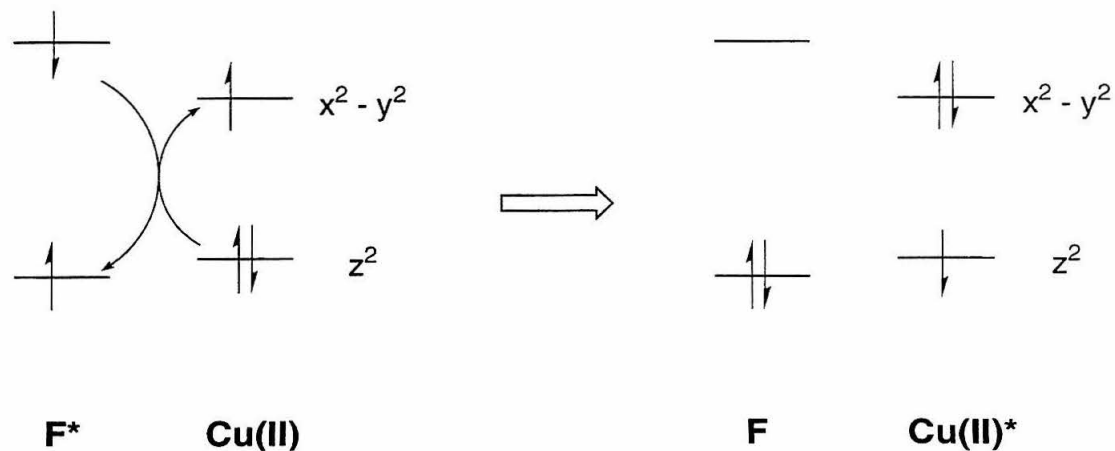


**Figure 4-4.** Mechanisms for fluorescence quenching by the  $Cu(II)$  ion. a. Electron transfer from the  $Cu(II)$  ion reduces the excited fluorophore to form the radical anion. b. The excited fluorophore transfers its energy to the  $Cu(II)$  ion *via* FRET.

**Investigation of the role of the fluorophore in signaling.**

To increase the sensitivity of the fluorescence signal, alternate fluorophores were investigated. As described earlier, both mechanisms of electron transfer or energy transfer are accessible to these chemosensors. Furthermore, changing the fluorophore could result in different quenching mechanism being accessed for an otherwise identical compound. For this reason, no single fluorophore can be identified as a “best” choice for application and, as a consequence, a *functional* screen of reporting fluorophores was initiated. However, in the event that an energy transfer quenching mechanism is being accessed, insight into this process does allow for the judicious selection of fluorophores. Since the emission of the fluorophore and the absorption of the donor must overlap for FRET quenching, fluorophores were chosen that would span the appropriate spectral range.

The structures of the fluorophores 2-benzoxazole (BZX), 9-carboxamido-anthracene (ANT), coumarin 343 (COM), and Rhodamine B (RHD), together with their excitation and emission maxima are shown in Figure 4-5. These fluorophores were selected for chemosensor incorporation since their emission maxima in water span the absorption profile of the ATCUN-Cu(II) complex. Differences in the overlap between the fluorophore emission and the metal center absorbance should result in varied quenching efficiency. Additionally, these fluorophores are all more efficient energy donors, having greater extinction coefficients and quantum yields than does the DNS group. This property is advantageous as it may theoretically enable metal cation determinations at lower concentrations. The spectral overlap for these fluorophores, as well as for the DNS moiety, in relation to the absorption band of an ATCUN-Cu(II) complex, are presented in Figure 4-6.

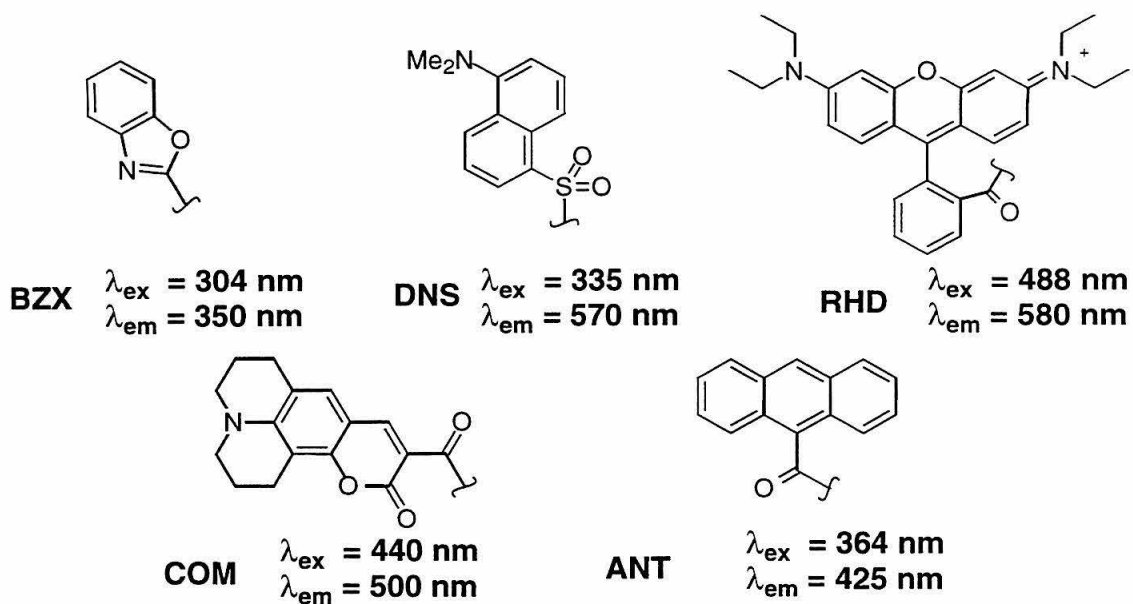


**Figure 4-5.** Fluorophores investigated to increase the sensitivity of the sensors to Cu(II) or Ni(II) quenching.

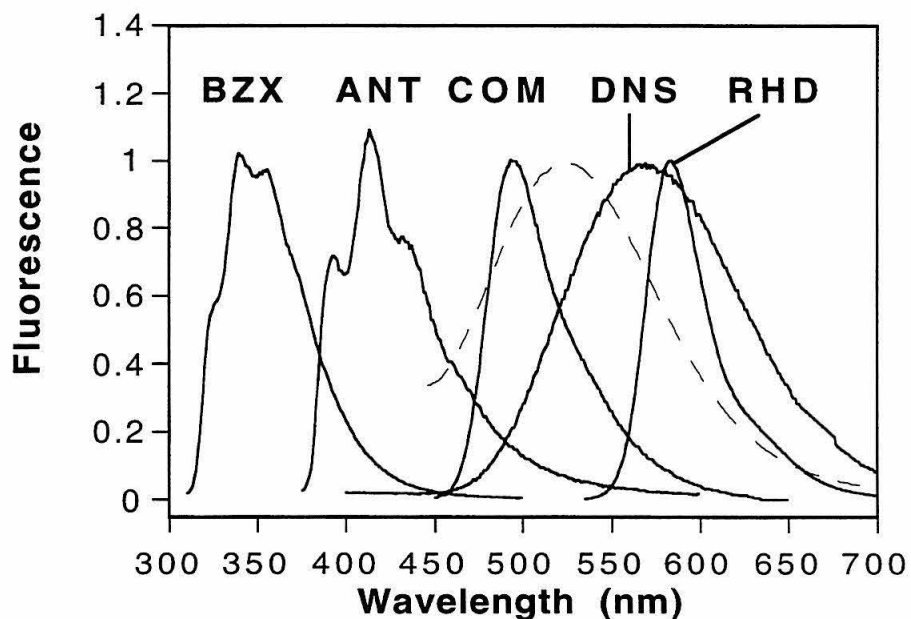
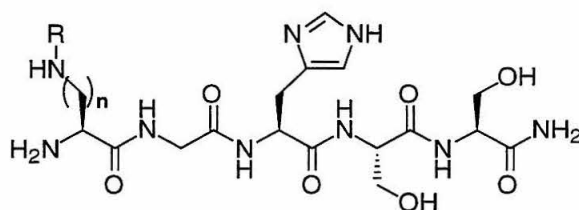


**Figure 4-6.** Fluorescence emission spectra (solid lines) of the listed fluorophores, compared with the absorption band of an ATCUN·Cu(II) complex (dashed line). Spectra were acquired in 50 mM HEPES, 150 mM NaCl, pH 7.0 and have been normalized to be of equal height at their emission/absorption maxima.

In order to test the ability of these new fluorophores to provide a more sensitive spectroscopic handle for Ni(II) and/or Cu(II) ion sensing, a second generation of peptidyl chemosensors (**4-8**) was prepared. Other than the choice of fluorophore introduced, modifications to the peptidyl template were kept to a minimum. Similarly to the first series of peptides, Dab or Orn residues were chosen for incorporation at the first position, and the Gly-His-Ser-Ser-NH<sub>2</sub> sequence was included in each of the peptides. The chemical identity of compounds **4-8** are summarized in Figure 4-7.



	compound				
	<b>4</b>	<b>5</b>	<b>6</b>	<b>7</b>	<b>8</b>
n	2	2	3	3	3
R	BZX	ANT	RHD	ANT	COM

**Figure 4-7.** Structures of the second series of peptides used to investigate the role of the fluorophore in the preparation of fluorescent chemosensors. The structures of the fluorophores are presented in Figure 4-5.

Spectroscopic studies of **4-8** convincingly demonstrated that the inclusion of a robust fluorophore is critical for overall chemosensor performance. Unfortunately, the compounds containing the RHD (**6**) and COM (**8**) moieties displayed fluorophore-related complications including photobleaching or degradation. While the benzoxazole-containing compound (**4**) did not exhibit these limitations, its fluorescence emission was insensitive to added Ni(II) and Cu(II). Finally, the anthracene containing compounds (**5, 7**) exhibited Ni(II)- and Cu(II)-dependent fluorescence. Interestingly these compounds exhibited greater Ni(II)-induced fluorescence sensitivity than the

corresponding DNS-compounds, but were less sensitive to Cu(II) (Figure 4-8). To take advantage of this bias towards greater Cu(II) sensitivity provided by the DNS fluorophore, subsequent chemosensors incorporated that group for signaling.

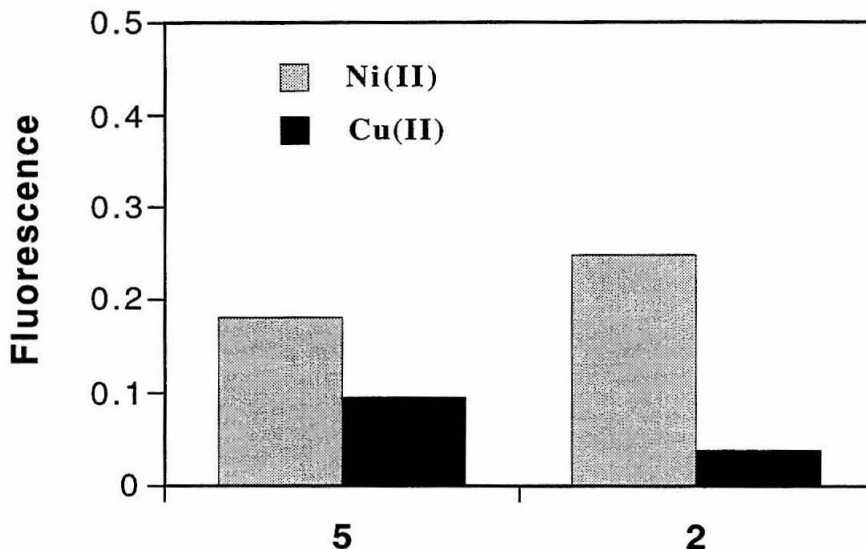


**Figure 4-8.** Fluorescence intensity 10  $\mu\text{M}$  **5** (ANT fluorophore) compared with that of 10  $\mu\text{M}$  **2** (DNS fluorophore) upon the addition of an equivalent of Ni(II) or Cu(II). Measurements were made at the emission maximum of the relevant compound (**5**, 413 nm; **2**, 570 nm). Intensities are normalized such that in the absence of divalent metal cations, the fluorescence is equal to unity. Excitation performed at 364 nm (**5**), or 333 nm (**2**).

Additionally, during the course of studies on the first two series of peptides, it was noted that Ni(II) binding was slow, particularly at low concentrations of chemosensor ( $\leq 1 \mu\text{M}$ ). This behavior is characteristic of the Ni(II) ion, which exhibits slow ligand exchange (even for the hexa-aquo species) relative to Cu(II),<sup>37,38</sup> and which may be expected to be accentuated due to the kinetic chelate effect.<sup>39</sup> Unfortunately, this property of the cation makes the determination of its concentration with complexing reagents problematic when it is present at trace ( $< 1 \mu\text{M}$ ) levels. Consequently, focus was shifted towards increasing the Cu(II) binding selectivity of the peptidyl motif.

**Investigations of the role of the position 3 residue in metal ion binding.**

To achieve greater binding selectivity between Ni(II) and Cu(II), modifications to the coordination environment presented to the metal by the peptidyl motif were investigated. While both Ni(II) and Cu(II) will support square-planar coordination geometries, Ni(II) is more stringent in this regard.<sup>22,28,38,40</sup> By virtue of its  $d^9$  electronic configuration, Cu(II) can accommodate distorted square-planar coordination better than Ni(II). Additionally, Cu(II) favors the inclusion of a fifth ligand to form square-pyramidal or trigonal bipyramidal complexes,<sup>41,42</sup> particularly those incorporating a long axial ligand-metal bond.<sup>43</sup> In addition to ligand geometry, varying the ligand type (hard or soft,  $\pi$ -acidity) could provide a handle for differentiation between Ni(II) and Cu(II). In this light, the residue in the third position of the peptidyl template is of particular importance. The side chain imidazole of the histidine residue at position 3 is required for high affinity binding in naturally-derived peptides. Chemical synthesis, however, allows greater flexibility in constructing analogous motifs, thereby permitting the modification of both coordination geometry and ligand type.

A third set of peptides (**9-18**), incorporating appropriate residues in the second and third positions to either deliver an additional axial ligand, or to replace the equatorial imidazole of L-histidine were synthesized (Figure 4-9). The residues selected to deliver the putative axial ligand included cysteine, aspartic acid, and glutamic acid. Additionally, a peptide incorporating a valine in the second position was prepared to probe the effect of additional steric bulk at that position upon metal binding. Both naturally-derived and nonstandard residues were chosen for position 3. The most simple change made was to incorporate D-histidine in place of its enantiomer within some of the peptides. Incorporation of the heterochiral residue could potentially alter the presentation of auxiliary ligands included within residue 2. In addition to D-histidine, the L-enantiomers of glutamic acid (Glu), glutamine (Gln), homocysteine (Hcs), 4-thiazolylalanine (Thz), and 2-pyridylalanine (Pya) were investigated as replacements

for the third residue. Importantly, the residues Hcs, Thz, and Pya preserve the opportunity to form a 6-membered chelate, analogous to that of the native ligand (illustrated in Figure 4-1).

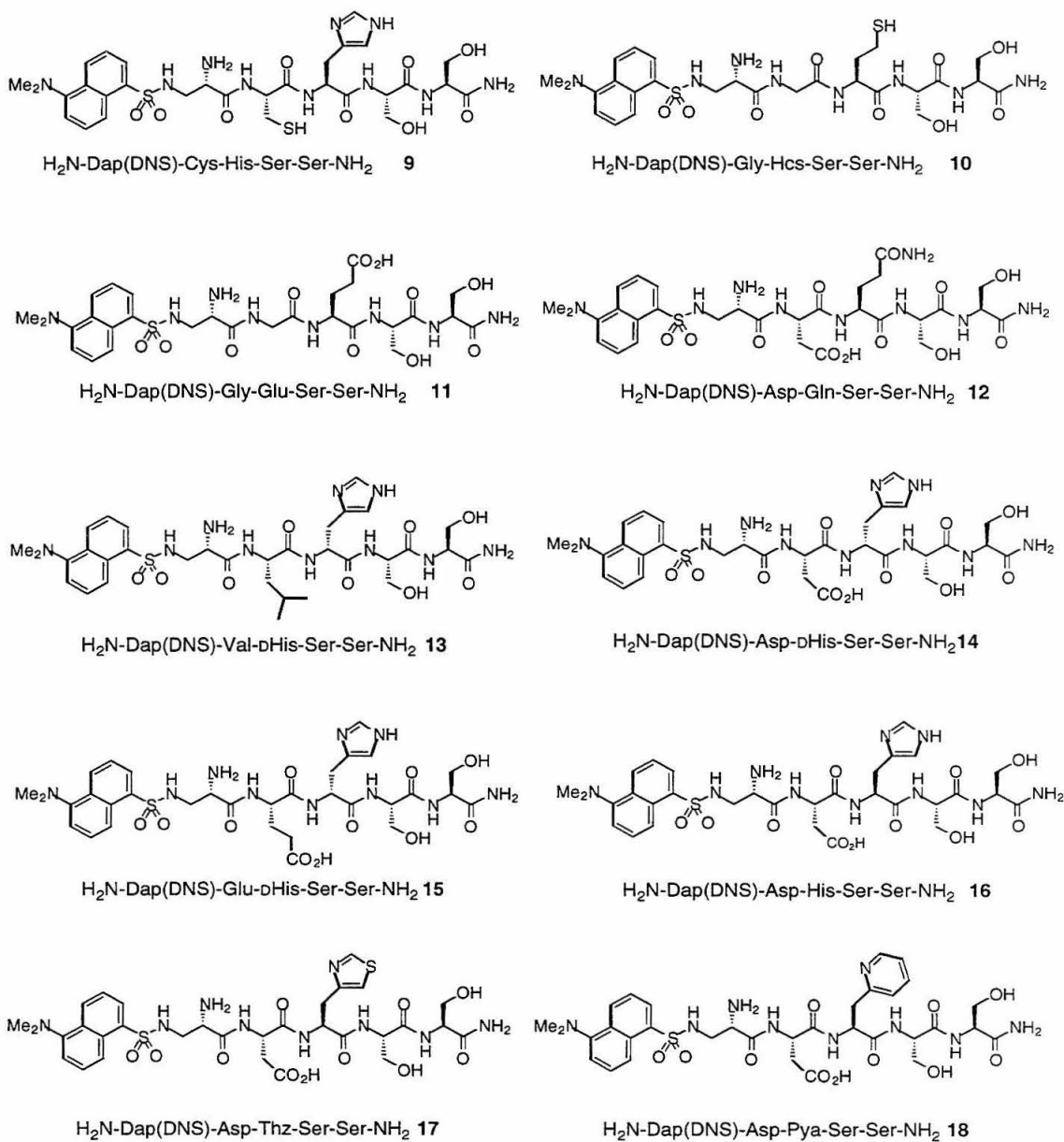


**Figure 4-9.** Structures of the third series of peptidyl chemosensors prepared (9-18).

Compounds **9-18** were assayed for their fluorescence response to both Ni(II) and Cu(II). Although the thiol-containing compounds (**9, 10**) suffered from oxidative problems which precluded a thorough investigation of their properties, the remainder of the compounds displayed Cu(II)-dependent fluorescence changes. Interestingly, both **11** and **12**, which incorporated glutamic acid and glutamine respectively at position 3, displayed little fluorescence response to an equivalent of added Ni(II) (Figure 4-10). Encouraged by these findings, the concentration of chemosensor was lowered from 10  $\mu\text{M}$  to 1  $\mu\text{M}$  to observe correspondingly lower concentrations of Cu(II). Under these conditions, however, compounds **11** and **12** were essentially insensitive to sub-stoichiometric quantities of Cu(II), suggesting that their binding affinities were diminished relative to the parent ATCUN motif.

In the remainder of the peptides (**13-18**) which contained either D- or L-histidine, Thz, or Pya in position 3, no significant difference could be seen in binding selectivity for Ni(II) and Cu(II). Furthermore, no distinction could be made between the spectral behavior of the peptides containing D-histidine and those with L-histidine. Under standard assay conditions, all were quenched by Cu(II), and less effectively by Ni(II). Thus, neither changing the identity of ligand contributed by the side chain of residue 3, nor presenting an auxiliary ligand from the side chain of residue 2 was sufficient to provide observable binding selectivity. However, all peptides that contained a Glu or an Asp residue at position 2 displayed more rapid Ni(II)-induced quenching, while **13** (which contains a valine at that position) shows slowed Ni(II)-induced quenching (Figure 4-11.) By comparison, the Cu(II)-induced effect for all compounds was complete by the time a measurement could be obtained (~5 minutes). These results demonstrate that the inclusion of an axial ligand at the second position of an ATCUN motif can accelerate ligand exchange for the corresponding Ni(II) complex. Furthermore, exploitation of this fact may be important for the future development of Ni(II) chemosensors.

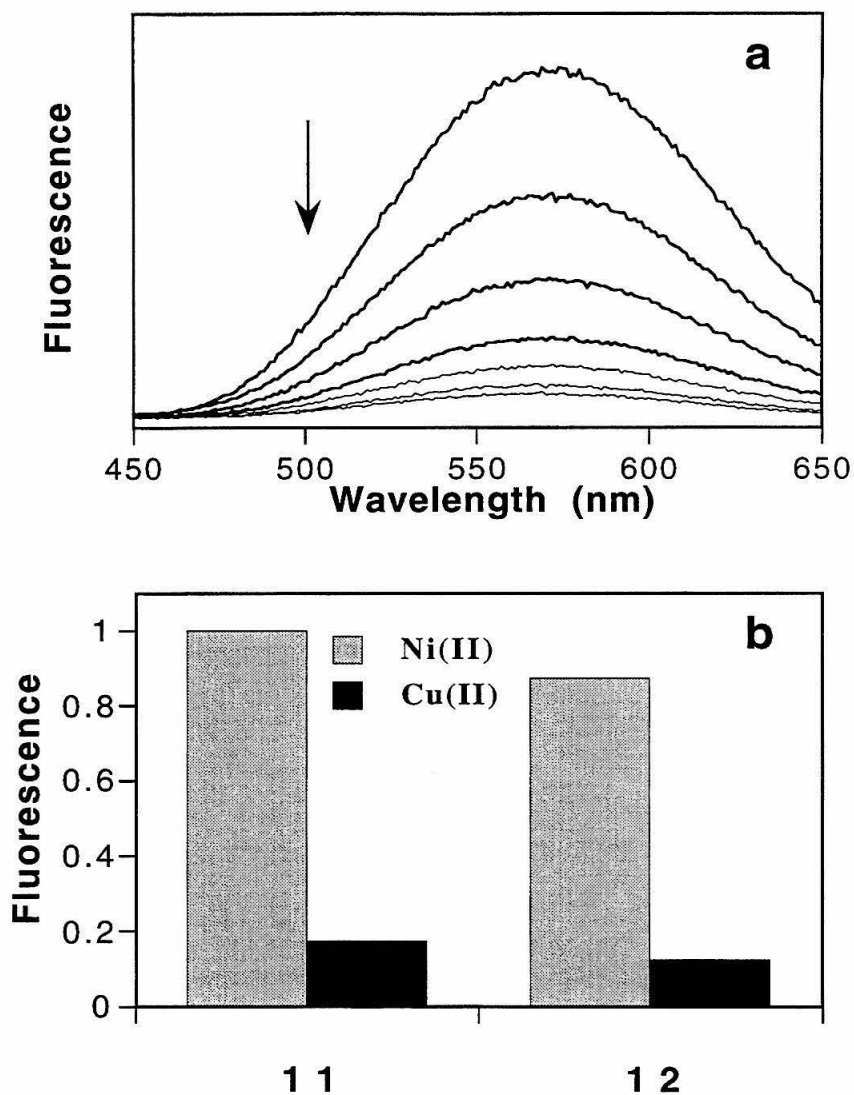


**Figure 4-10.** Compounds Dap(DNS)-Gly-Glu-Ser-Ser-NH<sub>2</sub> (**11**) and Dap(DNS)-Asp-Gln-Ser-Ser-NH<sub>2</sub> (**12**) show selectivity for Cu(II) over Ni(II). a. Fluorescence emission spectra of **11** (10  $\mu$ M, 0.15 M NaCl, 50 mM HEPES, pH 7.0) to increasing concentrations of Cu(II) (0, 0.25, 0.5, 0.75, 1.0, 1.25, and 1.5 equivalents respectively). b. Fluorescence emission at 570 nm of **11** and **12**, with an added equivalent of Ni(II) or Cu(II) (10  $\mu$ M chemosensor). The data have been scaled such that in the absence of metal ions, the fluorescence is equal to unity. The effect of Ni(II)-induced quenching is diminished relative to that observed for sensors **1-3** (compare with Figure 4-3). Excitation at 333 nm.

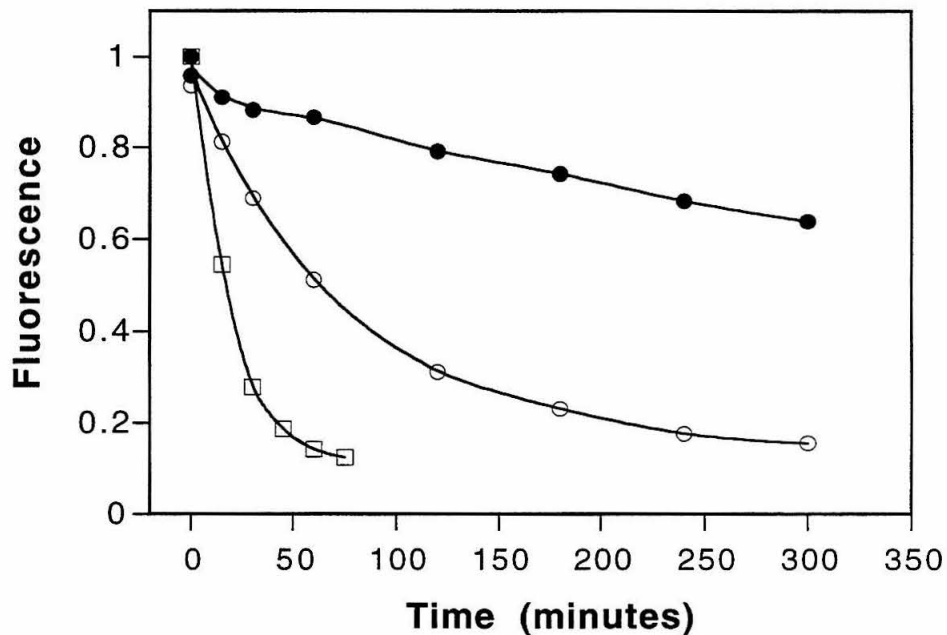


**Figure 4-11.** Fluorescence emission, measured at 570 nm for 10  $\mu\text{M}$  solutions of Dap(DNS)-Asp-His-Ser-Ser-NH<sub>2</sub> (**16**, open squares), Dap(DNS)-Gly-His-Ser-Ser-NH<sub>2</sub> (**1**, open circles), and Dap(DNS)-Val-DHis-Ser-Ser-NH<sub>2</sub> (**13**, filled circles) in the presence of one equivalent of Ni(II). The rate of Ni(II)-induced quenching is dependent upon the identity of second residue for these compounds which are aspartic acid, glycine, and valine, respectively.

Modifications to the parent ATCUN motif that augment the coordination sphere geometry, or ligand type, were not found to produce viable chemosensors for monitoring trace Cu(II) or Ni(II) concentrations. Where selective Cu(II) binding was observed (**11**, **12**), so was greatly diminished binding affinity. Compounds with residue 3 ligand modifications that preserved high affinity binding (**13-18**) did not exhibit metal binding selectivity. Compounds **1-18** all preserve the backbone connectivity of the parent compound, and thus may adopt a square planar coordination geometry. In order to force a change in the binding geometry, an additional compound (**19**, Figure 4-12) incorporating  $\beta$ -alanine ( $\beta$ Ala) at position 2 was prepared.

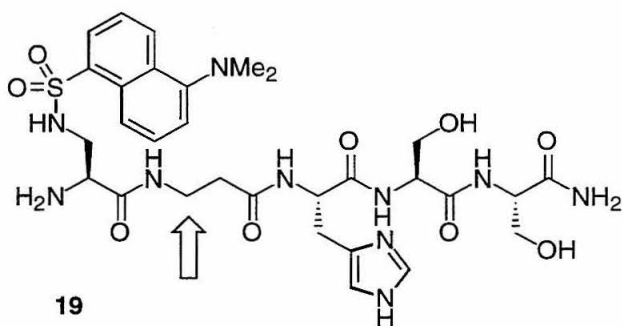


**Figure 4-12.** The structure of **19**, a sensitive and selective chemosensor for Cu(II). The nonstandard residue,  $\beta$ -alanine ( $\beta$ Ala) in position 2, is highlighted.

Remarkably, although **19** differs from **3** only by the inclusion of an extra methylene within the backbone of the second residue, this chemosensor exhibited highly sensitive and selective sensing of Cu(II), whereas **3** did not. The fluorescence emission properties of compound **19** are highly responsive to added Cu(II), even with low concentrations ( $1 \mu\text{M}$ ) of chemosensor. Under these conditions, incremental additions of  $100 \text{ nM}$  concentrations of divalent copper are easily discernible, with the fluorescence response linear in the range  $100\text{-}1000 \text{ nM}$  (Figure 4-13).

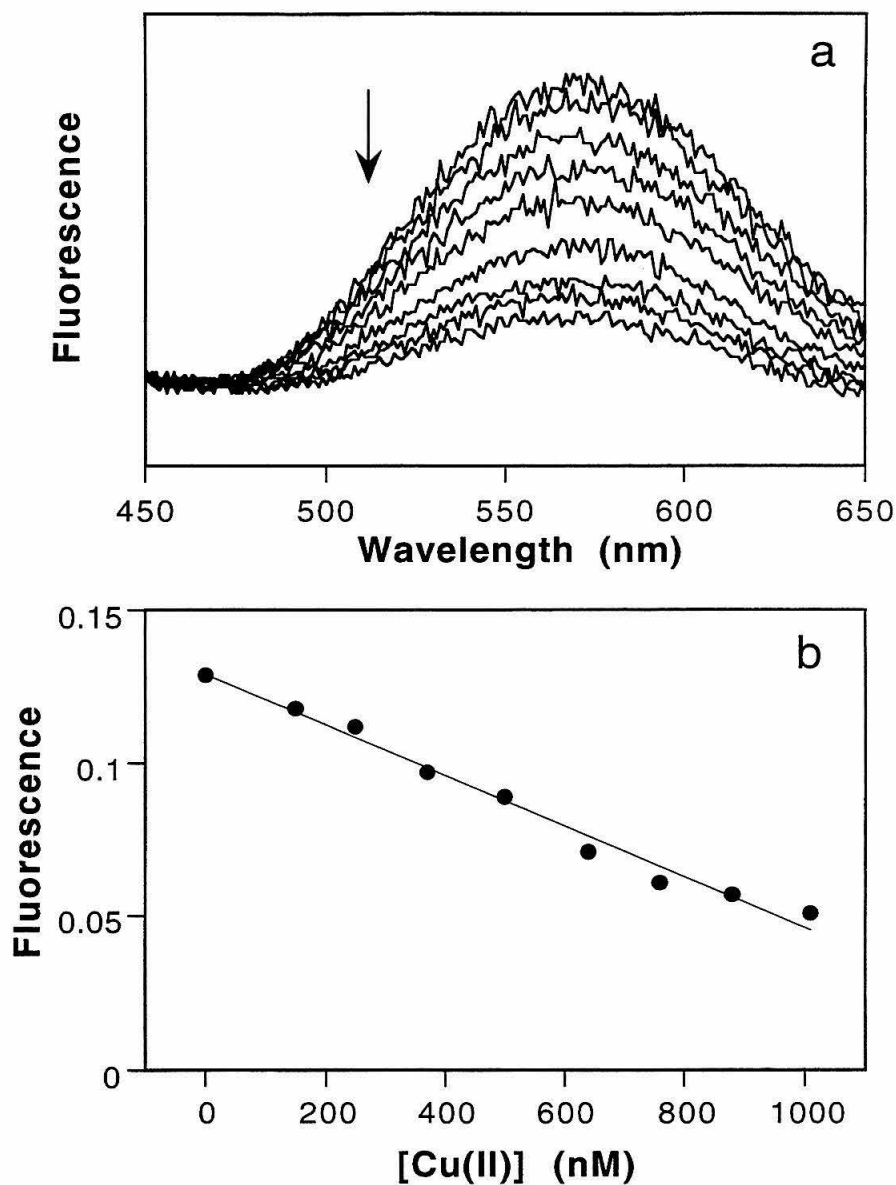


**Figure 4-13.** a. Fluorescence emission spectra of 1  $\mu\text{M}$  Dap(DNS)- $\beta\text{Ala-His-Ser-Ser-NH}_2$  (**19**) in 50 mM HEPES, 150 mM NaCl, pH 7.0 with increasing concentrations of Cu(II). The effect of 0, 0.12, 0.25, 0.37, 0.50, 0.64, 0.76, 0.88, and 1.0 equivalents of added Cu(II) are shown. Excitation at 333 nm. b. The change in fluorescence emission at 570 nm, extracted from the experiment shown in tile a.

In order to further probe the metal binding selectivity demonstrated by this chemosensor, experiments were performed with a wide variety of other metal ions. Cross reactivity of a 10  $\mu\text{M}$  solution of **19** with an equivalent each of Mn(II), Fe(II), Co(II), Ni(II), Zn(II), Cd(II), Mg(II), and Ca(II) was found to be minimal (Figure 4-14). Furthermore, this behavior does not appear to be a kinetic effect; extended preincubation of **19** with Ni(II) did not influence the outcome of subsequent Cu(II) titrations (data not shown).

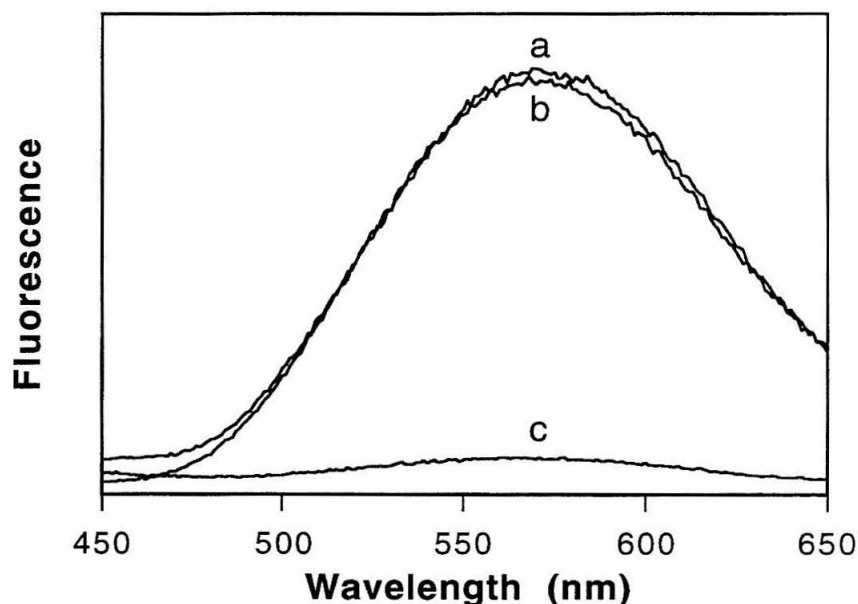
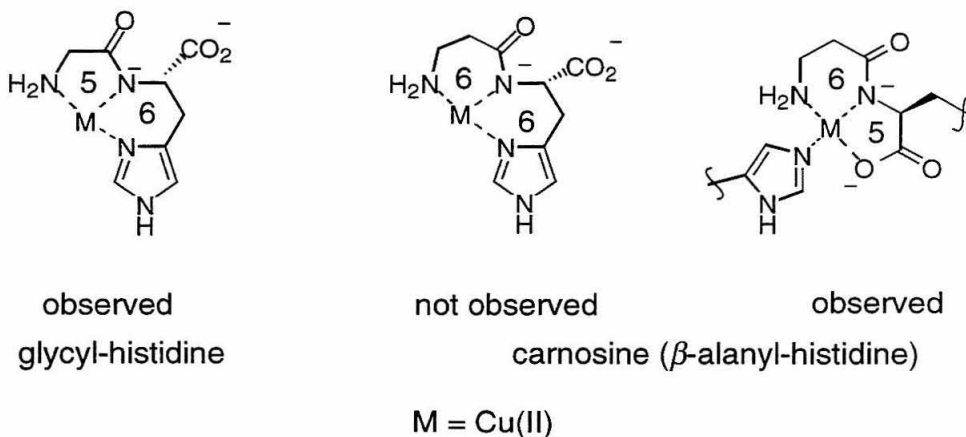


Figure 4-14. Fluorescence emission spectra of 10  $\mu\text{M}$  **19** in 0.15 M NaCl, 50 mM HEPES, pH 7.0, excitation at 333 nm. a. With no added divalent metal ions; b, after the addition of 10  $\mu\text{M}$  each Mg(II), Ca(II), Mn(II), Fe(II), Co(II), Ni(II), Zn(II), and Cd(II); c, after the addition of 1 equivalent Cu(II).

The success of **19** as a chemosensor for Cu(II) may be rationalized in light of the promiscuity of Cu(II) ligand binding geometry. In order to attain tetradentate binding through the *N*-terminal amine, the side chain of histidine 3, and the two intervening amides, a distortion of the square planar coordination geometry exhibited by the modified ATCUN motif *must* occur. This result is supported by both structural studies of the

Cu(II) complex of carnosine ( $\beta$ -alanyl-L-histidine),<sup>44</sup> and glycyl-histidine,<sup>45</sup> as well as thermodynamic investigation of the Ni(II)- and Cu(II)-binding preferences of  $\beta$ -alanine containing peptides.<sup>46</sup> These studies have shown that the peptide ligand (with the deprotonated peptide nitrogen) cannot accommodate the formation of two adjacent 6-membered rings and preserve its planarity.<sup>22</sup> Indeed, the energetic cost of this effect is great enough that while glycyl-histidine will crystallize as a planar tridentate species, carnosine will instead form a bridged 2-center chelate (Figure 4-15). Moreover, this effect can be observed in simple molecular models of the proposed **19**·Cu(II) complex, constrained to preserve a square-planar coordination geometry, wherein sizable distortions to the two adjacent 6-membered chelate rings result (Figure 4-16). This result suggests that a relaxation from true square planar coordination results for Cu(II) complexes of this type, and that Ni(II) coordination would be comparatively disfavored.



**Figure 4-15.** A comparison of the structures of the Cu(II) complexes for glycyl-histidine and carnosine highlight the fact that the formation of two adjacent 6-membered chelate rings is disfavored.

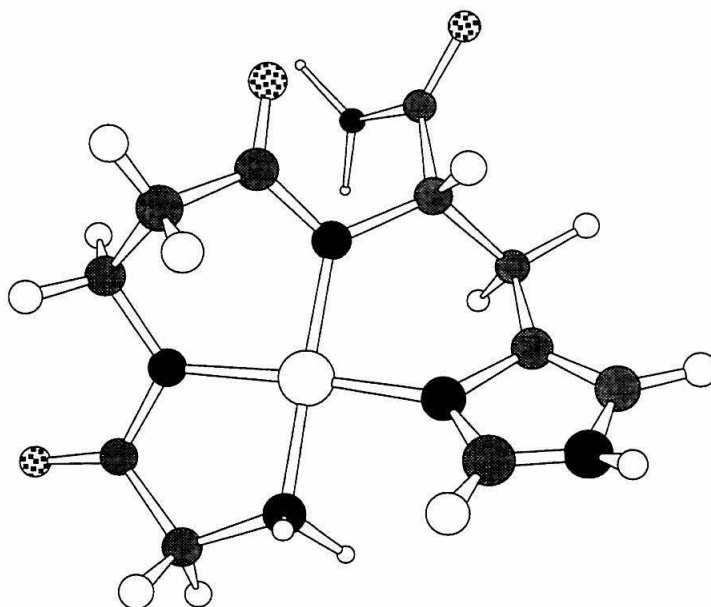


**Figure 4-16.** Molecular model of a Gly- $\beta$ Ala-His tripeptide bound to Cu(II) that was constrained to maintain a square planar coordination geometry. To accommodate this constraint, deformations result in the 6-membered chelate rings, suggesting that a relaxation from true square planar coordination probably results in complexes of this general form.

### **Solid phase immobilization studies.**

Concomitant with the studies presented above, efforts were made to convert these solution-based reagents to renewable devices through the attachment of the peptidyl chemosensors to a solid phase handle. In addition to producing a renewable chemosensor, potentially capable of real time measurements, the attachment of fluorosensors to the solid phase has other advantages. In particular, compounds that are as synthetically simple as these ATCUN-based motifs, are ideal candidates for the application of combinatorial techniques. Preparing chemosensors on the solid phase enables multiple compounds to be synthesized and assayed quickly and in parallel. Furthermore, the density of fluorophore loading on a single bead of typical peptide-synthesis resin ( $\sim 0.2$  mmole per g resin) is sufficient to be able to detect fluorescence emission with the naked eye. This final advantage is of significant importance as the

steps required to characterize the response of a *single* solution-phase fluorosensor with several metals can take several days.

As an initial examination of the feasibility of making metal ion measurements with solid-phase attached measurements, the peptide Dap(DNS)- $\beta$ Ala-His-Ser-Ser was prepared on “Tentagel” (polystyrene–poly(ethyleneglycol)–tentacle copolymer) resin, to yield the sensing material **1T**. Tentagel resin was selected, by virtue of its ability to be solvated in polar media (i.e., water).<sup>47,48</sup> As an added advantage, this resin is also commercially available in lots that have very consistent bead size. This property has been noted to be important when quantitative assessments of colorimetric or fluorescence changes are to be made in the screening of a combinatorial library.<sup>49,50</sup>

The response of **1T** to solutions of metal cations in aqueous solution was assessed. Unfortunately, when incubated at room temperature in 150 mM NaCl, 50 mM HEPES, pH 7.0 buffer containing 10–100  $\mu$ M Cu(II), no significant quenching was observed, even after 2 days. Further studies revealed that by the addition of organic cosolvent (20% v/v methanol), and incubating at 50 °C, quenching could be observed for 100  $\mu$ M concentrations of Cu(II), but not with Fe(II), Co(II), Ni(II) or Zn(II) after 4–6 hours. These results indicated that resin-supported fluorescent chemosensors could be screened, and that metal binding selectivities could be observed. However, these findings also demonstrated that the resin bound peptide was only partially solvated in water and not generally acceptable for continued development.

In light of this shortcoming of the solid support, others were considered with emphasis given to the ability of the resin to swell in water. One such recently-developed material is a polyethyleneglycol-poly-(*N,N'*-dimethylacrylamide) copolymer (PEGA). Unlike Tentagel, which is formed by polymerizing high molecular weight polyethylene glycol to the surface of a styrene/divinylbenzene matrix,<sup>48,51</sup> PEGA is composed of 2-acrylamidoprop-1-yl[2-aminoprop-1-yl]-PEG<sub>300</sub>, bis-2-acrylamidoprop-1-yl-PEG<sub>1900</sub>, and *N,N'*-dimethyl acrylamide (Figure 4-17), and thus consists solely of hydrophilic

material.<sup>52</sup> Indeed the aqueous solvation of compounds attached to PEGA is remarkable, even in comparison to other “water-swelled” resins.<sup>48</sup> For example, it has been demonstrated that peptides covalently attached to this resin are accessible to the action of ~50 kDa enzymes.<sup>53,54</sup> Consequently, further studies were performed using this resin as it was expected to provide easy access of metal ions to attached chemosensors.

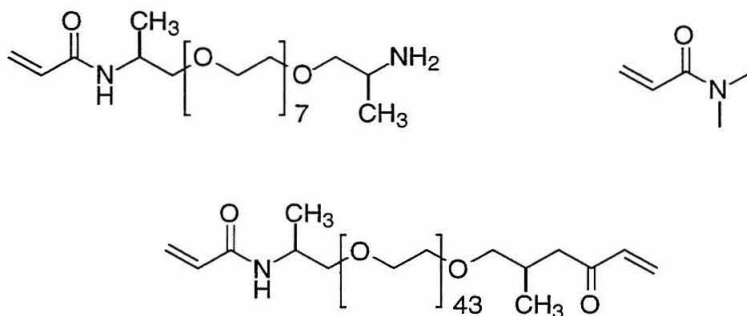


**Figure 4-17.** Monomers that comprise PEGA resin are all hydrophilic.

A small library of PEGA-attached fluorescent chemosensors was designed, with the aid of preliminary information obtained from the solution-state studies described above. However, it was clear that rather simple changes to the peptidyl motif could have important consequences for the metal binding properties of the resulting compounds. Given the relative ease with which peptides can be prepared, a mini “combinatorial scan” was performed in order to investigate the importance of individual residues of the ATCUN motif on a position by position basis. However, in order to be able to compare the behavior of the resin-bound peptides on as even a basis as possible, the *N*-terminal residue (Dap) and the attached fluorescent probe (DNS) were kept invariant. Replacements for the second and third residues (referred to as the “Xaa” and “Yaa” residues respectively) were considered that were anticipated to augment the metal-binding properties of the parent ATCUN motif (Figure 4-18).

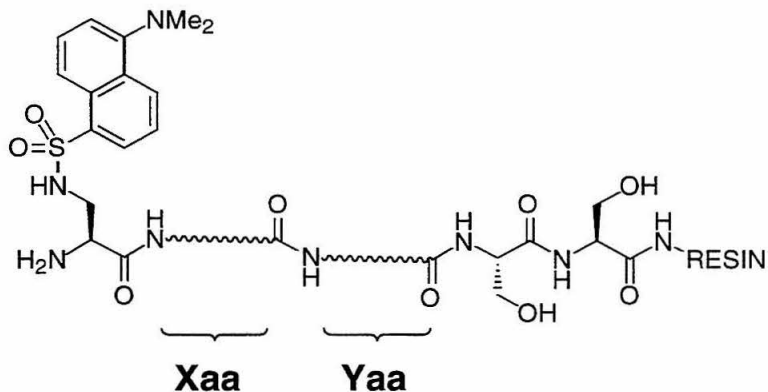


**Figure 4-18.** The second (Xaa) and third (Yaa) residues of the ATCUN motif chosen for replacement.

A total of four residues were chosen to replace the second (Xaa) position and three residues for the third (Yaa) position. Residues chosen for replacement of the Xaa residue were selected to provide a “standard” linkage (Gly), an “extended” linkage ( $\beta$ Ala), an “interfering” linkage (Sar, *N*-methyl glycine, or sarcosine), and an “axial ligand” linkage (Asp). Residues chosen for application as Yaa were selected to mimic the  $sp^2$   $\delta$ -nitrogen of the native histidine, while providing differing electronic characteristics. As a consequence, 2-pyridylalanine (2-Pya) and 4-thiazolylalanine (4-Thz) were selected. Each of these may donate an  $sp^2$ -hybridized nitrogen from a position *ortho* to the point of the ring attachment to the  $\beta$ -carbon. The family of 12 PEGA-bound peptides resulting from the appropriate combination of all possible substitutions of Xaa and Yaa-residues was synthesized. The sequences of these are delineated in Table 4-1.

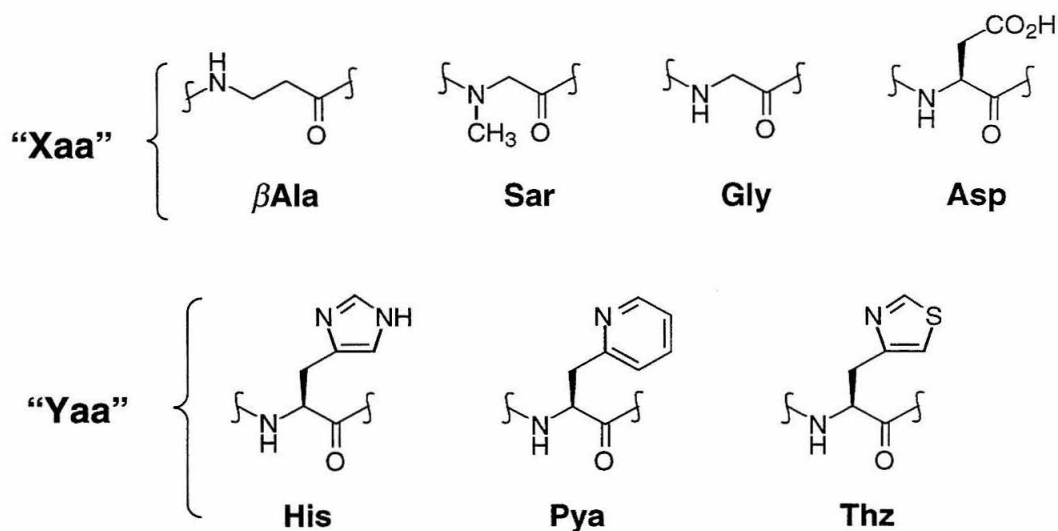


**Figure 4-19.** Amino acid derivatives chosen for the replacement of the “Xaa” and “Yaa” residues of the ATCUN motif.

**Table 4-1.** Identities of the PEGA resin-bound peptides prepared.

identifier	peptide sequence
1P	H <sub>2</sub> N-Dap(DNS)- $\beta$ Ala-His-Ser-Ser-PEGA
2P	H <sub>2</sub> N-Dap(DNS)-Gly-His-Ser-Ser-PEGA
3P	H <sub>2</sub> N-Dap(DNS)-Asp-His-Ser-Ser-PEGA
4P	H <sub>2</sub> N-Dap(DNS)-Sar-His-Ser-Ser-PEGA
5P	H <sub>2</sub> N-Dap(DNS)- $\beta$ Ala-Pya-Ser-Ser-PEGA
6P	H <sub>2</sub> N-Dap(DNS)-Gly-Pya-Ser-Ser-PEGA
7P	H <sub>2</sub> N-Dap(DNS)-Asp-Pya-Ser-Ser-PEGA
8P	H <sub>2</sub> N-Dap(DNS)-Sar-Pya-Ser-Ser-PEGA
9P	H <sub>2</sub> N-Dap(DNS)- $\beta$ Ala-Thz-Ser-Ser-PEGA
10P	H <sub>2</sub> N-Dap(DNS)-Gly-Thz-Ser-Ser-PEGA
11P	H <sub>2</sub> N-Dap(DNS)-Asp-Thz-Ser-Ser-PEGA
12P	H <sub>2</sub> N-Dap(DNS)-Sar-Thz-Ser-Ser-PEGA

The chemosensing ability of **1P-12P** were initially probed for the effect of various concentrations of Cu(II) on fluorescence. However, a preliminary assay was conducted with the Dap(DNS)-Gly-His-Ser-Ser-PEGA peptide (**2P**) only in completely aqueous pH 7 buffer (150 mM NaCl, 50 mM HEPES) in order to confirm that improved quenching kinetics could be observed. Because an entirely empirical approach was used, a qualitative scale was used to judge fluorescence quenching. For each observation, the fluorescence was described as + (no quenching),  $\pm$  (slight quenching), - (mostly quenched), Q (total quenching). Assays were conducted at room temperature with a small number of **2P** beads (5-20), and the effect of Cu(II) in concentrations ranging from 10-500  $\mu$ M were observed. The data obtained from a typical study are displayed in Table 4-2.

While these results showed that the PEGA support did provide better solvation to the attached chemosensor, significant metal ion concentration-dependent delays in the quenching response remained. Furthermore, after four days, even samples containing no Cu(II) ion appeared quenched, indicating that with protracted incubation times chemosensor degradation occurs. Based upon these results, a similar concentration-effect assay was performed, but with the addition of 20% v/v methanol to the buffer solution. The data obtained from this assay are presented in Table 4-3. With 20% methanol cosolvent, the quenching effect of 100  $\mu$ M Cu(II) is observed over a period of 24 hours. It was reasoned that this amount of time would be optimal for providing opportunity to observe potential differences in quenching kinetics for other peptides, while being short enough to avoid sample decomposition. Consequently, further assays were conducted with 100  $\mu$ M metal cation concentrations in buffer containing 20% v/v methanol cosolvent.

**Table 4-2.** Time-dependent quenching of Dap(DNS)-Gly-His-Ser-Ser-PEGA. Measurements were conducted in 150 mM NaCl, 50 mM HEPES, pH 7.0 buffer.

time (h)	[CuCl <sub>2</sub> ] $\mu$ M						
	EDTA	10	20	50	100	200	500
.25	+	+	+	+	+	+	+
.50	+	+	+	+	+	+	+
1	+	+	+	+	+	+	$\pm$
2	+	+	+	+	+	$\pm$	-
4	+	+	+	+	$\pm$	-	Q
8	+	+	+	+	$\pm$	-	Q
12	+	+	+	$\pm$	$\pm$	Q	Q
24	+	+	$\pm$	$\pm$	Q	Q	Q
4 days	Q	Q	Q	Q	Q	Q	Q

Key: + = full fluorescence;  $\pm$  = slight decrease; - = mostly quenched; Q = total quenching.

**Table 4-3.** Time dependent quenching of Dap(DNS)-Gly-His-Ser-Ser-PEGA. Measurements were conducted in 150 mM NaCl, 50 mM HEPES, pH 7.0 buffer, 20% v/v methanol.

time (h)	[CuCl <sub>2</sub> ] $\mu$ M						
	EDTA	10	20	50	100	200	500
.25	+	+	+	+	+	+	+
.50	+	+	+	+	+	+	$\pm$
1	+	+	+	+	+	$\pm$	-
2	+	+	+	$\pm$	-	-	Q
4	+	+	+	-	-	-	Q
8	+	+	+	-	-	Q	Q
12	+	+	+	-	-	Q	Q
24	+	$\pm$	$\pm$	-	Q	Q	Q
4 days	Q	Q	Q	Q	Q	Q	Q

The same criteria for grading quenching were used as described in Table 4-1.

Employing these conditions, each of the 12 peptides were tested for reaction with Al(III), Mn(II), Fe(II), Fe(III), Co(II), Ni(II), Cu(II), Zn(II), and EDTA. Of these, Al(III), Mn(II), Fe(II), Fe(III), Co(II), Zn(II), and EDTA showed no significant change in fluorescence after 16 hours. The remaining cations, Ni(II) and Cu(II), were far more potent quenchers of fluorescence both kinetically and statistically (number of peptides quenched). For example, Co(II) only produced slight quenching in one peptide—Dap(DNS)-Asp-His-Ser-Ser-PEGA (**3P**), and that only after 24 hours. In contrast, Ni(II) and Cu(II) produced quenching in all of the peptides after 4 hours. The results from typical assays of Cu(II)- and Ni(II)-induced quenching are displayed in Table 4-4 and Table 4-5 respectively. (Although these results were all obtained with 20% v/v methanol, it should be noted that subsequent studies revealed that the addition of only 10 % v/v methanol enhanced the rate of Cu(II)-induced quenching similarly.)

Analysis of these data revealed trends in the kinetic behavior of peptide quenching. For example, the most rapid Ni(II)-induced quenching was observed for peptides that had an aspartic acid as the central residue of the metal-binding triad. Furthermore, Cu(II) in all cases produced a quenching effect more rapidly than did Ni(II). While these measurements were made using a subjective scoring system, the trends observed have been entirely substantiated by the solution-state data that was obtained concomitantly. This fact highlights one of the primary benefits of assaying prospective chemosensors on the solid phase; whereas testing of the entire library with numerous metals takes approximately a week, performing a similar screen *via* solution state measurements takes weeks or months.

**Table 4-4.** Results from a typical Cu(II) quenching assay.

time (h)	resin-bound peptide											
	1P	2P	3P	4P	5P	6P	7P	8P	9P	10P	11P	12P
1	+	+	+	+	+	+	+	+	+	+	+	±
2	±	+	+	+	±	+	+	+	+	+	+	-
3	Q	±	±	+	±	±	+	+	±	+	+	Q
4	Q	±	±	+	±	±	+	+	±	+	+	Q
8	Q	-	-	±	-	-	+	+	-	±	±	Q
12	Q	Q	Q	Q	Q	Q	±	±	-	±	±	Q
16	Q	Q	Q	Q	Q	Q	±	-	Q	-	±	Q
20	Q	Q	Q	Q	Q	Q	-	Q	Q	-	±	Q
24	Q	Q	Q	Q	Q	Q	-	Q	Q	-	±	Q

Measurements were conducted in 100  $\mu$ M Cu(II), 150 mM NaCl, 50 mM HEPES, pH 7.0 buffer, 20% v/v methanol. The same criteria for grading quenching were used as described in Table 4-1.

**Table 4-5.** Results from a typical Ni(II) quenching assay.

time (h)	resin-bound peptide											
	1P	2P	3P	4P	5P	6P	7P	8P	9P	10P	11P	12P
1	+	+	+	+	+	+	+	+	+	±	+	+
2	+	+	+	+	+	+	+	+	+	±	+	+
3	+	±	+	+	+	+	±	+	+	±	+	+
4	+	±	±	+	+	+	±	+	+	±	+	+
8	±	±	±	+	+	+	±	+	+	±	+	+
12	±	±	±	±	+	+	±	+	+	-	+	+
16	±	±	-	±	+	±	±	+	+	-	+	+
20	±	±	-	±	+	±	±	±	+	-	±	+
24	±	±	-	±	±	±	±	±	+	-	±	+

Measurements were conducted in 100  $\mu$ M Ni(II), 150 mM NaCl, 50 mM HEPES, pH 7.0 buffer, 20% v/v methanol. The same criteria for grading quenching were used as described in Table 4-1.

An additional benefit of these solid phase chemosensors is the relative ease with which particular sensors with exceptional properties can be identified. For example, the selective fluorescence response of Dap(DNS)- $\beta$ Ala-His-Ser-Ser-PEGA (**1P**) can clearly be seen. A picture of a typical assay of this chemosensor with various divalent metal cations (taken after a 2 h incubation) is shown in Figure 4-20. Measurements were made at room temperature in 50 mM HEPES, 150 NaCl (pH 7.0), and 10% v/v methanol, and contain 100  $\mu$ M of the metal ion.

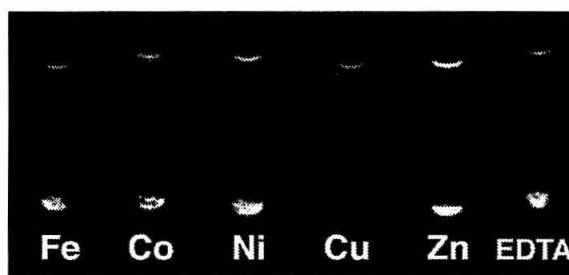


**Figure 4-20.** Typical solid-phase quenching assay of Dap(DNS)- $\beta$ Ala-His-Ser-Ser-PEGA (**1P**). The samples shown are in 50 mM HEPES, 150 mM NaCl, pH 7.0 with 10% v/v methanol and contain 100  $\mu$ M of the appropriate divalent metal cation or EDTA. Fluorescence excitation was provided with a hand-held low-wattage mineral lamp set on “long wavelength” (365 nm). The image was acquired after 2 h of incubation.

In addition to **1P**, another resin-bound peptide produced particularly interesting results from the quenching studies. The Dap(DNS)-Sar-Thz-Ser-Ser-PEGA material showed the fastest quenching by Cu(II), and was completely resistant to quenching by all the other metal cations tested, including Ni(II). This result was surprising in light of the fact that one of the ionizable amides of the parent ATCUN motif had been substituted with the *N*-methyl amide of the sarcosine residue. Nonetheless, this result also provides a strong argument for the inclusion of diverse functionality within a library to be screened.

To further probe (and confirm) this effect, the peptide **20** was synthesized and a solution study initiated.

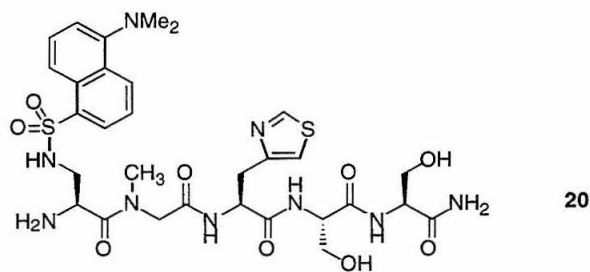


**Figure 4-21.** The structure of Dap(DNS)-Sar-Thz-Ser-Ser-NH<sub>2</sub> (**20**).

Fluorescence studies of **20** confirmed that this compound exhibits rapid Cu(II) binding, yet exhibits much lower affinity for Cu(II) than observed for the analogous peptides, Dap(DNS)-Gly-His-Ser-Ser-NH<sub>2</sub> (**1**) and Dap(DNS)-Asp-Thz-Ser-Ser-NH<sub>2</sub> (**17**), that retain an ionizable amide linking the first and second residues. At  $\sim 10 \mu\text{M}$  concentrations of this chemosensor, it requires  $> 6$  equivalents of Cu(II) to saturate the peptide. In addition, the extent of fluorescence quenching was less than for the parent compound (Figure 4-22). A binding isotherm, calculated from titration of **20** with CuCl<sub>2</sub>, is presented in Figure 4-23; the binding properties of this chemosensor are well described by an apparent dissociation constant for the **20**·Cu(II) complex of  $8 \mu\text{M}$  (Figure 4-23). This is approximately 6 orders of magnitude less avid Cu(II) binding than exhibited by the native C-terminal metal binding domain of the serum albumins.<sup>12</sup>

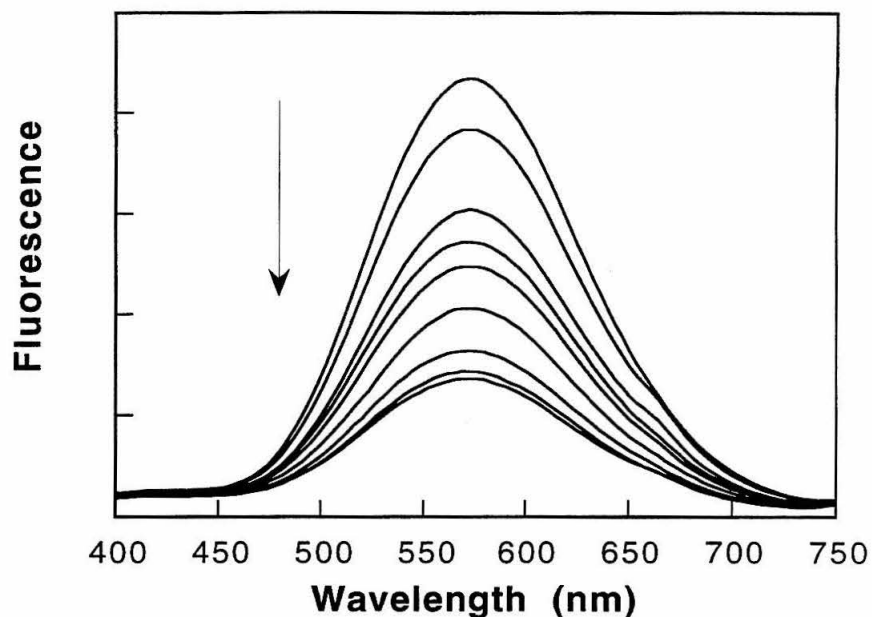


**Figure 4-22.** Fluorescence emission spectra of an 8.7  $\mu\text{M}$  solution of Dap(DNS)-Sar-Thz-Ser-Ser-NH<sub>2</sub> (**20**) in 150 mM NaCl, 50 mM HEPES, pH 7.0 with increasing amounts of added CuCl<sub>2</sub> (in equivalents): 0, 0.5, 1.0, 1.5, 2.0, 3.0, 4.0, 5.0, 6.0. Excitation was performed at 333 nm.

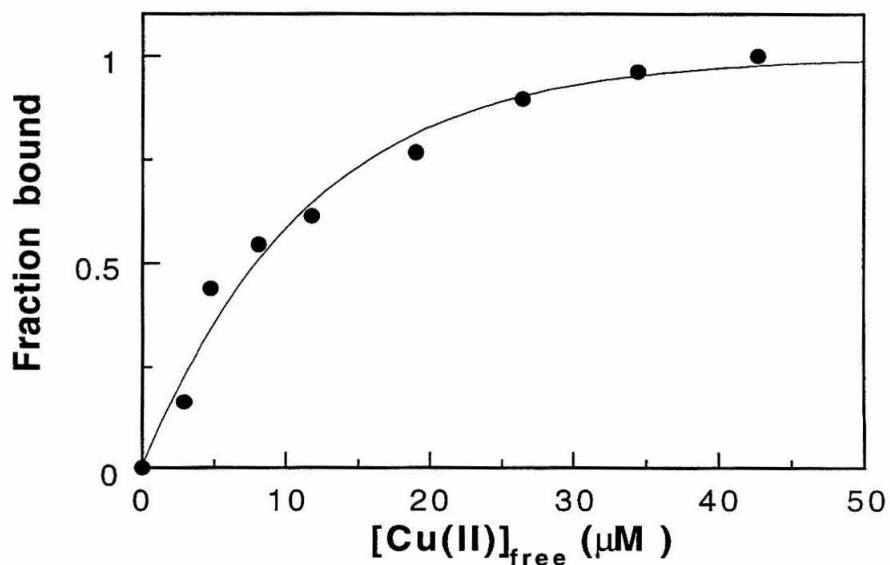


**Figure 4-23.** Cu(II) binding isotherm for **20**, obtained from the data presented in Figure 4-22. The apparent dissociation constant calculated for the **20**·Cu(II) complex is 8  $\mu\text{M}$ .

Despite the large loss of Cu(II) binding affinity observed for **20**, this chemosensor exhibits a high degree of selectivity for against Ni(II) binding. No change in fluorescence was observed upon the addition of 0.1 mM Ni(II) to a 10  $\mu$ M solution of chemosensor, even after 24 hours. However, this lower affinity binding of Cu(II) does not necessarily mean that it is “worse” than the other Cu(II)-selective peptidyl chemosensor produced by this research, Dap(DNS)- $\beta$ Ala-His-Ser-Ser-NH<sub>2</sub>; rather **20** could be useful for the detection of Cu(II) at higher levels (1-100  $\mu$ M)– namely concentrations of Cu(II) that are toxic.<sup>37,55</sup>

The study of the solid phase-supported chemosensors using the qualitative methods described thus far has been of tremendous use for the rapid discovery and preliminary characterization of chemosensors for Cu(II). However, an additional goal in producing these solid phase devices is to conduct real time measurements of metal cations. In other words, quantitative measurements on the solid phase are desired. Toward this end, studies of the Cu(II)-induced quenching of Dap(DNS)- $\beta$ Ala-His-Ser-Ser-PEGA have been conducted by fluorescence microscopy, with the optical output recorded with a charge-coupled devoid (CCD) camera. Figure 4-24 presents a series of pictures captured at 1 second intervals after the addition of 1 mM Cu(II) to **1P**.

By analyzing the signal information captured in the individual frames, quantitative measurements of fluorescence intensity (and therefore kinetic) information may be obtained. The results from a typical data regression, in this case for the “leftmost” bead shown in Figure 4-24 is presented in Figure 4-25. While the studies required to exhaustively calibrate the response of these sensing materials to varying levels of metal ions have not yet been done, these measurements do provide the “proof of concept,” demonstrating that quantitative Cu(II) analysis with the solid phase-attached peptidyl sensors presented herein is possible. Similar studies are ongoing in the Imperiali labs.

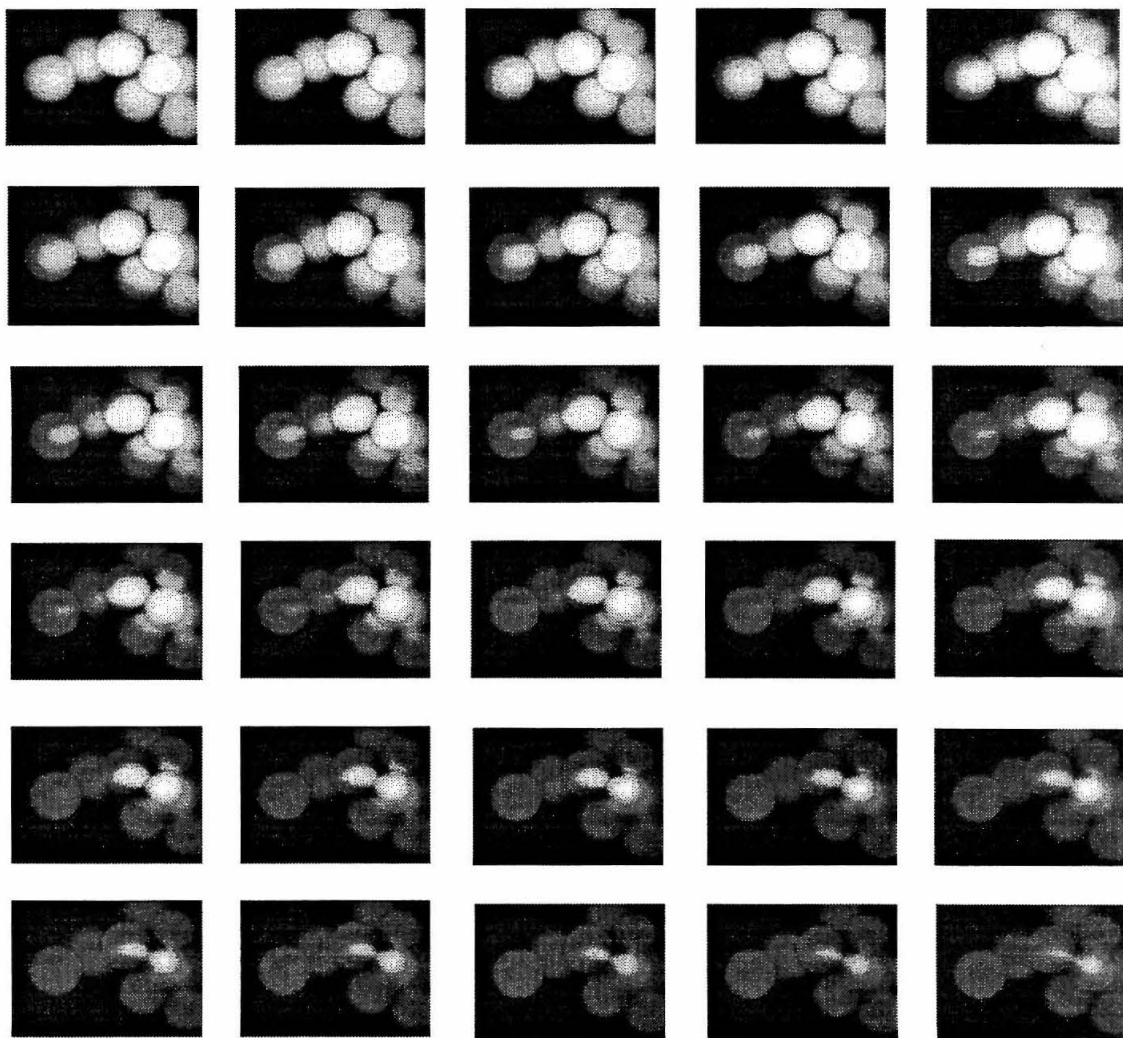


**Figure 4-24.** Fluorescence quenching of Dap(DNS)- $\beta$ Ala-His-Ser-Ser-PEGA after the addition of 1 mM Cu(II). Images were captured at 1 second intervals.

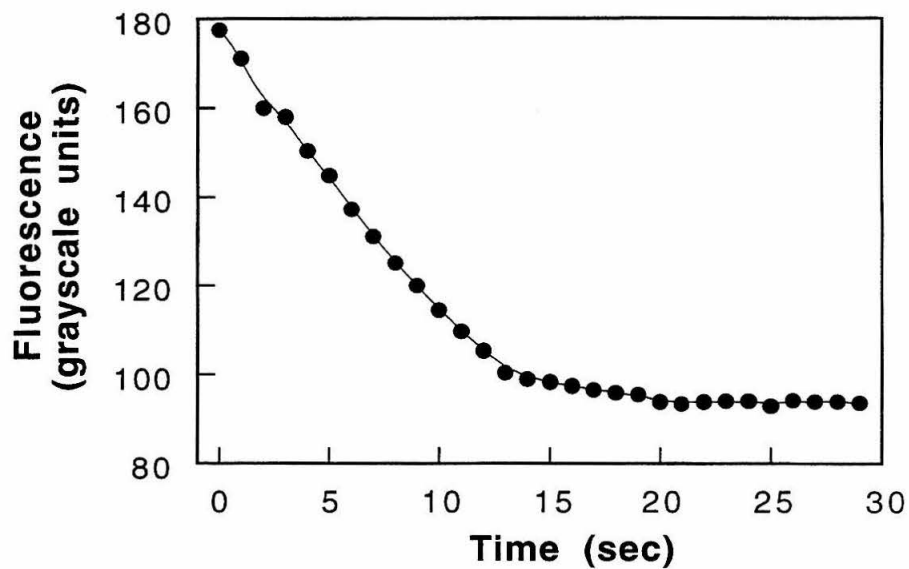


**Figure 4-25.** Quantitative measurement of on-bead fluorescence quenching kinetics; data extracted from the data set presented in Figure 4-24. Grayscale units are analogous to intensity, and for the camera used span between 255 (white) and 0 (black).

## Conclusion

The ATCUN motif of the serum albumins has been exploited for the design of fluorescent peptidyl chemosensors for Cu(II). By combining the strengths of combinatorial synthesis and rapid qualitative screening of solid phase-attached chemosensors with quantitative solution state studies, significant success has been achieved in the production of fluorescent chemosensors selective for Cu(II). As a result of this research, the compound Dap(DNS)- $\beta$ Ala-His-Ser-Ser-NH<sub>2</sub> (**19**) has been identified as a highly selective reporter of divalent copper. This chemosensor has been shown to enable the measurement of sub-micromolar concentrations of Cu(II) in aqueous solution and is unaffected by 100  $\mu$ M concentrations of Ni(II). The compound Dap(DNS)-Sar-Thz-Ser-Ser-NH<sub>2</sub> (**20**) is similarly unaffected by elevated Ni(II) concentrations, and is sensitive to Cu(II) concentrations in the 5-100  $\mu$ M range. Additionally, Dap(DNS)-Gly-Glu-Ser-Ser-NH<sub>2</sub> (**11**) and Dap(DNS)-Asp-Gln-Ser-Ser-NH<sub>2</sub> (**12**) demonstrated reduced sensitivity to Ni(II)-induced quenching, a result that may be worthy of further study.

In the course of these studies, it was noted that the rate of Ni(II) binding by the ATCUN motif at low concentrations of metal and peptide ( $\sim 1 \mu$ M) is slow, requiring hours to come to equilibrium for peptides containing glycine in the second position. Furthermore, this effect was exacerbated when a bulky residue (valine) was incorporated at that position. However, if aspartic acid was included at that position, which putatively could contribute an axial ligand to a bound metal ion through its side chain functionality, the rate of Ni(II) binding was dramatically increased. The exploitation of this fact may be useful in the future design of chemosensors for the Ni(II) ion.

## Acknowledgment

The work presented in this chapter was done in conjunction with Dr. Alicia Torrado, who synthesized and tested many of the solution-based peptidyl chemosensors.

Without her companionship on this project, much less could have been done; I wish to thank her for the tremendous amount of work that she did, and for being a wonderfully kind and enthusiastic collaborator. A portion of the work presented in this chapter is presented in the following publication:

“Exploiting Polypeptide Motifs for the Design of Selective Cu(II) Ion Chemosensors,”  
Torrado, A.; Walkup, G. K.; Imperiali, B. *J. Am. Chem. Soc.* **1997**, *120*, 609-610.

## **Experimental**

### **Solution-phase studies.**

#### *Peptide Synthesis.*

Fmoc-protected amino-acids for solid phase peptide synthesis were obtained from PerSeptive or Bachem. Solvents and reagents for chemical synthesis were obtained from PerSeptive, Aldrich or Fluka, and used without further purification. Peptides were synthesized using standard Fmoc chemistry using Pal-PEG-PS resin (PerSeptive), or "macro crowns" (Chiron). Activation was generally performed using a four-fold excess of the appropriate Fmoc-pentafluorophenyl ester derivatives, or when free acid monomers were used, 1,3-diisopropylcarbodiimide/1-hydroxybenzotriazole (DIPCDI/HOBt) chemistry. However, when coupling onto *N*-methyl amino acid sarcosine, 1-Hydroxy-7-azabenzotriazole/*O*-(7-Azabenzotriazol-1-yl)-1,1,3,3-tetramethyluronium hexafluorophosphate (HOAt/HATU) activation was used, again with a four-fold excess of acylating reagent to resin-bound amine. Peptide cleavage was performed 90:5:3:2 trifluoroacetic acid : thioanisole : ethanedithiol : anisole. Crude peptides were obtained by trituration with 2:1 ether:hexanes, resuspended in water and then lyophilized. All peptides were purified to homogeneity by reverse phase (C<sub>18</sub>) HPLC with water/acetonitrile (0.01% v/v TFA) gradient elution. The integrity of the purified peptides was confirmed by electrospray mass spectroscopy.

*Fluorophore coupling.*

All fluorophore derivatives were obtained from Aldrich and used without further purification. In general, couplings were performed with 5 equivalents of labeling reagent, and 5 equivalents of diisopropylethylamine in sufficient quantity of DMF to result in a solution 0.1 M in fluorophore. Couplings were allowed to proceed for a minimum of 2 h, and were monitored periodically by the Kaiser test for completeness. The fluorophores DNS and BZX were introduced by reaction with 5-*N,N'*-dimethylamino-naphthalene-1-sulfonyl chloride or 2-chlorobenzoxazole respectively. The remainder of the fluorophores (ANT, RHD, COM) were obtained as the free-acid derivatives and coupled using standard benzotriazole-1-yloxy-tris(dimethylamino)-phosphoniumhexafluorophosphate (BOP) activation chemistry.

*Fluorescence spectroscopy.*

Standard assays were performed using  $\sim 10 \mu\text{M}$  chemosensor at ambient temperature in 50 mM HEPES, 0.15 M NaCl (pH 7.0) using an SLM-Aminico SPF-500c spectrofluorometer. Emission spectra were acquired with the following parameters: HVA=975 V, excitation bandpass = 4 nm, emission bandpass = 2 nm, filter (time constant) = 3, gain = 10 or 100 depending upon sample concentration. All buffers and solutions were prepared using high purity water obtained from a Mili-Q (Millipore) filtration apparatus. Adventitious metal ions were removed from prepared buffer solutions by transport through a column (2 cm by 30 cm) of activated (sodium form) Chelex resin (Bio Rad Labs.), followed by re-adjustment of the buffer pH to 7.0 if necessary. Metal stock solutions were prepared as the chloride salts, except for Fe(II) which was prepared from ferrous ammonium sulfate. Analytical grade reagents were used in all cases, and the concentration of stock solutions determined by titration with standardized solutions of EDTA (Aldrich) in the presence of an appropriate metallochromic indicator.

*Determination of apparent dissociation constant for the 20·Cu(II) complex*

The Cu(II) binding studies were carried out according to the procedures presented in Chapter 2. In brief, aqueous solutions of known peptide concentrations ( $\sim 10 \mu\text{M}$ ) were titrated with a standardized  $\text{CuCl}_2$  solution at room temperature in 50 mM HEPES buffer, 150 mM NaCl at pH 7.0. The apparent dissociation constants ( $K_D$ ) were calculated using an iterative process based on the Scott equation<sup>56</sup> (with the additional modifications to the parameters used, necessary to reflect the fact that fluorescence, and not absorption spectroscopy, was used):

$$\frac{b \cdot [M]}{\Delta F} = \frac{[M]}{[\text{Pep}]_t \cdot \Delta\Phi} + \frac{K_D}{[\text{Pep}]_t \cdot \Delta\Phi}$$

where  $b$  = cell path length,  $[M]$  = free metal cation concentration,  $\Delta F$  = change in fluorescence due to complex formation,  $[\text{Pep}]_t$  = total peptide in solution,  $\Delta\Phi$  = change in “quantum yield” due to complex formation. This latter parameter is not a true quantum yield, but is dependent upon the instrument used for the measurements.

**Solid phase studies.***Peptide synthesis.*

Peptides were assembled on PEGA-1900 resin<sup>52</sup> (0.2 mmole/g) using standard Fmoc/OPfp chemistry batch synthesis techniques.<sup>57</sup> In general, coupling reactions were carried out using 0.1 M active ester in DMF for 8-12 h. For coupling steps performed upon intermediates terminating with an *N*-methyl glycine residue, HOAt/HATU activation was employed.<sup>58</sup> Iterative removal of the Fmoc protecting group was performed with piperidine (20% v/v in DMF) for 0.5 h followed by washing with DMF ( $5 \times 2$  mL). Final peptide deprotection was achieved with 5% v/v triisopropylsilane in trifluoroacetic acid. The deprotected resin was then washed with DCM ( $5 \times 2$  mL), DMF ( $3 \times 2$  mL), lyophilized, then stored at 4 °C until used.

*Quenching assay.*

Assays were performed on a small number of beads (5-20) placed in disposable glass culture tubes. Buffered metal solutions were prepared from a stock buffer solution (150 mM NaCl, 50 mM HEPES, pH 7.0), analytically determined stock metal solutions, and were diluted by the addition of 20% v/v methanol to yield solutions 100  $\mu$ M in divalent metal cation. Assays were initiated by the addition of these buffered metal solutions (500  $\mu$ L) to the culture tube and then stoppered and vortexed briefly (2 sec). The extent of quenching was evaluated on a qualitative scale using the following scoring categories: + (full fluorescence),  $\pm$  (slight diminution in intensity), - (obvious decrease in fluorescence), Q (total quenching of fluorescence). Illumination was provided by a low-power hand-held mineral lamp set on "long wavelength" (365 nm), and measurements were always made in reference to a solid black background.

*Fluorescence microscopy.*

Fluorescent chemosensors beads were placed in a well of a 96-well microtiter plate (Falcon) and 200  $\mu$ L of buffer (150 mM NaCl, 50 mM HEPES, pH 7.0) added. The microtiter plate was mounted on the observation stage of an Olympus IX-50. Excitation was provided by a 100 W Hg lamp, using an Olympus U-MWU optical filter set (excitation bandpass 330-385 nm, emission cutoff  $\leq$  420 nm). The assay was initiated by the addition of an aliquot of CuCl<sub>2</sub> from a concentrated stock solution. Images were recorded as 8-bit grayscale TIFF files *via* a charge-coupled device (CCD) camera (COHU Inc., San Diego, CA) attached to a computer running the Image Pro Plus software package (Media Cybernetics, Silver Spring, MD). The captured images were analyzed with the NIH Image v1.61 software package (available on-line from <http://rsb.info.nih.gov/nih-image/>) on a Macintosh computer. Using this software the area occupied by an individual bead in successive images was defined to be the region of interest (ROI), and the mean pixel intensity of the ROI at each time point was determined.

H<sub>2</sub>N-Dap(DNS)-Gly-His-Ser-Ser-NH<sub>2</sub> (1).

MS (ESI) calcd for C<sub>29</sub>H<sub>41</sub>O<sub>9</sub>N<sub>10</sub>S [M+H]<sup>+</sup> 705.3 found 705. HPLC (Beckman C<sub>18</sub> 0.46 × 15 cm column; flow rate 1.0 mL/min; solvent A = H<sub>2</sub>O, 0.1% v/v TFA, solvent B = MeCN 0.1% TFA; gradient 0% B 5 min, 0-70 % B over 25 min) retention = 21.3 min.

H<sub>2</sub>N-Dab(DNS)-Gly-His-Ser-Ser-NH<sub>2</sub> (2)

MS (ESI) calcd for C<sub>30</sub>H<sub>43</sub>O<sub>9</sub>N<sub>10</sub>S [M+H]<sup>+</sup> 719.3 found 719. HPLC (Beckman C<sub>18</sub> 0.46 × 15 cm column; flow rate 1.0 mL/min; solvent A = H<sub>2</sub>O, 0.1% v/v TFA, solvent B = MeCN 0.1% TFA; gradient 0% B 5 min, 0-70% B over 25 min) retention = 21.5 min.

H<sub>2</sub>N-Orn(DNS)-Gly-His-Ser-Ser-NH<sub>2</sub> (3)

MS (ESI) calcd for C<sub>31</sub>H<sub>45</sub>O<sub>9</sub>N<sub>10</sub>S [M+H]<sup>+</sup> 733.3 found 733. HPLC (Beckman C<sub>18</sub> 0.46 × 15 cm column; flow rate 1.0 mL/min; solvent A = H<sub>2</sub>O, 0.1% v/v TFA, solvent B = MeCN 0.1% TFA; gradient 0% B 5 min, 0-70% B over 25 min) retention = 21.7 min.

H<sub>2</sub>N-Dab(BZX)-Gly-His-Ser-Ser-NH<sub>2</sub> (4)

MS (ESI) calcd for C<sub>25</sub>H<sub>35</sub>O<sub>8</sub>N<sub>10</sub> [M+H]<sup>+</sup> 603.3 found 603. HPLC (Beckman C<sub>18</sub> 0.46 × 15 cm column; flow rate 1.0 mL/min; solvent A = H<sub>2</sub>O, 0.1% v/v TFA, solvent B = MeCN 0.1% TFA; gradient 0% B 5 min, 0-70% B over 25 min) retention = 20.5 min.

H<sub>2</sub>N-Dab(ANT)-Gly-His-Ser-Ser-NH<sub>2</sub> (5)

MS (ESI) calcd for C<sub>33</sub>H<sub>40</sub>O<sub>8</sub>N<sub>9</sub> [M+H]<sup>+</sup> 690.3 found 690. HPLC (Beckman C<sub>18</sub> 0.46 × 15 cm column; flow rate 1.0 mL/min; solvent A = H<sub>2</sub>O, 0.1% v/v TFA, solvent B = MeCN 0.1% TFA; gradient 10% B 1 min, 10-40% B over 25 min) retention = 25.3 min.

H<sub>2</sub>N-Orn(RHD)-Gly-His-Ser-Ser-NH<sub>2</sub> (6)

MS (ESI) calcd for C<sub>47</sub>H<sub>62</sub>O<sub>9</sub>N<sub>11</sub> [M+H]<sup>+</sup> 924.5 found 924. HPLC (Beckman C<sub>18</sub> 0.46 × 15 cm column; flow rate 1.0 mL/min; solvent A = H<sub>2</sub>O, 0.1% v/v TFA, solvent B = MeCN 0.1% TFA; gradient 0% B 5 min, 0-70% B over 25 min) retention = 25.1 min.

**H<sub>2</sub>N-Orn(ANT)-Gly-His-Ser-Ser-NH<sub>2</sub> (7)**

MS (ESI) calcd for C<sub>34</sub>H<sub>42</sub>O<sub>8</sub>N<sub>9</sub> [M+H]<sup>+</sup> 704.3 found 704. HPLC (Beckman C<sub>18</sub> 0.46 × 15 cm column; flow rate 1.0 mL/min; solvent A = H<sub>2</sub>O, 0.1% v/v TFA, solvent B = MeCN 0.1% TFA; gradient 0% B 5 min, 0-70% B over 25 min) retention = 25.0 min.

**H<sub>2</sub>N-Orn(COM)-Gly-His-Ser-Ser-NH<sub>2</sub> (8)**

MS (ESI) calcd for C<sub>35</sub>H<sub>47</sub>O<sub>10</sub>N<sub>10</sub> [M+H]<sup>+</sup> 767.3 found 767. HPLC (Beckman C<sub>18</sub> 0.46 × 15 cm column; flow rate 1.0 mL/min; solvent A = H<sub>2</sub>O, 0.1% v/v TFA, solvent B = MeCN 0.1% TFA; gradient 0% B 5 min, 0-70% B over 25 min) retention = 27.0 min.

**H<sub>2</sub>N-Dap(DNS)-Cys-His-Ser-Ser-NH<sub>2</sub> (9)**

MS (ESI) calcd for C<sub>30</sub>H<sub>43</sub>O<sub>9</sub>N<sub>10</sub>S<sub>2</sub> [M+H]<sup>+</sup> 751.3 found 751. HPLC (Beckman C<sub>18</sub> 0.46 × 15 cm column; flow rate 1.0 mL/min; solvent A = H<sub>2</sub>O, 0.1% v/v TFA, solvent B = MeCN 0.1% TFA; gradient 0% B 5 min, 0-70% B over 25 min) retention = 21.7 min.

**H<sub>2</sub>N-Dap(DNS)-Gly-Hcs-Ser-Ser-NH<sub>2</sub> (10)**

MS (ESI) calcd for C<sub>27</sub>H<sub>41</sub>O<sub>9</sub>N<sub>8</sub>S [M+H]<sup>+</sup> 685.2 found 685. HPLC (Beckman C<sub>18</sub> 0.46 × 15 cm column; flow rate 1.0 mL/min; solvent A = H<sub>2</sub>O, 0.1% v/v TFA, solvent B = MeCN 0.1% TFA; gradient 0% B 5 min, 0-70% B over 25 min) retention = 23.3 min.

**H<sub>2</sub>N-Dap(DNS)-Gly-Glu-Ser-Ser-NH<sub>2</sub> (11)**

MS (ESI) calcd for C<sub>28</sub>H<sub>41</sub>O<sub>11</sub>N<sub>8</sub>S [M+H]<sup>+</sup> 697.3 found 697. HPLC (Beckman C<sub>18</sub> 0.46 × 15 cm column; flow rate 1.0 mL/min; solvent A = H<sub>2</sub>O, 0.1% v/v TFA, solvent B = MeCN 0.1% TFA; gradient 0% B 5 min, 0-70% B over 25 min) retention = 21.5 min.

**H<sub>2</sub>N-Dap(DNS)-Asp-Gln-Ser-Ser-NH<sub>2</sub> (12)**

MS (ESI) calcd for C<sub>30</sub>H<sub>44</sub>O<sub>12</sub>N<sub>9</sub>S [M+H]<sup>+</sup> 754.3 found 754. HPLC (Beckman C<sub>18</sub> 0.46 × 15 cm column; flow rate 1.0 mL/min; solvent A = H<sub>2</sub>O, 0.1% v/v TFA, solvent B = MeCN 0.1% TFA; gradient 0% B 5 min, 0-70% B over 25 min) retention = 21.6 min.

**H<sub>2</sub>N-Dap(DNS)-Val-DHis-Ser-Ser-NH<sub>2</sub> (13)**

MS (ESI) calcd for C<sub>32</sub>H<sub>47</sub>O<sub>9</sub>N<sub>10</sub>S [M+H]<sup>+</sup> 747.3 found 747. HPLC (Beckman C<sub>18</sub> 0.46 × 15 cm column; flow rate 1.0 mL/min; solvent A = H<sub>2</sub>O, 0.1% v/v TFA, solvent B = MeCN 0.1% TFA; gradient 0% B 5 min, 0-70% B over 25 min) retention = 21.5 min.

**H<sub>2</sub>N-Dap(DNS)-Asp-DHis-Ser-Ser-NH<sub>2</sub> (14)**

MS (ESI) calcd for C<sub>31</sub>H<sub>43</sub>O<sub>11</sub>N<sub>10</sub>S [M+H]<sup>+</sup> 763.3 found 763. HPLC (Beckman C<sub>18</sub> 0.46 × 15 cm column; flow rate 1.0 mL/min; solvent A = H<sub>2</sub>O, 0.1% v/v TFA, solvent B = MeCN 0.1% TFA; gradient 0% B 5 min, 0-70% B over 25 min) retention = 21.1 min.

**H<sub>2</sub>N-Dap(DNS)-Glu-DHis-Ser-Ser-NH<sub>2</sub> (15)**

MS (ESI) calcd for C<sub>32</sub>H<sub>45</sub>O<sub>11</sub>N<sub>10</sub>S [M+H]<sup>+</sup> 777.3 found 777. HPLC (Beckman C<sub>18</sub> 0.46 × 15 cm column; flow rate 1.0 mL/min; solvent A = H<sub>2</sub>O, 0.1% v/v TFA, solvent B = MeCN 0.1% TFA; gradient 0% B 5 min, 0-70% B over 25 min) retention = 21.4 min.

**H<sub>2</sub>N-Dap(DNS)-Asp-His-Ser-Ser-NH<sub>2</sub> (16)**

MS (ESI) calcd for C<sub>31</sub>H<sub>43</sub>O<sub>11</sub>N<sub>10</sub>S [M+H]<sup>+</sup> 763.3 found 764. HPLC (Beckman C<sub>18</sub> 0.46 × 15 cm column; flow rate 1.0 mL/min; solvent A = H<sub>2</sub>O, 0.1% v/v TFA, solvent B = MeCN 0.1% TFA; gradient 0% B 5 min, 0-70% B over 25 min) retention = 20.5 min.

**H<sub>2</sub>N-Dap(DNS)-Asp-Thz-Ser-Ser-NH<sub>2</sub> (17)**

MS (ESI) calcd for C<sub>31</sub>H<sub>42</sub>O<sub>11</sub>N<sub>9</sub>S<sub>2</sub> [M+H]<sup>+</sup> 780.2 found 780. HPLC (Beckman C<sub>18</sub> 0.46 × 15 cm column; flow rate 1.0 mL/min; solvent A = H<sub>2</sub>O, 0.1% v/v TFA, solvent B = MeCN 0.1% TFA; gradient 0% B 5 min, 0-70% B over 25 min) retention = 23.5 min.

**H<sub>2</sub>N-Dap(DNS)-Asp-Pya-Ser-Ser-NH<sub>2</sub> (18)**

MS (ESI) calcd for C<sub>33</sub>H<sub>44</sub>O<sub>11</sub>N<sub>9</sub>S [M+H]<sup>+</sup> 774.3 found 774. HPLC (Beckman C<sub>18</sub> 0.46 × 15 cm column; flow rate 1.0 mL/min; solvent A = H<sub>2</sub>O, 0.1% v/v TFA, solvent B = MeCN 0.1% TFA; gradient 0% B 5 min, 0-70% B over 25 min) retention = 21.7 min.

H<sub>2</sub>N-Dap(DNS)-βAla-His-Ser-Ser-NH<sub>2</sub> (**19**)

MS (ESI) calcd for C<sub>30</sub>H<sub>43</sub>O<sub>9</sub>N<sub>10</sub>S [M+H]<sup>+</sup> 719.3 found 719. HPLC (Beckman C<sub>18</sub> 0.46 × 15 cm column; flow rate 1.0 mL/min; solvent A = H<sub>2</sub>O, 0.1% v/v TFA, solvent B = MeCN 0.1% TFA; gradient 0% B 5 min, 0-70% B over 25 min) retention = 21.5 min.

H<sub>2</sub>N-Dap(DNS)-Sar-His-Ser-Ser-NH<sub>2</sub> (**20**)

MS (ESI) calcd for C<sub>30</sub>H<sub>43</sub>O<sub>9</sub>N<sub>10</sub>S [M+H]<sup>+</sup> 719.3 found 719. HPLC (Beckman C<sub>18</sub> 0.46 × 15 cm column; flow rate 1.0 mL/min; solvent A = H<sub>2</sub>O, 0.1% v/v TFA, solvent B = MeCN 0.1% TFA; gradient 0% B 5 min, 0-70% B over 25 min) retention = 21.2 min.

## References

1. "Desperately seeking sensors," Czarnik, A. W. *Chem. Bio.* **1995**, *2*, 423-428.
2. "Fiber Optic Biosensor for Co(II) and Cu(II) Based on Fluorescence Energy Transfer with an Enzyme Transducer," Thompson, R. B.; Ge, Z.; Patchan, M.; Huang, C. C.; Fierke, C. A. *Biosensors & Bioelectronics* **1996**, *11*, 557-564.
3. "A Fluorescent Chemosensor Signalling Only Hg(II) and Cu(II) in Water," Yoon, J.; Ohler, N. E.; Vance, D. H.; Aumiller, W. D.; Czarnik, A. W. *Tetrahedron Lett.* **1997**, *38*, 3845-3848.
4. "Fluorescent Chemosensor for Organic Guests and Copper(II) Ion Based on Dansyldiethylenetriamine-Modified β-Cyclodextrin," Corradini, R.; Dossena, A.; Galaverna, G.; Marchelli, R.; Panagia, A., et al. *J. Org. Chem.* **1997**, *62*, 6283-6289.
5. "An Anthracene-Based Fluorescent Sensor for Transition Metal Ions," Fabbriizzi, L.; Licchelli, M.; Pallavicini, P.; Perotti, A.; Sacchi, D. *Angew. Chem. Int. Ed. Engl.* **1994**, *33*, 1975-1977.
6. "Fluorescent Sensors for Transition Metals Based on Electron-Transfer and Energy-Transfer Mechanisms," Fabbriizzi, L.; Licchelli, M.; Pallavicini, P.; Perotti, A.; Taglietti, A., et al. *Chemistry a European Journal* **1996**, *2*, 75-82.

7. "A Fluorescent Chemosensor for the Copper(II) Ion," De Santis, G.; Fabbrizzi, L.; Licchelli, M.; Mangano, C.; Sacchi, D., et al. *Inorg. Chem. Acta* **1997**, *257*, 69-76.
8. "Metal-Induced Dispersion of Lipid Aggregates: A Simple, Selective, and Sensitive Fluorescent Metal Ion Sensor," Sasaki, D. Y.; Shnek, D. R.; Pack, D. W.; Arnold, F. H. *Angew. Chem. Int. Ed. Engl.* **1995**, *34*, 905-907.
9. "A Long-Wavelength Fluorescent Chemodosimeter Selective for Cu(II) Ion in Water," Dujols, V.; Ford, F.; Czarnik, A. W. *J. Am. Chem. Soc.* **1997**, *119*, 7386-7387.
10. "Copper-binding Motifs in Catalysis, Transport, Detoxification and Signaling," Koch, K. A.; Peña, M. M. O.; Thiele, D. J. *Chem. Bio.* **1997**, *4*, 549-560.
11. "Amino Terminal Cu(II)- and Ni(II)-Binding (ATCUN) Motif of Proteins and Peptides: Metal Binding, DNA Cleavage, and Other Properties," Harford, C.; Sarkar, B. *Acc. Chem. Res.* **1997**, *30*, 123-130.
12. "Intrinsic Stoichiometric Equilibrium Constants for the Binding of Zinc(II) and Copper(II) to the High Affinity Site of Serum Albumin," Masuoka, J.; Hegenauer, J.; Van Duke, B. R.; Saltman, P. *J. Biol. Chem.* **1993**, *268*, 21533-21537.
13. "Zinc(II) and Copper(II) Binding to Serum Albumin," Masuoka, J.; Saltman, P. *J. Biol. Chem.* **1994**, *269*, 25557-25561.
14. "Kinetic and Thermodynamic Studies of Copper(II) and Nickel(II) Complexes of Glycylglycyl-L-Histidine," Hay, R. W.; Hassan, M. M.; You-Quan, C. *J. Inorg. Biochem.* **1993**, *52*, 17-25.
15. "Molecular Design to Mimic the Copper(II) Transport Site of Human Albumin: Studies of Equilibria Between Copper(II) and Glycylglycyl-L-histidine-N-methyl amide and Comparison with Human Albumin," Kruck, T. P. A.; Lau, S.; Sarkar, B. *Can. J. Chem.* **1976**, *54*, 1300-1308.
16. "A Peptide Molecule Mimicking the Copper(II) Transport Site of Human Serum Albumin," Lau, S.; Kruck, T. P. A.; Sarkar, B. *J. Biol. Chem.* **1974**, *249*, 5878-5884.

17. "Proton and Metal Ion Interactions with Glycylglycylhistamine, a Serum Albumin Mimicking Pseudopeptide," Gajda, T.; Henry, B.; Aubry, A.; Delpuech, J. *Inorg. Chem.* **1996**,
18. "Ligand Displacement of Glycylglycyl-L-histidine from Its Copper(II) Complex. A Proton-Assisted Mechanism Initiated at a Nonterminal Position," Cooper, J. C.; Wong, L. F.; Venezky, D. L.; Margerum, D. W. *J. Am. Chem. Soc.* **1974**, *96*, 7560-7562.
19. "Synthesis and Copper(II)-Binding Properties of the *N*-terminal Peptide of Human  $\alpha$ -Fetoprotein," Lau, S.; Laussac, J.-P.; Sarkar, B. *Biochem. J.* **1989**, *257*, 745-750.
20. "Further Characterization of the *N*-Terminal Copper(II)- and Nickel(II)-Binding Motif of Proteins," Predki, P. F.; Harford, C.; Brar, P.; Sarkar, B. *Biochem. J.* **1992**, *287*, 211-215.
21. "Synthesis of the Native Copper(II)-Transport Site of Human Serum Albumin and its Copper(II)-Binding Properties," Iyer, K. S.; Lau, S.-J.; Laurie, S. H.; Sarkar, B. *Biochem. J.* **1978**, *169*, 61-69.
22. "Coordinating Properties of the Amide Bond. Stability and Structure of Metal Ion Complexes of Peptides and Related Ligands," Sigel, H.; Martin, R. B. *Chem. Rev.* **1982**, *82*, 385-426.
23. "Metallopeptide-DNA Interactions: Site-Selectivity Based on Amino Acid Composition and Chirality," Liang, Q.; Eason, P. D.; Long, E. C. *J. Am. Chem. Soc.* **1995**, *117*, 9625-9631.
24. "Design and Synthesis of a Versatile DNA-Cleaving Metallopeptide Structural Domain," Shullenberger, D. F.; Eason, P. D.; Long, E. C. *J. Am. Chem. Soc.* **1993**, *115*, 11038-11039.
25. "Metal Ions as Donors and Acceptors of Fluorescence," In *Methods for Determining Metal Ion Environments in Proteins*; Holmquist, B.; Darnall, W. D.; Wilkins, R. G.; Elsevier, New York, 1980; pp 75-93.

26. "Principles of Fluorescence Spectroscopy," Lakowicz, J. R.; Plenum Press: New York, 1983.
27. "Electron-Transfer Kinetics of the Reactions Between Copper(III/II) and Nickel(III/II) Deprotonated-Peptide Complexes," Owens, G. D.; Phillips, D. A.; Czarnecki, J. J.; Raycheba, J. M. T.; Margerum, D. W. *Inorg. Chem.* **1984**, *23*, 1345-1353.
28. "Coordination Chemistry: Theory," In *Inorganic Chemistry*; Huheey, J. E.; HarperCollins, New York, 1983; 359-463.
29. "Sensors and Switches from Supramolecular Chemistry," Fabbrizzi, L.; Poggi, A. *Chem. Soc. Rev.* **1995**, 197-202.
30. "Luminescence and Charge Transfer. Part 2. Aminomethyl Anthracene Derivatives as Fluorescent PET (Photoinduced Electron Transfer) Sensors for Protons," Bissell, R. A.; Calle, E.; de Silva, A. P.; de Silva, S. A.; Gunaratne, H. Q. N., et al. *J. Chem. Soc., Perkin Trans. II* **1992**, 1559-1564.
31. "Molecular Fluorescent Signalling with 'Fluor-Spacer-Receptor' Systems: Approaches to Sensing and Switching Devices via Supramolecular Photophysics," Bissell, R. A.; de Silva, A. P.; Gunaratne, H. Q. N.; Lynch, P. L. M.; Maguire, G. E. M., et al. *Chem. Soc. Rev.* **1992**, 187-195.
32. "Fluorescent PET (Photoinduced Electron Transfer) Sensors," Bissell, R. A.; de Silva, A. P.; Gunaratne, H. Q. N.; Lynch, P. L. M.; Maguire, G. E. M., et al. *T. Curr. Chem.* **1993**, *168*, 223-264.
33. "Luminescence and Charge Transfer. Part 3. The Use of Chromophores with ICT (Internal Charge Transfer) Excited States in the Construction of Fluorescent PET (Photoinduced Electron Transfer) pH Sensors and Related Absorption pH Sensors with Aminoalkyl Side Chains," de Silva, A. P.; Gunarantne, H. Q. N.; Lynch, P. L. M.; Patty, A. J.; Spence, G. L. *J. Chem. Soc., Perkin Trans. II* **1993**, 1611-1616.

34. "Luminescence and Charge Transfer. Part 4. 'On-off' Fluorescent PET (Photoinduced Electron Transfer) Sensors with Pyridine Receptors: 1,3-Diaryl-5-pyridyl-4,5-dihydropyrazoles," de Silva, A. P.; Gunaratne, H. Q. N.; Lynch, P. L. M. *J. Chem. Soc., Perkin Trans. II* **1995**, 685-690.
35. "Signaling Recognition Events with Fluorescent Sensors and Switches," de Silva, A. P.; Gunaratne, H. Q. N.; Gunnlaugsson, T.; Huxley, A. J. M.; McCoy, C. P., et al. *Chem. Rev.* **1997**, *97*, 1515-1566.
36. "A Fluorescent Photoinduced Electron Transfer Sensor for Cations With an Off-On-Off Proton Switch," de Silva, S. A.; Zavaleta, A.; Baron, D. E.; Allam, O.; Isidor, E. V., et al. *Tetrahedron Lett.* **1997**, *38*, 2237-2240.
37. "The Biological Chemistry of the Elements: The Inorganic Chemistry of Life," Fraústo da Silva, J. J. R.; Willams, R. J. P.; Clarendon Press: New York, 1993.
38. "*d*-Metal Complexes," In *Inorganic Chemistry*; Shriver, D. E.; Atkins, P. W.; Langford, C. H.; W. H. Freeman, New York, 1990; pp 191-227.
39. "The Chelate, Macrocyclic, and Cryptate Effects," In *Coordination Chemistry: A Century of Progress*; Martel, A. E.; Hancock, R. D.; Kaufmann, G. B.; ACS, Washington D. C., 1994; pp 240-254.
40. "Crystal Structures of Metal-Peptide Complexes," Freeman, H. C. *Adv. Prot. Chem.* **1967**, *22*, 257-424.
41. "Chapter 20.2, Amino Acids, Peptides and Proteins," In *Comprehensive Coordination Chemistry*; Laurie, S. H.; Wilkinson, G.; Pergamon Press, New York, 1987; pp 739-776.
42. "Metal Complexes of Amino Acids and Peptides," Nolan, K. B.; Soudi, A. A.; Hay, R. W. *Amino Acids, Peptides and Proteins* **1994**, *25*, 282-332.
43. "Advanced Inorganic Chemistry," Cotton, F. A.; Wilkinson, G.; Wiley: New York, 1988.

44. "Crystallographic Studies of Metal—Peptide Complexes. V. ( $\beta$ -Alanyl-L-histidinato)copper(II) Dihydrate," Freeman, H. C.; Szymanski, J. T. *Acta Cryst.* **1967**, *22*, 406-416.
45. "Association of Divalent Cations with Acylated Histidine Derivatives," Martin, R. B.; Edsall, J. T. *J. Am. Chem. Soc.* **1960**, *82*, 1107.
46. "Stability of Binary and Ternary  $\beta$ -Alanine Containing Dipeptide Copper(II) Complexes," Sigel, H.; Prijs, B.; Martin, R. B. *Inorg. Chem. Acta* **1981**, *56*, 45-49.
47. "Peptide-Synthesis on the New Polyoxyethylene-Polystyrene Graft Copolymer, Synthesis of Insulin-B21-30," Bayer, E.; Dengler, M.; Hemassi, B. *Int. J. Pep. Protein Res.* **1985**, *25*, 178-186.
48. "Supports for Solid-Phase Organic Synthesis," In *Combinatorial Peptide and Nonpeptide Libraries: A Handbook*; Winter, M.; Jung, G.; VCH, New York, 1996; pp 465-510.
49. "Combinatorial Library Based on the One-Bead-One-Compound Concept," In *Combinatorial Peptide and Nonpeptide Libraries*; Lam, K. S.; Lebl, M.; Jung, G.; VCH, New York, 1996; pp 173-201.
50. "The "One-Bead-One-Compound" Combinatorial Library Method," Lam, K.; Lebl, M.; Krchnak, V. *Chem. Rev.* **1997**, *97*, 411-448.
51. "PEG Grafted Polystyrene Tentacle Polymers: Physico-Chemical Properties and Application in Chemical Synthesis," In *Combinatorial Peptide and Nonpeptide Libraries: A Handbook*; Rapp, W.; Jung, G.; VCH, New York, 1996; pp 425-464.
52. "PEGA: A Flow Stable Polyethylene Glycol Dimethyl Acrylamide Copolymer for Solid Phase Synthesis," Meldal, M. *Tetrahedron Lett.* **1992**, *33*, 3077-3080.
53. "Direct Visualization of Enzyme Inhibitors Using a Portion Mixing Inhibitor Library Containing a Quenched Fluorogenic Peptide Substrate. Part 1. Inhibitors for Subtilisin Carlsberg," Meldal, M.; Svendsen, I. *J. Chem. Soc., Perkin Trans. 1* **1995**, 1591-1596.

54. "A PEGA Resin for use in the Solid-phase Chemical—Enzymatic Synthesis of Glycopeptides," Meldal, M.; Auzanneau, F.-I.; Hindsgaul, O.; Palcic, M. M. *J. Chem. Soc., Chem. Commun.* **1994**, 1849-1850.
55. "Trace Elements in Natural Waters," Salbu, B.; Steinnes, E.; CRC: Boca Raton, 1995.
56. "Binding Constants: The Measurement of Molecular Complex Stability," Connors, K. A.; Wiley-Interscience: New York, 1987.
57. "Solid-Phase Peptide Synthesis Utilizing 9-Fluorenylmethoxycarbonyl Amino-Acids," Fields, G. B.; Noble, R. L. *Int. J. Pep. Protein Res.* **1990**, 35, 161-214.
58. "Advantageous Applications of Azabenzotriazole (Triazolopyridine)-based Coupling Reagents to Solid-phase Peptide Synthesis," Carpino, L. A.; El-Faham, A.; Minor, C. A.; Albericio, F. *J. Chem. Soc. Chem. Comm.* **1994**, 201-203.

**Chapter 5. Chemosensors for Ni(II) Based Upon the ATCUN Motif that Employ a FRET-Based Mechanism for Signal Transduction**

## Introduction

The exploitation of the amino-terminal Cu(II)- and Ni(II)-binding (ATCUN) domain of the serum albumins for the design of sensitive and selective chemosensors for Cu(II) has been demonstrated in the studies presented in Chapter 4. The mechanism of analyte detection employed for those sensors, namely the intramolecular quenching of an appended fluorophore, is one that has been commonly used in the design of chemosensors for Ni(II) and Cu(II).<sup>1-5</sup> (See also the discussion of these presented in Chapter 1.) However, a concern that arises for the application of such fluorosensors, is that it can be difficult to distinguish between the presence of the analyte and degradation of the sensing molecule. While the fluorosensors presented in Chapter 4 displayed reversible binding of the Cu(II) ion, and therefore the possibility of chemosensor degradation could be probed by the addition of a chelating agent such as EDTA to the sample, the requirement of doing so would add an undesired burden to the task of performing real time sensing.

To address this issue, efforts have been directed toward the production of sensors that operate through a different fluorescence signaling mechanism, but that employ the ATCUN motif for metal binding. One particularly attractive means of producing fluorescence modulation is to exploit the quantum-mechanical effect of fluorescence resonance energy transfer (FRET).<sup>6,7</sup> FRET occurs when a fluorophore in an excited state (donor) comes into proximity with an energy acceptor. If the absorption spectrum of the acceptor overlaps with the emission of the donor, then energy may be transferred between them *via* a nonradiative dipole-induced dipole interaction. If the acceptor is a fluorophore, it may then relax to the ground state, with the observation of enhanced acceptor emission. Quantum-mechanics dictate that the outcome of this dipole-induced dipole interaction is strongly distance-dependent, with the efficiency of energy transfer described as in equation 1:<sup>8</sup>

$$Efficiency = \frac{R_0^6}{(R^6 + R_0^6)} \quad (1)$$

where  $R$  is the distance between the donor and acceptor, and the quantity  $R_0$  is a parameter that is characteristic of the particular donor and acceptor, namely the distance at which energy transfer between them is 50% efficient.

As a consequence of this exquisite sensitivity to distance, FRET has traditionally been exploited for the elucidation of interatomic distances.<sup>9-12</sup> However, there are significant advantages inherent to the construction of FRET-based chemosensors. Primary among these is the fact that both donor and acceptor emissions are generally observed, thereby enabling ratiometric analysis. In contrast to the fluorescence mechanism employed by the chemosensors for Cu(II) presented in Chapter 4, this technique would afford an increase in acceptor fluorescence thereby circumventing the problem of determining whether chemosensor degradation has occurred.<sup>13,14</sup> Additionally, fluorophores which are excited at longer wavelengths (~ 400 nm) may be used, decreasing the potential for interference from fluorescence-active compounds (such as tryptophan or reduced pyridine-nucleotide cofactors) commonly found in biological samples.<sup>13,15</sup> As a consequence an emphasis in these studies has been the development of a so-called “long wavelength” chemosensor.

In order to exploit this method of fluorescence signaling, it was envisioned that the metal-induced contraction of the ATCUN motif could be used to drive changes in the distance separating an appended fluorescent donor and acceptor pair, as shown schematically in Figure 5-1. In the absence of Cu(II) or Ni(II), the peptidyl motif is extended, but when bound to an appropriate metal ion, the interfluorophore distance is decreased, leading to enhanced acceptor emission.

It should be noted, however, that the production of a FRET sensor for Cu(II) or Ni(II) using a small peptidyl template in which the fluorophores and bound metal ion are all in close proximity could be complicated by competition between the intended energy acceptor (fluorophore) and the metal cation for the energy available from the donor. Indeed, a variety of quenching mechanisms could result including electron transfer from

the metal to the excited state of the donor,<sup>4</sup> or FRET to a *d-d* transition of the metal cation.<sup>16</sup> (A discussion of these is presented in Chapter 4.) Although the quenching behavior of the metal cations is undesirable, only *total* quenching of the donor would necessarily preclude FRET as a sensing mechanism. Partial donor quenching, with observed acceptor emission, would still allow two separate fluorescence emission bands to be observed. In other words, if the system is not totally quenched, then even with metal interference in the FRET process, long-wavelength emission sensors may be produced.

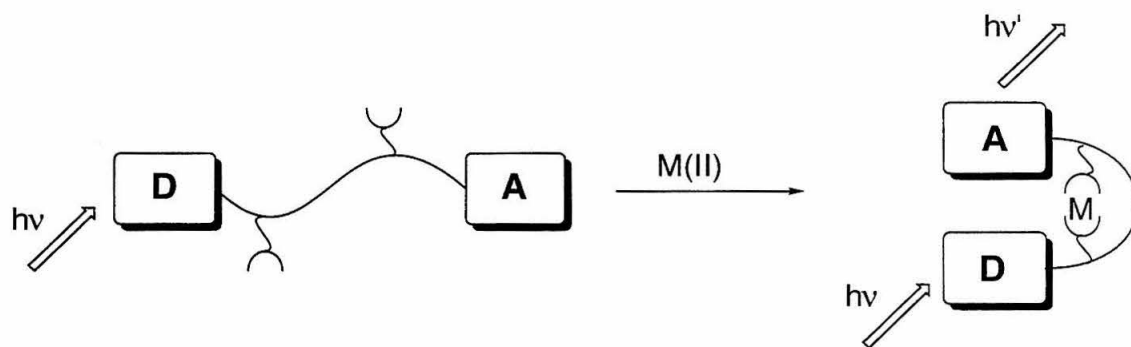


**Figure 5-1.** A representation of a FRET-based fluorosensor for a divalent metal cation. In the absence of metal, the motif is extended, and energy transfer from the donor fluorophore (D) to the acceptor fluorophore (A) is low. In the presence of a metal cation, the D to A distance is reduced, and enhanced acceptor emission is observed.

In order to maximize the sensitivity of the FRET response for a given metal ion-induced (peptidyl) conformational change, the mathematical consequences of the relationship between interfluorophore distance and efficiency of energy transfer (equation 1) should be considered. A plot of FRET efficiency against interfluorophore distance is presented in Figure 5-2. A critical aspect of this relationship is that for all pairs of fluorophores, changes in their distance-dependent exchange of energy is described by the same general function, one that is scaled by the magnitude of  $R_0$  for that particular fluorophore pair. A consequence of this is that no one pair of fluorophores is “best” for

the production of FRET-based sensors. Instead, fluorophores should be chosen by virtue of the value of their  $R_0$ .

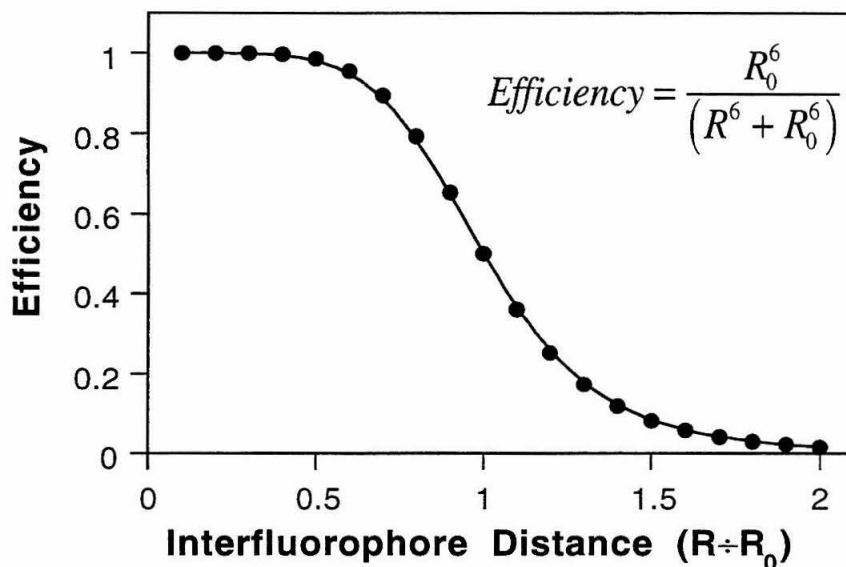


**Figure 5-2.** The distance-dependence of FRET efficiency is a function of the characteristic  $R_0$  for a donor and acceptor pair.

Analysis of Figure 5-2 suggests two different approaches for selecting FRET donor and acceptor pairs in order to “tune” their response to the magnitude of the particular interfluorophore distance change. The first approach is to choose fluorophore pairs such that the distance between them when in the metal-free (extended) state is  $\approx 2 R_0$ . In this situation, the *ratio* of acceptor emission to donor emission will be maximized with a metal-induced contraction of interfluorophore distance. The second approach is to choose fluorophore pairs such that the distance between them in the extended state is  $\approx R_0$ . In this case, the *relative* change in efficiency is maximized.

With these criteria in mind, an ATCUN-based peptidyl scaffold has been modeled in order to identify judicious sites for the introduction of two fluorophores for FRET-based signaling. Additionally, estimates of interfluorophore distances were measured and used for the selection of fluorophores to be included within ATCUN-based peptidyl chemosensors.

## Results and Discussion

### Modeling studies.

In order to estimate interfluorophore distances characteristic of in the extended, and metal bound states of a representative peptidyl template, Lys-Gly-His-Ser-Ser-Ser-NH<sub>2</sub> was used as a model compound (Figure 5-3). It was envisioned that the two fluorophores used for FRET would be attached through the side chain of the *N*-terminal residue, and through the side chain of the residue 1, 2, or 3 residues after the histidine in position 3 (sites a, b, or c, respectively). Two different sites of fluorophore attachment were considered for the first (*N*-terminal) residue, to model both a lysine-attached fluorophore (I) or a diaminopropanoic acid-attached fluorophore (II). With these varying points of attachment considered, a total of six theoretical interfluorophore distances were measured.

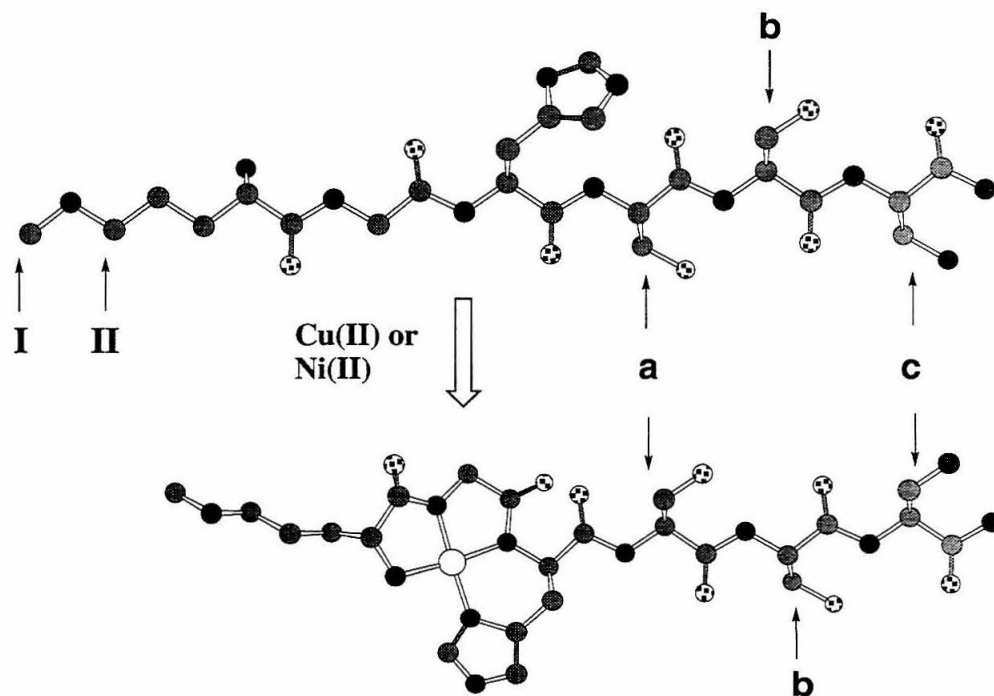


**Figure 5-3.** Molecular model of an ATCUN motif in an extended, and metal-bound state. Positions considered as potential sites for fluorophore introduction at the *N*-terminus (I, II) and *C*-terminus (a, b, and c) are highlighted.

To represent the metal ion-free state, the model was constrained with the backbone held in an extended geometry. The metal ion-bound state was modeled by constraining the metal ligating residues to be square planar, yet preserving the remainder of the backbone in an extended conformation. As these modeling studies were conducted with the intention of providing only a rough estimate of interatomic distances, no attempt was made to model the dynamic behavior of the peptide. The interatomic distances that were measured are presented in Table 5-1.

**Table 5-1.** Interatomic distances measured for the model ATCUN motif.

distance pair	extended distance (Å)	M(II)-bound distance (Å)	$\Delta$ (Å)
I-a	17.0	14.3	2.7
I-b	20.7	18.5	2.2
I-c	24.3	21.6	2.7
II-a	14.7	12.2	2.5
II-b	18.4	16.3	2.1
II-c	21.9	19.4	2.5

These data highlight two aspects of the ATCUN motif. First, it is very compact. The greatest interatomic distance measured (I  $\rightarrow$  a; Figure 5-3) was  $< 25$  Å. Second, the peptidyl conformational change upon binding a metal cation results in only a small compression of the backbone. Regardless of which pairs of interatomic distances are measured, the net change in distance is  $\sim 2.5$  Å. Both of these facts suggest that fluorophore pairs with small ( $< 20$  Å)  $R_0$ s are optimal for signal transduction for these sensors. Additionally, to maximize the relative change in energy transfer efficiency, the peptide corresponding to the substitution at positions I and a was chosen to be the host.

Accordingly, fluorophore pairs were investigated to find a suitable set (or sets) for the signaling event.

### **Selection of fluorophore pairs.**

Several reviews containing compilations of fluorophore pairs and their respective  $R_0$ s are available.<sup>9,11,14,17,18</sup> In this regard, the work of Van Der Meer<sup>6</sup> is an exceptionally useful source, deserving of special mention. This latter source contains an extensive, critically reviewed, listing fluorophore pairs by  $R_0$ , wavelength of donor excitation, and chemical family of the donor fluorophore, as well as quantum yields. Yet despite the wealth of information available regarding the  $R_0$ s for FRET pairs, there is a striking absence of fluorophore pairs with a small  $R_0$  ( $< 20 \text{ \AA}$ ) reported, unless a fluorophore with a very short excitation wavelength (such as tryptophan or tyrosine) is the donor.

This fact can best be understood from inspection of the quantum-mechanical relation from which the  $R_0$  for an energy donor and acceptor pair may be calculated. This is shown in equation 2:

$$R_0 = \left[ \frac{9000(\ln 10)}{128\pi^5 N_{AV}} \Phi_D \kappa^2 n^{-4} J \right]^{1/6} \quad (2)$$

where  $\Phi_D$  is the donor quantum yield,  $\kappa$  is an orientation factor,  $n$  is the index of refraction, and  $J$  the overlap integral for the donor emission and acceptor absorption. Thus, longer  $R_0$ s result when the donor quantum yield increases and when the overlap integral is large. This latter quantity,  $J$ , is described in a simplified fashion and can be thought of as the area in the shaded region of Figure 5-4.

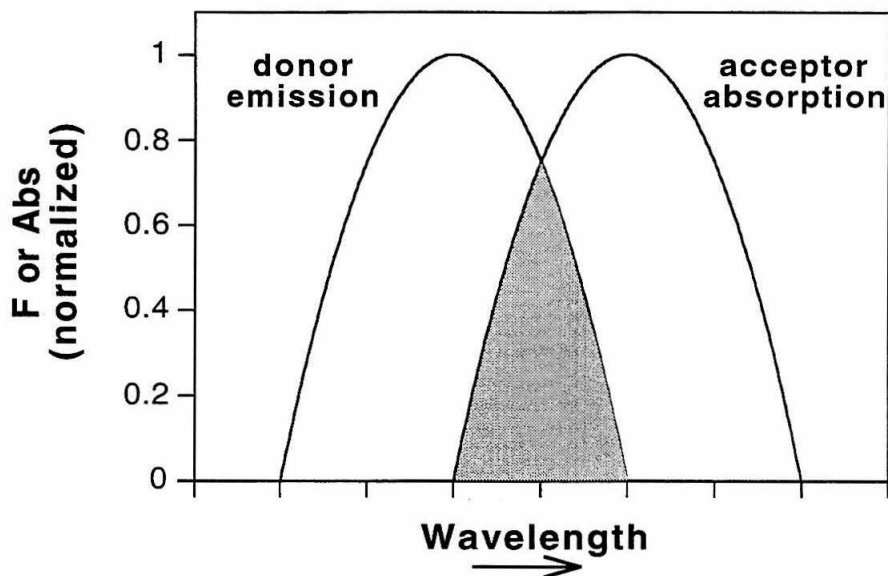


**Figure 5-4.** A typical donor-acceptor overlap, as required for FRET. The area in the shaded region is involved in the calculation of the overlap integral,  $J$ .

While the approximation of fluorophore overlaps is very useful for an estimation of their ability to transfer energy, a more precise definition of  $J$  is shown in equation 3.<sup>8</sup>

$$J = \frac{\int_0^{\infty} F_D(\lambda) \epsilon_A(\lambda) \lambda^4 d\lambda}{\int_0^{\infty} F_D(\lambda) d\lambda} \quad (3)$$

$F_D(\lambda)$  is the donor emission spectrum and

$\epsilon_A(\lambda)$  is the acceptor absorption (extinction) spectrum

$\lambda$  is the wavelength

As can be seen from the formal definition of  $J$ , this quantity has a fourth-order dependence on wavelength. In other words, overlap of donor emission and acceptor absorption at shorter wavelengths accounts for less efficient energy transfer, leading to shorter  $R_0$ s. In this regard, it is not surprising that there are few, if any, reports of fluorophores pairs that may be excited at long wavelengths and that have short  $R_0$ s. As mentioned previously, the historical application of FRET has been for the measurement of molecular distances, and

the accuracy of these determinations are greater when fluorophore pairs with substantial overlap (large values of  $J$ ) are used.<sup>14</sup>

For the of design of these chemosensors, the issue of decreased accuracy is of little consequence. The ability to produce metal-induced fluorescence modulation is of primary concern, rather than measurement of an interfluorophore distance change itself. As a consequence, three donor fluorophores were selected by virtue of their well characterized emission properties, resistance to photodegradation, and isomeric purity. (Many commercially available fluorophores are available only as isomeric mixtures.) These include the 5-*N,N'*-dimethylamino-naphthalene-1-sulfonyl (DNS) group, as well as two coumarin derivatives, 7-dimethylamino-coumarin-4-acetic acid (DM) and 7-diethylamino-coumarin-3-carboxylic acid (DE). The structures of these donor fluorophores and their fluorescence excitation and emission maxima in water are shown in Figure 5-5.

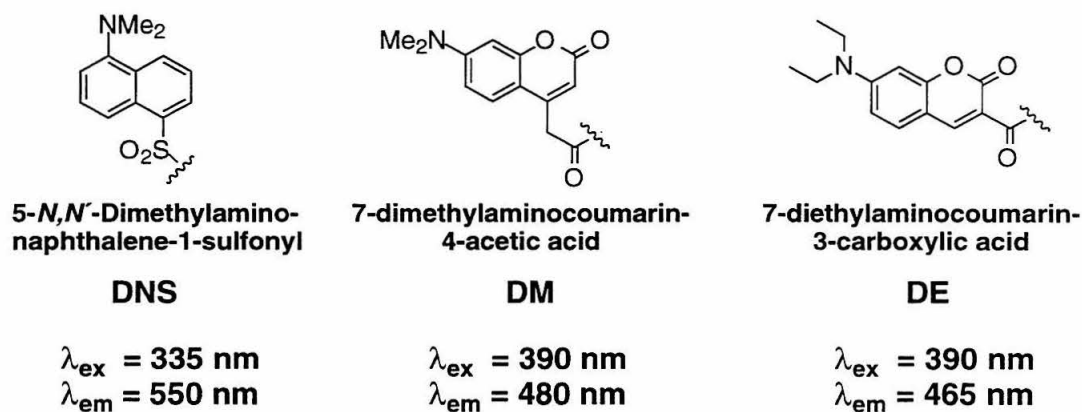
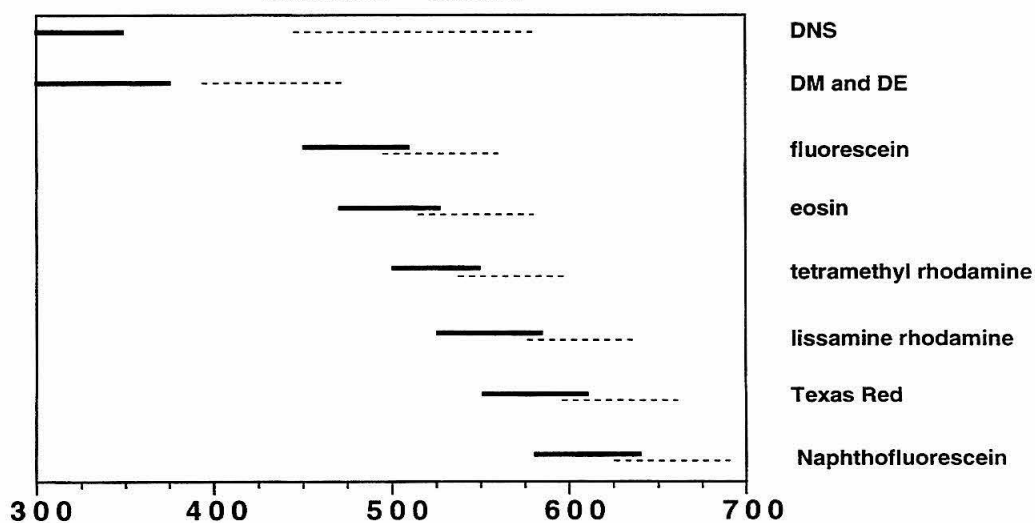
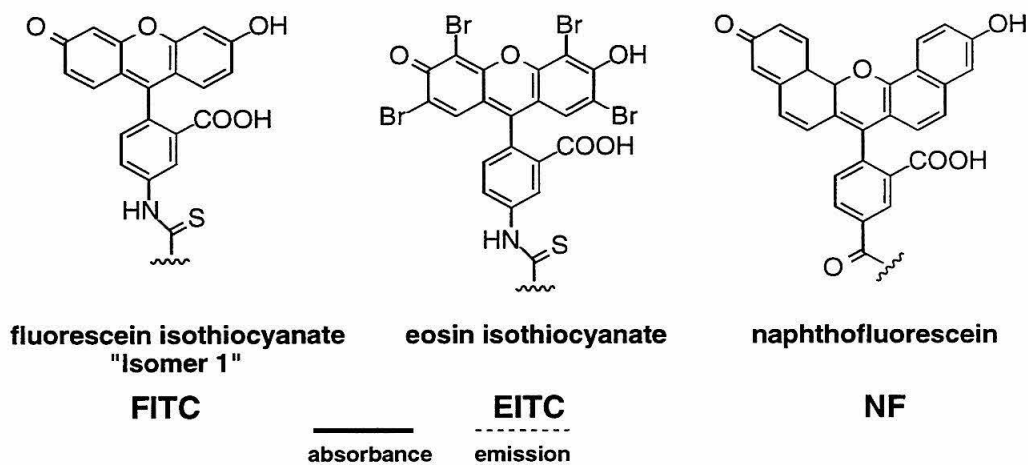


**Figure 5-5.** Structures and spectral properties of the donor fluorophores selected.

With donor fluorophores chosen, the spectral properties of several commercially available fluorophores that can be excited at wavelengths  $\geq 500 \text{ nm}$  were investigated. These include fluorescein isothiocyanate (FITC), eosin isothiocyanate (EITC), tetramethyl rhodamine isothiocyanate (TR-ITC), lissamine rhodamine (LR), Texas red (TR), and naphthofluorescein (NF). The structures of these, and a summary of their absorption and emission wavelengths, are presented in Figure 5-6. To judge (qualitatively) the extent of

donor emission overlap with acceptor absorption, the reported  $R_0$ s for several FRET pairs were considered in order to achieve a crude “calibration.” For example, the DNS/FITC couple has a reported  $R_0$  of 20-40 Å,<sup>17</sup> whereas that for a DM/FITC couple is 43 Å.<sup>6</sup> (Variance in the former is the large changes in quantum yield of the donor and in the overlap integral due to the polarity-dependence of the DNS group.)

The FITC, EITC, TMR-ITC, LR, and TR all have similar extinction coefficients ( $\sim 8 \times 10^5 \text{ M}^{-1} \text{ cm}^{-1}$ ), suggesting similar acceptor ability; smaller  $R_0$ s should be observed for those with the most red-shifted absorption, and hence the smallest overlap integrals. Yet of these potential acceptors, EITC was eliminated due to its exceptional sensitivity towards generation of singlet oxygen.<sup>14,19</sup> The TMR-ITC fluorophore was also eliminated in favor of the (slightly) longer-wavelength, and vastly less expensive LR. Further, TR was eliminated due to the propensity of TR-labeled molecules to precipitate from aqueous solution.<sup>15</sup> In summary, the acceptor fluorophores chosen for incorporation within peptidyl chemosensors were LR and NF, as well as the well-characterized FITC group, for it provided an experimental control with well-known  $R_0$ s with the selected donor partners.

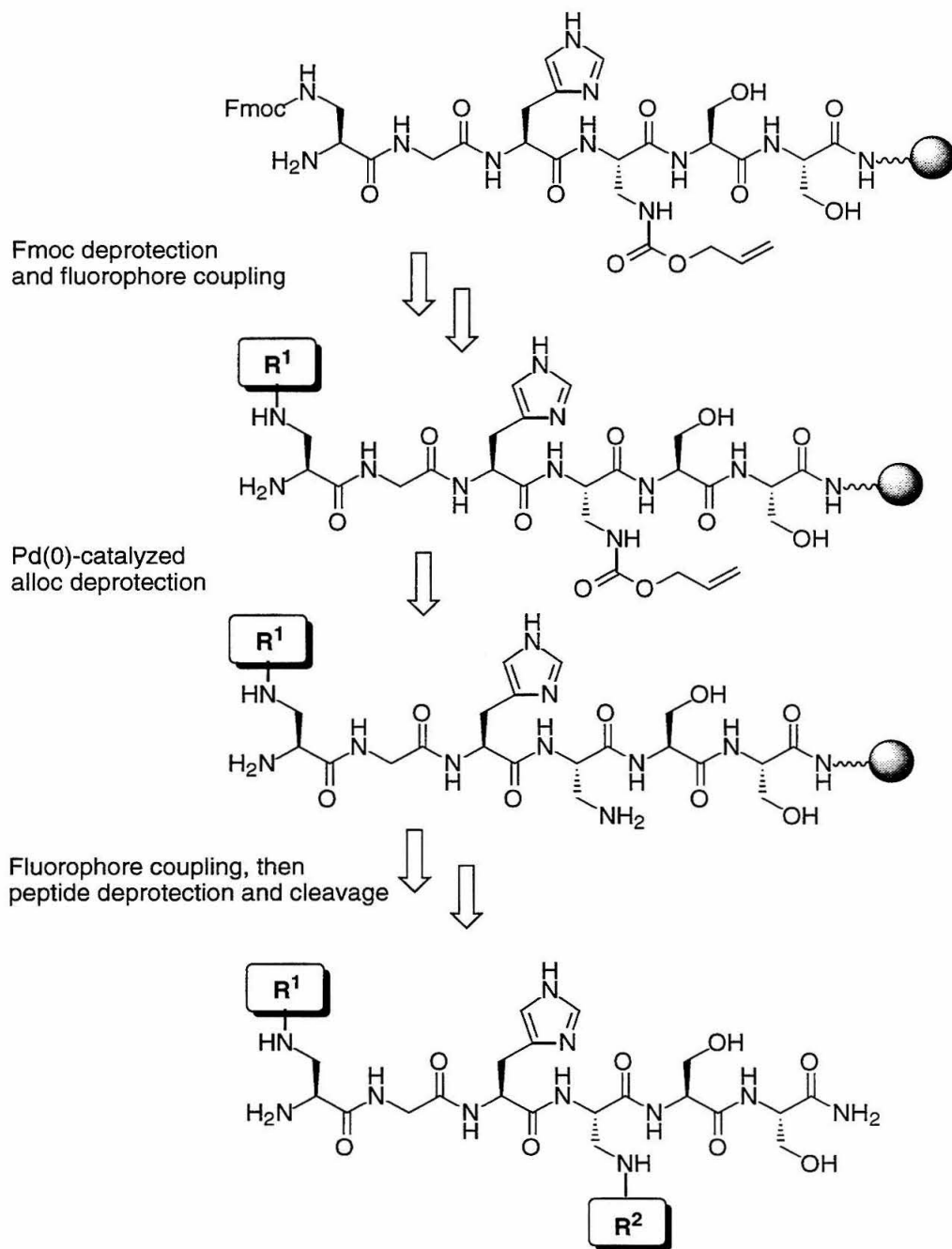


**Figure 5-6.** Structures of potential energy acceptors and their spectral properties in relation to those of the energy donors.

### Synthesis of chemosensors.

A family of peptides were prepared from a common precursor consisting of the resin-bound protected peptide Boc-Dap(Fmoc)-Gly-His(Boc)-Dap(alloc)-Ser(<sup>t</sup>Bu)-Ser(<sup>t</sup>Bu)-PAL-PEG-PS (Scheme 5-1). This template peptide was constructed using the differentially protected *N*<sup>α</sup>-Boc-*N*<sup>β</sup>-Fmoc-(*S*)-2,3-diaminopropanoic acid monomer at the *N*-terminus to facilitate attachment of the first fluorophore to the side chain amine of that residue similarly to a standard iteration of peptide elongation. Alternately, the residue *N*<sup>α</sup>-Fmoc-*N*<sup>β</sup>-allyloxycarbonyl-(*S*)-2,3-diaminopropanoic acid (Fmoc-Dap(alloc)-OH) was incorporated for the internal Dap residue. The allyloxycarbonyl (alloc) amine protecting group is deprotected orthogonally to the acid- or base-intensive methods typically used for Boc- or Fmoc-based peptide synthesis respectively through the use of a palladium catalyst.<sup>20</sup> Thus, after completion of the (*N*-terminal) fluorophore coupling, deprotection of the alloc group affords a selectively unmasked amine for coupling of the second fluorophore, resulting in FRET peptides **F1-F5**. In the case of control peptides (**C1-C5**), which contain only one fluorophore, the fluorescent probe was attached *via* the side chain of the *N*-terminal residue and the alloc side chain protecting group was left intact.

The structure of the resulting peptides are thus all described as variants of the final structure in Scheme 5-1, where R<sup>1</sup> represents an attached fluorophore, and R<sup>2</sup> represents either the alloc group or a second fluorophore. At the completion of synthesis and cleavage of the peptide from the resin, all peptides were purified to homogeneity by reverse-phase (C<sub>18</sub>) HPLC. Due to the fact that several of the fluorescent labeling compounds are not available in isomeric purity, multiple isomers were collected for many of the compounds. In all cases, these were separated, and the fluorescence properties tested only on isomerically pure materials. The compilation of the fluorophores incorporated within these peptides, and the number of isomers collected for each, is illustrated in Table 5-2.

**Scheme 5-1.** Synthetic strategy for the preparation of fluorescent peptides.

**Table 5-2.** Sequences of the peptides, and the number of pure isomers collected by HPLC.

peptide	sequence	isomers
<b>C 1</b>	H <sub>2</sub> N-Dap(DNS)-Gly-His-Dap(alloc)-Ser-Ser-CONH <sub>2</sub>	1
<b>C 2</b>	H <sub>2</sub> N-Dap(DM)-Gly-His-Dap(alloc)-Ser-Ser-CONH <sub>2</sub>	1
<b>C 3</b>	H <sub>2</sub> N-Dap(DE)-Gly-His-Dap(alloc)-Ser-Ser-CONH <sub>2</sub>	1
<b>C 4</b>	H <sub>2</sub> N-Dap(LR)-Gly-His-Dap(alloc)-Ser-Ser-CONH <sub>2</sub>	2
<b>C 5</b>	H <sub>2</sub> N-Dap(NF)-Gly-His-Dap(alloc)-Ser-Ser-CONH <sub>2</sub>	2
<b>F 1</b>	H <sub>2</sub> N-Dap(DNS)-Gly-His-Dap(FITC)-Ser-Ser-CONH <sub>2</sub>	1
<b>F 2</b>	H <sub>2</sub> N-Dap(DE)-Gly-His-Dap(FITC)-Ser-Ser-CONH <sub>2</sub>	1
<b>F 3</b>	H <sub>2</sub> N-Dap(LR)-Gly-His-Dap(DNS)-Ser-Ser-CONH <sub>2</sub>	4
<b>F 4</b>	H <sub>2</sub> N-Dap(LR)-Gly-His-Dap(DM)-Ser-Ser-CONH <sub>2</sub>	3
<b>F 5</b>	H <sub>2</sub> N-Dap(LR)-Gly-His-Dap(DE)-Ser-Ser-CONH <sub>2</sub>	4
<b>F 6</b>	H <sub>2</sub> N-Dap(LR)-Gly-His-Dap(FITC)-Ser-Ser-CONH <sub>2</sub>	2

**Fluorescence characterization.**

A series of background experiments were performed in order to characterize the fluorescence behavior of these compounds. Absorption, fluorescence excitation and fluorescence emission spectra were obtained for each of the control peptides (**C1-C5**) in 150 mM NaCl, 50 mM HEPES, pH 7.0 buffer. The respective wavelengths of maximum excitation determined in these studies were used in the acquisition emission spectra for the two-fluorophore compounds. During these initial studies it was discovered that the NF fluorophore is only slightly fluorescent at neutral pH; large changes are observed in both the absorbance and fluorescence emission spectra for this fluorophore between pH 7 and 9. (As a consequence no NF-containing dual-fluorophore compounds were prepared.)

To probe the effect of Cu(II) and Ni(II) on these peptides, emission spectra were acquired with 10  $\mu$ M solutions of chemosensor in 150 mM NaCl, 50 mM HEPES, pH 7.0 buffer, and the effect of an added equivalent of NiCl<sub>2</sub> or CuCl<sub>2</sub> measured. While the emission of all of the compounds (both for single-fluorophore control peptides and for dual-fluorophore FRET peptides) were strongly quenched by the addition of Cu(II), this was not the case for all peptides upon the addition of Ni(II). This trend mirrors the results obtained in the analysis of the quenching sensors based on the ATCUN motif, presented in Chapter 4. As in those studies, the Ni(II) ion was found here to be both a statistically and quantitatively less potent quencher of fluorescence. Quenching was observed for peptides **C1**, **C2**, **C3**, and **F3**, but no Ni(II)-induced change in emission was observed for peptides **C4**, **C5**, **F1**, and **F2**. A summary of the fluorescence emission response of all the peptides to both Ni(II) and Cu(II) is presented in Table 5-3.

**Table 5-3.** Spectral properties of the fluorescent peptides.

peptide	[R <sup>1</sup> ] <sup>a</sup>	[R <sup>2</sup> ] <sup>a</sup>	$\lambda_{\text{ex}}$ (nm)	$\lambda_{\text{em}}$ (nm)	+ Ni(II) <sup>b</sup>	+ Cu(II) <sup>b</sup>
<b>C1</b>	DNS	alloc	333	360	–	–
<b>C2</b>	DM	alloc	390	480	–	–
<b>C3</b>	DE	alloc	400	470	–	–
<b>C4</b>	LR	alloc	525 <sup>c</sup> , 560	590	0	–
<b>C5</b>	NF	alloc	570	660	0	–
<b>F1</b>	DNS	FITC	333	520	0	–
<b>F2</b>	DE	FITC	400	470 <sup>c</sup> , 520	0	–
<b>F3</b>	LR	DNS	333	590	–	–
<b>F4</b>	LR	DM	390	590	+	–
<b>F5</b>	LR	DE	400	590	+	–
<b>F6</b>	LR	FITC	490	590	–	–

<sup>a</sup>Indicates the identity of the side chain modification as depicted in Scheme 5-1.

<sup>b</sup>Fluorescence response to added divalent metal: – decrease; 0 no change;

+ enhancement of acceptor emission.

<sup>c</sup>Indicates minor feature.

Of particular interest, two of the peptides tested, **F4** and **F5**, showed an increase in acceptor fluorescence after the addition of Ni(II), although the response of **F5** is more pronounced. Likewise for both peptides, the increase in fluorescence approached equilibrium over a period of hours (Figure 5-7), indicating that Ni(II) binding is slow. Furthermore, the fluorescence response is reversible, albeit slowly, with the addition of EDTA. This behavior is characteristic of the Ni(II) ion, and has been seen in the studies of ATCUN-based sensors presented previously. Based upon those studies it is anticipated that the inclusion of an acidic residue (such as aspartic acid) as the second amino acid of the

peptide would increase the rate of Ni(II) binding. (For further details, please refer to Chapter 4.) Furthermore, the fluorescence behavior of 1  $\mu$ M solutions of **F5** is insensitive to 100  $\mu$ M concentrations of Mn(II), Fe(II), Fe(II), Co(II), Zn(II) as well as 10 mM concentrations of Mg(II) and Ca(II), with less than 10% changes in the fluorescence intensity observed.

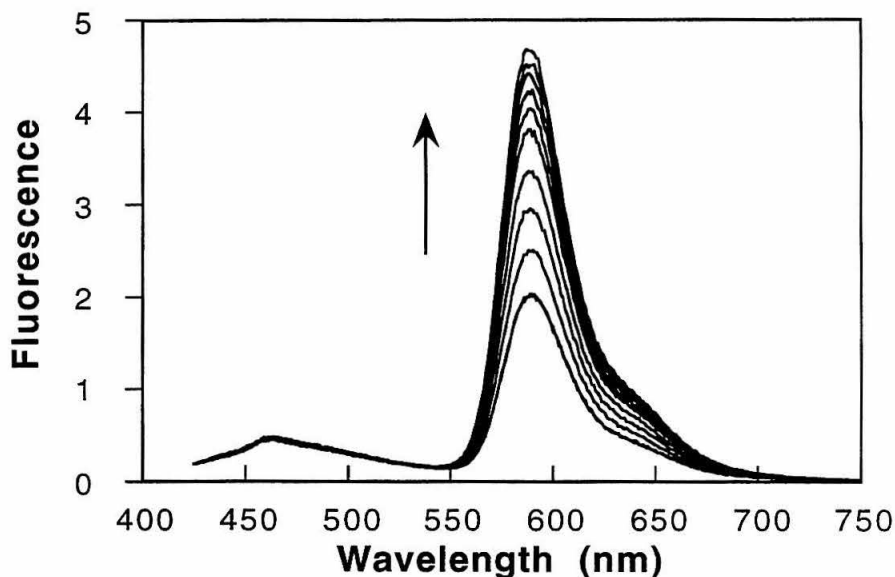


**Figure 5-7.** Fluorescence emission spectra of a 1  $\mu$ M solution of peptide **F5** in 150 mM NaCl, 50 mM HEPES, pH 7.0 after the addition of an equivalent of NiCl<sub>2</sub>. Spectra were acquired every 15 minutes for 2.5 hours. Excitation was performed at 400 nm.

### Calculation of $R_0$ s.

In addition to characterizing the fluorescence response of these peptidyl constructs to metal ions, studies were undertaken to determine the  $R_0$ s for the fluorophore pairs used. Accordingly, steady-state emission data were used to calculate quantum yields ( $\Phi$ ) of the donor fluorophores DM, DE, and DNS in 0.15 M NaCl, 50 mM HEPES, pH 7.0. Quinine in 0.1 N H<sub>2</sub>SO<sub>4</sub> was used as a standard ( $\Phi = 0.55$ ), also taking into account the wavelength-dependent changes of quantum yield of the standard.<sup>21</sup> It should be noted that although literature values of the quantum yield for these fluorophores are available,<sup>14,15</sup> the

measurement should be made under the exact conditions of the FRET assay. The buffer solution contains a high concentration of chloride ions which may cause partial quenching of the donor fluorescence.<sup>8</sup> The quantum yields calculated for the donor fluorophores are shown in Table 5-4.

**Table 5-4.** Quantum yields of the donor fluorophores measured in 0.15 M NaCl, 50 mM HEPES, pH 7.0.

fluorophore	$\Phi$
DM	0.17
DE	0.15
DNS	0.02(5)

FRET overlap integrals ( $J$ ) were calculated from steady state emission spectra of the donors and absorption spectra of acceptors.<sup>22</sup> Extinction coefficients of FITC ( $80,000 \text{ M}^{-1} \text{ cm}^{-1}$  at 490 nm) and LR ( $88,000 \text{ M}^{-1} \text{ cm}^{-1}$  at 570 nm) were obtained from the literature.<sup>15</sup> Distances of 50% energy transfer ( $R_0$ ) were calculated using the quantum yields obtained above, and the integrated overlap integrals. The calculated values of  $J$  and  $R_0$  are shown in Table 5-5. Furthermore, the  $R_0$ s calculated for those fluorophore pairs for which literature values are available (provided for comparison) are in good agreement.

**Table 5-5.** Integrated overlap integrals ( $J$ ) and distances of 50% energy transfer ( $R_0$ ) calculated for several fluorophore pairs.<sup>a</sup>

FRET pair	$J$ (OLI) <sup>b</sup>	$R_0$ (Å)	lit. value
DNS → FITC	2.3	22	20-40 <sup>c 17</sup>
DM → FITC	19.2	43	43 <sup>6</sup>
DE → FITC	19.7	42	43 <sup>6</sup>
DNS → LR	30.4	35	n/a
DM → LR	12.1	39	n/a
DE → LR	6.9	32	n/a

<sup>a</sup>Calculated with the assumption  $\kappa^2 = 2/3$ , and  $n = 1.34$ .

<sup>b</sup>The “OLI” units are scaled such that 1 OLI =  $1 \times 10^{-14} \text{ M}^{-1} \text{ cm}^{-3}$ .

<sup>c</sup>Variance due to the polarity-dependence of the donor quantum yield.

## Conclusion

These studies have resulted in the production of fluorescent chemosensors that selectively report the presence of the Ni(II) ion. Because these chemosensors employ the metal binding properties of the ATCUN motif, and have not been augmented to decrease their affinity for Cu(II), the reason for their Ni(II)-selectivity may be attributed to the selective binding of that ion only in part. While the ATCUN motif selectively binds a subset of the divalent metal ions, Cu(II) and Ni(II), the metal-enhanced FRET response is observed only for the Ni(II) ion. Thus, while peptide **P5** can be used for the measurement of sub-micromolar concentrations of divalent nickel in aqueous solution, the presence of equivalent concentrations of Cu(II) preclude successful measurements of the Ni(II) ion.

In agreement with the studies presented in Chapter 4, the response of these ATCUN-based peptidyl motifs to Ni(II) at low concentrations of chemosensor and metal ion ( $\sim 1 \mu\text{M}$ ) are slow, requiring several hours to reach equilibrium. In light of the previously presented research, this feature of the FRET sensors may be addressed. (The

incorporation of an amino acid with an acidic side chain in the second position of the peptidyl motif has been demonstrated to enhance the rate of binding the Ni(II) ion.)

## Acknowledgment

Dr. Dierdre Pearce has performed further studies on the production of FRET-based chemosensors for Ni(II). Her insights and contributions to this project have been invaluable for the furthering of this research, for which I sincerely thank her. A manuscript describing the results obtained by Dr. Pearce, combined with some of those described in this chapter has been prepared:

"Peptidyl Chemosensors Incorporating a Fret Mechanism for Detection of Ni(II)," Pearce, D. A.; Walkup, G. K.; Imperiali, B., submitted to *Biorg. Med. Chem. Lett.*, **1998**.

## Experimental

### Fluorescence measurements.

Steady state fluorescence spectra were acquired on an SLM-Aminco 500c spectrofluorometer. All measurements were performed using 150 mM NaCl, 50 mM HEPES buffer, pH 7.0, prepared with high purity water obtained from a Milli-Q filtration apparatus. Adventitious divalent metal cations were removed from the prepared buffer solution by passage through a Chelex column (BioRad).<sup>23</sup> Measurements were performed on 1-10  $\mu$ M solutions of peptides. Stock solutions of Ni(II) and Cu(II) were prepared as the chloride salt from analytical grade reagents. The concentrations of these were determined by titration with standardized solutions of EDTA in the presence of an appropriate metallochromic indicator.

### Calculation of $R_0$ s.

UV absorbance spectra were acquired using a Beckman DU7000. In both cases, data was transferred to a Macintosh computer. Further manipulation of the data was performed using Kaleidagraph version 3.0.5 (Adelback Software). Quantum yields of

donor fluorophores ( $\Phi_D$ ) were determined from the integrated emission intensity using equation 4, with quinine in 0.1 N H<sub>2</sub>SO<sub>4</sub> as the standard. The quantum yield of the standard was taken to be 0.55 when excited at 333 nm, and 0.62 when excited at 370 nm.<sup>21</sup>

$$\Phi_D = \Phi_{std} \cdot \frac{F_D}{F_S} \cdot \frac{A_S}{A_D} \quad (4)$$

$\Phi_{std}$  is the quantum yield of the standard

$F_S$  integrated fluorescence of the standard

$F_D$  integrated fluorescence of the donor

$A_S$  absorbance of the standard at  $\lambda_{ex}$

$A_D$  absorbance of the donor at  $\lambda_{ex}$

Fluorescence overlap integrals,  $J$ , were calculated using equation 5.

$$J = \frac{\int_0^{\infty} F_D(\lambda) \varepsilon_A(\lambda) \lambda^4 d\lambda}{\int_0^{\infty} F_D(\lambda) d\lambda} \quad (5)$$

$F_D(\lambda)$  is the donor emission spectrum

$\varepsilon_A(\lambda)$  is the acceptor absorbance (extinction) spectrum, with units of M<sup>-1</sup> cm<sup>-1</sup>.

$\lambda$  is the wavelength (in cm)

$R_0$  values were calculated by substituting the values of  $\Phi_D$  and  $J$  obtained as above into equation 6, assuming  $\kappa^2 = 2/3$ , and taking  $n$  (the index of refraction) as 1.34.

$$(6) \quad R_0 = \left[ \frac{9000(\ln 10)}{128\pi^5 N_{AV}} \Phi_D \kappa^2 n^{-4} J \right]^{1/6}$$

When  $J$  has been calculated, using the unit conventions described above, equation 6 simplifies to equation 7.

$$(7) \quad R_0 = 9.78 \times 10^3 \left[ \Phi_D \kappa^2 n^{-4} J \right]^{1/6} \text{ (with } J \text{ in units of M}^{-1} \text{ cm}^3\text{)}$$

## Peptide synthesis.

The peptide Boc-Dap(Fmoc)-Gly-His(Boc)-Dap(alloc)-Ser(<sup>t</sup>Bu)-Ser(<sup>t</sup>Bu) was synthesized on PAL-PEG-PS resin, 0.22 mmole/g (PerSeptive Biosystems) using a Millipore 9050 automated peptide synthesizer and employing 1,3-diisopropylcarbodiimide/1-hydroxybenzotriazole (DIPCDI/HOBt) activation. Coupling of the carboxylate-containing fluorophores DM, DE, and NF was performed using five equivalents of fluorophore, five equivalents of bromo-tris-pyrrolidino-phosphonium hexafluorophosphate (PyBrOP), 10 equivalents of diisopropylethylamine (DIEA), and 0.2 equivalents of 4-*N,N'*-dimethylaminopyridine (DMAP) in a minimal quantity of DMF. The LR and DNS fluorophores were coupled using the sulfonyl chlorides (3 equivalents per resin-bound amine), with 3 equivalents of DIPEA in a minimal volume of DMF. Coupling of FITC was performed similarly as described for the LR and DNS labels. Final peptide deprotection and cleavage from the resin was achieved with 5% v/v triisopropylsilane in trifluoroacetic acid. The crude cleavage mixture was reduced in volume, triturated with 1:1 ether:hexanes, dissolved in water, filtered, and lyophilized. All peptides were purified to homogeneity by RP (C<sub>18</sub>) HPLC, and characterized by electrospray mass spectrometry.

H<sub>2</sub>N-Dap(DNS)-Gly-His-Dap(alloc)-Ser-Ser-NH<sub>2</sub> (C1)

MS (ESI) calcd for C<sub>36</sub>H<sub>51</sub>O<sub>12</sub>N<sub>12</sub>S [M+H]<sup>+</sup> 875.4 found 875. HPLC (Beckman C<sub>18</sub> 0.46 × 15 cm column; flow rate 1.0 mL/min; solvent A = H<sub>2</sub>O, 0.1% v/v TFA, solvent B = MeCN 0.1% TFA; gradient 0% B 5 min, 0-70% B over 25 min) retention = 15.8 min.

H<sub>2</sub>N-Dap(DM)-Gly-His-Dap(alloc)-Ser-Ser-NH<sub>2</sub> (C2)

MS (ESI) calcd for C<sub>37</sub>H<sub>51</sub>O<sub>13</sub>N<sub>12</sub> [M+H]<sup>+</sup> 871.4 found 871. HPLC (Beckman C<sub>18</sub> 0.46 × 15 cm column; flow rate 1.0 mL/min; solvent A = H<sub>2</sub>O, 0.1% v/v TFA, solvent B = MeCN 0.1% TFA; gradient 0% B 5 min, 0-70% B over 25 min) retention = 17.5 min.

**H<sub>2</sub>N-Dap(DE)-Gly-His-Dap(alloc)-Ser-Ser-NH<sub>2</sub> (C3)**

MS (ESI) calcd for C<sub>38</sub>H<sub>53</sub>O<sub>13</sub>N<sub>12</sub> [M+H]<sup>+</sup> 885.4 found 885. HPLC (Beckman C<sub>18</sub> 0.46 × 15 cm column; flow rate 1.0 mL/min; solvent A = H<sub>2</sub>O, 0.1% v/v TFA, solvent B = MeCN 0.1% TFA; gradient 0% B 5 min, 0-70% B over 25 min) retention = 19.6 min.

**H<sub>2</sub>N-Dap(LR)-Gly-His-Dap(alloc)-Ser-Ser-NH<sub>2</sub> (C4)**

MS (ESI) calcd for C<sub>51</sub>H<sub>69</sub>O<sub>16</sub>N<sub>13</sub>S<sub>2</sub> [M+H]<sup>2+</sup> m/z = 591.7 found 592. HPLC (Beckman C<sub>18</sub> 0.46 × 15 cm column; flow rate 1.0 mL/min; solvent A = H<sub>2</sub>O, 0.1% v/v TFA, solvent B = MeCN 0.1% TFA; gradient 0% B 5 min, 0-70% B over 25 min) retention = 20.7 min (minor isomer), 21.2 min (major isomer).

**H<sub>2</sub>N-Dap(NF)-Gly-His-Dap(alloc)-Ser-Ser-NH<sub>2</sub> (C5)**

MS (ESI) calcd for C<sub>53</sub>H<sub>54</sub>O<sub>16</sub>N<sub>11</sub> [M+H]<sup>+</sup> 1100.4 found 1100. HPLC (Beckman C<sub>18</sub> 0.46 × 15 cm column; flow rate 1.0 mL/min; solvent A = H<sub>2</sub>O, 0.1% v/v TFA, solvent B = MeCN 0.1% TFA; gradient 25% B 5 min, 25-35% B over 20 min) retention = 19.8 min (isomer 1), 20.5 min (isomer 2).

**H<sub>2</sub>N-Dap(DNS)-Gly-His-Dap(FITC)-Ser-Ser-NH<sub>2</sub> (F1)**

MS (ESI) calcd for C<sub>53</sub>H<sub>58</sub>O<sub>15</sub>N<sub>13</sub>S<sub>2</sub> [M+H]<sup>+</sup> 1180.4 found 1181. HPLC (Beckman C<sub>18</sub> 0.46 × 15 cm column; flow rate 1.0 mL/min; solvent A = H<sub>2</sub>O, 0.1% v/v TFA, solvent B = MeCN 0.1% TFA; gradient 0% B 5 min, 0-70% B over 25 min) retention = 18.8 min; gradient 15% B 5 min, 15-35% B over 20 min, retention = 20.2 min.

**H<sub>2</sub>N-Dap(DE)-Gly-His-Dap(FITC)-Ser-Ser-NH<sub>2</sub> (F2)**

MS (ESI) calcd for C<sub>55</sub>H<sub>60</sub>O<sub>16</sub>N<sub>13</sub>S [M+H]<sup>+</sup> 1190.4 found 1190. HPLC (Beckman C<sub>18</sub> 0.46 × 15 cm column; flow rate 1.0 mL/min; solvent A = H<sub>2</sub>O, 0.1% v/v TFA, solvent B = MeCN 0.1% TFA; gradient 0% B 5 min, 0-70% B over 25 min) retention = 20.6 min; gradient 25% B 5 min, 25-35% B over 20 min, retention = 18.7 min.

**H<sub>2</sub>N-Dap(LR)-Gly-His-Dap(DNS)-Ser-Ser-NH<sub>2</sub> (F3)**

MS (ESI) calcd for C<sub>59</sub>H<sub>76</sub>O<sub>16</sub>N<sub>14</sub>S<sub>3</sub> [M+H]<sup>2+</sup> m/z = 666.3 found 666. HPLC (Beckman C<sub>18</sub> 0.46 × 15 cm column; flow rate 1.0 mL/min; solvent A = H<sub>2</sub>O, 0.1% v/v TFA, solvent B = MeCN 0.1% TFA; gradient 0% B 5 min, 0-70% B over 25 min) retention = 21.4 min.

**H<sub>2</sub>N-Dap(LR)-Gly-His-Dap(DM)-Ser-Ser-NH<sub>2</sub> (F4)**

MS (ESI) calcd for C<sub>60</sub>H<sub>76</sub>O<sub>17</sub>N<sub>14</sub>S<sub>2</sub> [M+H]<sup>2+</sup> m/z = 664.7 found 664. HPLC (Beckman C<sub>18</sub> 0.46 × 15 cm column; flow rate 1.0 mL/min; solvent A = H<sub>2</sub>O, 0.1% v/v TFA, solvent B = MeCN 0.1% TFA; gradient 0% B 5 min, 0-70% B over 25 min) retention = 22.8 min.

**H<sub>2</sub>N-Dap(LR)-Gly-His-Dap(DE)-Ser-Ser-NH<sub>2</sub> (F5)**

MS (ESI) calcd for C<sub>61</sub>H<sub>78</sub>O<sub>17</sub>N<sub>14</sub>S<sub>2</sub> [M+H]<sup>2+</sup> m/z = 671.3 found 671. HPLC (Beckman C<sub>18</sub> 0.46 × 15 cm column; flow rate 1.0 mL/min; solvent A = H<sub>2</sub>O, 0.1% v/v TFA, solvent B = MeCN 0.1% TFA; gradient 0% B 5 min, 0-70% B over 25 min) retention = 22.5 min.

**H<sub>2</sub>N-Dap(LR)-Gly-His-Dap(FITC)-Ser-Ser-NH<sub>2</sub> (F6)**

MS (ESI) calcd for C<sub>30</sub>H<sub>43</sub>O<sub>9</sub>N<sub>10</sub>S [M+H]<sup>+</sup> 719.3 found 719. HPLC (Beckman C<sub>18</sub> 0.46 × 15 cm column; flow rate 1.0 mL/min; solvent A = H<sub>2</sub>O, 0.1% v/v TFA, solvent B = MeCN 0.1% TFA; gradient 0% B 5 min, 0-70% B over 25 min) retention = 21.2 min.

**References**

1. "Fluorescent Chemosensor for Organic Guests and Copper(II) Ion Based on Dansyldiethylenetriamine-Modified β-Cyclodextrin," Corradini, R.; Dossena, A.; Galaverna, G.; Marchelli, R.; Panagia, A., et al. *J. Org. Chem.* **1997**, *62*, 6283-6289.

2. "A Fluorescent Chemosensor for the Copper(II) Ion," De Santis, G.; Fabbriizzi, L.; Licchelli, M.; Mangano, C.; Sacchi, D., et al. *Inorg. Chem. Acta* **1997**, 257, 69-76.
3. "An Anthracene-Based Fluorescent Sensor for Transition Metal Ions," Fabbriizzi, L.; Licchelli, M.; Pallavicini, P.; Perotti, A.; Sacchi, D. *Angew. Chem. Int. Ed. Engl.* **1994**, 33, 1975-1977.
4. "Fluorescent Sensors for Transition Metals Based on Electron-Transfer and Energy-Transfer Mechanisms," Fabbriizzi, L.; Licchelli, M.; Pallavicini, P.; Perotti, A.; Taglietti, A., et al. *Chemistry a European Journal* **1996**, 2, 75-82.
5. "A Fluorescent Chemosensor Signalling Only Hg(II) and Cu(II) in Water," Yoon, J.; Ohler, N. E.; Vance, D. H.; Aumiller, W. D.; Czarnik, A. W. *Tetrahedron Lett.* **1997**, 38, 3845-3848.
6. "Resonance Energy Transfer," Van Der Meer, B. W.; Coker, G. I.; Chen, S.-Y. S.; VCH: New York, 1994.
7. "Fluorescence Resonance Energy Transfer," Selvin, P. R. *Meth. Enzym.* **1995**, 246, 300-334.
8. "Principles of Fluorescence Spectroscopy," Lakowicz, J. R.; Plenum Press: New York, 1983.
9. "Fluorescence Energy Transfer as a Spectroscopic Ruler," Stryer, L. *Ann. Rev. Biochem.* **1978**, 47, 819-846.
10. "Energy Transfer: A Spectroscopic Ruler," Stryer, L.; Haugland, R. P. *Proc. Natl. Acad. Sci. U.S.A.* **1967**, 38, 719-725.
11. "The Use of Singlet-Singlet Energy Transfer to Study Macromolecular Assemblies," Fairclough, R. H.; Cantor, C. R. *Meth. Enzym.* **1976**, 278, 347-379.
12. "Intramolecular Transfer of Excitation from Tryptophan to 1-Dimethylaminonaphthalene-5-sulfonamide in a Series of Model Compounds," Conrad, R. H.; Brand, L. *Biochemistry* **1968**, 7, 777-787.

13. "Fluorescent and Photochemical Probes of Dynamic Biochemical Signals inside Living Cells," In *Fluorescent Chemosensors for Ion and Molecule Recognition*; Tsien, R. Y.; Czarnik, A. W.; ACS, Washington D.C., 1993; pp 130-146.
14. "Fluorescent Probes in Cellular and Molecular Biology," Slavik, J.; CRC Press: Boca Raton, 1994.
15. "Handbook of Fluorescent Probes and Research Chemicals," Haugland, R. P.; Molecular Probes: 1996.
16. "Metal Ions as Donors and Acceptors of Fluorescence," In *Methods for Determining Metal Ion Environments in Proteins*; Holmquist, B.; Darnall, W. D.; Wilkins, R. G.; Elsevier, New York, 1980; pp 75-93.
17. "Fluorescence Resonance Energy Transfer Measurements of Distances in Actin and Myosin. A Critical Evaluation.," dos Remedios, R. G.; Miki, M.; Barden, J. A. *J. Muscle Res. Cell Motil.* **1987**, *8*, 97-117.
18. Steinberg, I. Z. *Annual Review of Biochemistry* **1971**, *40*, 83-114.
19. "Covalent Fluorescent Probes," In *Excited states of biopolymers*; Haugland, R. P.; Sheiner, R. F.; Plenum, New York, 1983; pp 29-58.
20. "Automated Allyl Cleavage for Continuous-Flow Synthesis of Cyclic and Branched Peptides," Kates, S. A.; Daniels, S. B.; Albericio, F. *Anal. Biochem.* **1993**, *212*, 303-310.
21. "Some Characteristics of the Fluorescence of Quinine," Chen, R. F. *Anal. Biochem.* **1967**, *19*, 374-387.
22. "Practical Fluorescence; Theory, Methods, and Techniques," Guilbault, G. G.; Marcel Dekker: New York, 1973.
23. "Elimination of Adventitious Metals," Holmquist, B. *Meth. Enzym.* **1988**, *158*, 6-12.